Evolutionary landscape of bacterial adaptation to diverse environmental niches

Hu, Guohai

Publication date:
2023

Document Version
Publisher's PDF, also known as Version of record

Technical University of Denmark

Evolutionary landscape of bacterial adaptation to diverse environmental niches

Guohai Hu

PhD thesis

March 2023

Bacterial Interactions and Evolution group

Department of Biotechnology and Biomedicine

Technical University of Denmark

DTU Bioengineering

Department of Biotechnology and Biomedicine

Guohai Hu

Evolutionary landscape of bacterial adaptation to diverse environmental niches

Supervisors:

Professor Ákos T. Kovács

Associate Professor Mikael Lenz Strube (Co-supervisor)

PREFACE

This Ph.D. thesis was submitted as partial fulfilment of the requirements to obtain a Ph.D. degree from the Technical University of Denmark (DTU). The work described in this thesis was carried out from March 2020 to March 2023 in the Bacterial Interactions and Evolution group at the Department of Biotechnology and Biomedicine, DTU and China National GeneBank.

The Ph.D. project was supervised by Professor Ákos T. Kovács, co-supervised by Associate Professor Mikael Lenz Strube.

The project was funded by the DTU Bioengineering and China National GeneBank.

Guohai Hu (胡国海)

March 2023

ACKNOWLEDGEMENTS

It is an amazing experience for me to complete this PhD. First of all, I am grateful to my supervisor Ákos T. Kovács, for providing me with guidance, support and motivating discussions throughout my doctoral journey no matter when I was in Denmark or in China. You always encouraged me and gave me confidence to finish my project step by step, from study plan to data analysis and manuscript writing, that's a feeling I never had before. I learned a lot from your guidance, and it will be very helpful for my career. I also would like to thank my co-supervisor Mikael Lenz Strube for inspiring discussions and guidance during my Ph.D. project.

As a DTU-BGI collaboration Ph.D., I would like to thank DTU and BGI group for providing me with this opportunity. I am grateful to Bo Wang, Ren Wang, and many other colleagues from BGI side for their continuous support and encouragement throughout my research journey.

Special thanks to Yicen, Mathilde, Chris, Anna, and you for providing me with the "living fossil" samples from your experiments, which form the basis of my project. I would also like to acknowledge the co-authors of my studies for excellent collaborations. Thanks to Yue Wang, it was a happy collaboration with you.

Moreover, I'd like to thank Xinming, Xinli, Caja, Jiyu, Carlos, Lasse, Mark, Rune and Adele from the BIE group, for all the help, lunches and talks we had together.

Finally, I am deeply grateful to my family and friends. Your love and belief in me kept me motivated and focused during the challenging times. To my wife and son, I apologize for the absence of your life during this period.

Thank you all for being a part of this journey and for helping me to achieve this significant milestone.

ABSTRACT

Numerous species of the *Bacillus* genus are used in green biotechnology to improve plant growth. An important plant-growth-promoting rhizobacterium (PGPR) is *Bacillus subtilis* that is commonly isolated in association with plants and their rhizosphere. Likewise, *Bacillus thuringiensis* is commonly used as a biological pesticide. Both species are prevalent biofilm formers in diverse environments. Biofilms are matrix-enclosed microbial communities that adhere to biotic or abiotic surfaces. Experimental evolution has been previously utilized to study how these two *Bacillus* species adapt to different environmental niches, e.g., floating or plastic bead attached biofilms and during plant root colonization. However, the full understanding of the dynamic mutational landscapes was lacking over the full experimental evolution setup. The purpose of this PhD project was to unveil the evolutionary landscape how *Bacillus* adapts to diverse environmental niches using whole-population genome sequencing.

By comparing the genetic adaptive mechanisms between *B. subtilis* and *B. thuringiensis* when these two species were adapted to the same environment and when one species is adapted to two distinct environments, we detected higher number of mutations, greater genotypic diversity, and higher evolvability in the populations evolved in biotic conditions. Our results also uncovered the influence of insertion sequences on the adaptation of *B. thuringiensis*. Finally, the higher degree of genetic diversification observed in biotic selective environments suggests an increased spatial niche heterogeneity and a nutritional source difference created by the plant host that provided a strong selection during the adaptation process.

Subsequently, we investigated how *B. subtilis* evolves on *Arabidopsis thaliana* and tomato seedlings, as well as in an alternating host regime of the two plants. We identified parallel evolution across multiple levels of biological organization in all conditions. We also observed species-specific adaptation at genetic level, which was potentially provoked by specific host plant-imposed selection, either due to root exudates or certain stress conditions. Additionally, motility-biofilm trade-off was also revealed in the mutational landscape of related genes, confirming the experimentally observed reduced motility of evolved isolates. Lastly, we identified both condition-specific and shared list of mutated genes of *B. subtilis* when evolved in different biofilm environments.

In the final approach, a simple Bacterial-Fungal Interactions (BFIs) system was explored to reveal the effects of a long-term cultivation of *B. subtilis* in the presence of *Aspergillus niger* with focus on the evolution of *B. subtilis*. In specific populations, *B. subtilis* was selected with enhanced surfactin production and spreading behavior, which was mimicked by recreation of specific mutations in genes encoding DegS-DegU two-component system. Increased surfactin production and niche colonization by the bacterium dismantled fungal expansion and acidification of the medium, in addition to introduction of cell wall stress in *A. niger*.

In conclusion, this PhD project has contributed to the understanding the genetic mechanisms on how two *Bacillus* species adapt to different environmental niches, and deepen our understanding of bacterial interactions with plants and fungi, which will likely to support strain improvements for sustainable agriculture in the future.

DANSK RESUMÉ

Adskillige arter af *Bacillus*-slægten anvendes inden for grøn bioteknologi til at forbedre plantevækst. En vigtig plantevækstforøgende rodbakterie er *Bacillus subtilis* som ofte isoleres i forbindelse med planter og deres rhizosfære. Ligeledes bruges *Bacillus thuringiensis* ofte som et biologisk pesticid. Begge arter producerer hyppigt biofilm i forskellige miljøer. Biofilm er matrix-omsluttede mikrobielle samfund der fæstner til biotiske eller abiotiske overflader. Eksperimentel evolution er tidligere blevet brugt til at undersøge hvordan disse to *Bacillus*-arter tilpasser sig forskellige miljønicher, f.eks. i flydende eller plastikperlefæstnede biofilm og under planterodskolonisering. Imidlertid manglede den fulde forståelse af det dynamiske mutationslandskab henover hele eksperimentel evolution-opsætningen. Formålet med dette Ph.d.-projekt var at klarlægge det evolutionære landskab over hvordan *Bacillus* tilpasser sig forskellige miljønicher ved brug af helpopulations-genom-sekventering.

Ved at sammenligne de genetiske tilpasningsmekanismer mellem *B. subtilis* og *B. thuringiensis,* når disse to arter blev tilpasset det samme miljø og når en art blev tilpasset to forskellige miljøer, fandt vi et højere antal mutationer, større genotypisk variation og højere evolutionsevne i populationerne udviklet under biotiske forhold. Vores resultater klarlagde også betydningen af *insertion sequences* på evolutionen af *B. thuringiensis.* Endelig tyder den højere grad af genetisk diversificering observeret i biotisk selektive miljøer på, at en øget rummelig niche-heterogenitet og en næringskildeforskel skabt af planteværten bidrog til en stærk selektion under tilpasningsprocessen.

Efterfølgende undersøgte vi hvordan *B. subtilis* udvikler sig på *Arabidopsis thaliana* og frøplanter af tomat, såvel som i et skiftende værtsregime af de to planter. Vi identificerede parallel evolution på tværs af flere niveauer af biologisk organisation under alle forholdene. Vi observerede også artsspecifik tilpasning på det genetiske niveau, hvilket muligvis var fremprovokeret af specifik værtsplante-pålagt selektion, enten på grund af rodeksudater eller bestemte stressfaktorer. Derudover afsløredes også et motilitets-biofilm *trade-off* i mutationslandskabet af relaterede gener, hvilket bekræfter den eksperimentelt observerede reduktion i motilitet af udviklede isolater. Til sidst identificerede vi både miljø-specifikke og delte muterede gener af *B. subtilis* når udviklet i forskellige biofilm-miljøer.

I den endelige tilgang blev et simpelt bakterie-svampe interaktionssystem undersøgt for at klarlægge konsekvensen af langtidskultivering af *B. subtilis* i tilstedeværelse af *Aspergillus niger,* med fokus på evolutionen af *B. subtilis.* I bestemte populationer blev *B. subtilis* med øget surfactin-produktion og spreder-adfærd selekteret, hvilket blev efterlignet ved genskabelse af specifikke mutationer i gener kodende for DegS-DegU to-komponent-systemet. Øget surfactin-produktion og nichekolonisering af bakterien forhindrede svampens udvidelse og forsuring af mediet, udover at introducere cellevægsstress i *A. niger.*

Afslutningsvis har dette Ph.d.-projekt bidraget til forståelsen af de genetiske mekanismer hvorved to *Bacillus* arter tilpasser sig forskellige miljønicher, og udvidet vores forståelse af bakteriers interaktioner med planter og svampe, hvilket sandsynligvis vil hjælpe med forbedringen af bakteriestammer til bæredygtigt landbrug i fremtiden.

TABLE OF CONTENTS

PUBLICATIONS

This Ph.D. thesis is based on the following research articles:

Study 1: Mathilde Nordgaard, Christopher Blake, Gergely Maróti, **Guohai Hu**, Yue Wang, Mikael Lenz Strube, Ákos T. Kovács. Experimental evolution of *Bacillus subtilis* on *Arabidopsis thaliana* roots reveals fast adaptation and improved root colonization (2022). *iScience* 25, 104406

Study 2: Guohai Hu, Yue Wang, Xin Liu, Mikael Lenz Strube, Bo Wang, Ákos T. Kovács. Species and condition shape the mutational spectrum in experimentally evolved biofilms (2023). *To be revised in mSystem*, preprint deposited in bioRxiv: https://www.biorxiv.org/content/10.1101/2022.12.07.519423v1

Study 3: Guohai Hu, Yue Wang, Christopher Blake, Mathilde Nordgaard, Xin Liu, Bo Wang, Ákos T. Kovács. Parallel genetic adaptation of *Bacillus subtilis* to different plant species (2023). *Submitted to Microbial Genomics,* preprint deposited in bioRxiv: *https://www.biorxiv.org/content/10.1101/2023.03.17.533125v1*

Study 4: Anne Richter, Felix Blei, **Guohai Hu**, Jan W. Schwitalla, Carlos N. Lozano-Andrade, Scott A Jarmusch, Mario Wibowo, Bodil Kjeldgaard, Surabhi Surabhi, Theresa Jautzus, Christopher Phippen, Olaf Tyc, Mark Arentshorst, Yue Wang, Paolina Garbeva, Thomas Ostenfeld Larsen, Arthur F.J. Ram, Cees A.M. van den Hondel, Gergely Maróti, Ákos T. Kovács. Enhanced niche colonization and competition during bacterial adaptation to a fungus (2023). *To be submitted,* preprint deposited in bioRxiv: *https://www.biorxiv.org/content/10.1101/2023.03.27.534400v1*

Chapter 1 General introduction and thesis outline

The global population reached 8 billion on 15 November 2022 according to the United Nations, and it is projected to reach 9.8 billion by 2050[1]. The continuously growing world population increases the demand for food, which emphasizes the importance of sustainable agriculture to help increase crop yield and food production. Insects and pathogens that affect crops are among the biggest threats to modern food production and lead to huge economic losses worldwide[2]. In order to counteract crop losses, pesticides, herbicides, and other agrochemicals are often applied excessively during the last decades, however, such substances can cause environmental issues, and also affect human health[2,3]. Additionally, the consistent use of these chemicals will lead to the emergence of resistant plant pathogens[4], which increases the urge to develop alternative strategies even further.

Biocontrol agents promise a sustainable and innocuous alternative to chemical-based control[5], and biological control is regarded as one of the most environmentally safe and economically profitable ways to manage plant diseases and pests[5,6]. Plant-growth-promoting rhizobacterium (PGPR) can benefit plant growth and development directly or indirectly via different ways[7,8]. In general, PGPR enhance plant growth directly by either assisting in the acquisition of nutrients (nitrogen[9,10] and phosphorus[11]) or modulating plant hormone levels[12,13], or indirectly by acting as biocontrol agents[14–16] to reduce the inhibitory effects of a variety of pathogens on plant growth and development.

Numerous species of the *Bacillus* genus are used in green biotechnology to improve plant growth. An important PGPR is *Bacillus subtilis* that is

commonly isolated in association with plants and their rhizosphere[8,17]. Likewise, *Bacillus thuringiensis* is commonly used as a biological pesticide[18,19], it also can colonize plants in a phylogeny-dependent manner[20,21]. To exert their beneficial effects, PGPR usually must colonize and persist on the root surface efficiently, which mainly depends on their ability to form biofilms.

Experimental evolution provides a powerful tool to study microbial adaptation to different environments in real-time, it has been previously utilized to study how these two *Bacillus* species adapt to different environmental niches, e.g., floating or plastic bead attached biofilms[22,23] and during plant root colonization[24,25]. However, due to the lack of whole population level mutational data, the full understanding of the dynamic mutational landscapes was missing over the full experimental evolution setup.

The purpose of this PhD project was to unveil the evolutionary landscape how *Bacillus* adapts to diverse environmental niches. I aimed to expand our knowledge and understanding of the genetic mechanisms on how two *Bacillus* species adapt to different environmental niches, and to deepen our understanding of bacterial interactions with plants and fungi, which will likely to support strain improvements for sustainable agriculture in the future. Several research aspects were explored in this project:

- How *B. subtilis* genetically adapts to *A. thaliana* roots under hydroponic, axenic conditions (**Study 1**)?

- What are the differences and similarities of genetic adaptive mechanisms between *B. subtilis* and *B. thuringiensis* when these two species were adapted to the same environment and when one species is adapted to two distinct environments (**Study 2**).

- Do plant colonizing bacteria adapt differently in an alternating host regime compared with a setup where the same plant is used throughout the experiment (**Study 3**)?

- How *B. subtilis* adapts to the environment in the presence of *A. niger* (**Study 4**)?

The general introduction of this thesis starts with an introduction of Experimental Evolution in **Chapter 2**, including several models used in biofilm adaptation studies and sequencing based approaches and tools used in evolution experiments, as well as some genetic mechanisms in adaptation evolution. **Chapter 3** includes a general introduction to the *Bacillus* genus and then focuses on biofilm formation and its regulation in *B. subtilis*. **Chapter 4** introduces the evolution experiments performed on *B. subtilis*, including domestication, sporulation adaptation, as well as its adaptation to extreme environments, and highlights the biofilm studies performed on *B. subtilis* and *B. thuringiensis* adapting to different environments. Lastly, **Chapter 5** includes the final remarks and perspectives, and **0** includes the full-length research articles included in this Ph.D. thesis.

The next chapter will focus on Experimental Evolution.

Chapter 2 Experimental evolution

When Darwin developed his theory of natural selection, he believed that evolution was too slow to be studied directly and that could only be studied indirectly by comparing living species and/or fossils[26]. However, it has been shown that evolutionary changes can occur within shorter timeframes for many organisms, especially for microorganisms. Experimental evolution has transformed evolutionary biology from a historical science in which unseen processes are inferred from evolutionary end points to one that can examine evolution in real time, it has provided great understanding of phenotypic evolution and the genetic evolutionary landscapes underlying it.

Experimental evolution is the study of evolutionary processes occurring in experimental populations in response to certain conditions. It has been used to address diverse questions in a wide range of areas of evolutionary biology[27], including understanding how populations adapt to particular environmental conditions[28,29], studying evolutionary trade-offs and constraints[30], estimating population genetic parameters[31,32], testing evolutionary theories[33], and in medicine and technology studies such as vaccine screening[34] and biocatalysts and biocontrol agents production[35].

2.1 Experimental evolution in microorganisms

Perhaps the first experimental evolution was performed by William Dallinger, a contemporary of Darwin, in which protozoa was shown to be selected over time to grow at extreme temperatures far exceeding the thermal range of their ancestors[36]. However, microbial experimental evolution was not widely used until Richard Lenski and colleagues published their research on the long-term adaptation of the bacterium *Escherichia coli* in the early 1990s[37].

Several characteristics of microorganisms make them ideal models for setting up evolution experiments in diverse research[26]. Firstly, they are small and divide quickly, and can be propagated easily in simple growing conditions in large and highly replicated populations, allowing us to observe bacterial adaptation to specific environments within days or months. In addition, the ability to preserve populations samples cryogenically indefinitely from intermediate time points, providing researcher a 'living fossil record' for further analysis[37]. Moreover, microorganisms' small and well understood genomes, allowing both genetic manipulation and underlying causes of evolution are much more feasible. Furthermore, new analysis can be made as soon as new or better techniques emerged, one example is the continuously decreasing sequencing costs enable single evolved isolates as well as population samples to be sequenced deeply, allowing an understanding of the genetic basis of adaptation as well as the genetic diversity and its dynamics[38], respectively. Based on the archived evolving populations samples at periodic time points from six experimental evolutions studies[22–25,39], I performed whole-population genome sequencing to study genetic evolutionary landscapes of these populations, these "living fossils" make the foundation of this Ph.D. thesis.

Plenty of evolutionary studies have been performed on planktonic forms of bacteria and yeasts, under diverse environmental conditions[37,40–45]. The most famous example is the Long-Term Evolution Experiment (LTEE) conducted by Richard Lenski and collaborators with *E. coli* began in 1988 and have recently reaching 75,000 generations[46], with its 12 populations in media by batch culture. The bacterial cultures were grown in minimal medium with low levels of glucose as the sole accessible carbon source, then 1% of the overnight cultures were transferred to fresh medium initiating a new cycle of overnight batch growth. Numerous insights have been gained through the LTEE into evolutionary dynamics over short and long timescales, such as the dynamics of adaptation and divergence[37,47], parallelism from morphological [47] to genetic levels[40,48], forces maintaining diversity[49], evolvability[37], clonal interference and frequency-dependent interactions[50] and the effects of insertion sequence mediated mutations on evolvability[51]. Notably, it also inspired the conduction of later LTEE experiments in batch cultures[52,53].

2.2 Experimental evolution in biofilm populations

Contrast to evolutionary studies widely been performed on planktonic forms, only a relatively limited number of evolution experiments have been performed with biofilm populations[54–59]. Biofilm formation is a specifically complex process that strongly depends on environmental and experimental factors, which can influence the matrix composition and structure of the biofilm. With biofilms, the diffusion of molecules is limited, which enables the establishment of gradients, and eventual exhibit considerable structural, chemical and biological heterogeneity[60]. Biofilm evolutionary studies have provided many important insights into biofilms, several biofilm models have been used for experimental evolution. The experimental setup employed to study biofilms then can significant impact what one finds. The study of biofilms faces a strong tension between simplicity and complexity.

2.2.1 Static models

The simplest static model, used in one of the first evolution experiments in biofilms, uses glass tubes culturing *Pseudomonas fluorescens* under static condition[61]. Driven by spatially structured environments and the resulting physicochemical gradients, the bacteria rapidly diversified into three distinct colony morphotypes that exploited distinct niches. Therefore, this model is useful for studying factors driving the formation of biofilms, as well as further diversification within biofilms. Over the last two decades, this model of adaptive radiation has been applied for many studies of evolution, ecology, and genetics on this topic[62–64].

Another simple static model, colonies growth on a solid growth medium is used. Under this situation, as gradients are present, mutation rates increase in older colonies, and a spatially structured environment is formed[65]. This model was widely used in mutation accumulation experiments[48,66], in which mutations are allowed to drift to fixation in inbred lines and allow one to estimate the intrinsic rates and the effects of new mutations. This model was used in **Study 4** to study the bacterial-fungal interactions and how bacteria evolve in the presence of fungal partner on agar surface. This model of interaction between *B. subtilis* and *Aspergillus niger* is described in detail in **Chapter 3**.

One static air-medium floating biofilm transfer mode, which was employed to *B. subtilis* recently[22]. *B. subtilis* diversified into four distinct colony variants that dramatically differed in biofilm formation abilities and expression of biofilm-related genes. This study is described in detail in **Chapter 3**.

2.2.2 Bead transfer model

Similar to the LTEE, in 2011, Poltak and Cooper devised an innovative model to study biofilm evolution by transferring biofilm-associated cells that adhered to a plastic bead floating in a test tube in gentle rotating condition[55]. This model includes one bacterium, *Burkholderia cenocepacia*, which forms biofilms on the polystyrene beads floating in a gently shaking tubes. Each day, a new bead was colonized and a new biofilm was formed, selecting for a regular cycle of colonization and dispersal. In this way, only bacteria capable of attaching to and dispersing from the beads can attach to the new beads and evolve forward. Since the first report of the model, multiple follow-up studies have confirmed the model's resilience in different research aspects including mutational patterns[57], niche complementarity effect[67], and antibiotic resistance[68,69].

negative frequency-dependent[70], biodiversity arises and maintenance[59], and parallel adaptation across environments[71].

Adaptation and phenotypic diversification of *B. thuringiensis* biofilm was studied using the beads transfer model[23]. In this study, all evolved lineages displayed significantly enhanced biofilm production accompanied by the appearance of a *B. thuringiensis* fuzzy spreader (FS) colony morphotype variant. And the importance of insertion sequences of *B. thuringiensis* for its adaptation to the plastic bead-attached biofilm environment was revealed. The genetic dynamic landscape is investigated in **Study 2.**

2.2.3 Plant colonization models

Plant growth-promoting rhizobacteria are known to benefit plants by stimulating their growth or protecting them against phytopathogens. Rhizobacteria must colonize and persist on plant roots effectively to exert their benefits. In a gnotobiotic system with carbon-free silver sand, *Pseudomonas protegens* was inoculated on Arabidopsis roots grown within several plant growth cycles. Detailed genome analysis of the evolved derivatives was performed to identify the genes that explained *P. protegens* adaptation to Arabidopsis rhizosphere[58] and to understand how *P. protegens* rapidly evolve along the parasitism-mutualism continuum.

Another plant colonization models, inspired by the beads transfer model, how two *Bacilli* adapting to *A. thaliana* and/or tomato roots were studied in (static) hydroponic setups[24,25,39]. These hydroponic setups are described in detail in **Chapter 3**, and the genetic mechanism under these adaptations were investigated in **Study 1, Study 2 and Study 3**.

2.2.4 In vivo models

In vivo evolution models have mainly focused on human pathogens, like *Streptococcus pneumoniae* and *Pseudomonas aeruginosa*. Cooper and collaborators reported a model in which replicate experimentally evolved populations of *S. pneumoniae* propagated by repeated murine nasal colonization with the aim of identifying gene products under strong selection as well as the population genetic dynamics of infection cycles[54]. These studies indicate that biofilm experimental evolution can be applied to a more widely area to help resolving health-relevant issues.

2.3 Sequencing based approaches used in experimental evolution

Not a single genome of bacterium had been sequenced when the LTEE was launched, it was unaffordable for many years for whole genome sequencing, let alone whole-population genome sequencing for this project[72]. Since the launch of Human Genome Project, during the past decades, the sequencing cost has reduced drastically. Combine with the new developed bioinformatic tools, the genome sequencing has revolutionized studies using experimental evolution of microbes because it readily provides comprehensive insight into the genetic bases of adaptation[38]. In addition, many newer technologies will become more readily accessible for microbiology and experimental evolution research, like long-reads sequencing, single-cell sequencing[73–75] and spatial in situ transcriptome sequencing[76,77].

2.3.1 Isolates sequencing

To sequence the complete genome sequence of individual evolved isolates to understand evolution is the most straightforward use of genome sequencing technology. Genome sequencing provides the mutation number, type, and targets, and it clearly reveals that these mutations are linked together as a specific genotype. By sequencing isolates from 120 separate populations of *E. coli* evolved to grow at 42.2°C, a set of primary functional targets of high temperature were detected, and pervasive presence of epistasis among beneficial mutations were inferred, which shaped adaptive trajectories into at least two distinct pathways[78]. These results revealed that multiple distinct evolutionary trajectories were possible. When sequencing many isolates from

multiple timepoints in a single population or several populations, it becomes possible to study clonal dynamics and parallelism evolutions of these populations[48,50]. By sequencing 264 complete genomes from 12 *E. coli* populations from LTEE, their dynamics over 50,000 generations were characterized[48]. Results also showed that with the population retained the ancestral mutation rate, most fixed mutations are beneficial, and most mutations that reached high frequency were favored by selection.

The short reads of next generation sequencing were thought often fail to detect structural variants[79]. By the nanopore long reads sequencing, numerous genome rearrangements in the evolved isolates were revealed in an experimental evolution study which *B. thuringiensis* biofilm repeatedly evolved on plastic beads[23]. Also, the parallel distribution of these insertion sequence mediated mutations revealed these mutations possibly promoted the evolutionary adaptation of *B. thuringiensis* biofilm on abiotic surface[23].

2.3.2 Metagenomic sequencing of populations

In 2010, the first human gut microbial gene catalogue was established by metagenomic sequencing, which revealed the substantial diversity of the gut microbiome between healthy individuals[80]. This study showed that short-read metagenomic sequencing can be used for global characterization of the genetic potential of ecologically complex environments. Since then, metagenomic sequencing has become increasingly used by sequencing the total genomic DNA of evolving populations to examine their genetic diversity across time points and/or replicates.

As the sequencing cost decreases and the new analysis pipelines applied in the evolution experiment, the study of genetic diversity and dynamic has matured greatly[40]. By using population metagenome sequencing, the allele detecting sensitivity depends on the sequencing depth of coverage and allele abundance, with the increased sequencing quality and improved analysis methods, the alleles that rise to multiple percent of the population can be confidently identified. Another challenge is that these data lack linkage information between the detected variants, and thus we don't know directly which alleles are present on the same genetic background. With the additional information, such as the correlation between time points in an evolution experiment, and new developed pipeline, it is possible to infer the predict genotypes and lineages over time within populations across time points[69], this new pipeline is described in detail in **2.3.3**.

By sequencing 1,431 mixed-population samples taken at 500-generation intervals across 60,000 generations of evolution in each of the twelve LTEE populations, a complex adaptive process with clonal interference, genetic drift, and eco-evolutionary feedback playing important roles was revealed[40]. In addition, the targets of selection shift over time, and the long-term adaptation to a fixed environment can be characterized by a rich and dynamic set of population genetic processes.

During the LTEE, insertion sequences mediated mutations were detected in all 12 populations[51]. While the long-term dynamics of IS elements and their effects on bacteria are poorly understood, by using the genomic and metagenomic data from two studies[40,48], their effects on *E. coli* long-term adaptation were studied. Data showed that insertions of IS elements can result in both gene inactivation and activation or alter the expression of neighboring

genes. In addition, IS-mediated changes have been described to both promote and constrain evolvability of *E. coli* in LTEE [51].

Notably, in **Study 2**, by using the same mutation calling analysis pipeline[51], we were successful to detect fourteen IS mediated mutations in eight out of nine lineages in *B. thuringiensis* 407 population samples, which is consistent with the mutations detected by nanopore long reads sequencing[23]. The detailed result is described in **3.1.2**. The mutation calling analysis pipeline used here is described in detail in **2.3.3**.

2.3.3 Two useful bioinformatic tools in experimental evolution

(1) Mutation calling using *breseq* from NGS short read

Comprehensively determining genetic variation is pivotal for understanding the rate and character of genome evolution in laboratory experiments[81], which include single-nucleotide variation (SNV), short insertion or deletion (indel) variation and structural variation (SV). The SV were thought difficult to be detected using reads from next generation sequencing[79].

breseq is an open-source computational pipeline which can identify and annotate genetic differences detected in whole-genome and whole-population NGS data from haploid microbes where a high-quality reference genome is available[82]. In contrast to workflows developed for analyzing mainly human genomes, *breseq* has been optimized for haploid microbial-sized genomes (<20 Mb), which can detect not only SNV and indel, but also can detect SV[83]. Additionally, the *breseq* pipeline produces output in an annotated html format that is accessible to non-experts. We used this pipeline to call SNV, indel and SV mutations in all population samples in all **Studies**.

(2) Mutational trajectories within and/or across different lineages

For better understand of genealogical structure of each lineage and visualize changes in genotype frequencies, Mullor plots were frequently used in many experimental studies[44,50,57,84]. Muller plots are an intuitive visualization of phylogenetic trees to display the frequency of genotypes over time. Compare the tedious steps of other plot method, Cooper and colleagues developed the ***lolipop*** software package (https://github .com/cdeitrick/lolipop) that identifies linked genotypes and ancestry from shared mutation trajectories over time[69]. The inferred results then were displayed as a Muller diagram that integrate both frequency and ancestry, a lineage frequency plots, and a genetic pedigree for each lineage analyzed. To summarize, these tools predict genotypes based on shared trajectories of mutations over time and test their probability of nonrandom genetic linkage. Muller plots can be manually colored to highlight parallelism genotypes or certain mutation you want. We performed genotype and genealogy analysis in **Study 2, Study 3, and Study 4** to compare the genotype diversity between different evolved conditions, and we repeatedly observed reveal the clonal interference, hitchhiking, parallel evolution and evolution trade-off in these experimental setups.

In **Study 2**, we revived the archived population samples from our four previous experimental evolution studies[22–24,39] and performed longitudinal whole-population genome sequencing, to understand the differences and similarities of the dynamic evolutionary landscapes of two model species from the *Bacillus* genus as they adapt to abiotic and biotic surfaces. The mutation spectrum, mutation tread, *dN/dS* ratio and genotype diversity of each lineage in each different condition were determined and compared (**Fig. 1**). In total, higher genetic diversity in biotic conditions was possibly due to potentially increased spatial niche heterogeneity and nutritional source difference created

by the plant host. In addition, there were more fixed mutations in biotic conditions in both species, and extremely more fixed cases were found in Bth_root which possibly related with the small population size. The *dN/dS* ratio is slightly higher in *B. thuringiensis* and we only detected IS mediated mutations in *B. thuringiensis*.

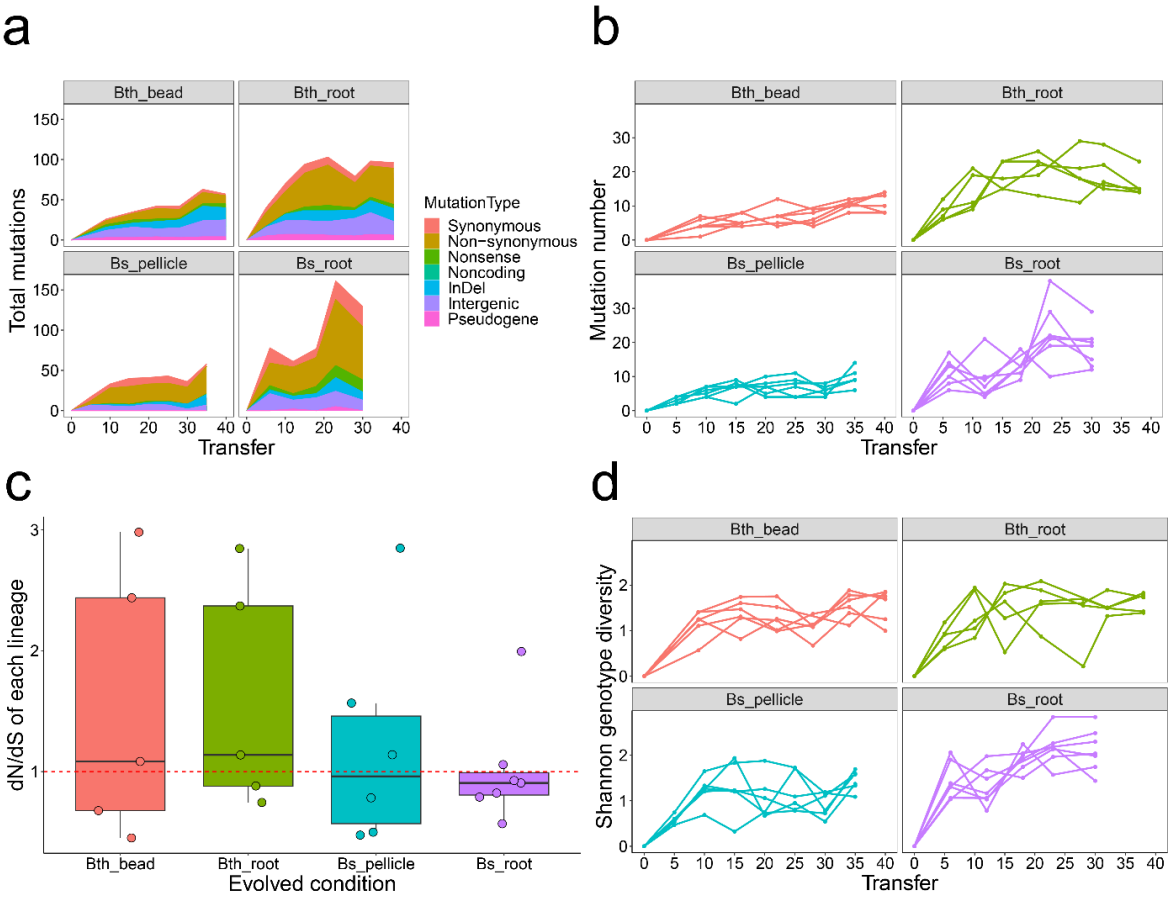

Fig. 1 Mutation spectrum, dynamics and diversity. a, Distribution of detected mutations of each type in four adaptation models over time. Shaded bars show the distribution of different mutation types in each time point or total. **b**, Dynamic distribution of detected mutations in each lineage over time. **c**, *dN/dS* ratio. The ratio of nonsynonymous to synonymous mutations (*dN/dS*) in the entire pool of detected mutations of each condition, this ratio is normalized by the relative number of synonymous and nonsynonymous sites of *B. thuringiensis* and *B. subtilis*, respectively. Boxes indicate Q1–Q3, lines indicate the median, black circles filling with different color indicate the ratio of each lineage. **d**, Genotype diversity**.** Dynamic distribution of genotype alpha diversity in each population of four adaptation models over time calculated using Shannon method. Genotypes and

frequencies were generated by *Lolipop* software package in Genotype and genealogy analysis. Figure from **Study 2**.

Then, we utilized the *Lolipop* to infer the genealogical structure of each lineage and visualize changes in lineage frequencies from shared, nested mutation trajectories over time. We observed frequency of clonal interference, which was stronger in biotic surface environments (**Fig. 2**). Additionally, nested fixations in some of the lineages were observed.

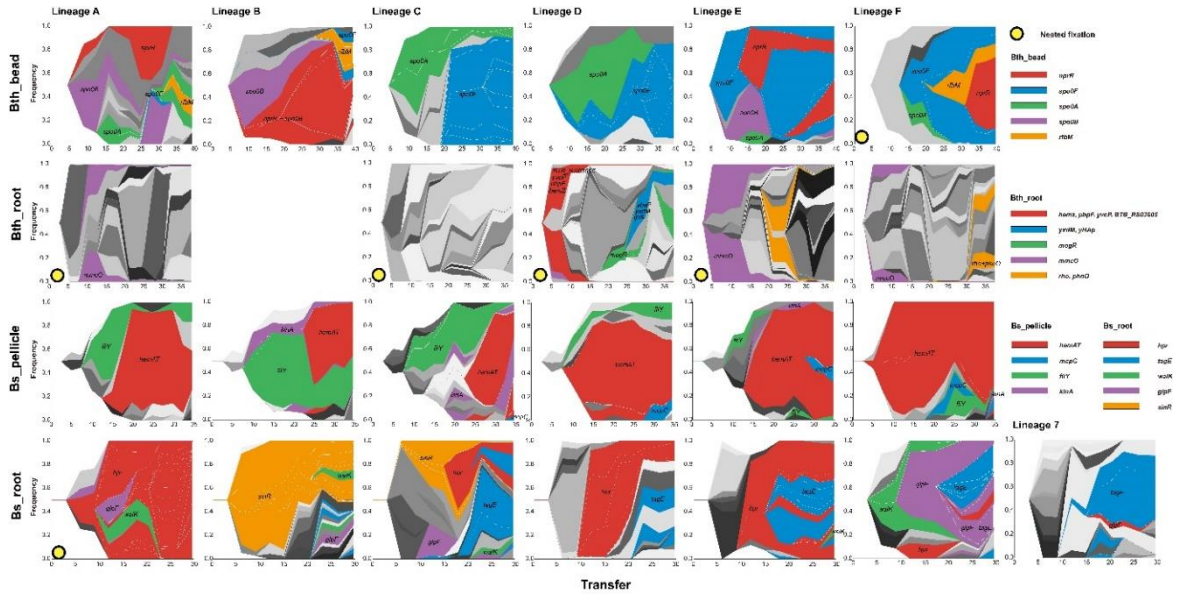

Fig. 2 Genealogy and genotype frequencies over time. Each shade or color represents a different genotype and vertical area corresponds to genotype frequency, inferred by Lolipop. Dominant genotypes that contain the high frequency mutated genes, which are shared in different populations, are highlighted in certain colors within each adaptation model. The nested genotypes of the dominant genotype are highlighted with the same color in in Bth_bead, Bs_pellicle, and Bs_root, except for the nested genotypes which also belong to the dominant genotypes. In Bth_root, for the complex combination of mutations among different lineages and early fix of new mutations, nested genotypes are not highlighted. Other genotypes are in gray. Figure from **Study 2**.

2.4 Genetic mechanisms in adaptive evolution

As mentioned above, technological advances in DNA sequencing have now made it affordable to determine genetic changes between ancestral and derived organisms on whole-genome and whole-population sequencing scale for any species. This enables scientists to reveal the underlying genetic mechanism of fitness improvement and phenotype diversification in evolution experiments, as well as the repeatability of evolution.

2.4.1 Clonal interference

Most evolution experiments are performed under conditions with sufficiently high mutation rates in sufficiently large populations for multiple mutations to be present simultaneously[85]. In the absence of recombination, the chances that several beneficial mutations occur in the same background at the same time are small, and most mutations likely occur in different individuals. This means any one of these mutations to sweep to fixation in the population is slowed because it must displace fitter competitors rather than only its ancestor[86]. This effect is called **clonal interference**, the competition between lineages arising from different beneficial mutations in an asexually reproducing population[87].

Clonal interference is ubiquitous in evolution experiments, observed by either NGS [44,50,59], or marker divergence studies[88,89], clearly affecting the dynamics of evolution. It is generally expected that a genotype with one or a combination of several beneficial mutations whose combined fitness is superior, may outcompete the other, less fit genotypes. However, the fate of such a genotype becomes uncertain by clonal interference, as potential new beneficial mutations can arise in a different background. Clonal interference

can increase genetic diversity in different ways[50], nonetheless, the diversity-promoting effects of clonal interference are only transient because eventually one genotype or another will prevail.

In **Study 2**, we frequently observed clonal interference in all experimentally evolving lineages (**Fig. 2**). Numerous mutations or groups of mutations rose to high frequency and then fall to extinction, while outcompeted by another group, and therefore many distinct mutations existed at a very low frequency (below 5%) during the earlier period of experiment and then rose to high frequency in the later period. The clonal interference was obviously much stronger in biotic surface environments than that in abiotic surface: we observed more mutations or genotypes appear and disappear in biotic surface environments, which is consistent with the mutation spectrum and genotype dynamic (**Fig. 1**).

2.4.2 Hitchhiking

Genetic dynamics become even more complex when considering that neutral and deleterious mutations continually occur alongside the beneficial mutations. In **Study 2 (Fig. 2)**, We observed nested fixations in three lineages of Bth_root, where beneficial mutation or mutations cohorts fix sequentially in the background of the previous fixed mutation(s)[50]. However, it is very unlikely that these mutations occurred simultaneously when considering the typical mutation rates in bacteria. One possible explanation is that the beneficial mutation(s) occurs in a background that already has a certain set of neutral or deleterious mutations, and therefore the **hitchhiker** and beneficial driver mutations fix at the same time[44]. We found this possible phenomenon frequently in Bth_root, in lineage D, the *ywdH*: T186T mutation is possibly a

neutral mutation as a background and the later beneficial co-drivers occurred sequentially and led the genotype contains the cohort to fix.

Genetic hitchhiking is the process by which a neutral or slightly deleterious mutation increases in frequency due to physically linkage to (a) beneficial mutation(s); can also refer to a weakly beneficial mutation increasing in frequency due to linkage to a more strongly beneficial one[90]. Clonal interference and hitchhiking are of widespread importance in determining the molecular dynamics of adaptation. The patterns of sequence evolution are driven by a balance between these chance effects of clonal interference and hitchhiking, resulting in increased stochastic variation in evolutionary outcomes and the deterministic action of selection on individual mutations, which favors **parallel evolutionary** solutions in replicate populations[44].

2.4.3 Parallel evolution

Genetic parallelism refers to the repeated evolution of the same phenotype or genotype in evolutionarily independent populations[91], which provides evidence for adaptation[81] and could help distinguish causal mutations from irrelevant ones. The replicated independent evolution of similar phenotypes or genotypes leads us to infer that evolution was driven natural selection[92]. Parallelism may occur at levels of biological organization from phenotypic, functional pathways, genes, and even to individual nucleotide[26,40,93], with a pattern that parallelism decreases, and the observed diversity increases. Several population genetic factors can affect evolutionary trajectories and degree of parallelism. Studies showed that differences in population sizes between populations exposed to similar conditions can affect the degree of

parallelism[44,91,94,95]. Additionally, selection environment differences also affect the degree of genetic parallelism, showed that similar environments led to higher levels of genetic parallelism[71] and significantly higher in a spatially structured, multiresource environment[93].

In **Study 3**, we identified repeated changes across multiple levels of biological organization from phenotypic, functional pathways, genes (**Fig. 3**), and even to individual nucleotide[93], and the degree of parallel evolution was significantly higher in the *B. subtilis* populations evolved in a heterogeneous, multi-resource spatially structured environment. Based on KEGG pathway analysis of the mutated genes, we found that bacterial motility proteins, genetic information processing and metabolism related genes were mutated more frequently and reached high frequencies, and bacterial motility proteins were the most selected in our experiment (**Fig. 3**).

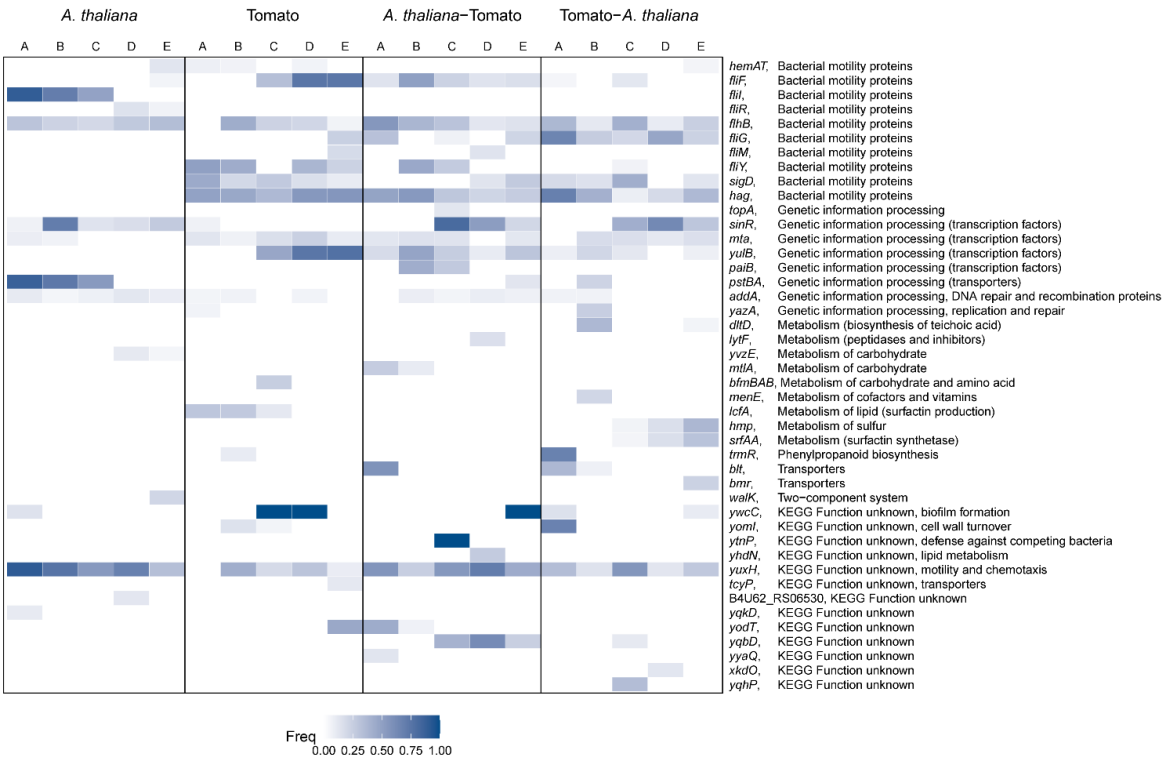

Fig. 3 Genes with mutation frequency > 10%. Each column represents one replicate lineage. Color indicates the highest frequency of mutations in that gene in that lineage. Figure from **Study 3**.

2.4.4 Trade-off

Many evolution experiments keep conditions constant, and it was widely used in studying evolutionary trade-offs[30,39,54,71,96,97]. Adaption to new conditions is often believed to acquiring a certain beneficial trait but show trade-offs in other, novel environments, also called the 'cost of adaptation'[26]. These trade-offs likely also contributed to the evolution of diversity in nature, which has been shown to occur in almost every important microbial characteristic[98], including bacterial biofilm formation, metabolism, motility, virulence, evolvability, DNA repair and resistance (**Fig. 4**). These traits are subject to constraints imposed by trade-offs, so adaptations that improve one trait may be at the cost of another.

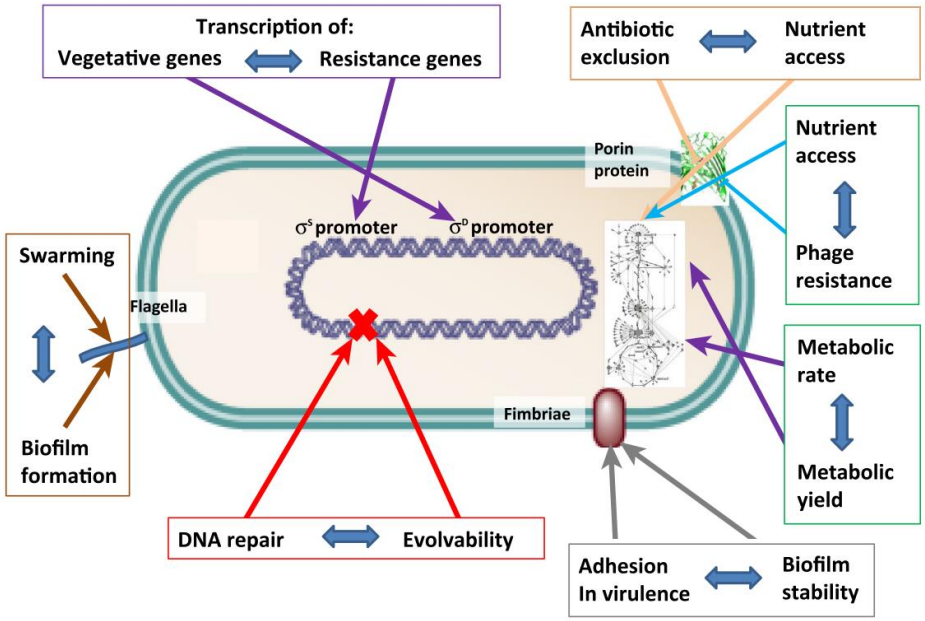

Fig. 4 Many prominent bacterial characteristics display **trade-off** to other traits in bacteria, in which an increase in one trait is accompanied by reduction in another. Image from reference[98].

These trade-offs can be caused by the mutation accumulation, in which the effects of these mutations are neutral in the selective environment, while becoming deleterious in newly encountered situations. Alternatively, trade-offs can result from antagonistic pleiotropy, also called adaptive trade-offs, in which the same mutation is beneficial under one condition while becoming maladaptive under another[99]. The latter could be caused by the selection between two mutual exclusiveness mechanisms, where they display negative correlation to each other. For example, the improved phosphate assimilation in *E. coli* was observed with reduced incorporation of carbon by shifting metabolic pathways after growth in low concentrations of inorganic phosphate (Pi) for 30 days[100].

In **Study 1**, we observed enhanced biofilm formation and impaired motility of isolates from populations 6 and 7, and detected mutations that involved in biofilm formation and motility (**Fig. 5**). Motility and biofilm formation are considered to be inversely regulated lifestyles with bacteria expressing genes necessary for either motility or biofilm matrix production but not both simultaneously [101,102]. We suggested that a **trade-off** between motility and biofilm development existed in this setup. Similar to **Study 1**, the evolved isolates from Bs_root_A and Bs_root_T exhibited either delayed, reduced or even impaired swarming abilities in **Study 3** (**Fig. 6**). As mentioned in **2.4.3**, bacterial motility proteins were the most selected in **Study 3** (**Fig. 3**), and all mutations in flagellar structure protein coding genes were nonsynonymous SNPs or InDels, suggesting these mutations to cause loss-of-function of flagella. Additionally, widespread and high frequency mutations in *sinR*, which encoding biofilm master regulator[103], *sigD*, encoding sigma factor D[104–106], which regulates flagella, motility, chemotaxis and autolysis of *B. subtilis*, *yuxH*, which is involved in c-di-GMP regulation in *B. subtilis*[107,108], and *pstBA*, which responsible for phosphate uptake under nutrient stress in *B. subtilis*[109], were all

predicted to regulate the motility-biofilm balance in *B. subtilis*. Revealed mutation in motility and biofilm genes help to reveal the underlying mechanisms behind the phenotypic observations in altered motility and biofilm development.

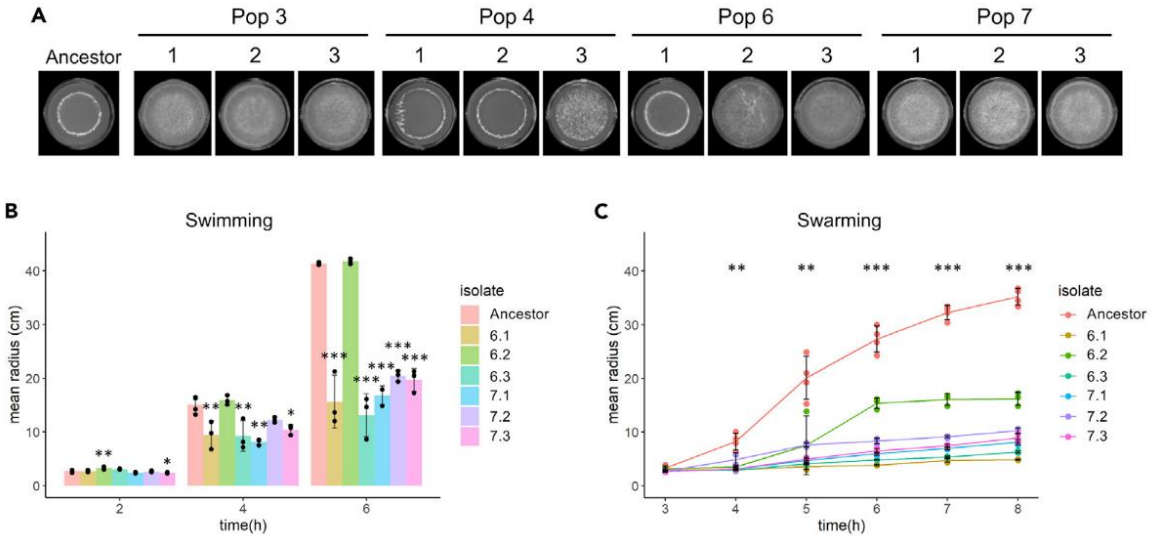

Fig. 5 Evolved isolates from T30 show altered pellicle biofilm formation in response to plant polysaccharides and impaired motility (**A**) Ancestor and evolved isolates from transfer 30 were inoculated into LB + 0.5% xylan at a starting OD_{600} of 0.05 in 24-well plates. Images were acquired after 48 h incubation at 30 °C using a stereomicroscope. Each image is representative of four replicates. Each well has 16 mm width. Evolved isolates were tested for swimming (**B**) and swarming (**C**) motility in LB medium supplemented with 0.3 or 0.7% agar, respectively.

(B) Bars represent the mean (N = 3-4) and error bars represent SD.

(C) Lines represent the mean (N = 2-4) and error bars the SD. For the motility assays, the following statistical analysis applies: For each time point, an ANOVA was performed on the log10-transformed data followed by a Dunnett's Multiple Comparison test with the ancestor as the control. For swarming motility, the asterisks show the least significance observed for the given time point. At 3 h, only isolate 7.3 was significantly reduced in swarming motility. *p < 0.05, **p < 0.01, ***p < 0.001. Figure from **Study 1**[39].

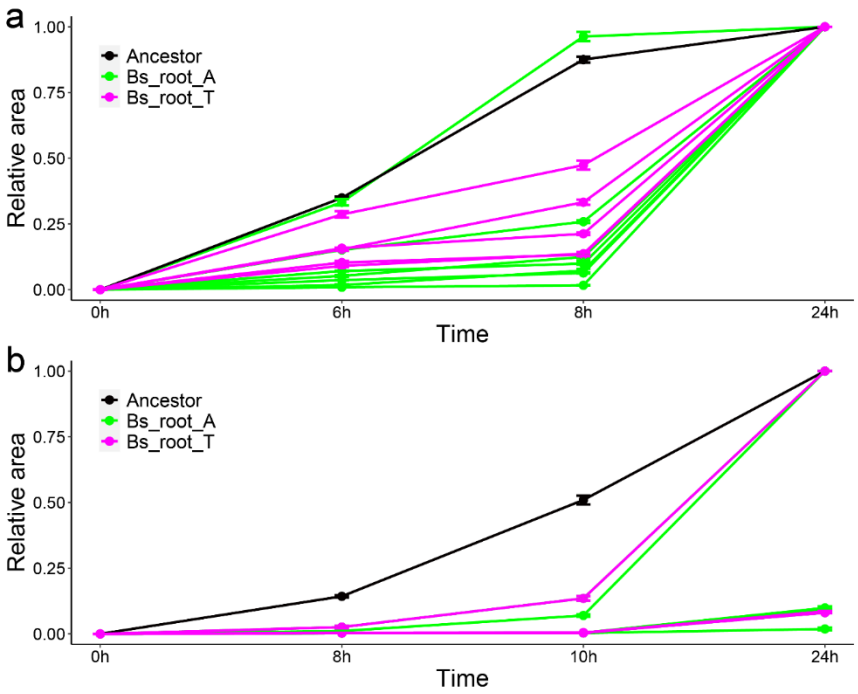

Fig. 6 Evolved isolates showed impaired motility. Swimming (**a**) and Swarming (**b**) motility of evolved isolates from Bs_root_A (green, 7 isolates) and Bs_root_T (magenta, 5 isolates) in comparison to the ancestor (Black). Notably, swarming motility of several isolates are similar and low, thus indistinguishable from each other in panel b. Data represent mean and error bars represent standard error, each isolate repeated for 3 times, the ancestor repeated for 9 times. Tested isolates include two SN from lineage A and E of Bs_root_A, two SM from lineage A and E of Bs_root_A, three WR from lineage A, D and E of Bs_root_A, and five WR from lineage A (1), B (2) and C (2) of Bs_root_T, respectively. Figure from **Study 3.**

Chapter 3 The genus *Bacillus* and biofilm formation

3.1 Genus of *Bacillus*

The genus *Bacillus* was described the first time by Ferdinand Cohn in 1872[110,111], is a phenotypically large, heterogeneous group of Gram-positive, rod shaped, aerobic or facultatively anaerobic and endospore-forming bacteria of the family *Bacillaceae* within the phylum Firmicutes.

For many decades, members of the *Bacillus* genus were classified as soil-dwelling organisms due to their endospores being isolated frequently from this environment[112]. However, these species are found to be ubiquitous and widespread in various habitats besides soil and rhizosphere, such as gastrointestinal track of humans and animals, hot spring, and water sediments[113–116].

One well known feature of *Bacillus* genus is their ability to form endospores, and the endospores of *Bacillus* could be isolated from places with pH = 2 or temperatures over 80 °C[117]. These species can form metabolically dormant endospores, which are highly resistant to many physical and chemical stresses, capable of surviving extremes of temperature, nutrient limitations, desiccation and ionizing radiation[118]. In response to environmental changes, especially nutrient limitations, the spore formation process was triggered in vegetative cells[119]. Endospores formation was initiated from an asymmetric cell division, resulting in the formation of a smaller cell, the forespore, and a larger cell, the mother cell, followed by engulfment of the forespore by the mother cell and the final release of the matured spore occur due to programmed cell lysis of the mother cell[119]. The spores can remain dormant for years until

favorable conditions reoccur by sensing with receptors germinants, such as the presence of amino acids, sugars, purine nucleotides or inorganic salts, which the spores can germinate and return to active growth[120].

Another well-studied characteristic of many *Bacillus* spp. is their ability to form biofilm. Biofilms are ubiquitous multicellular communities held together by a self-produced extracellular matrix[121]. Biofilm formation and its regulation is described more in detail in **3.2**.

The genus *Bacillus* constitutes a plethora of species and subspecies that have medical, environmental, and industrial applications[116]. At the time of writing, there are 228 species who have whole genome sequence in genus *Bacillus*, thereby representing it as one of the most studied and explored bacterial genera (https://www.ncbi.nlm.nih.gov/genome/?term=bacillus). To further clarify classification of *Bacillus* species, Gupta et al. (2020) performed a comprehensive phylogenomic and comparative analyses using 303 *Bacillus/Bacillaceae* genomes[122]. Based on their analysis, they assigned the *Bacillus* species to 17 novel distinct clades. Of them, the *Bacillus subtilis* group and *Bacillus cereus* group are the most intensely studied *Bacillus* species.

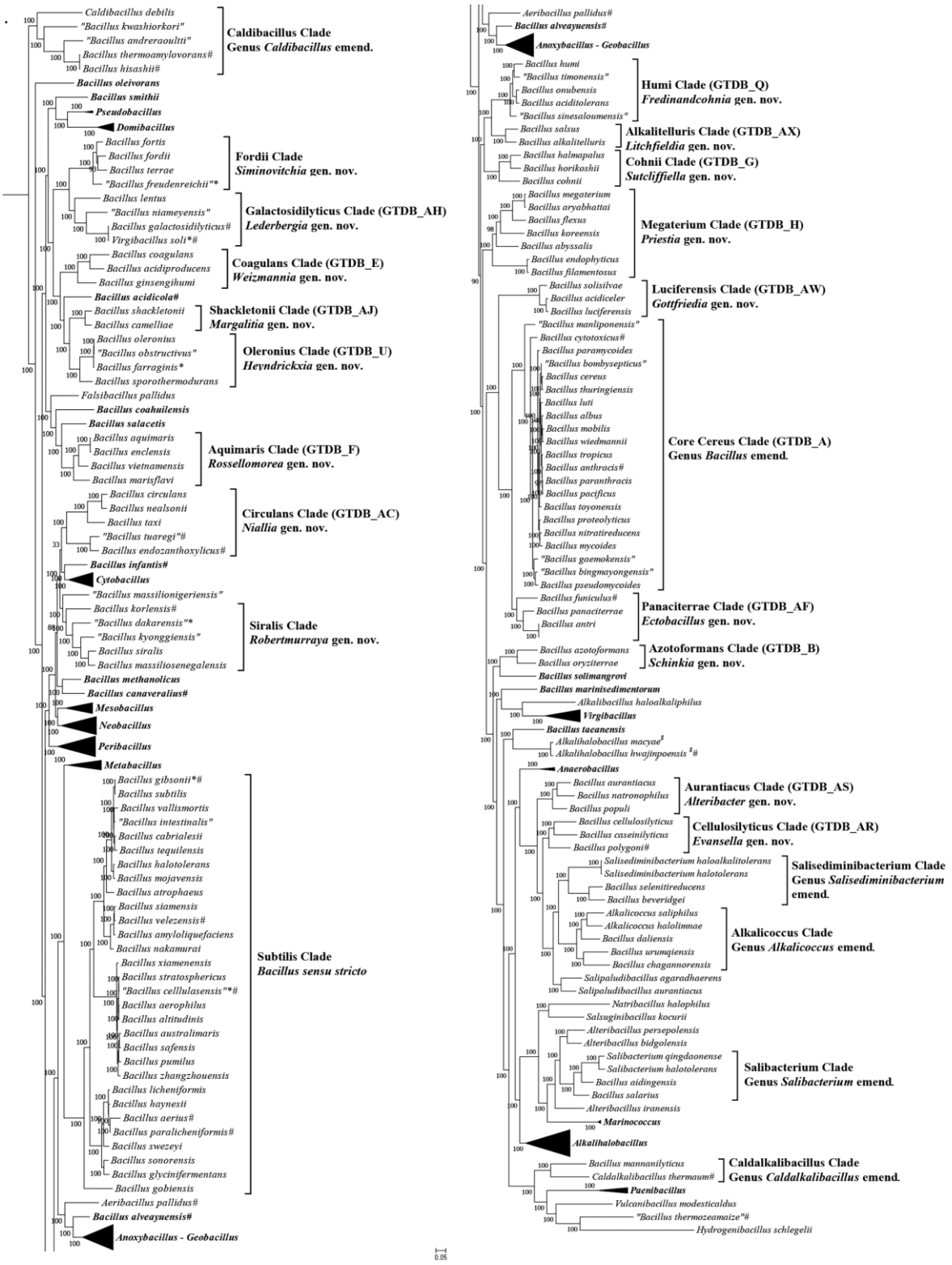

Fig. 7 A maximum- likelihood phylogenetic tree for 303 genome-sequenced *Bacillaceae* species including all named Bacillus species and species from related genera based on concatenated sequences for 650 core proteins for these genomes. Image from reference[122].

3.1.1 The *Bacillus subtilis* group

During the last seven decades, the members of the *B. subtilis* group have been widely applied in both food processes and crop protection industries. The *B. subtilis* group has four original species, including *B. subtilis*, *B. licheniformis*, *B. pumilus*, and *B. amyloliquefaciens*[123], which were discovered more than 40 years ago[124]. Since then, the evolution of their molecular, chemotaxonomic, and physiological characterizations was intensely studied. As new molecular methods and sequencing technologies are widely used, many novel species and subspecies have been described and assigned to this group. The current taxonomy of the *B. subtilis* group is presented in **Fig. 8**.

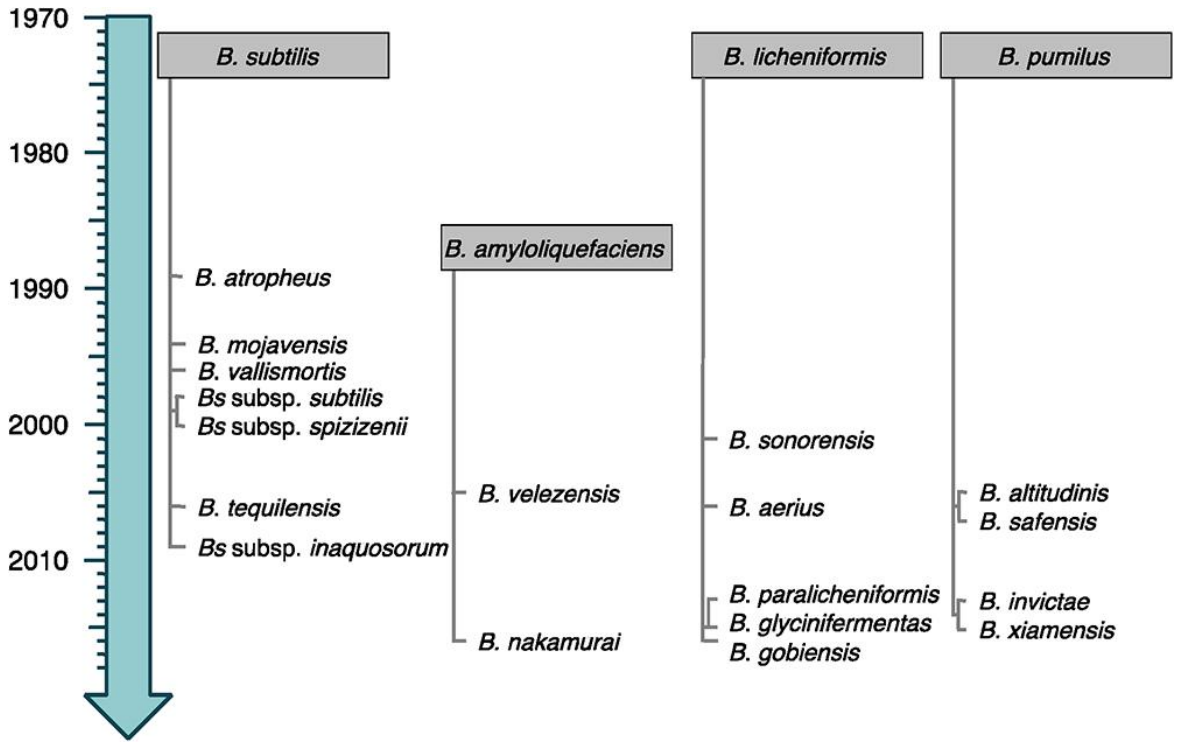

Fig. 8 Timeline emergence of the species from the *B. subtilis* group. The species are classified following their relatedness to the closest original member of the group (gray boxes). Heterotypic synonyms are not shown. Image from reference[124].

Due to its nature competence for uptake extracellular DNA and their rapid growth as dispersed cells, *B. subtilis* is the most studied species in the genus *Bacillus*. During the past decades, strains of this species were used as a model microorganism for studying cell division, protein secretion, bacterial motility, biofilm development, bacterial-plant interactions, or bacterial-fungal interactions, secondary metabolite production, and so on[125].

Wild type strain *B. subtilis* NCIB 3610 and the domesticated strain *B. subtilis* 168 are the most used frequently used in laboratory and industrial workhorse. The strain used in this study is DK1042 strain, which is a derivate of the wild strain NCIB 3610[126], originally isolated from hay infusion.

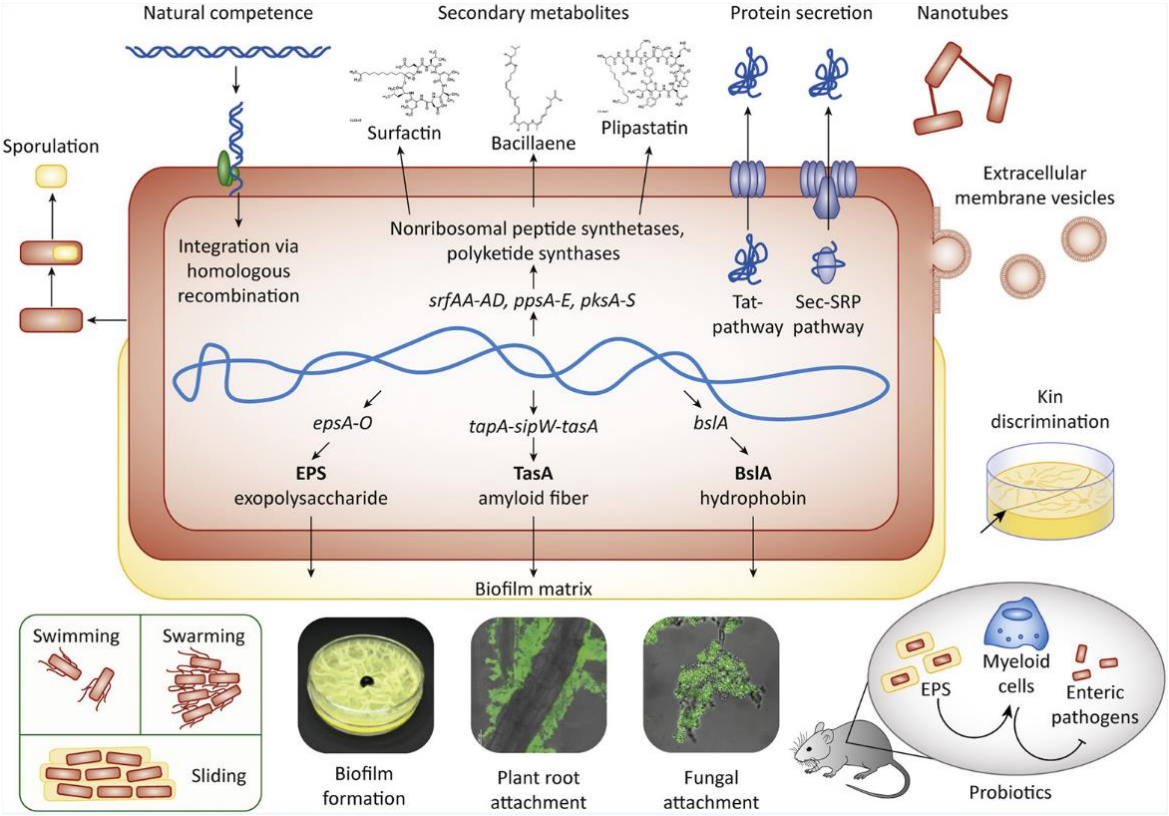

Fig. 9 *B. subtilis* as a model microorganism. Image from reference[125].

3.1.2 The *Bacillus cereus* group

The *Bacillus cereus* group includes at least eight closely related species: *B. cereus*, *B. thuringiensis* and *B. anthracis* as well as *B. mycoides*, *B. pseudomycoides*, *B. weihenstephanensis*, *B. cytotoxicus*, and *B. toyonensis*[127]. *B. anthracis*, *B. cereus* and *B. thuringiensis* are the most well-studied member of the group for their pathogenic potential, their genetics have therefore been thoroughly studied. *B. anthracis* was initially characterized by Koch and Pasteur as the etiologic agent of anthrax. It produces the toxin anthrax and capsule, which can induce a vascular shock and cause the death of the host at high concentrations[128]. *B. cereus* strains are commonly recognized as food poisoning agents, causing diarrhea and emesis due to the production of enterotoxins and the depsipetide toxin cereulide[129], which can also cause localized wound and eye infections as well as systemic disease[130]. *B. thuringiensis* was originally isolated in 1901 from infected silkworm larvae (*Bombyx mori*), which can cause the sotto disease (sudden-collapse disease), a lethal infection of silkworm[130]. *B. thuringiensis* was quickly commercialized and used as a biopesticide for pest control due to its entomopathogenic properties.

Bacillus subtilis and *Bacillus cereus* group share a large number of transcriptional factors, including Spo0A, σ^B, SinI, and SinR[131], which play crucial roles in the intertwined regulation of sporulation and biofilm formation[132–136]. Between these two species, however, there are also some important differences in the regulatory pathways and transposable elements. For example, SigD, the motility-specific sigma factor, and the DegU/DegS two-component system, are absent from the species of the *B. cereus sensu lato* group; while the virulence regulator PlcR, which plays an important role in *B.*

cereus and *B. thuringiensis* physiology[137,138], is absent in *B. subtilis*. Besides, diverse Insertion Sequences (ISs) have been described in different *B. thuringiensis* isolates[139–142], while only limited number of ISs have been reported in *B. subtilis*[143]. ISs are the simplest transposable elements and play important role in shaping their host genomes[144]. Insertions of IS elements can results in both gene inactivation and activation, or alter the expression of neighboring genes[145]. In addition, IS-mediated changes have been described to both promote and constrain evolvability of *Escherichia coli* in a long-term evolution experiment (LTEE)[51]. These differences may be the adaptation consequences of these species to different ecosystems.

We closer examined the genome sequences *B. subtilis* DK1042/NCIB 3610 and *B. thuringiensis* 407 Cry$^-$ (Bt407), we only found one incomplete transposase gene (186bp) in *B. subtilis* genome, while we found 10 types of transposase genes, with 1~12 copies having lengths from 213~1,562 bp (four ISs smaller than 900bp are presumably truncated IS), giving a total of 39 copies in the *B. thuringiensis* 407 genome (**Table 1**).

Table 1 Transposase gene in the *B. thuringiensis* 407 genome

Transposase gene	**Copies**
IS*110* family transposase	12
IS*110*-like element ISBth13 family transposase	5
IS*21*-like element IS*232* family transposase	5
IS*3* family transposase	5
transposase	5
IS*4* family transposase	2

Transposase gene	**Copies**
IS*4*-like element IS*231*A family transposase	2
IS*4*-like element IS*231*C family transposase	1
IS*607* family transposase	1
IS*66* family transposase	1

In **Study 2**, by perform a two-round strategy using *breseq* pipeline[51], we success to detect fourteen IS mediated mutations in eight out of nine lineages in *B. thuringiensis* 407 population samples, which is consistent with the mutations detected by nanopore long reads sequencing[23]. Among these mutations, 13 cases were mediated by IS*231*A and one by IS*110*. Seven genes and three intergenic regions were disrupted by the inserted IS*231*A elements. We found that the cupin domain-containing protein (BTB_RS26870, *rfbM* gene) was disrupted by IS*231*A in 4 out of the 6 lineages in Bth_bead with max frequencies from 11.94% to 49.73%, which show high parallelism of adaptation to the plastic bead attached biofilm environment. Importantly, when specifically sequencing FS colony morphotypes, IS*231*A insertion was detected within the *rfbM* gene in each of the 6 lineages[23]. A loss-of-function *rfbM* mutant, Bt407Δ*rfbM*, constructed previously, could re-create the FS phenotype and the robust biofilm formation. Our results showed that the insertion sequences of *B. thuringiensis* are critical for its adaptation to the plastic bead-attached biofilm environment, but insertion sequence mobility was a general phenomenon in this species independent of the selection condition.

Table 2 IS transposition cases detected in the experimentally evolved *B. thuringiensis* lineages in Study 2

Position	Insertion sequence*	Gene	Condition	Lineage	Highest frequency in lineage
397,547	I1(+) + 12bp	*glnP*	Bth_bead	B	6.12%
607,087	I1(-) + 11bp	*npr*	Bth_bead	E	5.23%
985,569	I1(+) + 11bp	BTB_RS05005/BTB_RS34715	Bth_bead	A	34.73%
1,233,591	I1(-) + 11bp	*rfbB*	Bth_bead	A	54.86%
2,650,349	I3(+) + 11bp	BTB_RS13370	Bth_bead	D	8.36%
5,263,506	I3(+) + 12bp	*rfbM*	Bth_bead	A	13.37%
5,263,506	I3(+) + 12bp	*rfbM*	Bth_bead	B	48.66%
5,263,506	I3(+) + 12bp	*rfbM*	Bth_bead	F	26.13%
5,289,559	I3(-) + 12bp	*nuoN*	Bth_bead	A	29.23%
493,064	I2(+) + 3bp	*wbpA*	Bth_root	F	8.59%
524,134	I1(+) + 11bp	BTB_RS02650	Bth_root	C	100.00%
1,915,321	I1(-) + 11bp	*braD*	Bth_root	F	18.75%
3,677,033	I3(+) + 12bp	*glnR/ynbB*	Bth_root	E	12.46%

3.1.3 Secondary metabolite of *Bacillus subtilis*

Bacterial metabolites can be divided into two categories, primary metabolites and secondary metabolites. Primary metabolites are the molecules that directly involved in normal growth, development, and proliferation, which dominate exponential phase growth[146]. In contrast, secondary metabolites are small molecular weight compounds, which, although not essential for growth, can facilitate the interaction of a microbe with its environment and contribute to it fitnes[146]. Bacteria can produce them throughout their growth cycle, but they typically dominate late exponential and stationary phase lifestyles.

However, we are only just beginning to understand how these specialized metabolites contribute to ecosystem functioning. In the first place, secondary metabolites are believed to serve primarily as biological weapons that give producer strains a competitive edge. Additionally, they can also function as signaling sues[147] or influencers of cellular differentiation[148] within microbial communities at subinhibitory concentrations.

For decades, *B. subtilis* group strains have been known to produce a wide range of secondary metabolites[124]. To this end, it is estimated that the average 4-5% of its genome is devoted to the secondary metabolites production[149]. These molecules are mainly antimicrobial peptides. *B. subtilis* is well known for its production of cyclic lipopeptides with antimicrobial and surfactant properties, including surfactins, iturins, and fengycins[150]. Fengycins and iturins are primarily known for their antifungal properties against a wide range of plant and human pathogenic fungi[150].

Surfactin is perhaps the best studied non-ribosomal peptide in *Bacilli*, also known as one of the most potent biosurfactants. Generally, surfactins exhibit

antiviral and antibacterial properties[151]. There are, however, some surfactins that can control important fungal plant and human pathogens, such as *Candida albicans*, *Rhizoctonia solani*, and *Aspergillus niger*[152–154]. Surfactins are biosynthesized by the surfactin synthetase complex, which is composed of four enzymatic units, including SrfA, SrfB, SrfC, and SrfD[155] coded by the *srfAA-AD* gene cluster[156], which is under the regulation of two quorum sensing system, ComX and CSF (competence and sporulation factor, the PhrC pentapeptide)[157]. Additionally, Spo0A plays an indispensable role in proper surfactin synthesis[157]. As signaling molecules, surfactin plays an important role in *B. subtilis* cell differentiation by trigger other cells to differentiate into non-motile cells, matrix producing cells, cannibals, and spores[157]. Furthermore, although surfactin alters biofilm development, it is not essential for biofilm formation[158].

In **Study 4**, we demonstrated that surfactin plays an important role in *B. subtilis* adaptation to the presence of a competitor fungus, *A. niger*.

3.2 *Bacillus subtilis* biofilm formation

Bacteria can be categorized into two life forms in nature, one is planktonic, in which bacteria appear as single, independent, free-floating cells, and the other one is biofilms, in which bacteria are organized in microbial aggregates[159]. Biofilms are matrix-enclosed microbial communities that adhere to biotic or abiotic surfaces. These complex assemblages confer emergent properties to their inhabitants and represent a much higher level of organization than free-living bacterial cells do[160,161]. The biofilm lifestyle not only protects bacteria to survive in harsh environments but also facilitates the colonization of new niches during dispersal from these microbial clusters. Bacteria form biofilms on almost all natural and artificial surfaces[60,161], utilizing diverse mechanisms that depend on environmental conditions and specific species[121]. Within biofilms, the diffusion of molecules is limited, which enables the establishment of gradients, and eventual exhibit considerable structural, chemical, and biological heterogeneity[60]. Furthermore, the spatial structure of biofilm also alters evolutionary adaptation[162].

B. subtilis is capable of forming various types of biofilms exhibiting either beneficial or pathogenic impact. Biofilms can be categorized into three models depending on the type of occupied niche, including pellicle biofilms at the air-liquid interface, colony biofilms at the air-solid interface, and submerged biofilms at the solid-liquid interface[163,164]. *B. subtilis* also can form biofilms on biotic surfaces, including fungal hyphae[165], plant roots[166]. *B. subtilis* has been used to determine the mechanisms that control matrix production and the subsequent transition from a motile planktonic state to a sessile biofilm state[167]. A simplified overview of the different stages on biofilm formation is shown in **Fig. 10**. Initiation of biofilm formation triggered by environmental signals

(such as the lipopeptide surfactin) that promote planktonic cells to switch to non-motile, matrix-producing cells that form chains surrounded by the extracellular matrix[168]. The extracellular matrix is vital to the integrity of the biofilm since it sticks the community together. Matrix producing cells initiate sporulation as the biofilm grows and matures, spores are released from the matrix[168].

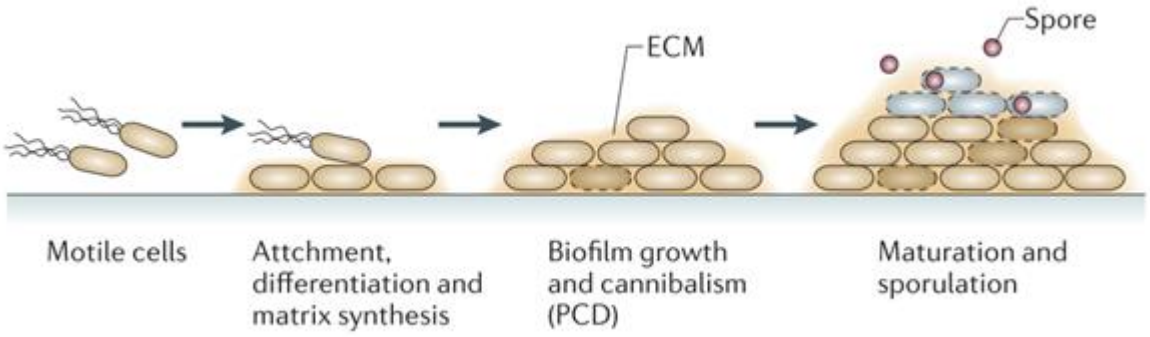

Fig. 10 Simplified overview of biofilm formation stages on *B. subtilis*. ECM, extracellular matrix; PCD, programmed cell death. Image from reference[169].

3.2.1 The extracellular matrix of *Bacillus subtilis*

The biofilm matrix is a structured and shared space, which is produced and regulated by the organisms within it. The *B. subtilis* extracellular matrix contains exopolysaccharide (EPS), which is synthesized by the products of the *epsA-O* operon[170], and protein fibres of TasA encoded by the *tapA–sipW–tasA* (*tapA*) operon[171], and a biofilm surface layer protein that confers hydrophobicity to the community[172,173]. eDNA has been identified as an important feature of the biofilm matrix, in *B. subtilis*, eDNA interacts with EPS in the early phases of biofilm development[174].

EPS is the main biofilm carbohydrate in *B. subtilis*, as well as acting as a signaling molecule, EPS is also required in forming complex colony structure, and pellicle formation[175,176]. Some of the 15 genes in the *epsA-O* operon have been studied individually. One of the most studied is EpsE, which is a bifunctional protein that coordinates the production of EPS and can inhibit flagellar motility as a molecular clutch by interacting with the flagellar motor switch protein, FliG[101,177]. TasA forms long amyloid-like fibres that are attached to the cell wall by TapA, besides, TapA also has a role in TasA fibres assembly[171,178]. The *tapA* operon also encodes SipW, a type I signal peptidase, which post-translationally modifies both TasA and TapA at the extracellular surface[179]. Both EPS and TasA are essential for the formation of strong and stable biofilms, since the mutants lacking either EPSs or TasA cannot establish pellicle biofilms in monocultures, while biofilm formation was restored when these two mutants are cocultured[97,180]. Due to it is a costly activity to produce EPS and TasA, these products are considered as public goods[180,181]. In addition, another secreted protein, BslA, a bacterial hydrophobin, forms a hydrophobic layer on the surface of the biofilm that acts as a barrier against environmental stress[172,173].

3.2.2 Master regulators govern biofilm regulation in *Bacillus subtilis*

Biofilm production is an energetically costly activity, the expression of matrix genes is often tightly regulated and controlled. Bacteria have developed complex regulatory networks to coordinate matrix gene expression as environmental conditions change in their natural habitat. In this section, three regulatory pathways that control biofilm formation are introduced, i.e., the Spo0A pathway, the DegS–DegU two-component system, and the Cyclic-di-

GMP pathway. The regulation of biofilm formation in *B. subtilis* has been extensively studied and reviewed[132,168], simplified schematic of this network is shown in **Fig. 11**.

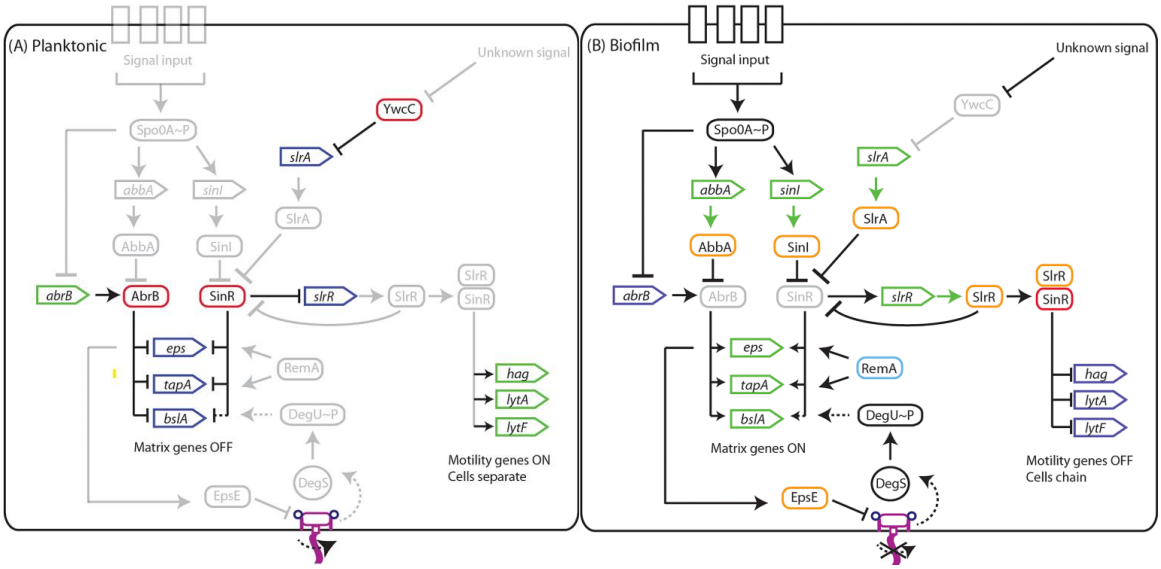

Fig. 11 Regulatory networks governing biofilm formation. Schematic of the complex regulatory pathways that control gene transcription during (A) planktonic growth and (B) growth as a biofilm. Rounded rectangles indicate proteins, triangles indicate open reading frames (ORFs), arrows indicate activation, T-bars indicate repression. Dashed arrows or T-bars indicate indirect activation and repression respectively. Green represents active gene transcription with a green arrow indicating translation, dark blue represents absence of gene transcription, red indicates a transcriptional repressor and orange indicates a protein–protein interaction. Light blue indicates a protein that is able to bind to DNA to activate transcription. Pink structure represents a flagellum, with the curved arrow indicating rotation and the cross indicating inhibition of flagellar rotation. Vertical rectangles labelled with "signal input" indicate sensor kinases for the Spo0A pathway, for more details see referebce[168]. Faded shading indicates parts of the pathway that are inactive. Image from reference[132].

(1) The Spo0A pathway

B. subtilis biofilm formation is regulated by transcription factor Spo0A, which directly controls the expression of more than 100 genes[182,183]. The activity of this protein is controlled by phosphorylation, and the concentration of phosphorylated Spo0A (Spo0A-P) in a given cell determines which sets of genes are expressed[182]. Moderate levels of Spo0A-P activates the expression of matrix genes, while high levels induces the genes involved in sporulation. At least four kinases (KinA, KinB, KinC and KinD) are involved in determining the concentration of Spo0A-P, that act either directly on Spo0A or indirectly via a phosphorelay, in which the phosphoryl groups are sequentially transferred from the kinases to Spo0F, to Spo0B and then to Spo0A[184].

At moderate levels of Spo0A-P, two parallel pathways of anti-repression are initiated, allowing transcription of operons essential for biofilm matrix production. **In the first pathway**, moderate levels of Spo0A-P repress the transcription of *abrB* directly and induces the expression of *abbA*, an AbrB anti-repressor, which binds to AbrB. **The second** anti-repression pathway involves the transcriptional repressor SinR, which inhibits the transcription of the *epsA-O* and *tapA* operon, this repressive effect of SinR is inactivated by SinI by binding to it, resulting in transcription of the matrix operons. Same as expression of AbbA, transcription of the *sinI* coding region is activated by moderate levels of Spo0A-P. While *sinR* is expressed in most cells, *sinI* is only expressed by a small subpopulation, likely contributing to three-dimensional spatial pattern of biofilm gene expression. Additionally, a second anti-repressor inhibitor of SinR is SlrA, which is under the control of the transcriptional repressor YwcC, although the signal that relieves this repression is unknown. Furthermore, the inhibition of SinR by high levels of SinI, allowing the expression of *slrR*. SlrR acts by binding to SinR, resulting

in SinR unable to bind the *epsA-O* and *tapA* operon and re-purposing of SinR function. The SlrR:SinR complex binds to and represses expression of genes involved in motility and autolysins, resulting in a simultaneously repression of motility (*hag*) and separation genes and the activation of matrix genes, thereby promoting the transition from a motile state to biofilm formation. The SlrR:SinR mediated repression leading to the cell chaining, which is essential at the initiation of biofilm formation. As SlrR re-purposes the SinR activity and prevents it from binding to target regions, including *slrR*, resulting a self-reinforcing negative feedback loop leading to high levels of SlrR. A cell can exist in a state in which SlrR levels are low where motility genes are expressed but matrix genes repressed, or in a state in which SlrR levels are high where cells exist as chains and express the genes involved in matrix production. Since the switch to the high SlrR state is self-reinforcing, it can persist for many generations and is regarded as an epigenetic switch.

In **Study 1, 2 and 3**, we frequently detected mutations in *sinR* or just few bp upstream of *sinR* gene (**Fig. 3**), which is potentially connected to the enhanced biofilm formation, and mutation in *kinA* is observed in **Study 1**[39].

(2) DegS–DegU two-component system

In B. subtilis, DegU plays a pivotal role in regulating a variety of processes such as competence, motility, biofilm formation, sporulation, and secretion of degradative enzymes, depending on the levels of phosphorylated DegU (DegU-P)[185]. The DegU is phosphorylated by its cognate sensor histidine kinase DegS. Intermediate-levels of DegU-P activates the biofilm formation while high-levels of it inhibits the biofilm formation, in the later situation, a

high percentage of the cells in the community enter the sporulation pathway[186]. Biofilm promotion occurs when DegU-P indirectly activates the expression of *bslA* and the PGA synthesis (*pgs*) operon[187–189]. Activation of the DegS-DegU pathway has been demonstrated by inhibiting flagellar rotation, as happens when the cell adheres to a surface[190]. These findings indicating that DegS phosphorylates DegU upon sensing a surface to promote transcription of target genes, including *bslA*. Thus, the arrest of flagellar rotation acts as an additional signal to initiate matrix production[190].

In **Study 4**, we identified that mutations in DegU and DegS contribute to adaptation to a fungus, and possibly to enhanced surfactin production.

(3) Cyclic-di-GMP

Bis-(3′-5′)-cyclic dimeric guanosine monophosphate (c-di-GMP) is a second messenger that regulates a number of cellular activities in bacteria, including motility, biofilm formation, cell-cell signaling, and host colonization[191]. Specifically, elevated c-di-GMP promotes sessility and biofilm formation; on the other hand, reduced c-di-GMP promotes biofilm dispersal and motility[191]. In response to external signals, c-di-GMP is synthesized from 2 GTP molecules by GGDEF domain-containing diguanylate cyclases (DGCs)[192–194]. The c-di-GMP can then bind intracellular effectors that regulating diverse phenotypes. The c-di-GMP is then hydrolyzed into the linear dinucleotide 5'-phosphoguanylyl-(3'-5')-guanosine (pGpG) by two classes of phosphodiesterases (PDEs) that contain either an EAL or HD-GYP domain [195–197]. However, c-di-GMP signaling has mainly been studied in Gram-negative bacteria until recently[107,108,198–200].

B. subtilis contains four GGDEF domain proteins (YdaK, GdpP, DgcK, and DgcP), two EAL domain proteins (YuxH/PdeH and YkuI), one GGDEF-EAL fusion protein and one PilZ domain protein[107,108]. Studies shown that the YuxH is a functional PDEin *in vitro*[108], the deletion of *yuxH* increasing cytoplasmic c-di-GMP levels and resulting impaired swarming motility of *B. subtilis*[107,108]. PilZ domain protein, YpfA, is a confirmed c-di-GMP receptor regulating flagellar motility in a post-translational mechanism, which is essential for c-di-GMP-dependent inhibition of flagellar motility[107,108]. However, the effect of c-di-GMP concentrations on biofilm formation is disputed.

In **Study 2**, several nonsynonymous and deletion mutation in gene *yuxH* were detected in Bs_root and Bs_pellicle, in low frequency (up to 28%) in 4 out of 13 lineages. However, mutations in gene *yuxH* were detected more frequently (only absent in one lineage in total twenty lineages) and in much higher frequency (up to 91%) in all evolved conditions in **Study 3**. *B. subtilis* contains a very small c-di-GMP regulatory network, with only four metabolic enzymes and one confirmed receptor protein identified to date, however, the repeated selected of gene *yuxH* in our evolution experiment, indicating c-di-GMP signaling pathway play an essential role when adapting to plant root conditions.

3.2.3 Bacterial motility

Motility and biofilm formation are described inversely regulated lifestyles with bacteria expressing genes necessary for either motility or biofilm matrix production but not both simultaneously[101,102]. Motility is vital for many bacteria, as this process enables them to explore resources and supports the dispersal of

progeny [201]. To better colonize diverse habitats, several motility mechanisms are employed by bacteria[202], which can be broadly divided into two types: cells either swim freely in aqueous media; or they move in aqueous media over solid surfaces. During the past decade, advances have been made in the field of bacterial motility, mechanisms of different types of motility have been elucidated and extensively reviewed, including swimming, swarming, twitching and gliding[201,203,204].

Here, I focus on two motility movement in *B. subtilis*, both are powered by rotating flagella, swimming, and swarming. Swimming motility takes place via individual cells moving in three dimensions of a liquid environments. In contrast, swarming motility involves groups of cells moving in two dimensions over solid surfaces[203]. The flagellar structure of *B. subtilis* is complex and is consisted of three architectural domains: the basal body, the hook, and the filament (**Fig. 12a**)[205]. The basal body is encoded by the *fla/che* operon, which contains 32 genes. Once hook is assembled, the sigma factor D (σ^D) is activated and resulting in expression of another set of genes dedicated to filament assembly and rotation. The filament is a helical propeller consisting of a repeating protein monomer called flagellin encoded by gene *hag*.

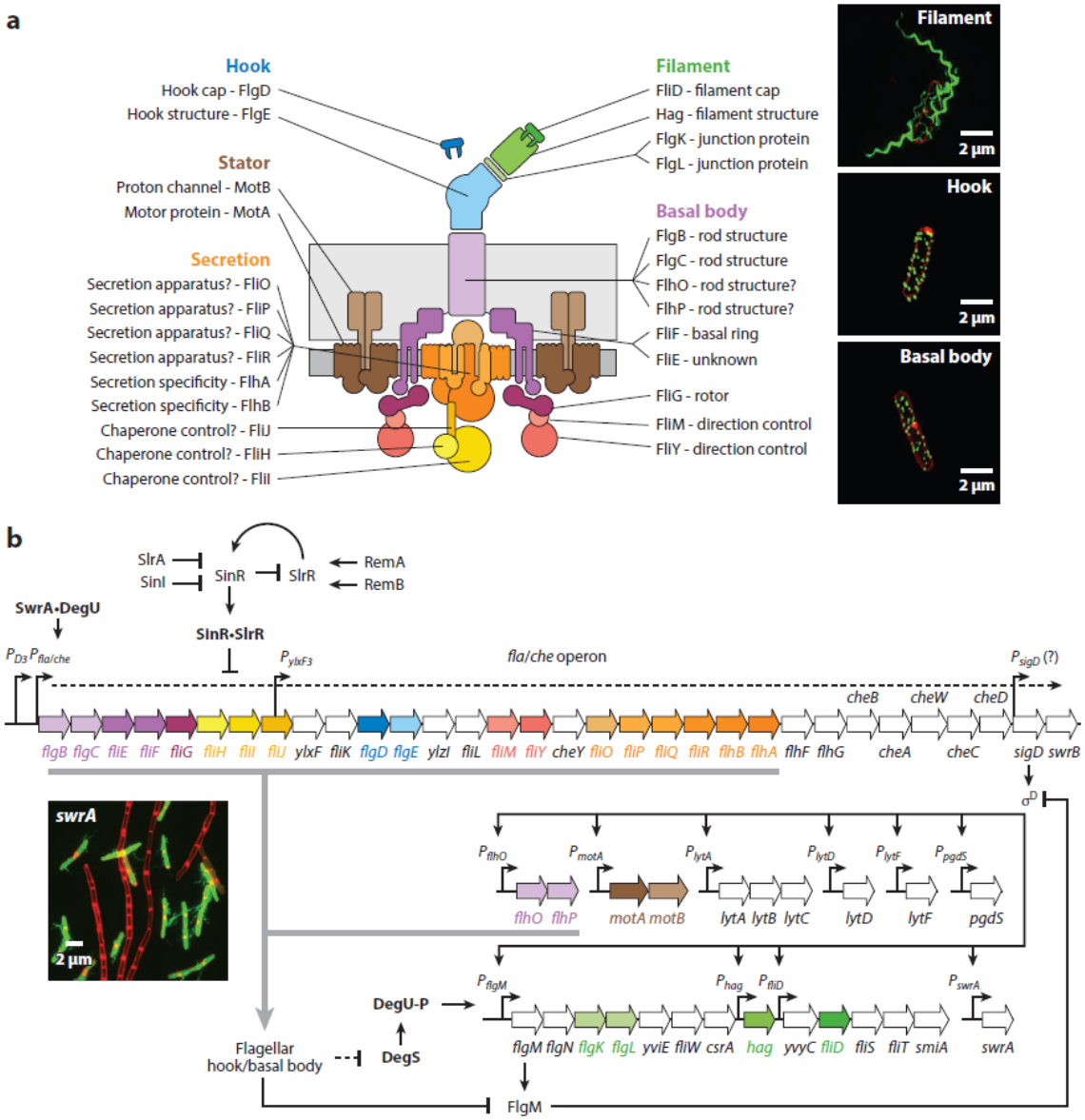

Fig. 12 Flagellar structure and genetic hierarchy. (**a**) Graphic depicting the putative structure of the *B. subtilis* flagellum based on empirical data and similarity to *Salmonella enterica*. Peptidoglycan is indicated in light gray. Membrane is indicated in dark gray. Flagellar components are colored and labeled. Micrographs are super-resolution fluorescence images of the indicated structures in wild-type cells: filament (maleimide-stained Hag^{T209C}), hook (maleimide-strained $FlgE^{T123C}$), and basal body (FliM-GFP fusion protein). (**b**) Graphic depicting genetic hierarchy of flagellar genes in B. subtilis. Open arrows are genes. Bent arrows are promoters. Closed arrows indicate activation; T bars indicate inhibition. Genes are color coded to match structures in panel a. Micrograph

indicates bistable gene expression found in a *swrA* mutant of *B. subtilis*. Membranes are red (stained with FM 4–64 dye). P_{hag} expression is colored green cytoplasmically (P_{hag}-YFP). Filaments are colored green extracellularly (maleimide-stained Hag^{T209C}). Only a subpopulation of cells expresses the filament gene hag and assembles filaments. Image from reference [205].

As shown **Fig. 11**, motility and biofilm formation are inversely regulated by several pathways, which affects the flagellar structural assembly state and gene expression. The fate of individuals in each subpopulation in *B. subtilis* are determined by the activity of σ^D. When the σ^D activity is "ON", cells produce Hag to complete flagellum assembly and produce LytF to separate individuals from chains, and the opposite when the σ^D activity is "OFF" (**Fig. 12b**)[206]. SwrA determines the transcriptionally activating of *fla/che* operon (including the *sigD* gene) which in turn increases expression of the σ^D regulon[207]. The *fla/che* operon may be indirectly activated by SwrA through its binding to and modulation of the response regulator DegU[208,209]. Additionally, SwrA increases σ^D-dependent gene expression by elevating σ^D levels above a threshold where motile cells contain high levels and chaining cells contain low levels[210]. σ^D protein levels are low in chains due to a failure of expression the *sigD* gene, the penultimate gene in the long 27-kb *fla/che* transcript[211,212]. This gradually decrease in *fla/che* operon transcript abundance is partly controlled by SlrA (**Fig. 12b**). SlrA overexpression results in enhanced distance-dependent decreases in *fla/che* operon transcript abundance, undetectable levels of σ^D protein, an OFF state for the entire σ^D regulon, and aflagellate cell chains, which is mediated by SlrR:SinR complex[213,214], as described in previous section. Furthermore, the activity of σ^D is promoted by hook–basal body completion through antagonism of the anti-sigma factor FlgM in two

different ways (**Fig. 13a**)[215], in one of which the DegS-DegU two-component system is involved. SwrB and YmdB are involved in the regulation of flagellar gene expression involves, whereas their mechanism are unknow yet. SwrB is produced immediately downstream of σ^D in the *fla/che* operon (**Fig. 13b**). Cytoplasmic concentration of the Hag is homeostatically auto-inhibited by a negative feedback loop which includes FliW and CsrA. However, this homeostasis is disrupted during periods of filament assembly in the present of flagellar filament chaperone FliS which binds to Hag and guides the exportation of Hag through the flagellar secretion apparatus[216]. At last, two functional flagellar inhibitors have been discovered in *B. subtilis*: YpfA (DgrA)[108,217] and EpsE[177], each through c-di-GMP signaling pathway or by binding to the rotor protein FliG, respectively (**Fig. 13c** and **d**). Both functions have been described in previous sections.

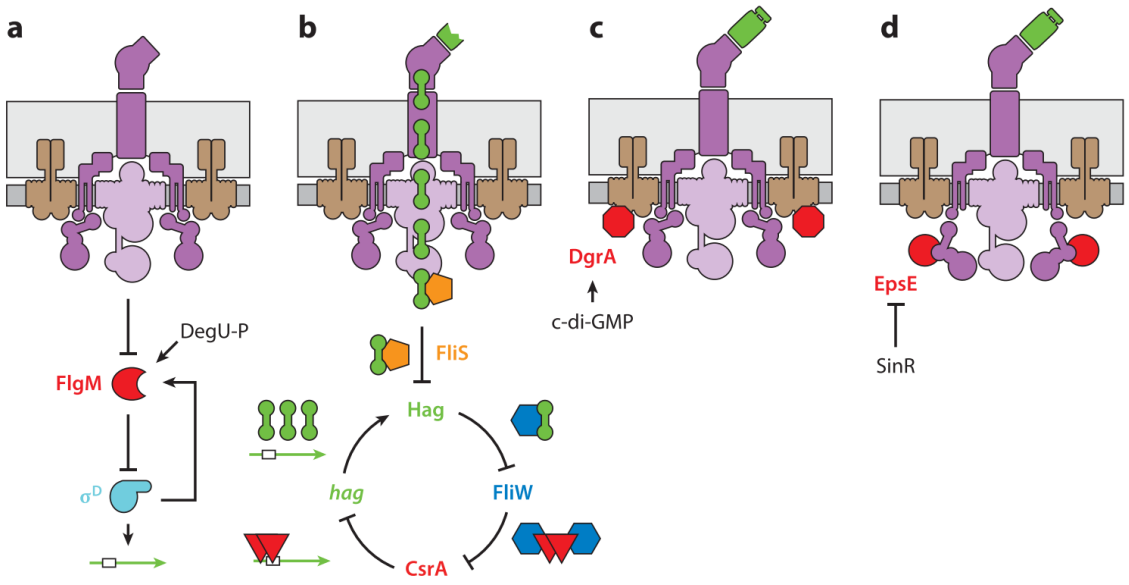

Fig. 13 Flagellar regulation. (**a**) FlgM (*red*) antagonizes σ^D (*cyan*), but σ^D activates FlgM expression prioritized by DegU-P. The autoinhibitory loop on σ^D is broken by completed hook–basal body structure by an unknown mechanism, and the hag transcript (*green arrow*) is synthesized. (**b**) CsrA (*red triangle*) binds to the Shine-Dalgarno sequence (*open box*) of the hag transcript and inhibits translation. When Hag (*green barbell*), aided by the secretion

chaperone FliS (*orange pentagon*), is secreted, FliW (*blue hexagon*) switches partners and antagonizes CsrA, which allows high-level Hag translation for the duration of filament assembly. (**c**) YpfA (DgrA) (*red octagon*) is activated by binding c-di-GMP and interacts with MotA to inhibit flagellar rotation. (**d**) EpsE (*red circle*) is relieved from SinR repression during biofilm formation and acts as a clutch by binding to FliG and disengaging the rotor (*purple*) from MotA (*brown*). Image from reference [205].

In our **Four Studies**, motility and biofilm formation seems to be a rapidly adapting phenotype of *B. subtilis*, as we observed that these change rapidly and the genes coding for regulators of these phenotypes are likely mutated (**Fig. 2**, **Fig. 3**).

Chapter 4 Experimental evolution of *Bacillus*

Microorganisms are ideal models for evolution experiments, as the most studied species in the genus *Bacillus*, powerful genetic and genomic methods are readily available for *B. subtilis* and several public and high-quality databases about its physiology, biochemistry, gene expression, and ecology can be used to help in interpreting results. *B. subtilis* has been used in many experimental evolution studies using different approaches. As an economically importance *Bacillus* species, several evolution experiments also performed using *B. thuringiensis*.

4.1 Domestication and sporulation adaptation studies

Many laboratory used model bacteria have been **domesticated** in laboratory conditions, bacteria can rapidly adapt and modify their phenotypes when a wild type from natural world is cultured in the lab. It is essential to understand how and the tempo of a natural isolate adapt to the new laboratory condition. *B. subtilis* strain 168, has lost a plasmid and acquired mutations in *sfp*, *epsC*, *swrA*, and *degQ* throughout its laboratory life, which results in the loss of traits likely to be important to the *B. subtilis* natural life cycle in the soil, root plants, or the gastrointestinal tract of various organisms[218]. Experimental evolution couple with whole-genome sequencing was used to study the domestication of a natural isolate of *B. subtilis* to laboratory environment[219]. In which, five independent populations from same natural isolate BSP160, were grown in LB with a daily 1:100 dilution for 16 days. New morphotypes were emerged

rapidly in all evolved populations and showed increased growth traits in the laboratory environment[219]. Further investigation showed that, mutation(s) in regulator DegU affects the DegU-dependent positive autoregulatory loop and leads to the loss of robust biofilm formation, impaired swarming motility, reduced secretion of exoproteases, and to changes in sporulation across environments, indicating that *degU* is a selection target during domestication[219]. Their study also emphasizes the importance to perform short-term cultivation of bacterial natural isolates to keep traits that may be important for the probiotic ability of *B. subtilis*.

Endospore formation is one well known feature of *Bacillus* genus, endospore has played a pivotal role in *Bacillus* evolution. The impact of stringent or relaxed selection for sporulation in the laboratory were intensively examined by using long-term evolution experiments and whole genome sequencing and several omics technologies. Five cultures of genetically marked congenic *B. subtilis* were propagated in a medium that repressed sporulation (Repressed, or R populations) with daily 100-fold dilutions and regrowth, and five cultures were propagated in a medium that induced sporulation (Sporulating, or S populations) with daily 100-fold dilutions and regrowth after subjected these S populations to heat shock (80°C, 10 min) to select for spores, both continued for 6,000 generations[220]. First, a large diversity of colony morphotypes and sporulation-defective (Spo^-) colonies emerged rapidly within 100-200 generations, and higher fitness was evolved, and auxotrophic mutations were cumulated in both S and R populations[220]. Further DNA microarray essay demonstrated that, most of the mutations result in the observed adaptive phenotypes over 6,000 generations were not caused by gross genomic losses, but more likely caused by small changes in the genome[221]. Then, isolates were isolated from R populations before and after a

distinct small-colony morphotype swept through the populations, respectively. Post-sweep strain WN716 showed a large competitive advantage against the ancestor and the pre-sweep strain WN715 both in pairwise competition and in mixed culture experiments[222]. Transcriptome profiles comparison analysis identified specific transcriptome files that are consistent with the observed phenotype characteristics in each isolate[222]. Additionally, genome sequencing of these two isolates revealed mutation involved in resistance to membrane-damaging agents and bacteriocins in sigma factor SigW, and in the *alsR* gene, which encoding the positive transcriptional regulator of acetoin fermentation[223]. While mutations responsible for the loss of motility and chemotaxis (*sigD*) in strain WN716 were not found. To validate the whether the inactivation of these pleiotropic regulators was indeed responsible for the increased fitness of strain WN716, mutants Δ*alsR*, Δ*sigW*, and Δ*sigD*, and in all possible combinations in ancestral strain WN624 were constructed, and their relative fitness versus the ancestor were measured[224]. By using this approach, some, but not all, factors responsible for the WN716 fitness improvement were revealed.

4.2 Extreme environment adaptation studies

Microorganisms, as a whole, can grow in an incredible wide range of physical extreme environments (temperature, pressure, extreme pH etc.), given any individual microbe, it can only survive within a limited subset of this range. What are the underlying molecular and genetic mechanism that determine at which environment a bacteria can survive and grow? Several studies have been performed to explore the directed evolution of *B. subtilis* to growth under the harsh environments, i.e., low pressure, and ultraviolet (UV) radiation, which are described in the below paragraphs.

4.2.1 Low-pressure

The mean atmospheric pressure at sea level on earth is around 101.3 kPa, the growth of *B. subtilis* is inhibited at pressures below 2.5 kPa[225], indicating that there exists a low-pressure limit to the growth of microbes. To reveal whether *B. subtilis* could evolve the ability to grow at lower pressure, *B. subtilis* was grown in liquid medium with a daily 1:100 dilution for 1,000 generations at 5 kPa, a pressure just above its inhibitory growth pressure[226]. The population exhibited a stepwise adaptation to growth at 5 kPa, and the isolate from the evolved endpoint, strain WN1106, out-competed the ancestral strain at 5 kPa, but not at Earth-normal pressure (101.3 kPa), which showed better growth under oxygen limitation[226]. Transcriptome profile comparison revealed higher levels of *des-desKR* gene cluster transcription of specifically in evolved stain in low pressure environment[227]. Genome sequencing determined the mutations in eight genes, one of which, *rnjB*, contain a 9bp in-frame deletion, encoding RNase J2, a component of the RNA degradosome[228]. Further competition

experiments between ancestor and mutant *rnjBΔ9* deletion showed combination of temperature and pressure used dependent consequence[229], which highlighted the linkage between temperature and pressure in environmental research.

4.2.2 Ultraviolet radiation

UV radiation was a ubiquitous environmental stress factor for microorganisms during the Archean eon. UV irradiation can cause several a variety of lesions on the cellular level of organisms, mainly DNA damage[230], microorganisms have to respond and adapt quite rapidly to survive in a change in the UV environment. Can *B subtilis* cells evolve higher resistance to UV if subjected to periodic exposure to polychromatic UV (200 to 400 nm)? To this end, *B. subtilis* was grown under non-sporulating conditions, and exposed to a pulse of polychromatic UV radiation every tenth generation with four replicates and a control without irradiation[231]. After about 700 generations, evolved populations, but not the control, exhibited a 4.5-fold increase in UV resistance relative to the ancestor. Increased resistance to X-rays and enhanced resistance to hydrogen peroxide were also exhibited in the evolved populations[231]. In addition, spores of the UV-adapted strains were also slightly more resistant to 254-nm UV than were spores of the ancestor (166). The adaptation experiments that the mechanisms of UV resistance in the evolved strain are mostly active in growing or stationary-phase cells, not in dormant spores[232].

4.3 Biofilm studies of *Bacillus*

Above mentioned evolution experiments were performed on planktonic forms. During the past two decades, several biofilm models have been used in *Bacillus* experimental evolution, such as static models, bead transfer models, plant colonization.

4.3.1 Diversification and hitchhiking

One of the early *B. subtilis* biofilm study was performed in a simple static model, in which, *B. subtilis* was grown in both a daily 1:50 dilution in 5mL LB under shaking condition and static culture in glass tubes transferred every two days, for 60 total days[64]. Bacteria rapidly diversified into diverse colony morphologies with different biofilm-forming ability within the first week in both under shaking and static conditions[64]. Wrinkled colony-forming evolved isolates were found to possess point mutations in the biofilm-regulatory gene *sinR* by genetic sequencing. The evolved biofilm phenotypes were restored by introducing these mutations into the ancestral strain suggesting that these mutations are sufficient for robust biofilm formation in wrinkled colony types. These results implying that adaptive specialization of *B. subtilis* can occur through mutations that modulate biofilm formation[64].

B. subtilis can form biofilms at air–liquid interfaces, that is, pellicles, a feasible experimental model system. As mentioned in **3.2.1**, biofilm matrix production depends on activation of *epsA-O* and *tapA* operons encoding for enzymes required for EPS and TasA, respectively. To explore the evolutionary diversification of pellicle biofilms of *B. subtilis*, a total 35 transfers of static

air-medium floating biofilm transfer (Bs_pellicle) was performed[22]. *B. subtilis* diversified into four distinct colony variants that dramatically differed in biofilm formation abilities and expression of biofilm-related genes (EPS and TasA). Interestingly, one of the morphotypes lost the biofilm formation ability can exploit the cooperative products of the other morphotypes. Genome comparison suggested that major phenotypic transformations between the morphotypes can be triggered by subtle genetic differences[22]. The periodic archived samples in this study were used in **Study 2** for further genetic studies.

As public goods, EPSs and TasA can both be shared within biofilms. Driven by heterogeneously activated regulatory pathways, clonal groups of *B. subtilis* develop into phenotypically heterogeneous cells that (1) either lack production of the biofilm matrix (non-producer), (2) solely secrete EPSs (specialist), and (3) produce both EPSs and TasA (generalists)[180]. Using an approach similar to Bs_pellicle evolutionary setup, EPS non-producers and wild-type *B. subtilis* were repetitively cocultured in an experiment[233]. Compared to the high phenotypic heterogeneity in *eps* expression of the ancestor strain, prolonged exposure of the wild-type EPS-producer cells to the presence of EPS-deficient cheaters results in an adaptive strategy, where most of the wild-type cells becomes a matrix overproducer[233].

Both pheno- and genetic diversification are frequently observed in biofilm adaptation. In our **Four Studies**, evolved clones diversified into distinct pheno- and/or genotypic colony variants in time, associating with increased biofilm development (**Study 1, 2 and 3**) or increased surfactin production (**Study 4**) of the isolated clones at the end of the experiments.

4.3.2 Plant colonization

The rhizosphere plays an important niche for the mutualistic relationships between plants and the microorganisms in the surrounding soil. Overall, plants exude up to 20% of fixed carbon and 15% of nitrogen into their environment[234,235], and these exudates shape the microbiome. Importantly, the amount and composition of exudates vary depending on the plant species, the stage of development, and the environmental stresses[236]. The exudates contribute a rhizobiome formation by recruiting plant-growth-promoting rhizobacterium (PGPR) and serving as nutrients[237], while PGPRs benefit plant growth and enhance plant tolerance to different abiotic and biotic stresses[238].

B. subtilis is a soil-dwelling, biofilm forming, Gram-positive PGPR that is commonly found in association with plants and their rhizosphere[167]. It has been widely recognized that this bacterial species aids plants in several direct and indirect ways[8]. Some *B. subtilis* strains have been applied as biocontrol agents within agriculture, but the effects vary immensely under field conditions[239,240]. Another *Bacillus*, *B. thuringiensis*, although less studied, has also been described as PGPR, indicating that *B. thuringiensis* has the intrinsic ability to colonize plants in a phylogeny-dependent manner[20,21]. To exert their beneficial effects, PGPR usually must colonize and persist on the root surface efficiently, which mainly depends on their ability to form biofilms.

To explore how adapt to plant root, experimental evolution of *B. subtilis* was performed on *A. thaliana* roots under gently shaking hydroponic conditions in **Study 1** (Bs_root)[39]. In this study, *B. subtilis* was shown to rapidly adapt to the *A. thaliana* root environment, several evolved isolates displayed altered colony morphologies. Two selected evolved isolates from independent populations from the final transfer outcompeted the ancestor

during root colonization. Re-sequencing of single evolved isolates from independent populations and different time points revealed mutations in genes related to different bacterial traits. The examined evolved isolates also displayed robust biofilm formation in response to plant polysaccharides, impaired motility, and altered growth on plant-derived compounds[39].

Similarly, experimental evolution of *B. thuringiensis* was performed on *A. thaliana* roots under gently shaking hydroponic conditions (Bth_root)[24]. In the Bth_root experiments, bacterial lineages displayed enhanced root colonization ability compared with the ancestral strain. Single isolates from two of the evolved lineages showed higher recolonization efficiency of new roots compared with the other lineages, in addition to exhibiting altered bacterial differentiation and pathogenicity. Investigation of a key mutation in the gene encoding the Rho transcription termination factor in these lineages demonstrated how transcriptional rewiring alters cell fate decisions in *B. thuringiensis*[24]. The periodic archived samples in two above mentioned studies were used in **Study 2** for further genetic studies.

In **Study 3**, we further investigated how *B. subtilis* evolves on *A. thaliana* and tomato seedlings, as well as in an alternating host regime of the two plants in a static hydroponic setup. We identified parallel evolution across multiple levels of biological organization in all conditions, and highest in two heterogeneous, multi-resource spatially structured environments in gene level (**Fig. 14**). Species-specific adaptation in genetic level was also observed, possibly caused by the selection stress imposed by different host plants. Further, the trade-off between motility and biofilm development was supported by the mutational changes in motility- and biofilm-related genes.

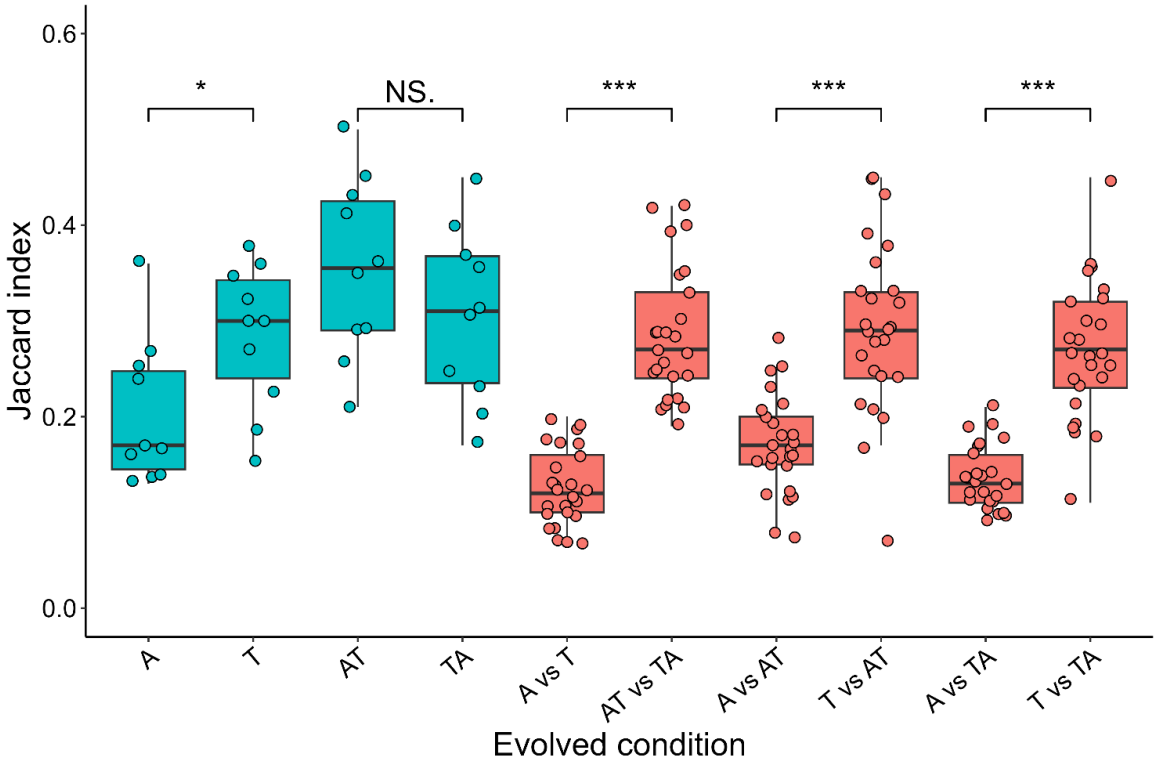

Fig. 14 Parallelism. Degree of parallelism within and between each evolved environment was estimated using the Jaccard index. Asterisks at the top indicate significant differences between different environment combinations (*p < 0.05, ***p < 0.001, by student's unpaired two-tailed t-test). Boxes indicate Q1–Q3, lines indicate the median, circles indicate the J value of each pair within (blue) or between (soft red) evolved conditions.

Taken together, results from these evolution experiments of *B. subtilis* evolved on plant roots demonstrate a common strategy used by *B. subtilis* when adapting to the plant rhizosphere in similar conditions and reveal the differences of genetic mechanism between the two different host plants, both will likely support strain improvements for sustainable agriculture.

4.3.3 Bacterial-fungal interactions

Bacteria and fungi share diverse habitats with each other and consequently, a wide span of interactions is observed between them ranging from mutualism to inhibition. These interactions not only influence the structure and ecology of the respective microbial community but also impact the development and evolution of the interacting species[241,242]. Bacteria and fungi can indirectly affect each other by sensing and responding to diffusible signals like chemoattractants, quorum sensing molecules, or volatile substances[243–245]. However, several bacterial-fungal interactions (BFIs) require a close vicinity, direct contact of the interaction partners. In certain cases, the bacterium resides inside the cells of its fungal host[242,245]. Often, a combination of indirect influence and physical contact define a BFI. In addition to influencing short-term microbial development, BFIs can also impact the evolution of an organism over longer time scales[246].

Direct interaction between the black mold causing fungus *Aspergillus niger* and *Bacillus subtilis* were observed[247,248]. Both organisms are commonly found in soil, thus they potentially coexist in the same habitat and influence each other. Attachment of *B. subtilis* cells to the fungal hyphae results in transcriptional changes. Specifically, the production of antimicrobial substances was downregulated in both microorganisms, including the *B. subtilis*-produced lipopeptide, surfactin. Further, genes related to motility and aerobic respiration were also downregulated in the bacterium during attachment. In **Study 4**, we investigated the effects of a long-term cultivation of *B. subtilis* in the presence of *A. niger* with focus on the evolution of the bacterium. During this laboratory adaptation experiment, *B. subtilis* was selected with enhanced surfactin production and spreading behavior, which

was mimicked by recreation of specific mutations in genes encoding DegS-DegU two-component system (**Fig. 15**). Increased surfactin production and niche colonization by the bacterium dismantled fungal expansion and acidification of the medium, in addition to introduction of cell wall stress in *A. niger*.

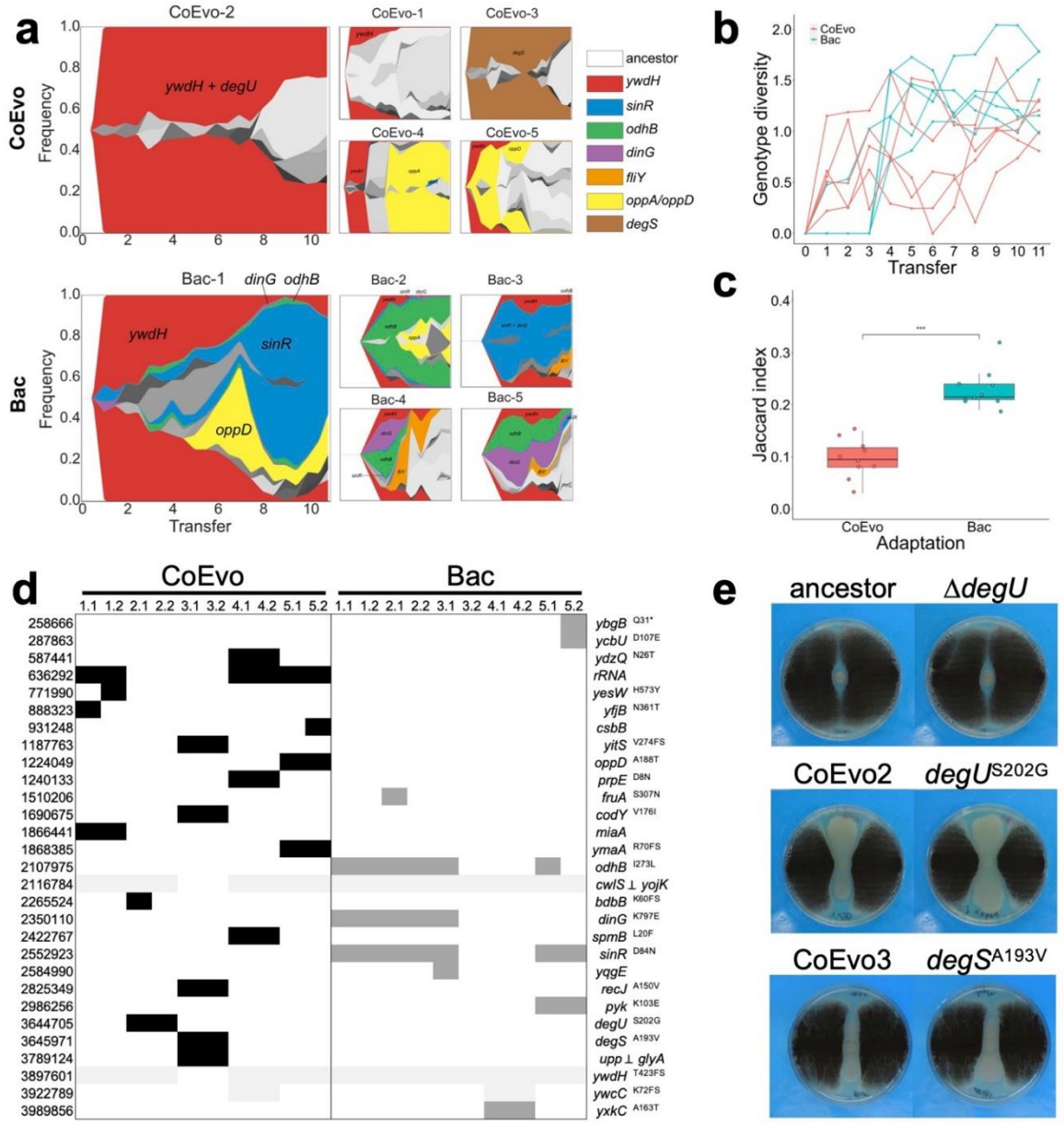

Fig. 15 Genetic characterization of *B. subtilis* adaptation to *A. niger*. a, Graphs represent the genealogy and genotype frequencies throughout the transfers. Each colour or shade represents a distinct genotype, the vertical area corresponds to genotype frequency as

inferred using *Lolipop*. Dominant genotypes with high mutated gene frequency, which are shared in different populations, are highlighted with matching colours within both adaptation models. **b,** Genotype diversity. Dynamic distribution of genotype alpha diversity in each population of the two adaptation models over time calculated using Shannon method. **c,** Degree of parallelism within both conditions estimated by Jaccard index. Asterisks denotes significant differences (***$p < 0.001$, Student's unpaired two-tailed t-test). Boxes indicate Q1–Q3, lines indicate the median, dots indicate the J value of each condition. **d,** Detected mutations in endpoint CoEvo and Bac isolates. Black indicates CoEvo specific mutations, dark grey denotes Bac-specific SNPs, while light grey refers to common mutations found in both experimental setups. ^ indicates intergenic region between the two genes depicted. * indicates an introduced stop codon. Amino acid changes are indicated unless synonymous mutation was determined. **e,** Bacterial colony growth between two lines of fungal streak. Plate size is 9 cm.

Our study demonstrates the potential of combining co-culture and laboratory evolution experiments to deepen our understanding of BFIs. Such co-culture adaptation methodology could offer a general, non-GMO approach to enhance antifungal activities of biocontrol bacteria against pathogenic fungi.

Chapter 5 Conclusions and perspectives

The Gram-positive bacterium *Bacillus subtilis* and *Bacillus thuringiensis* are used in green biotechnology to improve plant growth due to their beneficial properties. Both species are prevalent biofilm formers and found to be ubiquitous and widespread in various habitats. An in-depth understanding of genetic mechanisms on how these two *Bacillus* species adapt to different environmental niches and how these bacteria interact with plants and fungi will likely support strain improvements for sustainable agriculture in the future. In this Ph.D. study, I exposed the evolutionary landscape on how *Bacillus* adapts to diverse environmental niches using whole-population genome sequencing.

By performing whole-population genome sequencing, we provided the first comprehensive mutational landscape of two bacterial species' biofilms that is adapted to an abiotic and biotic surface. Our analysis revealed that different adaptation strategies were employed by each species in response to different environments, with a more diverse mutational spectrum observed under biotic conditions. Furthermore, our findings highlighted the impact of insertion sequences on the adaptation of *B. thuringiensis*, emphasizing the importance of considering the bacterial genome background when utilizing experimental evolution for strain improvements. Notably, we also observed a higher level of genetic diversification in biotic selective environments, indicating an increased spatial niche heterogeneity and a nutritional source difference created by the plant host that provided a strong strength of selection during the adaptation process. To better understand the influence of spatial niche heterogeneity created by the plant host on evolution and adaptation, future experiments should be performed with similar population sizes between abiotic and biotic adaptation environments, along with a known generation

number during each transfer. Such experimental setups would be instrumental in shedding light on the effects of these factors.

We performed an experimental evolution approach to study *B. subtilis* adaptation to *Arabidopsis thaliana* both under static and shaking hydroponic setups. We found that *B. subtilis* rapidly adapted to the plant root, exhibiting improved root colonization in both setups, alongside reduced or even impaired motility, supporting a biofilm-motility trade-off. Further, the trade-off between motility and biofilm development was supported by the mutational changes in motility-and biofilm-related genes. These findings suggest that experimental evolution can serve as an effective methodology for improving PGPR strains for potential use in sustainable agriculture. However, since motility has been shown to be pivotal for *B. subtilis* root colonization under soil conditions, reduced or even impaired motility of the evolved isolates might be undesirable in a biocontrol strain. Thus, it is important to conduct future experimental evolution studies under simulated soil conditions or in greenhouses. Our findings underscore the significance of carefully selecting the appropriate selective environment for experimental evolution for PGPR strains improvements.

Species-specific adaptation in genetic level was also observed when we compared *B. subtilis* evolves on *A. thaliana* and tomato seedlings, as well as in an alternating host regime of the two plants in a static hydroponic setup. It has been previously demonstrated that when different *Bacilli* are isolated from different plant species, those will display plant host-specific root colonize ability[249]. Our findings suggest that PGPR strains could be most beneficial when adapted to the specific plant species for which they are intended during the experimental evolution process.

We revealed numerous mutations in motility-and biofilm-related genes, which are crucial for adaptation to different environmental niches. We also identified several condition-specific and commonly targeted genes in different environments by comparing the three different *B. subtilis* biofilm adaptation settings from **Study 1, 2 and 3**. These results demonstrate a common strategy used by *B. subtilis* when adapting to the plant rhizosphere in similar conditions and also reveal the differences of genetic mechanism between the two different host plants, both will likely support strain improvements for sustainable agriculture. However, reintroduction of single mutations alone or in combination will be necessary in the future to precisely measure the influence of these mutations on fitness.

Moreover, the Ph.D. study used a simple Bacterial-Fungal Interactions (BFIs) system to reveal the effects of a long-term cultivation of *B. subtilis* in the presence of *Aspergillus niger* with focus on the evolution of *B. subtilis*. In specific populations, *B. subtilis* was selected with enhanced surfactin production and spreading behavior. Increased surfactin production and niche colonization by the bacterium dismantled fungal expansion and acidification of the medium, in addition to introduction of cell wall stress in *A. niger*. It has been shown that surfactin was neither required for biofilm formation nor root colonization in *B. subtilis* 3610 and various environmental strains. Our findings indicate that the surfactin production and the formation of biofilms are both important to the biocontrol properties of *B. subtilis*. Experiments could be conducted *in vivo* to determine the effect of surfactin on plant growth promotion and root colonization in the future.

From a technical perspective, we performed whole genome sequencing to unveil the dynamic evolutionary landscape by identifying genetic variations and mutations. However, we did not have access to gene expression levels at

different stages of the evolution experiment or during biofilm formation, let alone in single cell level. As technology advances, the use of single-cell sequencing and spatial transcriptome profiling will make experimental evolution an even more powerful tool in future studies.

In conclusion, this Ph.D. thesis adds knowledge on how different *Bacillus* adapt to diverse environmental niches, with a particular focus on their interactions with plants and fungi, thus supporting strain improvements for sustainable agriculture.

REFERENCE

1. United Nations, Department of Economic and Social Affairs, Population Division. World Population Prospects 2022: Summary of Results Ten key messages. (2022).
2. Pérez-García, A., Romero, D. & de Vicente, A. Plant protection and growth stimulation by microorganisms: biotechnological applications of *Bacilli* in agriculture. *Curr Opin Biotechnol* **22**, 187–193 (2011).
3. Carvalho, F. P. Pesticides, environment, and food safety. *Food Energy Secur* **6**, 48–60 (2017).
4. Keswani, C. *et al.* Antimicrobial secondary metabolites from agriculturally important bacteria as next-generation pesticides. *Appl Microbiol Biotechnol* **104**, 1013–1034 (2020).
5. van Lenteren, J. C., Bolckmans, K., Köhl, J., Ravensberg, W. J. & Urbaneja, A. Biological control using invertebrates and microorganisms: plenty of new opportunities. *BioControl* **63**, 39–59 (2018).
6. Heydari, A. & Pessarakli, M. A review on biological control of fungal plant pathogens using microbial antagonists. *Journal of Biological Sciences* **10**, 273–290 (2010).
7. Lugtenberg, B. & Kamilova, F. Plant-Growth-Promoting Rhizobacteria. *Annu Rev Microbiol* **63**, 541–556 (2009).
8. Blake, C., Christensen, M. N. & Kovács, Á. T. Molecular Aspects of Plant Growth Promotion and Protection by *Bacillus subtilis*. *Molecular Plant-Microbe Interactions* **34**, 15–25 (2021).
9. Elkoca, E., Kantar, F. & Sahin, F. Influence of Nitrogen Fixing and Phosphorus Solubilizing Bacteria on the Nodulation, Plant Growth, and Yield of Chickpea. *J Plant Nutr* **31**, 157–171 (2007).
10. van Rhijn, P. & Vanderleyden, J. The *Rhizobium*-plant symbiosis. *Microbiol Rev* **59**, 124–142 (1995).
11. Saeid, A., Prochownik, E. & Dobrowolska-Iwanek, J. Phosphorus Solubilization by Bacillus Species. *Molecules* **23**, 2897 (2018).
12. Nadeem, S. M., Zahir, Z. A., Naveed, M. & Arshad, M. Rhizobacteria containing ACC-deaminase confer salt tolerance in maize grown on salt-affected fields. *Can J Microbiol* **55**, 1302–1309 (2009).

13. Spaepen, S. & Vanderleyden, J. Auxin and Plant-Microbe Interactions. *Cold Spring Harb Perspect Biol* **3**, a001438 (2011).

14. Bhattacharyya, P. N. & Jha, D. K. Plant growth-promoting rhizobacteria (PGPR): emergence in agriculture. *World J Microbiol Biotechnol* **28**, 1327–1350 (2012).

15. Glick, B. R. Plant Growth-Promoting Bacteria: Mechanisms and Applications. *Scientifica (Cairo)* **2012**, 1–15 (2012).

16. Ahemad, M. & Kibret, M. Mechanisms and applications of plant growth promoting rhizobacteria: Current perspective. *J King Saud Univ Sci* **26**, 1–20 (2014).

17. Todorova, S. & Kozhuharova, L. Characteristics and antimicrobial activity of *Bacillus subtilis* strains isolated from soil. *World J Microbiol Biotechnol* **26**, 1207–1216 (2010).

18. Navon, A. *Bacillus thuringiensis* insecticides in crop protection — reality and prospects. *Crop Protection* **19**, 669–676 (2000).

19. Cannon, R. J. C. Prospects and progress for *Bacillus thuringiensis*-based pesticides. *Pestic Sci* **37**, 331–335 (1993).

20. Anwar, M. S. *et al.* Multitrait plant growth promoting (PGP) rhizobacterial isolates from *Brassica juncea* rhizosphere. *Commun Integr Biol* **7**, e27683 (2014).

21. Vidal-Quist, J. C., Rogers, H. J., Mahenthiralingam, E. & Berry, C. *Bacillus thuringiensis* colonises plant roots in a phylogeny-dependent manner. *FEMS Microbiol Ecol* **86**, 474–489 (2013).

22. Dragoš, A. *et al.* Evolution of exploitative interactions during diversification in *Bacillus subtilis* biofilms. *FEMS Microbiol Ecol* **94**, fix155 (2018).

23. Lin, Y., Xu, X., Maróti, G., Strube, M. L. & Kovács, Á. T. Adaptation and phenotypic diversification of Bacillus thuringiensis biofilm are accompanied by fuzzy spreader morphotypes. *NPJ Biofilms Microbiomes* **8**, 27 (2022).

24. Lin, Y. *et al.* Adaptation of Bacillus thuringiensis to Plant Colonization Affects Differentiation and Toxicity. *mSystems* **6**, e00864-21 (2021).

25. Blake, C., Nordgaard, M., Maróti, G. & Kovács, Á. T. Diversification of *Bacillus subtilis* during experimental evolution on *Arabidopsis thaliana* and the complementarity in root colonization of evolved subpopulations. *Environ Microbiol* **23**, 6122–6136 (2021).

26. Bram Van den Bergh, Toon Swings, Maarten Fauvart, J. M. Experimental Design, Population Dynamics, and Diversity in Microbial Experimental Evolution. *Microbiology and Molecular Biology Reviews* **82**, e00008-18 (2018).

27. Kawecki, T. J. *et al.* Experimental evolution. *Trends Ecol Evol* **27**, 547–560 (2012).

28. Bennett, A. F. & Lenski, R. E. EVOLUTIONARY ADAPTATION TO TEMPERATURE II. THERMAL NICHES OF EXPERIMENTAL LINES OF *ESCHERICHIA COLI*. *Evolution (N Y)* **47**, 1–12 (1993).

29. Kolss, M., Vijendravarma, R. K., Schwaller, G. & Kawecki, T. J. LIFE-HISTORY CONSEQUENCES OF ADAPTATION TO LARVAL NUTRITIONAL STRESS IN DROSOPHILA. *Evolution (N Y)* **63**, 2389–2401 (2009).

30. Fry, J. D. DETECTING ECOLOGICAL TRADE-OFFS USING SELECTION EXPERIMENTS. *Special Feature Ecology* **84**, 1672–1678 (2003).

31. Perfeito, L., Fernandes, L., Mota, C. & Gordo, I. Adaptive mutations in bacteria: High rate and small effects. *Science (1979)* **317**, 813–815 (2007).

32. Meyer, J. R. *et al.* Repeatability and contingency in the evolution of a key innovation in phage lambda. *Science (1979)* **335**, 428–432 (2012).

33. Beaumont, H. J. E., Gallie, J., Kost, C., Ferguson, G. C. & Rainey, P. B. Experimental evolution of bet hedging. *Nature 2009 462:7269* **462**, 90–93 (2009).

34. Plotkin, S. A. & Plotkin, S. L. The development of vaccines: how the past led to the future. *Nature Reviews Microbiology 2011 9:12* **9**, 889–893 (2011).

35. de Crecy, E., Jaronski, S., Lyons, B., Lyons, T. & Keyhani, N. Directed evolution of a filamentous fungus for thermotolerance. *BMC Biotechnol* **9**, 74 (2009).

36. I. On the life-history of a minute septic organisms with an account of experiments made to determine its thermal death point. *Proceedings of the Royal Society of London* **27**, 332–350 (1878).

37. Lenski, R. E., Rose, M. R., Simpson, S. C. & Tadler, S. C. Long-Term Experimental Evolution in *Escherichia coli*. I. Adaptation and Divergence During 2,000 Generations. *Am Nat* **138**, 1315–1341 (1991).

38. Bruger, E. L. & Marx, C. J. A decade of genome sequencing has revolutionized studies of experimental evolution. *Curr Opin Microbiol* **45**, 149–155 (2018).

39. Nordgaard, M. *et al.* Experimental evolution of Bacillus subtilis on Arabidopsis thaliana roots reveals fast adaptation and improved root colonization. *iScience* **25**, 104406 (2022).

40. Good, B. H., McDonald, M. J., Barrick, J. E., Lenski, R. E. & Desai, M. M. The dynamics of molecular evolution over 60,000 generations. *Nature* **551**, 45–50 (2017).

41. Johnson, M. S. *et al.* Phenotypic and molecular evolution across 10,000 generations in laboratory budding yeast populations. *Elife* **10**, e63910 (2021).

42. Nilsson, A. I. *et al.* Bacterial genome size reduction by experimental evolution. *Proc Natl Acad Sci U S A* **102**, 12112–12116 (2005).

43. Ackermann, M., Schauerte, A., Stearns, S. C. & Jenal, U. Experimental evolution of aging in a bacterium. *BMC Evol Biol* **7**, 126 (2007).

44. Lang, G. I. *et al.* Pervasive genetic hitchhiking and clonal interference in forty evolving yeast populations. *Nature* **500**, 571–574 (2013).

45. Koeppel, A. F. *et al.* Speedy speciation in a bacterial microcosm: new species can arise as frequently as adaptations within a species. *ISME J* **7**, 1080–1091 (2013).

46. Lenski, R. E. Revisiting the Design of the Long-Term Evolution Experiment with *Escherichia coli*. *J Mol Evol* (2023) doi:10.1007/S00239-023-10095-3.

47. Lenski, R. E. & Travisano, M. Dynamics of adaptation and diversification: a 10,000-generation experiment with bacterial populations. *Proceedings of the National Academy of Sciences* **91**, 6808–6814 (1994).

48. Tenaillon, O. *et al.* Tempo and mode of genome evolution in a 50,000-generation experiment. *Nature* **536**, 165–170 (2016).

49. Barrick, J. E. & Lenski, R. E. Genome-wide Mutational Diversity in an Evolving Population of *Escherichia coli*. *Cold Spring Harb Symp Quant Biol* **74**, sqb.2009.74.018 (2009).

50. Maddamsetti, R., Lenski, R. E. & Barrick, J. E. Adaptation, clonal interference, and frequency-dependent interactions in a long-term evolution experiment with *Escherichia coli*. *Genetics* **200**, 619–631 (2015).

51. Consuegra, J. *et al.* Insertion-sequence-mediated mutations both promote and constrain evolvability during a long-term experiment with bacteria. *Nat Commun* **12**, 980 (2021).

52. Dunham, M. J. *et al.* Characteristic genome rearrangements in experimental evolution of *Saccharomyces cerevisiae*. *Proceedings of the National Academy of Sciences* **99**, 16144–16149 (2002).

53. Hegreness, M., Shoresh, N., Hartl, D. & Kishony, R. An equivalence principle for the incorporation of favorable mutations in asexual populations. *Science (1979)* **311**, 1615–1617 (2006).

54. Cooper, V. S. *et al.* Experimental Evolution In Vivo To Identify Selective Pressures during *Pneumococcal Colonization*. *mSystems* **5**, e00352-20 (2020).

55. Poltak, S. R. & Cooper, V. S. Ecological succession in long-term experimentally evolved biofilms produces synergistic communities. *ISME Journal* **5**, 369–378 (2011).

56. Zhang, Q. *et al.* Acceleration of emergence of bacterial antibiotic resistance in connected microenvironments. *Science (1979)* **333**, 1764–1767 (2011).

57. Traverse, C. C., Mayo-Smith, L. M., Poltak, S. R. & Cooper, V. S. Tangled bank of experimentally evolved *Burkholderia* biofilms reflects selection during chronic infections. *Proceedings of the National Academy of Sciences* **110**, E250–E259 (2013).

58. Li, E. *et al.* Experimental-evolution-driven identification of arabidopsis rhizosphere competence genes in *Pseudomonas protegens*. *mBio* **12**, e00927-21 (2021).

59. Harris, K. B., Flynn, K. M. & Cooper, V. S. Polygenic Adaptation and Clonal Interference Enable Sustained Diversity in Experimental Pseudomonas aeruginosa Populations. *Mol Biol Evol* **38**, 5359–5375 (2021).

60. Stewart, P. S. & Franklin, M. J. Physiological heterogeneity in biofilms. *Nat Rev Microbiol* **6**, 199–210 (2008).

61. Rainey, P. B. & Travisano, M. Adaptive radiation in a heterogeneous environment. *Nature* **394**, 69–72 (1998).

62. Kassen, R. Toward a General Theory of Adaptive Radiation. *Ann N Y Acad Sci* **1168**, 3–22 (2009).

63. Spiers, A. J. A Mechanistic Explanation Linking Adaptive Mutation, Niche Change, and Fitness Advantage for the Wrinkly Spreader. *Int J Evol Biol* **2014**, 675432 (2014).

64. Leiman, S. A., Arboleda, L. C., Spina, J. S. & McLoon, A. L. SinR is a mutational target for fine-tuning biofilm formation in laboratory-evolved strains of *Bacillus subtilis*. *BMC Microbiol* **14**, 301 (2014).

65. Bjedov, I. *et al.* Stress-induced mutagenesis in bacteria. *Science (1979)* **300**, 1404–1409 (2003).

66. Halligan, D. L. & Keightley, P. D. Spontaneous Mutation Accumulation Studies in Evolutionary Genetics. *Annu Rev Ecol Evol Syst* **40**, 151–172 (2009).

67. Ellis, C. N., Traverse, C. C., Mayo-Smith, L., Buskirk, S. W. & Cooper, V. S. Character displacement and the evolution of niche complementarity in a model biofilm community. *Evolution (N Y)* **69**, 283–293 (2015).

68. Santos-Lopez, A., Marshall, C. W., Scribner, M. R., Snyder, D. J. & Cooper, V. S. Evolutionary pathways to antibiotic resistance are dependent upon environmental structure and bacterial lifestyle. *Elife* **8**, e47612 (2019).

69. Scribner, M. R. *et al.* Parallel evolution of tobramycin resistance across species and environments. *mBio* **11**, e00932-20 (2020).

70. Turner, C. B., Buskirk, S. W., Harris, K. B. & Cooper, V. S. Negative frequency-dependent selection maintains coexisting genotypes during fluctuating selection. *Mol Ecol* **29**, 138 (2020).

71. Turner, C. B., Marshall, C. W. & Cooper, V. S. Parallel genetic adaptation across environments differing in mode of growth or resource availability. *Evol Lett* **2**, 355–367 (2018).

72. Lenski, R. E. What is adaptation by natural selection? Perspectives of an experimental microbiologist. *PLoS Genet* **13**, e1006668 (2017).

73. Kuchina, A. *et al.* Microbial single-cell RNA sequencing by split-pool barcoding. *Science (1979)* **371**, aba5257 (2021).

74. Imdahl, F., Vafadarnejad, E., Homberger, C., Saliba, A. & Vogel, J. Single-cell RNA-sequencing reports growth-condition-specific global transcriptomes of individual bacteria. *Nat Microbiol* **5**, 1202–1206 (2020).

75. Westermann, A. J. & Vogel, J. Cross-species RNA-seq for deciphering host–microbe interactions. *Nat Rev Genet* **22**, 361–378 (2021).

76. Dar, D., Dar, N., Cai, L. & Newman, D. K. Spatial transcriptomics of planktonic and sessile bacterial populations at single-cell resolution. *Science (1979)* **373**, eabi4882 (2021).

77. Chen, A. *et al.* Spatiotemporal transcriptomic atlas of mouse organogenesis using DNA nanoball-patterned arrays. *Cell* **185**, 1777-1792.e21 (2022).

78. Tenaillon, O. *et al.* The Molecular Diversity of Adaptive Convergence. *Science (1979)* **335**, 457–461 (2012).

79. Levy, S. E. & Myers, R. M. Advancements in Next-Generation Sequencing. *Annu Rev Genomics Hum Genet* **17**, 95–115 (2016).

80. Qin, J. *et al.* A human gut microbial gene catalogue established by metagenomic sequencing. *Nature* **464**, 59–65 (2010).

81. Barrick, J. E. & Lenski, R. E. Genome dynamics during experimental evolution. *Nat Rev Genet* **14**, 827–839 (2013).

82. Deatherage, D. E. & Barrick, J. E. Identification of Mutations in Laboratory-Evolved Microbes from Next-Generation Sequencing Data Using breseq. *Methods Mol Biol* **1151**, 165–188 (2014).

83. Barrick, J. E. *et al.* Identifying structural variation in haploid microbial genomes from short-read resequencing data using breseq. *BMC Genomics* **15**, 1039 (2014).

84. Behringer, M. G. *et al. Escherichia coli* cultures maintain stable subpopulation structure during long-term evolution. *Proceedings of the National Academy of Sciences* **115**, E4642–E4650 (2018).

85. Levy, S. F. *et al.* Quantitative evolutionary dynamics using high-resolution lineage tracking. *Nature* **519**, 181–186 (2015).

86. Fogle, C. A., Nagle, J. L. & Desai, M. M. Clonal Interference, Multiple Mutations and Adaptation in Large Asexual Populations. *Genetics* **180**, 2163–2173 (2008).

87. Park, S. C. & Krug, J. Clonal interference in large populations. *Proc Natl Acad Sci U S A* **104**, 18135–18140 (2007).

88. Hegreness, M., Shoresh, N., Hartl, D. & Kishony, R. An equivalence principle for the incorporation of favorable mutations in asexual populations. *Science (1979)* **311**, 1615–1617 (2006).

89. Levy, S. F. *et al.* Quantitative evolutionary dynamics using high-resolution lineage tracking. *Nature* **519**, 181–186 (2015).

90. Cvijović, I., Nguyen Ba, A. N. & Desai, M. M. Experimental Studies of Evolutionary Dynamics in Microbes. *Trends in Genetics* **34**, 693–703 (2018).

91. Bailey, S. F., Blanquart, F., Bataillon, T. & Kassen, R. What drives parallel evolution?: How population size and mutational variation contribute to repeated evolution. *BioEssays* **39**, 1600176 (2017).

92. Bolnick, D. I., Barrett, R. D. H., Oke, K. B., Rennison, D. J. & Stuart, Y. E. (Non)Parallel Evolution. *Annu. Rev. Ecol. Evol. Syst* **49**, 303–333 (2018).

93. Bailey, S. F., Rodrigue, N. & Kassen, R. The Effect of Selection Environment on the Probability of Parallel Evolution. *Mol Biol Evol* **32**, 1436–1448 (2015).

94. Lachapelle, J., Reid, J. & Colegrave, N. Repeatability of adaptation in experimental populations of different sizes. *Proceedings of the Royal Society B: Biological Sciences* **282**, 20143033 (2015).

95. Miller, C. R., Joyce, P. & Wichman, H. A. Mutational Effects and Population Dynamics During Viral Adaptation Challenge Current Models. *Genetics* **187**, 185–202 (2011).

96. Tarkington, J. & Zufall, R. A. Temperature affects the repeatability of evolution in the microbial eukaryote *Tetrahymena thermophila*. *Ecol Evol* **11**, 13139 (2021).

97. Dragoš, A. *et al.* Collapse of genetic division of labour and evolution of autonomy in pellicle biofilms. *Nat Microbiol* **3**, 1451–1460 (2018).

98. Ferenci, T. Trade-off Mechanisms Shaping the Diversity of Bacteria. *Trends Microbiol* **24**, 209–223 (2016).

99. Philippe, N., Pelosi, L., Lenski, R. E. & Schneider, D. Evolution of penicillin-binding protein 2 concentration and cell shape during a long-term experiment with *Escherichia coli*. *J Bacteriol* **191**, 909–921 (2009).

100. Behrends, V. *et al.* A metabolic trade-off between phosphate and glucose utilization in *Escherichia coli*. *Mol. BioSyst.* **10**, 2820–2822 (2014).

101. Guttenplan, S. B. & Kearns, D. B. Regulation of flagellar motility during biofilm formation. *FEMS Microbiol Rev* **37**, 849–871 (2013).

102. van Ditmarsch, D. *et al.* Convergent evolution of hyperswarming leads to impaired biofilm formation in pathogenic bacteria. *Cell Rep* **4**, 697–708 (2013).

103. Kearns, D. B., Chu, F., Branda, S. S., Kolter, R. & Losick, R. A master regulator for biofilm formation by Bacillus subtilis. *Mol Microbiol* **55**, 739–749 (2005).

104. Marquez, L. M. *et al.* Studies of σ^D-dependent functions in *Bacillus subtilis*. *J Bacteriol* **172**, 3435–3443 (1990).

105. Hölscher, T. *et al.* Motility, Chemotaxis and Aerotaxis Contribute to Competitiveness during Bacterial Pellicle Biofilm Development. *J Mol Biol* **427**, 3695–3708 (2015).

106. Hölscher, T. *et al.* Impaired competence in flagellar mutants of Bacillus subtilis is connected to the regulatory network governed by DegU. *Environ Microbiol Rep* **10**, 23–32 (2018).

107. Chen, Y., Chai, Y., Guo, J.-H. & Losick, R. Evidence for Cyclic Di-GMP-Mediated Signaling in Bacillus subtilis. *J Bacteriol* **194**, 5080–5090 (2012).

108. Gao, X. *et al.* Functional Characterization of Core Components of the Bacillus subtilis Cyclic-Di-GMP Signaling Pathway. *J Bacteriol* **195**, 4782–4792 (2013).

109. Moreno-Letelier, A., Olmedo, G., Eguiarte, L. E., Martinez-Castilla, L. & Souza, V. Parallel Evolution and Horizontal Gene Transfer of the *pst* Operon in Firmicutes from Oligotrophic Environments. *Int J Evol Biol* **2011**, 781642 (2011).

110. Harwood, C. R. Introduction to the Biotechnology of *Bacillus*. in *Bacillus* 1–4 (Springer US, 1989). doi:10.1007/978-1-4899-3502-1_1.

111. Zeigler, D. R. & Perkins, J. B. The Genus *Bacillus*. in *Practical Handbook of Microbiology* 249–278 (CRC Press, 2021). doi:10.1201/9781003099277-24.

112. Nicholson, W. L. Roles of *Bacillus* endospores in the environment. *Cellular and Molecular Life Sciences* **59**, 410–416 (2002).

113. Hong, H. A. *et al. Bacillus subtilis* isolated from the human gastrointestinal tract. *Res Microbiol* **160**, 134–143 (2009).

114. Miranda, C. A. C., Martins, O. B. & Clementino, M. M. Species-level identification of *Bacillus* strains isolates from marine sediments by conventional biochemical, 16S rRNA gene sequencing and inter-tRNA gene sequence lengths analysis. *Antonie van Leeuwenhoek, International Journal of General and Molecular Microbiology* **93**, 297–304 (2008).

115. Barbosa, T. M., Serra, C. R., La Ragione, R. M., Woodward, M. J. & Henriques, A. O. Screening for *Bacillus* Isolates in the Broiler Gastrointestinal Tract. *Appl Environ Microbiol* **71**, 968 (2005).

116. Alcaraz, L. D. *et al.* Understanding the evolutionary relationships and major traits of *Bacillus* through comparative genomics. *BMC Genomics* **11**, 1–17 (2010).

117. Riesenman, P. J. & Nicholson, W. L. Role of the Spore Coat Layers in *Bacillus subtilis* Spore Resistance to Hydrogen Peroxide, Artificial UV-C, UV-B, and Solar UV Radiation. *Appl Environ Microbiol* **66**, 620 (2000).

118. Nicholson, W. L., Munakata, N., Horneck, G., Melosh, H. J. & Setlow, P. Resistance of *Bacillus* Endospores to Extreme Terrestrial and Extraterrestrial Environments. *Microbiology and Molecular Biology Reviews* **64**, 548–572 (2000).

119. Higgins, D. & Dworkin, J. Recent progress in *Bacillus subtilis* sporulation. *FEMS Microbiol Rev* **36**, 131–148 (2012).

120. Moir, A. & Cooper, G. Spore Germination. *Microbiol Spectr* **3**, (2015).

121. López, D., Vlamakis, H. & Kolter, R. Biofilms. *Cold Spring Harb Perspect Biol* **2**, a000398 (2010).

122. Gupta, R. S., Patel, S., Saini, N. & Chen, S. Robust demarcation of 17 distinct *Bacillus* species clades, proposed as novel *Bacillaceae genera*, by phylogenomics and comparative genomic analyses: Description of *Robertmurraya kyonggiensis* sp. nov. and proposal for an emended genus <. *Int J Syst Evol Microbiol* **70**, 5753–5798 (2020).

123. Jeyaram, K. *et al.* Distinct differentiation of closely related species of *Bacillus subtilis* group with industrial importance. *J Microbiol Methods* **87**, 161–164 (2011).

124. Caulier, S. *et al.* Overview of the Antimicrobial Compounds Produced by Members of the Bacillus subtilis Group. *Front Microbiol* **10**, 302 (2019).

125. Kovács, Á. T. *Bacillus subtilis*. *Trends Microbiol* **27**, 724–725 (2019).

126. Konkol, M. A., Blair, K. M. & Kearns, D. B. Plasmid-encoded comi inhibits competence in the ancestral 3610 strain of *Bacillus subtilis*. *J Bacteriol* **195**, 4085–4093 (2013).

127. Khurana, H. *et al.* Genomic insights into the phylogeny of *Bacillus* strains and elucidation of their secondary metabolic potential. *Genomics* **112**, 3191–3200 (2020).

128. Pilo, P. & Frey, J. Pathogenicity, population genetics and dissemination of *Bacillus anthracis*. *Infection, Genetics and Evolution* **64**, 115–125 (2018).

129. Granum, P. E. Spotlight on Bacillus cereus and its food poisoning toxins. *FEMS Microbiol Lett* **364**, fnx071 (2017).

130. Ehling-Schulz, M., Lereclus, D. & Koehler, T. M. The *Bacillus cereus* Group: Bacillus Species with Pathogenic Potential. in *Gram-Positive Pathogens* 875–902 (ASM Press, 2019). doi:10.1128/9781683670131.ch55.

131. Ivanova, N. *et al.* Genome sequence of Bacillus cereus and comparative analysis with *Bacillus anthracis*. *Nature* **423**, 87–91 (2003).

132. Cairns, L. S., Hobley, L. & Stanley-Wall, N. R. Biofilm formation by *Bacillus subtilis*: new insights into regulatory strategies and assembly mechanisms. *Mol Microbiol* **93**, 587–598 (2014).

133. Slamti, L., Perchat, S., Huillet, E. & Lereclus, D. Quorum sensing in *Bacillus thuringiensis* is required for completion of a full infectious cycle in the insect. *Toxins (Basel)* **6**, 2239–2255 (2014).

134. Fagerlund, A. *et al.* SinR controls enterotoxin expression in *Bacillus thuringiensis* biofilms. *PLoS One* **9**, e87532 (2014).

135. Tan, S. J. and T. Spore Formation in *Bacillus subtilis*. *Bone* **23**, 212–225 (2008).

136. Hamon, M. A. & Lazazzera, B. A. The sporulation transcription factor Spo0A is required for biofilm development in *Bacillus subtilis*. *Mol Microbiol* **42**, 1199–1209 (2001).

137. Verplaetse, E., Slamti, L., Gohar, M. & Lereclus, D. Two distinct pathways lead *Bacillus thuringiensis* to commit to sporulation in biofilm. *Res Microbiol* **168**, 388–393 (2017).

138. Gohar, M. *et al.* The PlcR Virulence Regulon of *Bacillus cereus*. *PLoS One* **3**, e2793 (2008).

139. Mahillon, J., Rezsöhazy, R., Hallet, B. & Delcour, J. IS*231* and other *Bacillus thuringiensis* transposable elements: A review. *Genetica* **93**, 13–26 (1994).

140. Joung, K. B. & Côté, J. C. Distribution analysis of IS*231*-like sequences among *Bacillus thuringiensis* serovars inferred from restriction fragment length polymorphisms. *Curr Microbiol* **47**, 417–424 (2003).

141. Mahillon, J., Seurinck, J., van Rompuy, L., Delcour, J. & Zabeau, M. Nucleotide sequence and structural organization of an insertion sequence element (IS*231*) from *Bacillus thuringiensis* strain berliner 1715. *EMBO J* **4**, 3895–3899 (1985).

142. Qiu, N. *et al.* Prevalence and diversity of insertion sequences in the genome of *Bacillus thuringiensis* YBT-1520 and comparison with other *Bacillus cereus* group members. *FEMS Microbiol Lett* **310**, 9–16 (2010).

143. Nagai, T., Tran, L. S. P., Inatsu, Y. & Itoh, Y. A new IS4 family insertion sequence, IS4Bsu1, responsible for genetic instability of poly-γ-glutamic acid production in *Bacillus subtilis*. *J Bacteriol* **182**, 2387–2392 (2000).

144. Miller, S. R. *et al.* Bacterial Adaptation by a Transposition Burst of an Invading IS Element. *Genome Biol Evol* **13**, evab245 (2021).

145. Schneider, D. & Lenski, R. E. Dynamics of insertion sequence elements during experimental evolution of bacteria. *Res Microbiol* **155**, 319–327 (2004).

146. Seyedsayamdost, M. R. Toward a global picture of bacterial secondary metabolism. *J Ind Microbiol Biotechnol* **46**, 301–311 (2019).

147. Romero, D., Traxler, M. F., López, D. & Kolter, R. Antibiotics as signal molecules. *Chem Rev* **111**, 5492–5505 (2011).

148. Straight, P. D., Willey, J. M. & Kolter, R. Interactions between *Streptomyces coelicolor* and *Bacillus subtilis*: Role of surfactants in raising aerial structures. *J Bacteriol* **188**, 4918–4925 (2006).

149. Stein, T. *Bacillus subtilis* antibiotics: structures, syntheses and specific functions. *Mol Microbiol* **56**, 845–857 (2005).

150. Kaspar, F., Neubauer, P. & Gimpel, M. Bioactive Secondary Metabolites from Bacillus subtilis: A Comprehensive Review. *J Nat Prod* **82**, 2038–2053 (2019).

151. Ongena, M. & Jacques, P. *Bacillus* lipopeptides: versatile weapons for plant disease biocontrol. *Trends Microbiol* **16**, 115–125 (2008).

152. Romano, A., Vitullo, D., Senatore, M., Lima, G. & Lanzotti, V. Antifungal cyclic lipopeptides from *Bacillus amyloliquefaciens* strain BO5A. *J Nat Prod* **76**, 2019–2025 (2013).

153. Qi, G. *et al.* Lipopeptide induces apoptosis in fungal cells by a mitochondria-dependent pathway. *Peptides (N.Y.)* **31**, 1978–1986 (2010).

154. Dimkić, I. *et al.* Characterization and evaluation of two *Bacillus* strains, SS-12.6 and SS-13.1, as potential agents for the control of phytopathogenic bacteria and fungi. *Biological Control* **65**, 312–321 (2013).

155. Peypoux, F., Bonmatin, J. M. & Wallach, J. Recent trends in the biochemistry of surfactin. *Appl Microbiol Biotechnol* **51**, 553–563 (1999).

156. Nakano, M. M. *et al. srfA* is an operon required for surfactin production, competence development, and efficient sporulation in Bacillus subtilis. *J Bacteriol* **173**, 1770–1778 (1991).

157. Rahman, F. Bin, Sarkar, B., Moni, R. & Rahman, M. S. Molecular genetics of surfactin and its effects on different sub-populations of *Bacillus subtilis*. *Biotechnology Reports* **32**, e00686 (2021).

158. Thérien, M. *et al.* Surfactin production is not essential for pellicle and root-associated biofilm development of *Bacillus subtilis*. *Biofilm* **2**, 100021 (2020).

159. Sauer, K. *et al.* The biofilm life cycle: expanding the conceptual model of biofilm formation. *Nat Rev Microbiol* **20**, 608–620 (2022).

160. Flemming, H. C. & Wuertz, S. Bacteria and archaea on Earth and their abundance in biofilms. *Nat Rev Microbiol* **17**, 247–260 (2019).

161. Hall-Stoodley, L., Costerton, J. W. & Stoodley, P. Bacterial biofilms: From the natural environment to infectious diseases. *Nature Reviews Microbiology* vol. 2 95–108 Preprint at https://doi.org/10.1038/nrmicro821 (2004).

162. Martin, M., Hölscher, T., Dragoš, A., Cooper, V. S. & Kovács, Á. T. Laboratory evolution of microbial interactions in bacterial biofilms. *J Bacteriol* **198**, 2564–2571 (2016).

163. Kovács, Á. T. & Dragoš, A. Evolved Biofilm: Review on the Experimental Evolution Studies of *Bacillus subtilis* Pellicles. *Journal of Molecular Biology* vol. 431 4749–4759 Preprint at https://doi.org/10.1016/j.jmb.2019.02.005 (2019).

164. Bais, H. P., Fall, R. & Vivanco, J. M. Biocontrol of Bacillus subtilis against Infection of Arabidopsis Roots by *Pseudomonas syringae* Is Facilitated by Biofilm Formation and Surfactin Production. *Plant Physiol* **134**, 307–319 (2004).

165. Kjeldgaard, B. *et al.* Fungal hyphae colonization by *Bacillus subtilis* relies on biofilm matrix components. *Biofilm* **1**, 100007 (2019).

166. Noirot-Gros, M. F. *et al.* Functional Imaging of Microbial Interactions With Tree Roots Using a Microfluidics Setup. *Front Plant Sci* **11**, 408 (2020).

167. Arnaouteli, S., Bamford, N. C., Stanley-Wall, N. R. & Kovács, Á. T. *Bacillus subtilis* biofilm formation and social interactions. *Nat Rev Microbiol* **19**, 600–614 (2021).

168. Vlamakis, H., Chai, Y., Beauregard, P., Losick, R. & Kolter, R. Sticking together: Building a biofilm the *Bacillus subtilis* way. *Nat Rev Microbiol* **11**, 157–168 (2013).

169. Claessen, D., Rozen, D. E., Kuipers, O. P., Søgaard-Andersen, L. & Van Wezel, G. P. Bacterial solutions to multicellularity: a tale of biofilms, filaments and fruiting bodies. *Nature Reviews Microbiology 2014 12:2* **12**, 115–124 (2014).

170. Branda, S. S., González-Pastor, J. E., Ben-Yehuda, S., Losick, R. & Kolter, R. Fruiting body formation by *Bacillus subtilis*. *Proceedings of the National Academy of Sciences* **98**, 11621–11626 (2001).

171. Romero, D., Aguilar, C., Losick, R. & Kolter, R. Amyloid fibers provide structural integrity to *Bacillus subtilis* biofilms. *Proc Natl Acad Sci U S A* **107**, 2230–2234 (2010).

172. Kobayashi, K. & Iwano, M. BslA(YuaB) forms a hydrophobic layer on the surface of *Bacillus subtilis* biofilms. *Mol Microbiol* **85**, 51–66 (2012).

173. Hobley, L. *et al.* BslA is a self-assembling bacterial hydrophobin that coats the *Bacillus subtilis* biofilm. *Proc Natl Acad Sci U S A* **110**, 13600–13605 (2013).

174. Peng, N. *et al.* The exopolysaccharide-eDNA interaction modulates 3D architecture of *Bacillus subtilis* biofilm. doi:10.1186/s12866-020-01789-5.

175. Branda, S. S. *et al.* Genes involved in formation of structured multicellular communities by *Bacillus subtilis*. *J Bacteriol* **186**, 3970–3979 (2004).

176. Seminara, A. *et al.* Osmotic spreading of *Bacillus subtilis* biofilms driven by an extracellular matrix. *Proc Natl Acad Sci U S A* **109**, 1116–1121 (2012).

177. Guttenplan, S. B., Blair, K. M. & Kearns, D. B. The EpsE Flagellar Clutch Is Bifunctional and Synergizes with EPS Biosynthesis to Promote *Bacillus subtilis* Biofilm Formation. *PLoS Genet* **6**, e1001243 (2010).

178. Romero, D., Vlamakis, H., Losick, R. & Kolter, R. An accessory protein required for anchoring and assembly of amyloid fibres in *B. subtilis* biofilms. *Mol Microbiol* **80**, 1155–1168 (2011).

179. Serrano, M. *et al.* A *Bacillus subtilis* secreted protein with a role in endospore coat assembly and function. *J Bacteriol* **181**, 3632–3643 (1999).

180. Dragoš, A. *et al.* Division of Labor during Biofilm Matrix Production. *Current Biology* **28**, 1903-1913.e5 (2018).

181. West, S. A., Griffin, A. S., Gardner, A. & Diggle, S. P. Social evolution theory for microorganisms. *Nature Reviews Microbiology 2006 4:8* **4**, 597–607 (2006).

182. Fujita, M., González-Pastor, J. E. & Losick, R. High- and low-threshold genes in the Spo0A regulon of *Bacillus subtilis*. *J Bacteriol* **187**, 1357–1368 (2005).

183. Molle, V. *et al.* The Spo0A regulon of *Bacillus subtilis*. *Mol Microbiol* **50**, 1683–1701 (2003).

184. Jiang, M., Shao, W., Perego, M. & Hoch, J. A. Multiple histidine kinases regulate entry into stationary phase and sporulation in *Bacillus subtilis*. *Mol Microbiol* **38**, 535–542 (2000).

185. Murray, E. J., Kiley, T. B. & Stanley-Wall, N. R. A pivotal role for the response regulator DegU in controlling multicellular behaviour. *Microbiology (N Y)* **155**, 1–8 (2009).

186. Marlow, V. L. *et al.* Phosphorylated DegU manipulates cell fate differentiation in the *Bacillus subtilis* biofilm. *J Bacteriol* **196**, 16–27 (2014).

187. Stanley, N. R. & Lazazzera, B. A. Defining the genetic differences between wild and domestic strains of *Bacillus subtilis* that affect poly-γ-dl-glutamic acid production and biofilm formation. *Mol Microbiol* **57**, 1143–1158 (2005).

188. Verhamme, D. T., Kiley, T. B. & Stanley-Wall, N. R. DegU co-ordinates multicellular behaviour exhibited by *Bacillus subtilis*. *Mol Microbiol* **65**, 554–568 (2007).

189. Verhamme, D. T., Murray, E. J. & Stanley-Wall, N. R. DegU and Spo0A jointly control transcription of two loci required for complex colony development by *Bacillus subtilis*. *J Bacteriol* **91**, 100–108 (2009).

190. Cairns, L. S., Marlow, V. L., Bissett, E., Ostrowski, A. & Stanley-Wall, N. R. A mechanical signal transmitted by the flagellum controls signalling in *Bacillus subtilis*. *Mol Microbiol* **90**, 6–21 (2013).

191. Hengge, R. Principles of c-di-GMP signalling in bacteria. *Nat Rev Microbiol* **7**, 263–273 (2009).

192. Purcell, E. B. & Tamayo, R. Cyclic diguanylate signaling in Gram-positive bacteria. *FEMS Microbiol Rev* **40**, 753–773 (2016).

193. Sadiq, F. A. *et al.* New mechanistic insights into the motile-to-sessile switch in various bacteria with particular emphasis on *Bacillus subtilis* and *Pseudomonas aeruginosa*: a review. *Biofouling* **33**, 306–326 (2017).

194. Luo, Y. & Helmann, J. D. A σ^D-dependent antisense transcript modulates expression of the cyclic-di-AMP hydrolase GdpP in *Bacillus subtilis*. *Microbiology (N Y)* **158**, 2732–2741 (2012).

195. Simm, R., Morr, M., Kader, A., Nimtz, M. & Römling, U. GGDEF and EAL domains inversely regulate cyclic di-GMP levels and transition from sessility to motility. *Mol Microbiol* **53**, 1123–1134 (2004).

196. Tischler, A. D. & Camilli, A. Cyclic diguanylate (c-di-GMP) regulates Vibrio cholerae biofilm formation. *Mol Microbiol* **53**, 857–869 (2004).

197. Schmidt, A. J., Ryjenkov, D. A. & Gomelsky, M. The ubiquitous protein domain EAL is a cyclic diguanylate-specific phosphodiesterase: Enzymatically active and inactive EAL domains. *J Bacteriol* **187**, 4774–4781 (2005).

198. Kunz, S. *et al.* Cyclic di-GMP Signaling in *Bacillus subtilis* Is Governed by Direct Interactions of Diguanylate Cyclases and Cognate Receptors. *mBio* **11**, e03122-19 (2020).

199. Bedrunka, P. & Graumann, P. L. Subcellular clustering of a putative c-di-GMP-dependent exopolysaccharide machinery affecting macro colony architecture in *Bacillus subtilis*. *Environ Microbiol Rep* **9**, 211–222 (2017).

200. Weiss, C. A., Hoberg, J. A., Liu, K., Tu, B. P. & Winkler, W. C. Single-Cell Microscopy Reveals That Levels of Cyclic di-GMP Vary among *Bacillus subtilis* Subpopulations. *J Bacteriol* **201**, e00247-19 (2019).

201. Wadhwa, N. & Berg, H. C. Bacterial motility: machinery and mechanisms. *Nat Rev Microbiol* **20**, 161–173 (2022).

202. Jarrell, K. F. & McBride, M. J. The surprisingly diverse ways that prokaryotes move. *Nature Reviews Microbiology 2008 6:6* **6**, 466–476 (2008).

203. Kearns, D. B. A field guide to bacterial swarming motility. *Nature Reviews Microbiology* vol. 8 634–644 Preprint at https://doi.org/10.1038/nrmicro2405 (2010).

204. Hazelbauer, G. L. Bacterial Chemotaxis: The Early Years of Molecular Studies. *Annu Rev Microbiol* **66**, 285–303 (2012).

205. Mukherjee, S. & Kearns, D. B. The structure and regulation of flagella in *Bacillus subtilis*. *Annu Rev Genet* **48**, 319–340 (2014).

206. Chen, R., Guttenplan, S. B., Blair, K. M. & Kearns, D. B. Role of the σ^D-dependent autolysins in *Bacillus subtilis* population heterogeneity. *J Bacteriol* **191**, 5775–5784 (2009).

207. Kearns, D. B. & Losick, R. Cell population heterogeneity during growth of *Bacillus subtilis*. *Genes Dev* **19**, 3083–3094 (2005).

208. Ogura, M. & Tsukahara, K. SwrA regulates assembly of *Bacillus subtilis* DegU via its interaction with N-terminal domain of DegU. *The Journal of Biochemistry* **151**, 643–655 (2012).

209. Mordini, S. *et al.* The Role of SwrA, DegU and PD3 in *fla/che* Expression in *B. subtilis*. *PLoS One* **8**, e85065 (2013).

210. Cozy, L. M. & Kearns, D. B. Gene position in a long operon governs motility development in *Bacillus subtilis*. *Mol Microbiol* **76**, 273–285 (2010).

211. Werhane, H. *et al.* The last gene of the *fla/che* operon in *Bacillus subtilis*, *ylxL*, is required for maximal σ^D function. *J Bacteriol* **186**, 4025–4029 (2004).

212. Marquez-Magana, L. M. & Chamberlin, M. J. Characterization of the sigD transcription unit of *Bacillus subtilis*. *J Bacteriol* **176**, 2427–2434 (1994).

213. Cozy, L. M. *et al.* SlrA/SinR/SlrR inhibits motility gene expression upstream of a hypersensitive and hysteretic switch at the level of σ^D in *Bacillus subtilis*. *Mol Microbiol* **83**, 1210–1228 (2012).

214. Chai, Y., Norman, T., Kolter, R. & Losick, R. An epigenetic switch governing daughter cell separation in *Bacillus subtilis*. *Genes Dev* **24**, 754–765 (2010).

215. Caramori, T., Barillà, D., Nessi, C., Sacchi, L. & Galizzi, A. Role of FlgM in sigma D-dependent gene expression in *Bacillus subtilis*. *J Bacteriol* **178**, 3113–3118 (1996).

216. Mukherjee, S., Babitzke, P. & Kearns, D. B. FliW and FliS function independently to control cytoplasmic flagellin levels in *Bacillus subtilis*. *J Bacteriol* **195**, 297–306 (2013).

217. Chen, Y., Chai, Y., Guo, J. hua & Losick, R. Evidence for cyclic Di-GMP-mediated signaling in *Bacillus subtilis*. *J Bacteriol* **194**, 5080–5090 (2012).

218. McLoon, A. L., Guttenplan, S. B., Kearns, D. B., Kolter, R. & Losick, R. Tracing the domestication of a biofilm-forming bacterium. *J Bacteriol* **193**, 2027–2034 (2011).

219. Barreto, H. C., Cordeiro, T. N., Henriques, A. O. & Gordo, I. Rampant loss of social traits during domestication of a *Bacillus subtilis* natural isolate. *Sci Rep* **10**, 18886 (2020).

220. Maughan, H. *et al.* THE POPULATION GENETICS OF PHENOTYPIC DETERIORATION IN EXPERIMENTAL POPULATIONS OF *BACILLUS SUBTILIS*. *Evolution (N Y)* **60**, 686–695 (2006).

221. Maughan, H., Birky, C. W. & Nicholson, W. L. Transcriptome Divergence and the Loss of Plasticity in *Bacillus subtilis* after 6,000 Generations of Evolution under Relaxed Selection for Sporulation. *J Bacteriol* **191**, 428–433 (2009).

222. Maughan, H. & Nicholson, W. L. Increased Fitness and Alteration of Metabolic Pathways during *Bacillus subtilis* Evolution in the Laboratory. *Appl Environ Microbiol* **77**, 4105–4118 (2011).

223. Brown, C. T. *et al.* Whole-Genome Sequencing and Phenotypic Analysis of *Bacillus subtilis* Mutants following Evolution under Conditions of Relaxed Selection for Sporulation. *Appl Environ Microbiol* **77**, 6867–6877 (2011).

224. Nicholson, W. L. Increased competitive fitness of *Bacillus subtilis* under nonsporulating conditions via inactivation of pleiotropic regulators AlsR, SigD, and SigW. *Appl Environ Microbiol* **78**, 3500–3503 (2012).

225. SCHUERGER, A. & NICHOLSON, W. Interactive effects of hypobaria, low temperature, and CO2 atmospheres inhibit the growth of mesophilic Bacillus spp. under simulated martian conditions. *Icarus* **185**, 143–152 (2006).

226. Nicholson, W. L. *et al.* Exploring the low-pressure growth limit: Evolution of *Bacillus subtilis* in the laboratory to enhanced growth at 5 kilopascals. *Appl Environ Microbiol* **76**, 7559–7565 (2010).

227. Fajardo-Cavazos, P. *et al.* Evolution of *Bacillus subtilis* to enhanced growth at low pressure: Up-regulated transcription of *des-desKR*, encoding the fatty acid desaturase system. *Astrobiology* **12**, 258–270 (2012).

228. Waters, S. M., Zeigler, D. R. & Nicholson, W. L. Experimental evolution of enhanced growth by *Bacillus subtilis* at low atmospheric pressure: Genomic changes revealed by whole-genome sequencing. *Appl Environ Microbiol* **81**, 7525–7532 (2015).

229. Zeigler, D. R. & Nicholson, W. L. Experimental evolution of *Bacillus subtilis*. *Environ Microbiol* **19**, 3415–3422 (2017).

230. Cadet, J., Sage, E. & Douki, T. Ultraviolet radiation-mediated damage to cellular DNA. *Mutation Research/Fundamental and Molecular Mechanisms of Mutagenesis* **571**, 3–17 (2005).

231. Wassmann, M., Moeller, R., Reitz, G. & Rettberg, P. Adaptation of *Bacillus subtilis* cells to archean-like uv climate: Relevant hints of microbial evolution to remarkably increased radiation resistance. *Astrobiology* **10**, 605–615 (2010).

232. Wassmann, M. *et al.* Survival of spores of the UV-Resistant *Bacillus subtilis* strain MW01 after exposure to low-earth orbit and simulated martian conditions: Data from the space experiment ADAPT on EXPOSE-E. *Astrobiology* **12**, 498–507 (2012).

233. Martin, M. *et al.* Cheaters shape the evolution of phenotypic heterogeneity in *Bacillus subtilis* biofilms. *ISME Journal* **14**, 2302–2312 (2020).

234. Haichar, F. el Z., Heulin, T., Guyonnet, J. P. & Achouak, W. Stable isotope probing of carbon flow in the plant holobiont. *Curr Opin Biotechnol* **41**, 9–13 (2016).

235. Venturi, V. & Keel, C. Signaling in the Rhizosphere. *Trends Plant Sci* **21**, 187–198 (2016).

236. Sasse, J., Martinoia, E. & Northen, T. Feed Your Friends: Do Plant Exudates Shape the Root Microbiome? *Trends Plant Sci* **23**, 25–41 (2018).

237. Lareen, A., Burton, F. & Schäfer, P. Plant root-microbe communication in shaping root microbiomes. *Plant Mol Biol* **90**, 575–587 (2016).

238. Vives-Peris, V., de Ollas, C., Gómez-Cadenas, A. & Pérez-Clemente, R. M. Root exudates: from plant to rhizosphere and beyond. *Plant Cell Rep* **39**, 3–17 (2020).

239. Peng, G. *et al.* Potential biological control of clubroot on canola and crucifer vegetable crops. *Plant Pathol* **60**, 566–574 (2011).

240. Wei, F., Hu, X. & Xu, X. Dispersal of Bacillus subtilis and its effect on strawberry phyllosphere microbiota under open field and protection conditions. *Scientific Reports 2016 6:1* **6**, 1–9 (2016).

241. Deveau, A. *et al.* Bacterial–fungal interactions: ecology, mechanisms and challenges. *FEMS Microbiol Rev* **42**, 335–352 (2018).

242. Frey-Klett, P. *et al.* Bacterial-Fungal Interactions: Hyphens between Agricultural, Clinical, Environmental, and Food Microbiologists. *Microbiology and Molecular Biology Reviews* **75**, 583–609 (2011).

243. Lowery, C. A., Dickerson, T. J. & Janda, K. D. Interspecies and interkingdom communication mediated by bacterial quorum sensing. *Chem Soc Rev* **37**, 1337–1346 (2008).

244. Effmert, U., Kalderás, J., Warnke, R. & Piechulla, B. Volatile Mediated Interactions Between Bacteria and Fungi in the Soil. *Journal of Chemical Ecology 2012 38:6* **38**, 665–703 (2012).

245. Sadiq, F. A. *et al.* Trans-kingdom interactions in mixed biofilm communities. *FEMS Microbiol Rev* **46**, (2022).

246. Zhang, M., Pereira e Silva, M. de C., Chaib De Mares, M. & van Elsas, J. D. The mycosphere constitutes an arena for horizontal gene transfer with strong evolutionary implications for bacterial-fungal interactions. *FEMS Microbiol Ecol* **89**, 516–526 (2014).

247. Kjeldgaard, B. *et al.* Fungal hyphae colonization by *Bacillus subtilis* relies on biofilm matrix components. *Biofilm* **1**, 100007 (2019).

248. Benoit, I. *et al. Bacillus subtilis* attachment to *Aspergillus niger* hyphae results in mutually altered metabolism. *Environ Microbiol* **17**, 2099–2113 (2015).

249. Zhang, N. *et al.* Effects of different plant root exudates and their organic acid components on chemotaxis, biofilm formation and colonization by beneficial rhizosphere-associated bacterial strains. *Plant Soil* **374**, 689–700 (2014).

Chapter 6 Research articles

6.1 Study 1

Experimental evolution of *Bacillus subtilis* on *Arabidopsis thaliana* roots reveals fast adaptation and improved root colonization

Mathilde Nordgaard, Christopher Blake, Gergely Maróti, **Guohai Hu**, Yue Wang, Mikael Lenz Strube, Kovács, Á. T. (2022). *iScience* 25, 104406

Note: supplementary figures and tables are attached at the end of the study, the **dataset** is available on iScience:

https://www.cell.com/iscience/fulltext/S2589-0042(22)00677-0

iScience

CellPress
OPEN ACCESS

Article

Experimental evolution of *Bacillus subtilis* on *Arabidopsis thaliana* roots reveals fast adaptation and improved root colonization

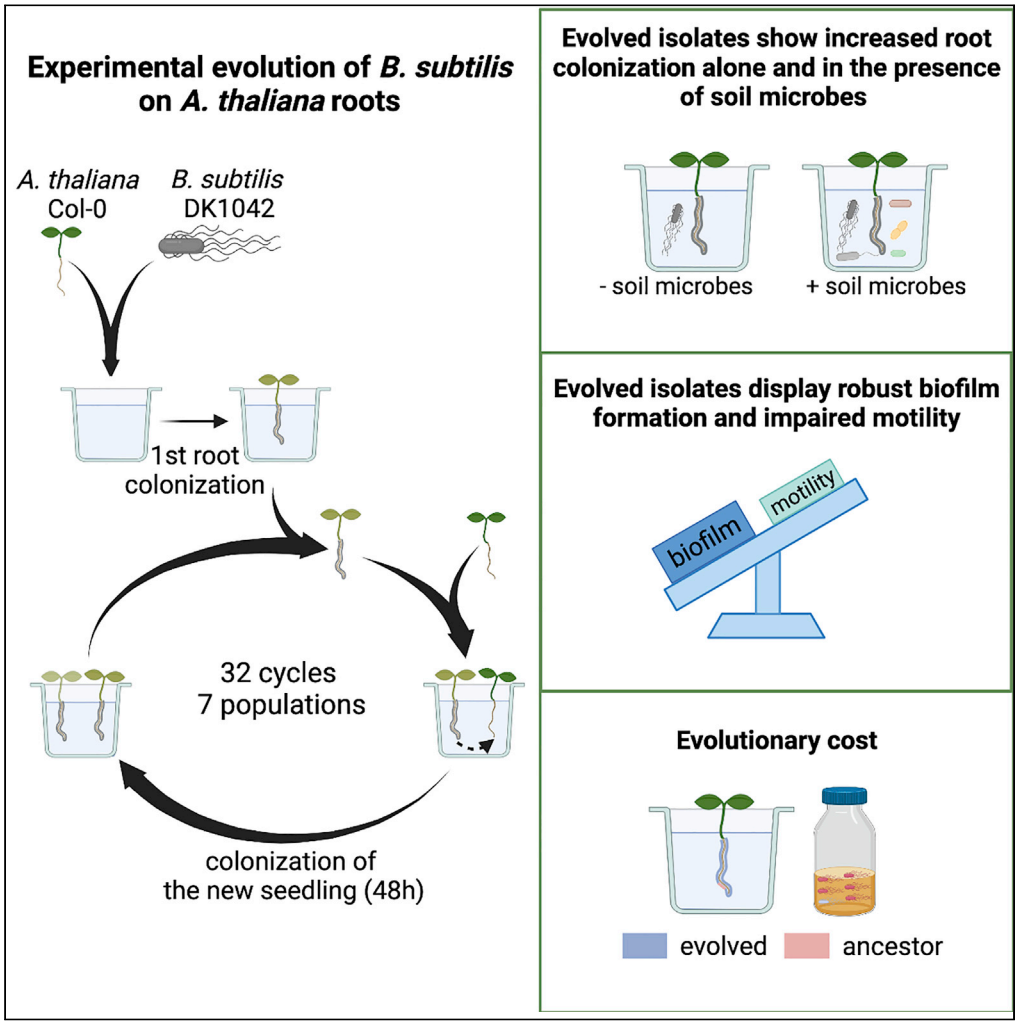

Mathilde Nordgaard, Christopher Blake, Gergely Maróti, Guohai Hu, Yue Wang, Mikael Lenz Strube, Ákos T. Kovács

atkovacs@dtu.dk

Highlights

Bacillus subtilis shows fast adaptation to *Arabidopsis thaliana* roots in a hydroponic setup

Evolved isolates exhibit robust biofilms in response to xylan and impaired motility

Adaptation to *A. thaliana* roots is accompanied by an evolutionary cost

An evolved isolate shows higher root colonization in the presence of soil bacteria

Nordgaard et al., iScience *25*, 104406
June 17, 2022
https://doi.org/10.1016/j.isci.2022.104406

iScience

CellPress
OPEN ACCESS

Article

Experimental evolution of *Bacillus subtilis* on *Arabidopsis thaliana* roots reveals fast adaptation and improved root colonization

Mathilde Nordgaard,[1] Christopher Blake,[1] Gergely Maróti,[2] Guohai Hu,[1,3] Yue Wang,[3,4] Mikael Lenz Strube,[5] and Ákos T. Kovács[1,6,*]

SUMMARY

***Bacillus subtilis* is known to promote plant growth and protect plants against disease. *B. subtilis* rapidly adapts to *Arabidopsis thaliana* root colonization, as evidenced by improved root colonizers already after 12 consecutive transfers between seedlings in a hydroponic setup. Re-sequencing of single evolved isolates and endpoint populations revealed mutations in genes related to different bacterial traits, in accordance with evolved isolates displaying increased root colonization associated with robust biofilm formation in response to the plant polysaccharide xylan and impaired motility. Interestingly, evolved isolates suffered a fitness disadvantage in a non-selective environment, demonstrating an evolutionary cost of adaptation to the plant root. Finally, increased root colonization by an evolved isolate was also demonstrated in the presence of resident soil microbes. Our findings highlight how a plant growth-promoting rhizobacterium rapidly adapts to an ecologically relevant environment and reveal evolutionary consequences that are fundamental to consider when evolving strains for biocontrol purposes.**

INTRODUCTION

The nutrient-rich rhizosphere is a hotspot for microbial activity, containing up to 10^{11} bacteria per gram root (Egamberdieva et al., 2008) and housing more than 30,000 prokaryotic species (Mendes et al., 2011). Among those are beneficial bacteria which are actively recruited by the plant through root exudate secretion and subsequently colonize the root from where they benefit the plant through various mechanisms (Berendsen et al., 2012, 2018; Mendes et al., 2011; Rudrappa et al., 2008; Trivedi et al., 2020). One well-known plant growth-promoting rhizobacterium (PGPR) is the spore-forming *B. subtilis* that has been isolated from various plant species (Cazorla et al., 2007; Fall et al., 2004; Huang et al., 2017; Pandey and Palni, 1997). Its plant-beneficial traits (Blake et al., 2021a) and promising role as a biocontrol agent (Fira et al., 2018; Kiesewalter et al., 2021; Ongena and Jacques, 2008) have fueled the interest in studying *B. subtilis*–plant interactions and led to the elucidation of mechanisms involved in the establishment of *B. subtilis* on the root and behind its plant beneficial properties.

An obvious prerequisite for successful root colonization is the ability of the bacterium to reach the plant root. Chemotaxis toward root exudates was shown to be important for the early colonization of *A. thaliana* roots by *B. subtilis* under hydroponic conditions (Allard-Massicotte et al., 2016), whereas solid surface motility has been suggested to play a role during tomato root colonization in vermiculites (Tian et al., 2021). After reaching the plant root, *B. subtilis* initiates biofilm formation (Allard-Massicotte et al., 2016; Bais et al., 2004; Beauregard et al., 2013; Chen et al., 2013). Similar to *in vitro* conditions, the formation of plant root-associated biofilms depends on the production of the matrix components EPS and TasA (Beauregard et al., 2013; Branda et al., 2006; Chen et al., 2013; Dragoš et al., 2018a). The expression of the operons involved in matrix production, *epsA-O* and *tapA-sipW-tasA*, is controlled by the biofilm repressor SinR (Chu et al., 2006; Kearns et al., 2005). In response to environmental cues, one or more of the five histidine kinases, KinA-E, are activated resulting in phosphorylation of the master regulator Spo0A through a phosphorelay (Jiang et al., 2000). At threshold concentrations of Spo0A ~ P, SinI is produced (Fujita et al., 2005), which binds to and inhibits SinR (Bai et al., 1993), resulting in matrix gene expression. As an environmental cue for root colonization, root exudates from tomatoes were shown to

[1]Bacterial Interactions and Evolution Group, DTU Bioengineering, Technical University of Denmark, 2800 Kongens Lyngby, Denmark

[2]Institute of Plant Biology, Biological Research Centre, Eötvös Loránd Research Network (ELKH), 6726 Szeged, Hungary

[3]China National GeneBank, BGI-Shenzhen, 518120 Shenzhen, China

[4]BGI-Beijing, BGI-Shenzhen, 100101 Beijing, China

[5]Bacterial Ecophysiology and Biotechnology Group, DTU Bioengineering, Technical University of Denmark, 2800 Kongens Lyngby, Denmark

[6]Lead contact

*Correspondence: atkovacs@dtu.dk

https://doi.org/10.1016/j.isci.2022.104406

trigger biofilm formation in *B. subtilis* in a KinD-dependent manner (Chen et al., 2012), whereas another study reported biofilm induction by plant polysaccharides via KinC and KinD (Beauregard et al., 2013). *B. subtilis* benefits from such microbe–plant interactions by acquiring carbon source from the plants. In turn, *B. subtilis* protects the plant against disease directly by producing antimicrobials (Asaka and Shoda, 1996; Bais et al., 2004; Chen et al., 2013; Kiesewalter et al., 2021) and indirectly through niche competition (Köhl et al., 2019; Lugtenberg and Kamilova, 2009) and elicitation of induced systemic resistance in the plant (Akram et al., 2015; Rudrappa et al., 2008). Moreover, *B. subtilis* promotes plant growth by improving nutrient availability and producing growth-promoting phytohormones (Blake et al., 2021a).

Mutualistic bacteria-plant interactions are a result of a long-term co-evolution of bacteria and plants that started with the colonization of land by ancestral plants 450 million years ago (Hassani et al., 2018). Here, we were interested in studying how *B. subtilis* adapts to plant roots on a much shorter evolutionary timescale. Experimental evolution (EE) provides a powerful tool to study microbial adaptation to different environments in real-time (Kawecki et al., 2012; Lenski, 2017). We recently studied EE of *B. subtilis* on *A. thaliana* plants roots, which revealed diversification of *B. subtilis* into three distinct morphotypes. A mix of the three morphotypes displayed increased root colonization compared with the sum of the three morphotypes in monocultures weighted by their initial relative abundance in the mix, which was demonstrated to be caused by complementarity effects (Blake et al., 2021b). Such morphological diversification has also been observed in EE of *B. subtilis* biofilm pellicles formed at the air-liquid interface (Dragoš et al., 2018b) as well as during EE of *Burkholderia cenocepacia* biofilms on polystyrene beads (Poltak and Cooper, 2011). In this study, we performed EE of *B. subtilis* on one-week-old *A. thaliana* roots under axenic conditions with the initial hypothesis that *B. subtilis* would adapt to the plant root environment by acquiring mutations that would provide the bacteria with a fitness advantage over the ancestor during root colonization. We found that *B. subtilis* rapidly adapted to the plant root as observed by improved root colonizers already after 12 consecutive transfers. In addition, two selected evolved isolates from independent populations from the final transfer (transfer 30) outcompeted the ancestor during root colonization. Furthermore, re-sequencing of single evolved isolates from independent populations and different time points as well as of the endpoint populations revealed mutations within (or upstream from) genes related to different bacterial traits. To further elucidate which bacterial traits were altered during the adaptation to plant roots, evolved isolates from the final transfer were subjected to additional phenotypic characterization. We found that evolved isolates from independent populations displayed robust biofilm formation in response to plant polysaccharides, impaired motility, and altered growth on plant compounds. Finally, we demonstrate that adaptation of *B. subtilis* to *A. thaliana* roots is accompanied by an evolutionary cost, and report an evolved isolate displaying increased root colonization also in the presence of resident soil microbes.

RESULTS

B. subtilis populations evolved on *A. thaliana* roots show a rapid increase in root colonization

To explore the evolutionary adaptation of *B. subtilis* to plant roots, we employed an experimental evolution (EE) setup previously established for another *Bacillus* species (Lin et al., 2021). In short, *B. subtilis* DK1042 (hereafter referred to as the ancestor) was inoculated onto *A. thaliana* seedlings under hydroponic conditions in seven parallel populations. The MSNg medium used in the EE is a minimal medium supplemented with a very low concentration of glycerol (0.05%), and the bacteria thereby move toward the plant root to access a carbon source. Every 48 h for a total of 64 days, the newly colonized seedling was transferred to a fresh medium containing a new sterile seedling, thereby enabling re-colonization (Figure 1A). We hypothesized, that during the successive transfers *B. subtilis* would adapt to the plant roots by acquiring mutations that would confer a fitness advantage over the ancestor during root colonization, resulting in these mutations being selected. In this setup, we specifically selected for a regular cycle of dispersal from the root-associated biofilm, chemotaxis toward the new root, and biofilm formation on the root surface. To follow potential changes in root colonization of the evolving populations during the ongoing EE, the productivity, i.e. colony-forming unit (CFU) per root, was quantified at different time points. All seven independent populations showed a rapid increase in root colonization within the first seven transfers, after which the productivity of the populations remained rather stable with slight increases and drops dependent on the certain population (Figure 1B). While this rapid increase in productivity could be owing to genetic adaptation to the plant root, the initial rise could also be caused by physiological adaptation to the experimental conditions. Interestingly, such a rapid increase in productivity of populations evolving on plant roots is consistent with our recent study where *B. subtilis* evolved on older *A. thaliana* roots (Blake et al., 2021b).

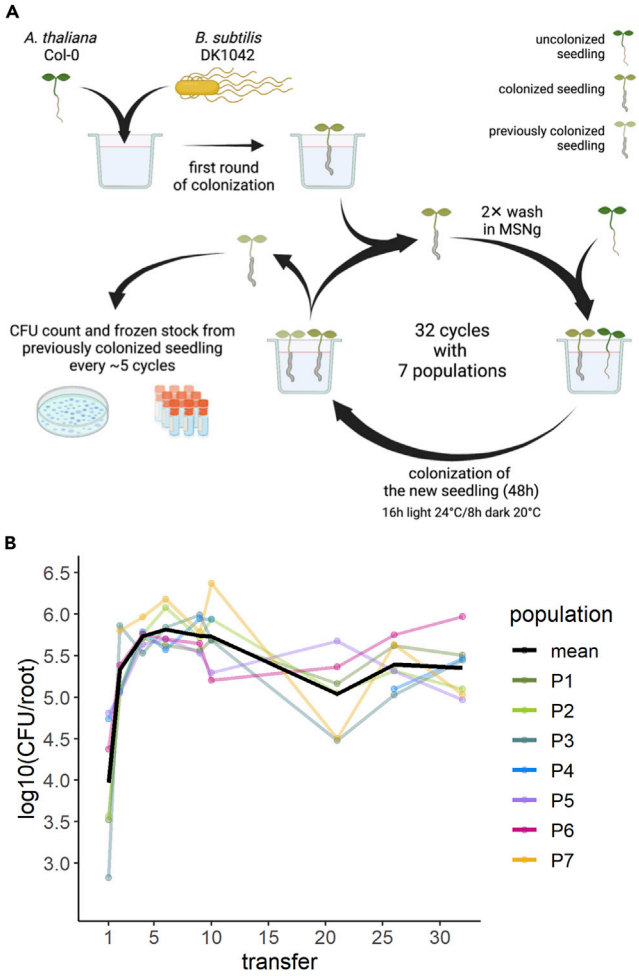

Figure 1. Overview of experimental evolution and productivity of evolving populations

(A) Overview of the experimental evolution approach. Created on BioRender.com.

(B) The *B. subtilis* populations rapidly increased in productivity during the experimental evolution on *A. thaliana* roots. The productivity (CFU/root) of the evolving populations was systematically quantified as CFU/root at nine different time points during the ongoing EE. The *y* axis displays the log10-transformed productivity. The black line represents the mean population productivity ($N = 7$).

Several evolved isolates display altered colony morphologies

To examine whether genetic adaptation to the plant root had taken place during the EE, single evolved isolates from the evolved populations were saved as frozen stocks and subjected to phenotypic and genotypic characterization. To represent different populations and time points during the EE, three isolates were randomly picked from each of population 3, 4, 6, and 7 at transfer 12, 18, and 30 (hereafter referred to as T12, T18, and T30). To detect possible changes in colony morphology, ON cultures of the ancestor and evolved isolates were spotted on LB agar and colonies inspected after 48-h incubation. On LB agar, the ancestor formed a round colony with a wrinkled periphery, whereas different colony morphologies were observed among the evolved isolates (Figure 2). At T12, some isolates displayed a colony morphology resembling the ancestor, e.g. isolate 3 from population 3 (3.3) and isolate 2 from population 7 (7.2), referred to as the "Wrinkled"-type. Several other isolates formed a colony with a white sharp edge along the wrinkled periphery (including isolates 3.2, 4.3, 6.1, and 7.3), hereafter referred to as the "Sharp-Wrinkled"-type. Additionally, isolate 7.1 formed a hyper-wrinkled, white colony, referred to as the "Snow"-type. These distinct colony morphologies were also observed at later time points (T18 and T30). Interestingly, the Snow-type was only observed in population 7. Furthermore, the three isolates from population 6 at T30 formed slightly less wrinkled colonies compared with the ancestor. We note that three isolates do not represent the entire population, and isolates with other colony morphologies could be present in

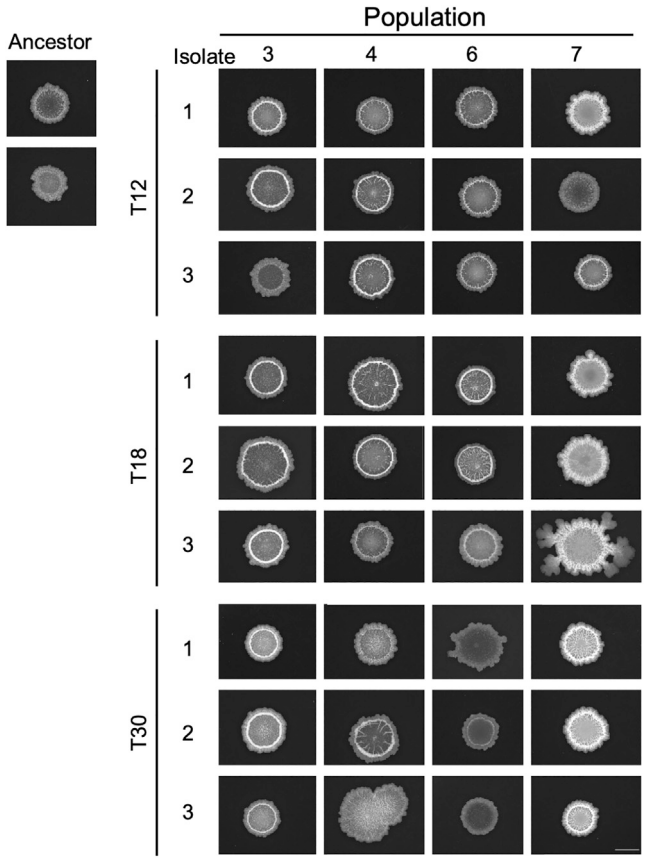

Figure 2. Distinct colony morphologies are observed among evolved isolates from different time points of the experimental evolution

ON cultures of the ancestor and evolved isolates from populations 3, 4, 6, and 7 at transfer 12, 18, and 30 were spotted on LB agar (1.5%) and imaged after incubation for 48 h at 30°C using a stereomicroscope. Ancestor represents *B. subtilis* DK1042. Each colony is representative of at least three replicates. Scale bar = 5 mm.

the populations. Nonetheless, the appearance of isolates with altered colony morphologies in the four populations indicates the presence of genetic changes. Furthermore, the occurrence of isolates with altered colony morphologies already at T12, and especially the presence of three different types (Wrinkled, Sharp-Wrinkled, and Snow) in population 7, at this early time point, suggests rapid diversification of *B. subtilis* during EE on *A. thaliana* roots. Such diversification into distinct morphotypes was also observed in our previous study on EE of *B. subtilis* on plant roots (Blake et al., 2021b) and has additionally been observed in EE of *B. subtilis* pellicle biofilms (Dragoš et al., 2018b), indicating successful adaptation to the selective environment.

Evolved isolates from different time points show increased colonization of *A. thaliana* roots

The design of the EE employed in this study should enable selection for bacteria that efficiently colonize the root. We, therefore, speculated whether the altered colony morphology of some of the evolved isolates was associated with improved productivity on the root (CFU/mm root). To test this, the ancestor and evolved isolates from the final time point (T30) were tested for individual colonization of *A. thaliana* seedlings under the same conditions applied during the EE. CFU quantification revealed that most evolved isolates tended to show increased root colonization, with five isolates from three different populations displaying significantly increased productivity on the root, with an up to circa 1.3-fold change relative to the ancestor (Figure 3). To track down when such improved root colonizers emerged during the EE, the randomly selected evolved isolates from T12 and T18 were similarly tested. Three and five evolved isolates at T12 and T18, respectively, displayed significantly increased productivity relative to the ancestor. In addition, a single isolate from T12 was significantly reduced in root colonization. These results confirm that

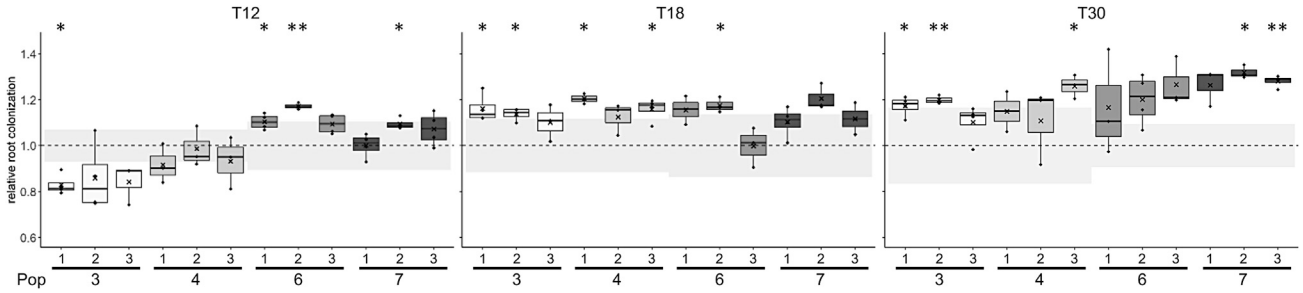

Figure 3. Evolved isolates from different time points show increased productivity on the root relative to the ancestor

The ancestor and evolved isolates from populations 3, 4, 6, and 7 at three different time points (T12, 18, 30) were tested for individual root colonization. For each evolved isolate, relative root colonization was calculated by dividing the log10-transformed productivity (CFU/mm root) of each replicate by the mean of the log10-transformed productivity of the ancestor from the same experimental setup. The cross represents the mean relative root colonization (N = 3-4). The dashed, horizontal line represents the mean of the ancestor (N = 3-4), whereas the grey-shaded rectangles represent the SD of the ancestor from the corresponding experiment. The normalized values were subjected to a One-sample t-test to test whether the mean was significantly different from 1. p-values have been corrected for multiple comparisons. *$p < 0.05$, **$p < 0.01$. See also Figure S2.

indeed the genetic adaptation of *B. subtilis* to the plant root took place during the EE. Furthermore, the observation of improved root colonizers already at T12 indicates that *B. subtilis* rapidly adapted to plant root colonization during the EE.

Selected evolved isolates display a fitness advantage over the ancestor that is specific to the plant root environment

While multiple evolved isolates displayed increased individual root colonization relative to the ancestor (Figure 3), we next wanted to test whether the evolved isolates had a noticeable fitness advantage over the ancestor during competition on the root. For this purpose, two selected evolved isolates from independent populations from T30 (Ev6.1 and Ev7.3, referring to isolate 1 from population 6 and isolate 3 from population 7, respectively) were competed against the ancestor on the plant root. Following 48 h of root colonization, CFU quantification revealed that both evolved isolates had outcompeted the ancestor on the root, and statistical analysis confirmed that the evolved isolates had a significantly higher fitness relative to the ancestor (Figure 4A; for calculation of relative fitness, see STAR Methods). This result was further supported by CLSM imaging: regardless of the fluorescence labeling combination, the two evolved isolates formed biofilms on the roots, as evidenced by aggregates along the root, whereas the ancestor was scarcely present (Figure 4C). Noticeably, the fluorescent images revealed that Ev6.1 formed fewer and smaller aggregates along the root compared with Ev7.3 (Figure 4C), consistent with the individual root colonization of the two isolates (Figure 3). To test whether the fitness advantage of Ev6.1 and Ev7.3 over the ancestor was specific to the plant root environment, the two evolved isolates competed against the ancestor in a non-selective environment, i.e. in LB supplemented with xylan, a plant polysaccharide (PP) found among others in the secondary cell walls of *A. thaliana* (Liepman et al., 2010), and under well-shaking conditions. In this non-selective environment, neither of the evolved isolates outcompeted the ancestor but instead seemed to suffer a fitness disadvantage compared with the ancestor, although the difference was statistically not significant (Figure 4B). Similar results were obtained for the permuted fluorescent combination (Figure S1). These results demonstrated that the evolved isolates had a fitness advantage over the ancestor specifically in the plant root environment. Furthermore, the loss of fitness in a different, non-selective environment suggests an evolutionary cost of adaptation to the plant roots (Bennett and Lenski, 2007; Elena and Lenski, 2003; van den Bergh et al., 2018).

Evolved isolates harbor mutations in genes related to different bacterial traits

To identify the genetic changes contributing to the increased root colonization (Figure 3) and fitness advantage over the ancestor during root colonization (Figures 4A and 4C), the genomes of selected evolved isolates were re-sequenced. To represent independent populations, the isolates from populations 6 and 7 at T30 were included. Furthermore, to track molecular evolution over time, the three isolates from population 7 at T12 and T18 were also re-sequenced. Finally, one isolate from population 1 (Ev1.1) at T30 was included for re-sequencing owing to its "Smooth" colony morphology and reduced root colonization (Figure S2). In the 13 re-sequenced isolates, we observed in total 51 unique mutations of which 37 were non-synonymous (Table S1). Isolate Ev1.1 harbored several mutations in *gtaB* encoding a UTP-glucose-1-phosphate

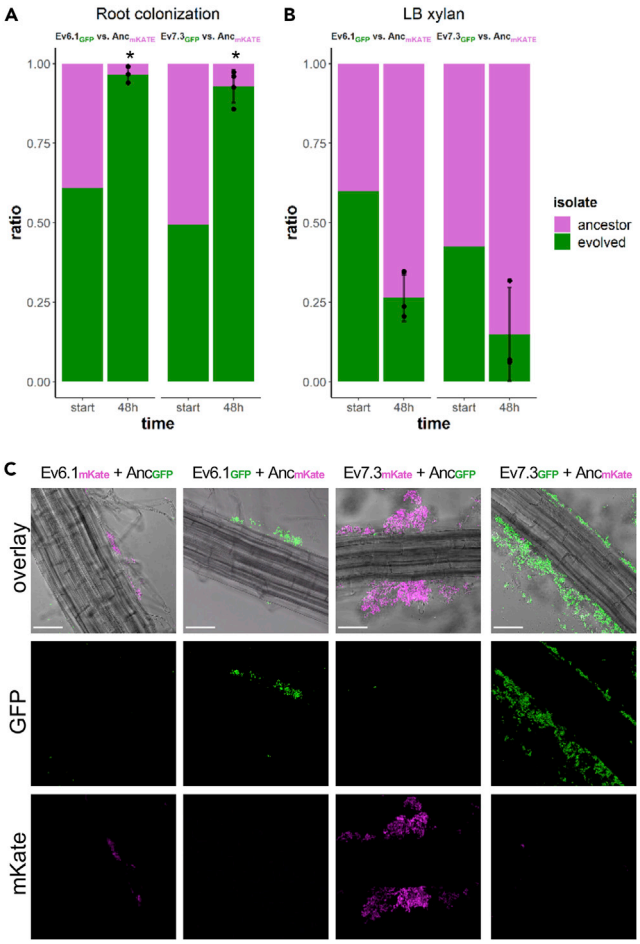

Figure 4. Two evolved isolates from transfer 30 outcompete the ancestor on the root but suffer a fitness disadvantage under shaking conditions in LB + xylan

(A and B) Pairwise competitions between ancestor (magenta) and evolved isolates (green) during root colonization (A) and in LB xylan (0.5%) under shaking conditions (B) for 48 h. In A and B, the bar plots show the starting ratio of the evolved isolate and ancestor in the mix, and the observed ratios after 48 h. Bars represent the mean (N = 3-4), the error bars represent the SD and the points show the replicates for the evolved (below) and ancestor (above). For statistical analysis, the relative fitness (r) of the evolved isolates was calculated by comparing the frequency of the evolved isolate at the beginning and end of the competition experiment. The log2-transformed relative fitness values were subjected to a One-sample t-test to test whether the mean was significantly different from 0. *$p < 0.05$.

(C) *A. thaliana* roots colonized by a 1:1 mix of ancestor and evolved isolates imaged by CLSM. Both fluorescence combinations are shown. The top row shows the overlay of the fluorescence channels and the bright field image. Images are representative of three independent *A. thaliana* seedlings. Color codes are shown at the top. Scale bar is 50 μm. See also Figure S1.

uridylyltransferase that synthesizes a nucleotide sugar precursor essential for the biosynthesis of exopolysaccharides (Varon et al., 1993) and for the synthesis of wall teichoic acids and lipoteichoic acid (Lazarevic et al., 2005). Two of the three isolates from population six at T30 (isolate Ev6.1 and Ev6.3) harbored a non-synonymous point mutation in the *fliM* gene, encoding a flagellar motor switch protein, part of the basal body C-ring controlling the direction of flagella rotation (Guttenplan et al., 2013). All three isolates in population 7 at T30 harbored a mutation in the intergenic region upstream from the *sinR* gene encoding a transcriptional repressor of the genes responsible for matrix production (Chu et al., 2006; Kearns et al., 2005). Interestingly, this mutation was also present in the three isolates in population 7 at T18 and in one of the isolates in this population at T12, suggesting that this mutation arose rather early in the EE and rose to a high frequency in population 7. Indeed, sequencing of the seven endpoint populations (i.e. the populations from T30) revealed that this mutation upstream from *sinR* was fixed in population 7 at the final time point, i.e. the mutation had reached a frequency of 1 in this population at T30 (Table S2). Furthermore, a

non-synonymous mutation within the *sinR* gene was detected at high frequencies in populations 2 and 3. In addition, non-synonymous mutations in genes related to flagellar motility were besides population 6 also observed in populations 3, 4, and 5 (*fliF*, *fliK*, *fliM*, and *hag*). Finally, mutations in genes related to cell wall metabolism (*gtaB*, *tagE*, and *walK*, encoded functions according to SubtiWiki (Zhu and Stülke, 2018)) were identified across all seven populations (Table S2). The detection of mutations within (or upstream from) genes related to biofilm formation, motility, and cell wall metabolism across independent populations supports the role of these mutations in the adaptation of *B. subtilis* to *A. thaliana* roots.

Evolved isolates show altered pellicle biofilm formation in response to plant polysaccharides

The fitness advantage of selected evolved isolates over the ancestor during root colonization (Figures 4A and 4C) and the detected mutations in the evolved isolates and endpoint populations (Tables S1 and S2) confirm our initial hypothesis, that *B. subtilis* adapted to the plant root by acquiring mutations that conferred a fitness advantage over the ancestor during root colonization.

Next, we wanted to elucidate which bacterial traits were altered during such adaptation to the plant root. For this purpose, evolved isolates from the final transfer (T30) were subjected to further phenotypic characterization. Given the detected mutations (Tables S1 and S2) and that both biofilm formation and motility are important for successful root colonization by *B. subtilis* (Allard-Massicotte et al., 2016; Beauregard et al., 2013; Chen et al., 2013; Tian et al., 2021), we hypothesized that these two bacterial traits would be under selection during the adaptation to the plant roots. To this end, plant polysaccharides (PPs) including xylan have been shown to induce biofilm formation in *B. subtilis* in a non-biofilm inducing medium (Beauregard et al., 2013). One way of adapting to the plant root could thereby be through enhanced biofilm formation in response to such PPs. To test whether the improved productivity on the root by the evolved isolates was associated with more robust biofilm formation in response to PPs, the ancestor and evolved isolates were tested for pellicle biofilm formation, a biofilm formed at the medium-air interface (Branda et al., 2001), in LB supplemented with xylan (LB + xylan). Importantly, a rich medium (LB) rather than the minimal medium (MSNg) was used in this assay to provide the bacteria with plenty of nutrients, allowing us to assess only the ability of the evolved isolates to form biofilm in response to xylan, and not the ability to utilize xylan for growth. We observed that a few isolates from T30 developed a pellicle biofilm similar to the ancestor, i.e. Ev4.1, Ev4.2, and Ev6.1 (Figure 5A). In contrast, the remaining isolates developed more robust pellicles with highly structured wrinkles indicative of enhanced matrix production. Especially the three isolates from population 7 developed hyper-robust, white pellicles, consistent with the Snow-type colony morphology observed for these isolates (Figure 2). The biofilms developed in response to xylan by the evolved isolates generally correlated with their productivity on the root. For example, isolates Ev4.1, Ev4.2, and Ev6.1 developing similar pellicles as the ancestor and isolates Ev7.1, Ev7.2, and Ev7.3 forming hyper-wrinkled, robust pellicles in response to xylan were among the ones showing the smallest and largest increase in individual root colonization (Figures 3 and 5A), respectively. This is in accordance with Chen et al. (2013) demonstrating that the ability of *B. subtilis* mutants to form robust biofilms *in vitro* correlated with that on the root. These results suggest that improved productivity on the root was associated with robust biofilm formation in response to xylan. To test whether this enhanced biofilm formation was specific to the presence of PPs, the ancestor and evolved isolates were tested for the ability to form pellicles in LB in the absence of xylan. In this medium, the pellicles developed by both the ancestor and evolved isolates were less robust (Figure S3). For most isolates, the improved biofilm formation was specific to the presence of PPs, whereas the isolates from population 7 displayed robust biofilms also in the absence of plant compounds suggesting a general improvement in biofilm formation in these isolates.

Evolved isolates show reduced swarming and swimming motility

To test whether the evolved isolates were affected in motility, the ancestor and evolved isolates from population 6 and 7 were tested for two types of motility: swimming motility, a single cell movement in aqueous environments powered by flagella rotation and swarming motility which is associated with a rapid multicellular movement of hyper-flagellated cells across a surface facilitated by self-produced surfactin (Kearns, 2010). Interestingly, most isolates were significantly impaired in both swimming and swarming motility (Figures 5B and 5C). Swimming motility was observed for the ancestor and evolved isolates after 4 h (Figure 5B). However, after 6 h only the ancestor and Ev6.2 had reached the edge of the Petri dish, whereas the remaining isolates reached at the most half of the swimming distance of the ancestor. Swarming was observed for the ancestor after 4 h which continued until the expanding colony almost reached the edge of the Petri dish after 8 h (Figure 5C). In contrast, the evolved isolates showed reduced or a complete

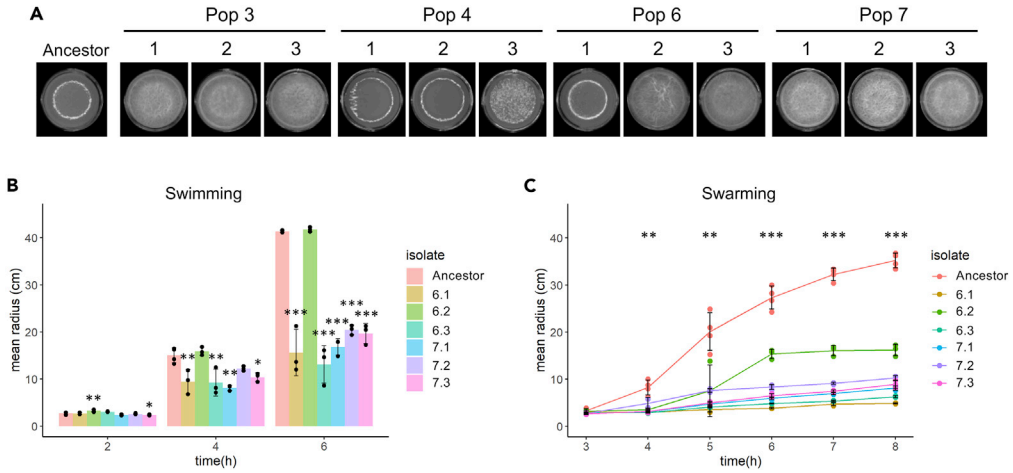

Figure 5. Evolved isolates from T30 show altered pellicle biofilm formation in response to plant polysaccharides and impaired motility

(A) Ancestor and evolved isolates from transfer 30 were inoculated into LB + 0.5% xylan at a starting OD_{600} of 0.05 in 24-well plates. Images were acquired after 48 h incubation at 30°C using a stereomicroscope. Each image is representative of four replicates. Each well has 16 mm width. Evolved isolates were tested for swimming (B) and swarming (C) motility in LB medium supplemented with 0.3 or 0.7% agar, respectively.

(B) Bars represent the mean (N = 3-4) and error bars represent SD.

(C) Lines represent the mean (N = 2-4) and error bars the SD. For the motility assays, the following statistical analysis applies: For each time point, an ANOVA was performed on the log10-transformed data followed by a Dunnett's Multiple Comparison test with the ancestor as the control. For swarming motility, the asterisks show the least significance observed for the given time point. At 3 h, only isolate 7.3 was significantly reduced in swarming motility. *$p < 0.05$, **$p < 0.01$, ***$p < 0.001$. See also Tables S1, S2, Figures S3, S4, and S5.

lack of swarming throughout the experiment. The evolution of motility-impaired isolates in independent populations could indicate that motility is not important for root colonization in the selective environment. Notably, during the EE the 48-well plates were continuously shaking at 90 rpm. We speculated, that these mildly shaking conditions could allow the bacteria to get into contact with the root by chance and thereby reducing the impact of motility on root colonization in the selective environment. To test whether motility is important during root colonization under shaking conditions, the ancestor (here referred to as "WT") was competed against a Δ*hag* mutant, deficient in the production of the flagellin protein, for three successive rounds of root colonization under static or shaking conditions (200 rpm). Under static conditions, the Δ*hag* mutant was significantly outcompeted by the WT (Figure S4). In contrast, under shaking conditions, the Δ*hag* mutant was able to co-colonize the root to similar levels as the WT. These results demonstrate that motility is important for competition on the root under static conditions but is not required under shaking conditions. Thereby, impaired motility of several of the evolved isolates is not expected to negatively influence the fitness of these isolates in the selective environment.

Evolved isolates show distinct growth profiles in a plant-mimicking environment

The minimal medium (MSNg) used in the EE should render the bacteria dependent on root exudates and dead plant material to survive. A simple way of adapting to this selective environment could be through the enhanced utilization of available plant compounds. To test this, we used a modified version of the minimal medium employed during the EE. Instead of 0.05% glycerol, the MSN medium was supplemented with 0.5% cellobiose (MSNc). Cellobiose is a disaccharide and a product of partial hydrolysis of cellulose, found in plant cell walls (Beauregard et al., 2013; Endler and Persson, 2011). In addition, MSNc was supplemented with 0.5% xylan. The ancestor showed a growth profile typical of bacterial growth under planktonic conditions (Figure S5). In contrast, several evolved isolates displayed distinct growth profiles, including 3.2, 7.1, 7.2, and 7.3, which showed no decline phase, but instead displayed a pro-longed stationary phase. When analyzing the carrying capacity (K), several isolates showed significantly increased carrying capacity (all three isolates from populations 3 and 7), whereas few isolates showed significantly decreased carrying capacity (Ev4.2, Ev4.3, and Ev6.2). While cellobiose and xylan do not completely represent the plant

compounds present in the selective environment, these results suggest that adaptation to the plant root could also be facilitated through the altered utilization of plant compounds.

An evolved isolate shows increased colonization of *A. thaliana* roots in the presence of a synthetic, soil-derived community

During the EE, *B. subtilis* was adapted to the plant root alone – in the absence of other microbes. This selective environment is far from its natural habitat in the rhizosphere, where *B. subtilis* encounters other microbial residents. In fact, the ancestor DK1042 is a derivate of the wild strain NCIB 3610, originally isolated from hay infusion (Cohn, 1930; Zeigler et al., 2008). To this end, we wondered how the pro-longed adaptation of *B. subtilis* to the plant root environment in the absence of other microbial species affected the ability to colonize the root in the presence of soil microbes. The ancestor and Ev7.3 were tested for their ability to colonize *A. thaliana* roots in the presence of a synthetic, soil-derived community (Lozano-Andrade et al., 2021). This community comprises four bacterial species, *Pedobacter* sp., *Rhodococcus globerulus*, *Stenotrophomas indicatrix* and *Chryseobacterium* sp. that were previously isolated from soil samples that also contained *B. subtilis*, thereby representing bacterial soil inhabitants that *B. subtilis* would normally encounter in nature. The isolate Ev7.3 was chosen for this test since it was highly adapted to the selective environment, i.e. the isolate displayed significantly increased individual root colonization (Figure 3) and outcompeted the ancestor during competition on the root, where it formed a robust biofilm along the root (Figures 4A and 4C). To capture any potential difference in the establishment on the root, here defined as root colonization after 48 h, between *B. subtilis* ancestor and Ev7.3 in the presence of the community, the ancestor or Ev7.3 was co-inoculated with the community in four different ratios: 0.1:1, 1:1, 10.1, and 100:1 of *B. subtilis* and community, respectively. When *B. subtilis* was initially under-represented or highly in excess, i.e. inoculation ratio 0.1:1 and 100:1, respectively, no significant difference was observed in the establishment on the root between *B. subtilis* ancestor and Ev7.3 within the same inoculation ratio (Figure 6). In contrast, when co-inoculated with the community in intermediate ratios, i.e. 1:1 and 10:1, isolate Ev7.3 showed significantly enhanced establishment on the root compared with the ancestor. Since Ev7.3 displayed increased carrying capacity in MSNc + xylan in monoculture compared with the ancestor (Figure S5), we wondered whether the enhanced establishment on the root by Ev7.3 in the presence of the community could be partly attributed to improved utilization of plant compounds. Indeed, growth profiles in MSNc + xylan of the ancestor or Ev7.3 in co-culture with the community revealed that Ev7.3 displayed a significantly increased carrying capacity at inoculation ratio 1:1, 10:1, and 100:1 compared with the ancestor (Figure S6). Finally, *in vitro* confrontation assays on LB agar (1.5%) showed no major difference in the inhibition of the community members by Ev7.3 compared with the ancestor (Figure S7). Taken together, these results show that even though *B. subtilis* was adapted to the plant root alone, isolate Ev7.3 displayed increased root colonization also in the presence of a synthetic, soil-derived community under certain inoculation ratios, possibly mediated by robust biofilm formation on the root and enhanced utilization of plant compounds.

DISCUSSION

Several studies have reported experimental evolution as a powerful tool to explore how bacteria adapt to ecologically relevant environments. A recent study investigated the adaptive response of the PGPR *Pseudomonas protegens* to the *A. thaliana* rhizosphere in a sand system, which revealed mutations in genes encoding global regulators and genes related to motility and cell surface structure across independent populations (Li et al., 2021b) and during such adaptation, the initially plant-antagonistic *P. protegens* bacterium evolved into mutualists (Li et al., 2021a). Furthermore, Lin et al. (2021) observed that adaptation of *Bacillus thuringiensis* to *A. thaliana* roots under hydroponic conditions led to the evolution of multicellular aggregating phenotypes, which, surprisingly, in certain lineages were accompanied by enhanced virulence against the *Galleria mellonella* larvae. Here, we employed experimental evolution to study the adaptation of *B. subtilis* to *A. thaliana* roots under hydroponic conditions. Our initial hypothesis was that *B. subtilis* would adapt to the plant roots by acquiring mutations that would provide the bacteria with a fitness advantage over the ancestor during root colonization. We could demonstrate that *B. subtilis* rapidly adapted to the plant roots, as observed by evolved isolates displaying improved root colonization relative to the ancestor already after 12 transfers and the detection of genetic changes in evolved isolates from transfer 12, 18, and 30. In addition, competition between the ancestor and two selected evolved isolates from the final transfer (T30) on the root revealed that both evolved isolates had a fitness advantage over the ancestor during root colonization, thereby confirming our hypothesis.

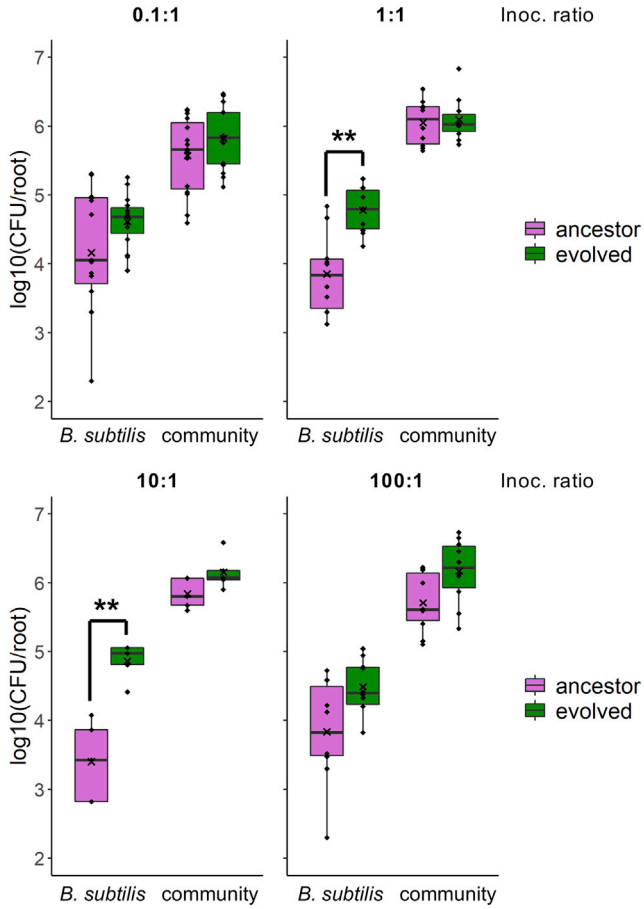

Figure 6. Root colonization by *B. subtilis* ancestor and isolate Ev7.3 in the presence of a synthetic, soil-derived community

The ancestor and evolved isolate, Ev7.3, were tested for the ability to colonize the root in the presence of a synthetic, soil-derived bacterial community. *B. subtilis* ancestor or Ev7.3 and the community were co-inoculated onto *A. thaliana* roots in four different ratios: 0.1:1, 1:1, 10:1, and 100:1 of *B. subtilis* and community, respectively. Root colonization after 48 h was quantified as log10-transformed productivity (CFU/root). Each plot shows the resulting root colonization at the given inoculation ratio of *B. subtilis* (left) and the co-inoculated community (right). Magenta: Ancestor and the corresponding community co-inoculated with the ancestor. Green: Ev7.3 and the community co-inoculated with Ev7.3. The cross represents the mean (N = 5–15). Within each inoculation ratio, statistical significance between *B. subtilis* ancestor and Ev7.3, and between the communities co-inoculated with the ancestor or with Ev7.3 was tested with a Two-sample t-test (Welch's Two-sample t-test when unequal variance). **$p < 0.01$. See also Figures S6 and S7.

Further phenotypic characterization of the evolved isolates from the final transfer revealed that most isolates across independent populations developed more robust biofilms in response to the plant polysaccharide xylan compared with the ancestor. Except for isolate Ev3.3, the robust biofilm formers tended to be increased in individual root colonization, indicating that robust biofilm formation is associated with adaptation to the plant root. Motility represents an important trait for many bacteria as it allows them to explore the environment for nutrients and escape unfavorable conditions. Of relevance to the adaptation of *B. subtilis* to plant roots, motility has been shown to be important for root colonization of different plant species under different conditions. For example, a *B. subtilis* Δ*hag* mutant was shown to be delayed or reduced in *A. thaliana* root colonization under hydroponic conditions as well as in tomato root colonization under vermiculites pot conditions (Allard-Massicotte et al., 2016; Tian et al., 2021). Yet, we found that five out of six isolates from two independent populations were impaired in both swimming and swarming motility, indicating that motility is not important for root colonization in the selective environment of the EE, i.e. under hydroponic, shaking conditions. Indeed, this was verified in a competition experiment between a non-motile Δ*hag* mutant and the WT, revealing that motility is not required for root colonization under shaking conditions. In contrast to our observations, Li et al. (2021a) observed several evolved isolates

of *P. protegens* improved in swimming motility following adaptation to the *A. thaliana* rhizosphere in a sand system (Li et al., 2021b), supporting that in sand (and thus possibly also in soil), motility is indeed important for root colonization and is therefore selected for.

In *B. subtilis*, motility and biofilm formation are incompatible processes: *B. subtilis* can exist as single, motile cells or in chains of sessile, matrix-producing cells which is regulated by an epigenetic switch involving SinR (Chai et al., 2010; Vlamakis et al., 2008). The enhanced biofilm formation and impaired motility of isolates from populations 6 and 7 (Ev6.3, Ev7.1, Ev7.2, and Ev7.3) could thereby indicate a possible biofilm-motility trade-off. An inverse evolutionary trade-off between biofilm formation and motility was observed when the opportunistic pathogen *Pseudomonas aeruginosa* was subjected to repeated rounds of swarming that lead to the evolution of hyper-swarmers that were impaired in biofilm formation (van Ditmarsch et al., 2013). Considering that the ability to form robust biofilm *in vitro* was shown to positively correlate with root colonization in *B. subtilis* (Chen et al., 2013), and the demonstration that motility is not important for root colonization under shaking conditions, a possible biofilm-motility trade-off could provide *B. subtilis* with enhanced fitness during root colonization in the selective environment. Indeed, isolate Ev7.3, which developed hyper-robust biofilms in LB + xylan and was impaired in motility, significantly outcompeted the ancestor during root colonization.

Re-sequencing of selected evolved isolates revealed that Ev7.1, Ev7.2, and Ev7.3 (from transfer 30) all harbored a single nucleotide polymorphism (SNP) two base pairs upstream from the start codon of the *sinR* gene (Agarwala et al., 2018), encoding a transcriptional repressor of matrix genes (Chu et al., 2006; Kearns et al., 2005). This SNP is located in the spacer region between the Shine Dalgarno sequence and the start codon in the ribosome binding site. Interestingly, the nucleotide composition of the spacer sequence has been shown to influence translation efficiency (Liebeton et al., 2014). The SNP upstream from *sinR* might thereby potentially affect the translation efficiency from the mRNA transcript, resulting in reduced levels of SinR. Reduced levels of SinR could in turn result in increased expression of matrix genes. This is supported by Richter et al. (2018) who demonstrated that a Δ*sinR* mutant shows increased matrix gene expression, and by Subramaniam et al. (2013) reporting that SinR translation and therefore protein level affects matrix gene expression. Potential increased matrix production caused by this mutation could contribute to the Snow-type colony morphology, as this colony morphology was exclusively observed for isolates harboring this mutation. Furthermore, in accordance with the robust biofilm formation and increased root colonization observed for Ev7.1, Ev7.2 and Ev7.3, a Δ*sinR* mutant was shown to form a hyper-robust biofilm in biofilm-inducing medium as well as on tomato roots (Chen et al., 2013), supporting the possible relevance of this mutation for the observed phenotypes of these isolates. Based on these previous studies, we therefore speculate that the mutation upstream from *sinR* results in increased matrix gene expression, which in turn enables more robust biofilm formation and increased root colonization as observed for the three isolates in population 7. These three isolates did not harbor mutations in motility-related genes. However, besides a possible effect of reduced SinR levels on the epigenetic switch (Chai et al., 2010) that could lock the cells in a sessile, matrix-producing stage, a potential reduction in SinR levels leading to overexpression of the *eps* operon could possibly reduce motility owing to the EpsE clutch (Blair et al., 2008). Such mutation and the observed corresponding phenotypes could be responsible for the biofilm-motility trade-off, and be an example of antagonistic pleiotropy (Elena and Lenski, 2003) in which the same mutation is beneficial in one environment, i.e. during root colonization under shaking conditions, but disadvantageous in another, i.e. where motility is required for survival. In addition, this mutation affecting a biofilm regulator could possibly explain why Ev7.1, Ev7.2, and Ev7.3 show improved biofilm formation also in the absence of xylan.

Isolate Ev6.1 and Ev6.3 harbored a non-synonymous point mutation in the *fliM* gene, which was not present in Ev6.2. This gene encodes a flagellar motor switch protein, part of the basal body C-ring controlling the direction of flagella rotation (Guttenplan et al., 2013). Interestingly, Ev6.1 and Ev6.3 were impaired in both forms of motility, whereas Ev6.2 showed similar swimming as the ancestor and was less affected in swarming. We speculate that the R326I substitution affects the function of FliM and consequently the flagellar machinery, resulting in hampered motility in these two isolates. Since we showed that motility was not important for root colonization under shaking conditions, a mutation hampering motility could provide the bacterium a fitness advantage during the adaptation to *A. thaliana* roots owing to the reduced cost of this apparently redundant trait. However, we do not expect the mutation in *fliM* to result in reduced cost; it merely changes an amino acid in a protein part of the flagellar machinery. Other mutations in the population six isolates must explain the robust biofilm formation by Ev6.2 and Ev6.3 and the

fitness advantage of Ev6.1 over the ancestor during root colonization. For example, isolate Ev6.1 and Ev6.3 harbor a mutation in *kinA* encoding a two-component sensor kinase which once activated initiates the phosphorelay leading to phosphorylation of the master regulator Spo0A (Jiang et al., 2000).

The isolate from population one at transfer 30 (Ev1.1) harbored a frameshift mutation in the *rsiX* locus, encoding an anti-sigma factor controlling the activity of SigX (Zhu and Stülke, 2018). Inconsistent with the smooth morphology and reduced root colonization of this isolate, an Δ*rsiX* mutant was shown to have increased *eps* expression (Martin et al., 2020). However, Ev1.1 additionally harbored several mutations in *gtaB* encoding a UTP-glucose-1-phosphate uridylyltransferase involved in the biosynthesis of a nucleotide sugar precursor for EPS biosynthesis (Varon et al., 1993). A study conducted by Reverdy et al. (2018) showed that acetylation of GtaB is important for biofilm formation of *B. subtilis* and that a *gtaB* mutant was reduced in pellicle formation. In addition, Xu et al. (2019) showed that a Δ*gtaB* mutant of *Bacillus velezensis* SQR9 was significantly decreased in colonization of cucumber roots compared with the WT, although the effect of *gtaB* on root colonization may be species-dependent. We therefore speculate that Ev1.1 may have first gained the mutation in *rsiX* and was selected for owing to increased *eps* expression, whereas later on the increased matrix production was reverted by the mutations in *gtaB*, resulting in a non-functional protein and thereby reduced precursors for EPS production, which was selected for owing to the reduced cost. In accordance with the mutations observed in this study, a non-synonymous mutation in *sinR* in two isolates forming Snow-type colonies and increased in root colonization as well as several mutations in *gtaB* in two isolates with a Smooth colony morphology were observed in our recent study on diversification of *B. subtilis* during adaptation to *A. thaliana* roots (Blake et al., 2021b).

To get a more general insight into the mutations arising in *B. subtilis* during EE on *A. thaliana* roots, the seven endpoint populations were also sequenced. This revealed mutations within (or upstream from) genes related to biofilm formation (*sinR*), flagellar motility (*fliF*, *fliK*, *fliM*, and *hag*), and cell wall metabolism (*gtaB*, *tagE*, and *walK*) (Zhu and Stülke, 2018) across independent populations. Taken together, our findings of evolved isolates displaying altered biofilm formation and motility properties and the detection of mutations within (or upstream from) genes related to biofilm formation and motility in single evolved isolates as well as across independent endpoint populations indicates that adaptation of *B. subtilis* to *A. thaliana* roots under the employed conditions is associated with alterations in these two bacterial traits.

While we found that the phenotypic and genetic changes of Ev6.1 and Ev7.3 conferred a fitness advantage over the ancestor during root colonization, adaptation to one certain environment may be accompanied by a loss of fitness in other environments (Elena and Lenski, 2003). This has been demonstrated for *Escherichia coli* which following adaptation to low temperature showed reduced fitness at high temperature (Bennett and Lenski, 2007). In the example of the evolution of hyper-swarmers of *P. aeruginosa*, the hyperswarmer clones outcompeted the ancestor in swarming, but lost in biofilm competitions (van Ditmarsch et al., 2013). In this study, we demonstrate that adaptation of *B. subtilis* to *A. thaliana* roots is accompanied by an evolutionary cost. When Ev6.1 and Ev7.3 each were competed against the ancestor in LB + xylan under shaking conditions, i.e. an environment where plant compounds are present but biofilm formation is not required for survival, both evolved isolates suffered a fitness disadvantage. The observation that two evolved isolates, from independent populations and with different phenotypes and genetic changes, both suffered a fitness disadvantage in a non-selective environment might suggest the generality of such an evolutionary cost accompanying adaptation to *A. thaliana* roots.

In our EE approach, *B. subtilis* was adapted to plant roots in the absence of other microbes. In the rhizosphere environment under natural conditions, *B. subtilis* is far from being the sole microbial inhabitant. Instead, it engages in cooperative and competitive interactions with other members of the rhizosphere microbiome (Hassani et al., 2018; Kiesewalter et al., 2021). We tested whether the evolved isolate, Ev7.3, displaying increased root colonization in the selective environment relative to the ancestor, would also show improved establishment on the root under more ecologically complex conditions. We found that in the presence of a synthetic, soil-derived community, Ev7.3 displayed enhanced establishment on the root compared with the ancestor in two out of four inoculation ratios. This enhanced establishment on the root by Ev7.3 is not expected to be caused by altered antagonistic activities toward the community members. First, no major changes in the inhibition of the community members were observed in confrontation colony assays. Secondly, an increased number of Ev7.3 cells on the root did not cause a reduction in the co-colonizing community. Finally, Ev7.3 did not harbor mutations in genes directly related to secondary metabolite production. Instead, enhanced establishment on the root by Ev7.3 in the presence of the

community is possibly enabled by robust biofilm formation facilitating stronger attachment to the root and enhanced utilization of plant compounds. Interestingly, a study by Molina-Santiago et al. (2019) showed that compared with a Δmatrix mutant, co-inoculation of *B. subtilis* WT with *Pseudomonas chlororaphis* on melon leaves enabled co-localization of the two species as well as the closer attachment of *B. subtilis* to the left surface (Molina-Santiago et al., 2019). The robust biofilm formed on the root by Ev7.3 possibly facilitated by increased matrix production may thereby not exclude the community members on the root but could rather allow them to incorporate into the matrix. This could also explain why the enhanced establishment of *B. subtilis* Ev7.3 on the root did not cause a reduction in the number of community cells attached to the root. Alternatively, the community may not be majorly affected by any difference in the establishment on the root between the ancestor and Ev7.3 owing to the low abundance of *B. subtilis* relative to the community. Further work is needed to elucidate the interactions between *B. subtilis* and this synthetic community during root colonization. In summary, these findings suggest that even though *B. subtilis* was evolved on *A. thaliana* in the absence of other microbes, it became highly adapted to the plant root environment enabling better establishment on the root also when the ecological complexity increases. How genetic adaptation to the plant root in the absence of other microbial species differs from adaptation to plant root environments with varying levels of ecological complexity is the scope of future studies.

The formation of root-associated biofilms is important for the biocontrol efficacy of *B. subtilis* (Chen et al., 2013). From an applied perspective, experimental evolution of *B. subtilis* on plant roots represents an unexplored approach for developing strains with improved root attachment abilities for agricultural use. However, a biofilm-motility tradeoff as observed here may be undesirable when developing biocontrol agents owing to the growing evidence of motility as an important trait for bacterial root colonization in soil systems (Li et al., 2021b; Tian et al., 2021). The phenotypes associated with the adaptation of *B. subtilis* to *A. thaliana* roots presented here as well as the accompanying evolutionary cost and the increased root colonization also in the presence of resident soil bacteria highlight the importance of considering the selective environment if evolving PGPR for biocontrol purposes.

Limitations of the study

This study on the evolutionary adaptation of *B. subtilis* to *A. thaliana* roots under hydroponic conditions revealed that *B. subtilis* rapidly adapted to the plant root environment as observed by improved root colonizers already after 12 transfers. Moreover, we found that one selected evolved isolate displayed increased root colonization also in the presence of resident soil bacteria. The findings from this study thereby highlight experimental evolution as an approach to developing *B. subtilis* strains with improved root colonization capacities to potentially support a sustainable agricultural production. However, such plant root adaptation might be condition-specific, and we do not know whether the evolved isolates also display increased root colonization under soil conditions reminiscent of those the bacteria will encounter under greenhouse or field conditions. To this end, motility has been shown to be important for root colonization under diverse conditions, including soil and sand conditions (Gao et al., 2016; Tian et al., 2021). Thereby, the biofilm-motility trade-off observed for several of the evolved isolates might be undesirable in a biocontrol strain used under field or greenhouse conditions. Future studies will therefore test the evolved isolates for root colonization under greenhouse soil conditions to reveal whether adaptation to plant roots under the simple axenic, hydroponic conditions employed in this study, manifests in increased root colonization also under agriculturally relevant conditions.

STAR★METHODS

Detailed methods are provided in the online version of this paper and include the following:

- KEY RESOURCES TABLE
- RESOURCE AVAILABILITY
  - Lead contact
  - Materials availability
  - Data and code availability
- EXPERIMENTAL MODEL AND SUBJECT DETAILS
  - Bacterial strains and culture media
  - Plant material
- METHOD DETAILS

- Experimental evolution of *B. subtilis* on *A. thaliana* seedlings
- Isolation of single evolved isolates and colony morphology assay
- Root colonization assay
- Pairwise competition experiments in LB + xylan
- Biofilm formation in response to plant polysaccharides
- Motility assays
- Growth in the presence of xylan
- Pairwise interactions of *B. subtilis* with community members
- Microscopy/confocal laser scanning microscopy (CLSM)
- Genome re-sequencing and genome analysis of single isolates and endpoint populations

- QUANTIFICATION AND STATISTICAL ANALYSIS
  - Data and statistical analysis

SUPPLEMENTAL INFORMATION

Supplemental information can be found online at https://doi.org/10.1016/j.isci.2022.104406.

ACKNOWLEDGMENTS

We thank Carlos N. Lozano-Andrade for the four bacterial species constituting the synthetic community. The work was supported by a DTU Bioengineering start-up fund to ÁTK. Fundings from Novo Nordisk Foundation for the infrastructure "Imaging Microbial Language in Biocontrol (IMLiB)" (NNFOC0055625), and within the INTERACT project of the Collaborative Crop Resiliency Program (NNF19SA0059360) are acknowledged. The position of M.L.S. is financed by the Danish National Research Foundation (DNRF137) for the Center for Microbial Secondary Metabolites. G.H. and Y.W. were supported by China National GeneBank (CNGB).

AUTHOR CONTRIBUTIONS

Conceptualization, M.N.C., Á.T.K.; investigation, M.N.C., C.B.; formal analysis, M.N.C., M.L.S, G.M., G.H.; resources, G.M., G.H., Y.W.; writing – original draft, M.N.C., Á.T.K.; writing – review and editing, G.H., Y.W., G.M., M.L.S.; supervision, Á.T.K.; funding acquisition, Á.T.K.

DECLARATION OF INTERESTS

The authors declare no competing interests.

Received: August 10, 2021
Revised: January 22, 2022
Accepted: May 5, 2022
Published: June 17, 2022

REFERENCES

Agarwala, R., Barrett, T., Beck, J., Benson, D.A., Bollin, C., Bolton, E., Bourexis, D., Brister, J.R., Bryant, S.H., Canese, K., et al. (2018). Database resources of the National center for biotechnology information. Nucleic Acids Res. *46*, D8–D13. https://doi.org/10.1093/nar/gkx1095.

Akram, W., Anjum, T., and Ali, B. (2015). Searching ISR determinant/s from *Bacillus subtilis* IAGS174 against *Fusarium* wilt of tomato. BioControl *60*, 271–280. https://doi.org/10.1007/s10526-014-9636-1.

Allard-Massicotte, R., Tessier, L., Lécuyer, F., Lakshmanan, V., Lucier, J.F., Garneau, D., Caudwell, L., Vlamakis, H., Bais, H.P., and Beauregard, P.B. (2016). *Bacillus subtilis* early colonization of *Arabidopsis thaliana* roots involves multiple chemotaxis receptors. MBio *7*, e01664-16. https://doi.org/10.1128/mBio.01664-16.

Asaka, O., and Shoda, M. (1996). Biocontrol of *Rhizoctonia solani* damping-off of tomato with *Bacillus subtilis* RB14. Appl. Environ. Microbiol. *62*, 4081–4085. https://doi.org/10.1128/aem.62.11.4081-4085.1996.

Bai, U., Mandic-Mulec, I., and Smith, I. (1993). SinI modulates the activity of SinR, a developmental switch protein of *Bacillus subtilis*, by protein-protein interaction. Genes Dev. *7*, 139–148. https://doi.org/10.1101/gad.7.1.139.

Bais, H.P., Fall, R., and Vivanco, J.M. (2004). Biocontrol of *Bacillus subtilis* against infection of Arabidopsis roots by *Pseudomonas syringae* is facilitated by biofilm formation and surfactin production. Plant Physiol. *134*, 307–319. https://doi.org/10.1104/pp.103.028712.

Beauregard, P.B., Chai, Y., Vlamakis, H., Losick, R., and Kolter, R. (2013). *Bacillus subtilis* biofilm induction by plant polysaccharides. Proc. Natl. Acad. Sci. U. S. A. *110*, E1621–E1630. https://doi.org/10.1073/pnas.1218984110.

Bennett, A.F., and Lenski, R.E. (2007). An experimental test of evolutionary trade-offs during temperature adaptation. Proc. Natl. Acad. Sci. U S A. *104*, 8649–8654. https://doi.org/10.17226/11790.

Berendsen, R.L., Pieterse, C.M.J., and Bakker, P.A.H.M. (2012). The rhizosphere microbiome and plant health. Trends Plant Sci. *17*, 478–486. https://doi.org/10.1016/j.tplants.2012.04.001.

Berendsen, R.L., Vismans, G., Yu, K., Song, Y., De Jonge, R., Burgman, W.P., Burmølle, M., Herschend, J., Bakker, P.A.H.M., and Pieterse, C.M.J. (2018). Disease-induced assemblage of a plant-beneficial bacterial consortium. ISME J. *12*, 1496–1507. https://doi.org/10.1038/s41396-018-0093-1.

Blair, K.M., Turner, L., Winkelman, J.T., Berg, H.C., and Kearns, D.B. (2008). A molecular clutch disables flagella in the *Bacillus subtilis* biofilm. Science *320*, 1636–1638. https://doi.org/10.1126/science.1157877.

Blake, C., Christensen, M.N., and Kovács, Á.T. (2021a). Molecular aspects of plant growth promotion and protection by *Bacillus subtilis*. Mol. Plant Microbe Interact. *34*, 15–25. https://doi.org/10.1094/MPMI-08-20-0225-CR.

Blake, C., Nordgaard, M., Maróti, G., and Kovács, Á.T. (2021b). Diversification of *Bacillus subtilis* during experimental evolution on *Arabidopsis thaliana* and the complementarity in root colonization of evolved subpopulations. Environ. Microbiol. *23*, 6122–6136. https://doi.org/10.1111/1462-2920.15680.

Branda, S.S., Chu, F., Kearns, D.B., Losick, R., and Kolter, R. (2006). A major protein component of the *Bacillus subtilis* biofilm matrix. Mol. Microbiol. *59*, 1229–1238. https://doi.org/10.1111/j.1365-2958.2005.05020.x.

Branda, S.S., González-Pastor, J.E., Ben-Yehuda, S., Losick, R., and Kolter, R. (2001). Fruiting body formation by *Bacillus subtilis*. Proc. Natl. Acad. Sci. U. S. A. *98*, 11621–11626. https://doi.org/10.1073/pnas.191384198.

Casadaban, M.J., Chou, J., and Cohen, S.N. (1980). In vitro gene fusions that join an enzymatically active B- galactosidase segment to amino-terminal fragments of exogenous proteins: *Escherichia coli* plasmid vectors for the detection and cloning of translational initiation signals. J. Bacteriol. *143*, 971–980. https://doi.org/10.1128/jb.143.2.971-980.1980.

Cazorla, F.M., Romero, D., Pérez-García, A., Lugtenberg, B.J.J., Vicente, A.D., and Bloemberg, G. (2007). Isolation and characterization of antagonistic *Bacillus subtilis* strains from the avocado rhizoplane displaying biocontrol activity. J. Appl. Microbiol. *103*, 1950–1959. https://doi.org/10.1111/j.1365-2672.2007.03433.x.

Chai, Y., Kolter, R., and Losick, R. (2010). An epigenetic switch governing daughter cell separation in *Bacillus subtilis*. Genes Dev. *24*, 754–765. https://doi.org/10.1111/j.1365-2958.2010.07335.x.

Chen, F.Z., You, L.J., Yang, F., Wang, L.N., Guo, X.Q., Gao, F., Hua, C., Tan, C., Fang, L., Shan, R.Q., et al. (2020). CNGBdb: China National GeneBank DataBase. Hereditas *42*, 799–809. https://doi.org/10.16288/j.yczz.20-080.

Chen, Y., Cao, S., Chai, Y., Clardy, J., Kolter, R., Guo, J.H., and Losick, R. (2012). A *Bacillus subtilis* sensor kinase involved in triggering biofilm formation on the roots of tomato plants. Mol. Microbiol. *85*, 418–430. https://doi.org/10.1111/j.1365-2958.2012.08109.x.

Chen, Y., Yan, F., Chai, Y., Liu, H., Kolter, R., Losick, R., and Guo, J.H. (2013). Biocontrol of tomato wilt disease by *Bacillus subtilis* isolates from natural environments depends on conserved genes mediating biofilm formation. Environ. Microbiol. *15*, 848–864. https://doi.org/10.1111/j.1462-2920.2012.02860.x.

Chen, Y., Chen, Y., Shi, C., Huang, Z., Zhang, Y., Li, S., Li, Y., Ye, J., Yu, C., Li, Z., et al. (2018). SOAPnuke: a MapReduce acceleration-supported software for integrated quality control and preprocessing of high-throughput sequencing data. Gigascience *7*, gix120. https://doi.org/10.1093/gigascience/gix120.

Chu, F., Kearns, D.B., Branda, S.S., Kolter, R., and Losick, R. (2006). Targets of the master regulator of biofilm formation in *Bacillus subtilis*. Mol. Microbiol. *59*, 1216–1228. https://doi.org/10.1111/j.1365-2958.2005.05019.x.

Cohn, H.J. (1930). The identity of *Bacillus subtilis*. J. Infect. Dis. *46*, 341–350.

Deatherage, D.E., and Barrick, J.E. (2014). Identification of mutations in laboratory-evolved microbes from Next-Generation Sequencing data using breseq. In Engineering and Analyzing Multicellular Systems. Methods in Molecular Biology (Methods and Protocols), L. Sun and W. Shou, eds. (Humana Press), pp. 165–188. https://doi.org/10.1007/978-1-4939-0554-6_1.

Dragoš, A., Kiesewalter, H., Martin, M., Hsu, C.Y., Hartmann, R., Wechsler, T., Eriksen, C., Brix, S., Drescher, K., Stanley-Wall, N., et al. (2018a). Division of labor during biofilm matrix production. Curr. Biol. *28*, 1903–1913.e5. https://doi.org/10.1016/j.cub.2018.04.046.

Dragoš, A., Lakshmanan, N., Martin, M., Horváth, B., Maróti, G., Falcón García, C., Lieleg, O., and Kovács, Á.T. (2018b). Evolution of exploitative interactions during diversification in *Bacillus subtilis* biofilms. FEMS Microbiol. Ecol. *94*, fix155. https://doi.org/10.1093/femsec/fix155.

Dragoš, A., Martin, M., Falcón García, C., Kricks, L., Pausch, P., Heimerl, T., Bálint, B., Maróti, G., Bange, G., López, D., et al. (2018c). Collapse of genetic division of labour and evolution of autonomy in pellicle biofilms. Nat. Microbiol. *3*, 1451–1460. https://doi.org/10.1038/s41564-018-0263-y.

Egamberdieva, D., Kamilova, F., Validov, S., Gafurova, L., Kucharova, Z., and Lugtenberg, B. (2008). High incidence of plant growth-stimulating bacteria associated with the rhizosphere of wheat grown on salinated soil in Uzbekistan. Environ. Microbiol. *10*, 1–9. https://doi.org/10.1111/j.1462-2920.2007.01424.x.

Elena, S.F., and Lenski, R.E. (2003). Evolution experiments with microorganisms: the dynamics and genetic bases of adaptation. Nat. Rev. Genet. *4*, 457–469. https://doi.org/10.1038/nrg1088.

Endler, A., and Persson, S. (2011). Cellulose synthases and synthesis in *Arabidopsis*. Mol. Plant *4*, 199–211. https://doi.org/10.1093/mp/ssq079.

Fall, R., Kinsinger, R.F., and Wheeler, K.A. (2004). A simple method to isolate biofilm-forming *Bacillus subtilis* and related species from plant roots. Syst. Appl. Microbiol. *27*, 372–379. https://doi.org/10.1078/0723-2020-00267.

Fira, D., Dimkić, I., Berić, T., Lozo, J., and Stanković, S. (2018). Biological control of plant pathogens by *Bacillus* species. J. Biotechnol. *285*, 44–55. https://doi.org/10.1016/j.jbiotec.2018.07.044.

Fujita, M., González-Pastor, J.E., and Losick, R. (2005). High- and low-threshold genes in the Spo0A regulon of *Bacillus subtilis*. J. Bacteriol. *187*, 1357–1368. https://doi.org/10.1128/JB.187.4.1357-1368.2005.

Gallegos-Monterrosa, R., Christensen, M.N., Barchewitz, T., Koppenhöfer, S., Priyadarshini, B., Bálint, B., Maróti, G., Kempen, P.J., Dragoš, A., and Kovács, Á.T. (2021). Impact of Rap-Phr system abundance on adaptation of *Bacillus subtilis*. Commun. Biol. *4*, 468. https://doi.org/10.1038/s42003-021-01983-9.

Gallegos-Monterrosa, R., Mhatre, E., and Kovács, Á.T. (2016). Specific *Bacillus subtilis* 168 variants form biofilms on nutrient-rich medium. Microbiology (United Kingdom) *162*, 1922–1932. https://doi.org/10.1099/mic.0.000371.

Gao, S., Wu, H., Yu, X., Qian, L., and Gao, X. (2016). Swarming motility plays the major role in migration during tomato root colonization by *Bacillus subtilis* SWR01. Biol. Control *98*, 11–17. https://doi.org/10.1016/j.biocontrol.2016.03.011.

Guo, X., Chen, F., Gao, F., Li, L., Liu, K., You, L., Hua, C., Yang, F., Liu, W., Peng, C., et al. (2020). CNSA: a data repository for archiving omics data. Database *2020*, baaa055. https://doi.org/10.1093/database/baaa055.

Guttenplan, S.B., Shaw, S., and Kearns, D.B. (2013). The cell biology of peritrichous flagella in *Bacillus subtilis*. Mol. Microbiol. *87*, 211–229. https://doi.org/10.1111/mmi.12103.

Hassani, M.A., Durán, P., and Hacquard, S. (2018). Microbial interactions within the plant holobiont. Microbiome *6*, 58. https://doi.org/10.1007/978-1-4419-9863-7_100630.

Huang, Y., Wu, Z., He, Y., Ye, B.C., and Li, C. (2017). Rhizospheric *Bacillus subtilis* exhibits biocontrol effect against *Rhizoctonia solani* in Pepper (*Capsicum annuum*). Biomed. Res. Int. *2017*, 1–9. https://doi.org/10.1155/2017/9397619.

Jiang, M., Shao, W., Perego, M., and Hoch, J.A. (2000). Multiple histidine kinases regulate entry into stationary phase and sporulation in *Bacillus subtilis*. Mol. Microbiol. *38*, 535–542. https://doi.org/10.1046/j.1365-2958.2000.02148.x.

Jousset, A., Rochat, L., Péchy-Tarr, M., Keel, C., Scheu, S., and Bonkowski, M. (2009). Predators promote defence of rhizosphere bacterial populations by selective feeding on non-toxic cheaters. ISME J. *3*, 666–674. https://doi.org/10.1038/ismej.2009.26.

Kawecki, T.J., Lenski, R.E., Ebert, D., Hollis, B., Olivieri, I., and Whitlock, M.C. (2012). Experimental evolution. Trends Ecol. Evol. *27*, 547–560. https://doi.org/10.1016/j.tree.2012.06.001.

Kearns, D.B. (2010). A field guide to bacterial swarming motility. Nat. Rev. Microbiol. *8*, 634–644. https://doi.org/10.1038/nrmicro2405.

Kearns, D.B., Chu, F., Branda, S.S., Kolter, R., and Losick, R. (2005). A master regulator for biofilm formation by *Bacillus subtilis*. Mol. Microbiol. *55*, 739–749. https://doi.org/10.1111/j.1365-2958.2004.04440.x.

Kiesewalter, H.T., Lozano-Andrade, C.N., Wibowo, M., Strube, M.L., Maróti, G., Snyder, D., Jørgensen, T.S., Larsen, T.O., Cooper, V.S., Weber, T., and Kovács, Á.T. (2021). Genomic and chemical diversity of *Bacillus subtilis* secondary metabolites against plant pathogenic fungi. mSystems *6*, e00770-20. https://doi.org/10.1101/2020.08.05.238063.

Köhl, J., Kolnaar, R., and Ravensberg, W.J. (2019). Mode of action of microbial biological control agents against plant diseases: relevance beyond efficacy. Front. Plant Sci. *10*, 1–19. https://doi.org/10.3389/fpls.2019.00845.

Konkol, M.A., Blair, K.M., and Kearns, D.B. (2013). Plasmid-encoded ComI inhibits competence in the ancestral 3610 strain of *Bacillus subtilis*. J. Bacteriol. *195*, 4085–4093. https://doi.org/10.1128/JB.00696-13.

Lazarevic, V., Soldo, B., Médico, N., Pooley, H., Bron, S., and Karamata, D. (2005). *Bacillus subtilis* alpha-phosphoglucomutase is required for normal cell morphology and biofilm formation. Appl. Environ. Microbiol. *71*, 39–45. https://doi.org/10.1128/AEM.71.1.39-45.2005.

Lenski, R.E. (2017). What is adaptation by natural selection? Perspectives of an experimental microbiologist. PLoS Genet. *13*, e1006668. https://doi.org/10.1371/journal.pgen.1006668.

Li, E., de Jonge, R., Liu, C., Jiang, H., Friman, V.P., Pieterse, C.M.J., and Bakker, P.A.H.M. (2021a). Rapid evolution of bacterial mutualism in the plant rhizosphere. Nat. Commun. *12*, 3829. https://doi.org/10.2139/ssrn.3650572.

Li, E., Zhang, H., Jiang, H., Pieterse, C.M.J., Jousset, A., Bakker, P.A.H.M., and de Jonge, R. (2021b). Experimental-evolution-driven identification of *Arabidopsis* rhizosphere competence genes in *Pseudomonas protegens*. mBio *12*, e00927-21. https://doi.org/10.1128/mbio.00927-21.

Liebeton, K., Lengefeld, J., and Eck, J. (2014). The nucleotide composition of the spacer sequence influences the expression yield of heterologously expressed genes in *Bacillus subtilis*. J. Biotechnol. *191*, 214–220. https://doi.org/10.1016/j.jbiotec.2014.06.027.

Liepman, A.H., Wightman, R., Geshi, N., Turner, S.R., and Scheller, H.V. (2010). Arabidopsis - a powerful model system for plant cell wall research. Plant J. *61*, 1107–1121. https://doi.org/10.1111/j.1365-313X.2010.04161.x.

Lin, Y., Alstrup, M., Pang, J.K.Y., Maróti, G., Er-Rafik, M., Tourasse, N., Økstad, O.A., and Kovács, Á.T. (2021). Adaptation of *Bacillus thuringiensis* to plant colonization affects differentiation and toxicity. mSystems *6*, e00864-21. https://doi.org/10.1128/msystems.00864-21.

Lozano-Andrade, C.N., Strube, M.L., and Kovács, Á.T. (2021). Complete genome sequences of four soil-derived isolates for studying synthetic microbial community assembly. Microbiol. Resour. Announc. *10*, e00848-21.

Lugtenberg, B., and Kamilova, F. (2009). Plant-growth-promoting rhizobacteria. Annu. Rev. Microbiol. *63*, 541–556. https://doi.org/10.1146/annurev.micro.62.081307.162918.

Martin, M., Dragoš, A., Otto, S.B., Schäfer, D., Brix, S., Maróti, G., and Kovács, Á.T. (2020). Cheaters shape the evolution of phenotypic heterogeneity in *Bacillus subtilis* biofilms. ISME J. *14*, 2302–2312. https://doi.org/10.1038/s41396-020-0685-4.

Mendes, R., Kruijt, M., De Bruijn, I., Dekkers, E., Van Der Voort, M., Schneider, J.H.M., Piceno, Y.M., DeSantis, T.Z., Andersen, G.L., Bakker, P.A.H.M., and Raaijmakers, J.M. (2011). Deciphering the rhizosphere microbiome for disease-suppressive bacteria. Science *332*, 1097–1100. https://doi.org/10.1126/science.1203980.

Mhatre, E., Sundaram, A., Hölscher, T., Mühlstädt, M., Bossert, J., and Kovács, Á. (2017). Presence of calcium lowers the expansion of *Bacillus subtilis* colony biofilms. Microorganisms *5*, 7. https://doi.org/10.3390/microorganisms5010007.

Molina-Santiago, C., Pearson, J.R., Navarro, Y., Berlanga-Clavero, M.V., Caraballo-Rodriguez, A.M., Petras, D., García-Martín, M.L., Lamon, G., Haberstein, B., Cazorla, F.M., et al. (2019). The extracellular matrix protects *Bacillus subtilis* colonies from *Pseudomonas* invasion and modulates plant co-colonization. Nat. Commun. *10*, 1919. https://doi.org/10.1038/s41467-019-09944-x.

Nordgaard, M., Mortensen, R.M.R., Kirk, N.K., Gallegos-Monterrosa, R., and Kovács, Á.T. (2021). Deletion of Rap-Phr systems in *Bacillus subtilis* influences in vitro biofilm formation and plant root colonization. Microbiologyopen *10*, e1212. https://doi.org/10.1002/mbo3.1212.

Ongena, M., and Jacques, P. (2008). *Bacillus* lipopeptides: versatile weapons for plant disease biocontrol. Trends Microbiol. *16*, 115–125. https://doi.org/10.1016/j.tim.2007.12.009.

Pandey, A., and Palni, L.M.S. (1997). *Bacillus* species: the dominant bacteria of the rhizosphere of established tea bushes. Microbiol. Res. *152*, 359–365. https://doi.org/10.1016/S0944-5013(97)80052-3.

Poltak, S.R., and Cooper, V.S. (2011). Ecological succession in long-term experimentally evolved biofilms produces synergistic communities. ISME J. *5*, 369–378. https://doi.org/10.1038/ismej.2010.136.

Reverdy, A., Chen, Y., Hunter, E., Gozzi, K., and Chai, Y. (2018). Protein lysine acetylation plays a regulatory role in *Bacillus subtilis* multicellularity. PLoS One *13*, e0204687. https://doi.org/10.1371/journal.pone.0204687.

Richter, A., Hölscher, T., Pausch, P., Sehrt, T., Brockhaus, F., Bange, G., and Kovács, Á.T. (2018). Hampered motility promotes the evolution of wrinkly phenotype in *Bacillus subtilis*. BMC Evol. Biol. *18*, 155. https://doi.org/10.1186/s12862-018-1266-2.

Ross-Gillespie, A., Gardner, A., West, S.A., and Griffin, A.S. (2007). Frequency dependence and cooperation: theory and a test with bacteria. Am. Nat. *170*, 331–342. https://doi.org/10.1086/519860.

Rudrappa, T., Czymmek, K.J., Paré, P.W., and Bais, H.P. (2008). Root-secreted malic acid recruits beneficial soil bacteria. Plant Physiol. *148*, 1547–1556. https://doi.org/10.1104/pp.108.127613.

Schindelin, J., Arganda-Carreras, I., Frise, E., Kaynig, V., Longair, M., Pietzsch, T., Preibisch, S., Rueden, C., Saalfeld, S., Schmid, B., et al. (2012). Fiji: an open-source platform for biological-image analysis. Nat. Methods *9*, 676–682. https://doi.org/10.1038/nmeth.2019.

Sprouffske, K., and Wagner, A. (2016). Growthcurver: an R package for obtaining interpretable metrics from microbial growth curves. BMC Bioinformatics *17*, 172. https://doi.org/10.1186/s12859-016-1016-7.

Subramaniam, A.R., Deloughery, A., Bradshaw, N., Chen, Y., O'Shea, E., Losick, R., and Chai, Y. (2013). A serine sensor for multicellularity in a bacterium. Elife *2*, e01501. https://doi.org/10.7554/eLife.01501.

Thérien, M., Kiesewalter, H.T., Auria, E., Charron-Lamoureux, V., Wibowo, M., Maróti, G., Kovács, Á.T., and Beauregard, P.B. (2020). Surfactin production is not essential for pellicle and root-associated biofilm development of *Bacillus subtilis*. Biofilm *2*, 100021. https://doi.org/10.1016/j.bioflm.2020.100021.

Tian, T., Sun, B., Shi, H., Gao, T., He, Y., Li, Y., Liu, Y., Li, X., Zhang, L., Li, S., et al. (2021). Sucrose triggers a novel signaling cascade promoting *Bacillus subtilis* rhizosphere colonization. ISME J. *15*, 2723–2737. https://doi.org/10.1038/s41396-021-00966-2.

Trivedi, P., Leach, J.E., Tringe, S.G., Sa, T., and Singh, B.K. (2020). Plant–microbiome interactions: from community assembly to plant health. Nat. Rev. Microbiol. *18*, 607–621. https://doi.org/10.1038/s41579-020-0412-1.

van den Bergh, B., Swings, T., Fauvart, M., and Michiels, J. (2018). Experimental design, population dynamics, and diversity in microbial experimental evolution. Microbiol. Mol. Biol. Rev. *82*. e00008-18. https://doi.org/10.1128/mmbr.00008-18.

van Ditmarsch, D., Boyle, K.E., Sakhtah, H., Oyler, J.E., Nadell, C.D., Déziel, É., Dietrich, L.E.P., and Xavier, J.B. (2013). Convergent evolution of hyperswarming leads to impaired biofilm formation in pathogenic bacteria. Cell Rep. *4*, 697–708. https://doi.org/10.1016/j.celrep.2013.07.026.

van Gestel, J., Weissing, F.J., Kuipers, O.P., and Kovács, Á.T. (2014). Density of founder cells affects spatial pattern formation and cooperation in *Bacillus subtilis* biofilms. ISME J. *8*, 2069–2079. https://doi.org/10.1038/ismej.2014.52.

Varon, D., Boylan, S.A., Okamoto, K., and Price, C.W. (1993). *Bacillus subtilis gtaB* encodes UDP-glucose pyrophosphorylase and is controlled by stationary-phase transcription factor σB. J. Bacteriol. *175*, 3964–3971. https://doi.org/10.1128/jb.175.13.3964-3971.1993.

Vlamakis, H., Aguilar, C., Losick, R., and Kolter, R. (2008). Control of cell fate by the formation of an architecturally complex bacterial community. Genes Dev. *22*, 945–953. https://doi.org/10.1101/gad.1645008.4.

Xu, Z., Zhang, H., Sun, X., Liu, Y., Yan, W., Xun, W., Shen, Q., and Zhang, R. (2019). *Bacillus velezensis* wall teichoic acids are required for biofilm formation and root colonization. Appl. Environ. Microbiol. *85*, e02116–e02118. https://doi.org/10.1128/aem.02116-18.

Zeigler, D.R., Prágai, Z., Rodriguez, S., Chevreux, B., Muffler, A., Albert, T., Bai, R., Wyss, M., and Perkins, J.B. (2008). The origins of 168, W23, and other *Bacillus subtilis* legacy strains. J. Bacteriol. *190*, 6983–6995. https://doi.org/10.1128/JB.00722-08.

Zhu, B., and Stülke, J. (2018). SubtiWiki in 2018: from genes and proteins to functional network annotation of the model organism *Bacillus subtilis*. Nucleic Acids Res. *46*, D743–D748. https://doi.org/10.1093/nar/gkx908.

STAR★METHODS

KEY RESOURCES TABLE

REAGENT or RESOURCE	SOURCE	IDENTIFIER
Chemicals, peptides, and recombinant proteins		
Lysogeny Broth (LB)	Carl Roth GmbH	Catalog # X964.2
Tryptic Soy Broth (TSB)	Sigma-Aldrich	Catalog # 22098-500G-F
Agar	Carl Roth GmbH	Catalog # 5210.2
Potassium Hydrogen Phosphate	Carl Roth GmbH	Catalog # P749.2
Potassium Dihydrogen Phosphate	Carl Roth GmbH	Catalog # 3904.1
MOPS	Carl Roth GmbH	Catalog # 6979.3
Magnesium chloride hexahydrate	Carl Roth GmbH	Catalog # 2189.1
Manganese(II) chloride	Carl Roth GmbH	Catalog # T881.3
Zinc chloride	Carl Roth GmbH	Catalog # T887.1
Thiamine	Carl Roth GmbH	Catalog # T911.1
Calcium chloride	Carl Roth GmbH	Catalog # 5239.1
Ammonium chloride	Carl Roth GmbH	Catalog # K298.2
Glycerol	Carl Roth GmbH	Catalog # 7533.1
Cellobiose	Carl Roth GmbH	Catalog # 5840.3
Xylan from beechwood	Carl Roth GmbH	Catalog # 4414.3
Starch from potatoes	Carl Roth GmbH	Catalog # 9441.1
Potassium hydroxide	Carl Roth GmbH	Catalog # 6751.1
Sodium hypochlorite	VWR	Catalog # 27900.296
Murashige and Skoog basal salts mixture	Sigma-Aldrich	Catalog # M5519
Spectinomycin dihydrochloride	VWR	J61820.14
Experimental models: Organisms/strains		
DK1042: *B. subtilis* NCIB 3610 *comI*^{Q12I}	(Konkol et al., 2013)	Strain DK1042
TB500.1: DK1042 *amyE*::$P_{hyperspank}$-*gfp* Spec^R	(Mhatre et al., 2017)	N/A
TB501.1: DK1042 *amyE*::$P_{hyperspank}$-*mKATE2* Spec^R	(Dragoš et al., 2018a)	N/A
TB530.1: DK1042 *amyE*::$P_{hyperspank}$-*gfp* Spec^R *hag*::Km^R		N/A
TB531.1: DK1042 *amyE*::$P_{hyperspank}$-*mKATE2* Spec^R *hag*::Km^R		N/A
DTUB310: DK1042 Ev6.1 *amyE*::$P_{hyperspank}$-*gfp* Spec^R	This study	N/A
DTUB311: DK1042 Ev6.1 *amyE*::$P_{hyperspank}$-*mKATE2* Spec^R		
DTUB312: DK1042 Ev7.3 *amyE*::$P_{hyperspank}$-*gfp* Spec^R		
DTUB313: DK1042 Ev7.3 *amyE*::$P_{hyperspank}$-*mKATE2* Spec^R		
D749: *Pedobacter* sp	(Lozano-Andrade et al., 2021)	N/A
D757: *Rhodococcus globerulus*		N/A
D763: *Stenotrophomas indicatrix*		N/A
D764: *Chryseobacterium* sp		N/A
MC1061: *Escherichia coli* K-12 F λ Δ(*ara-leu*)*7697* [*araD139*]$_{B/r}$ Δ(*codB-lacI*)*3 galK16 galE15* e14 *mcrA0 relA1 rpsL150*(Str^R) *spoT1 mcrB1 hsdR2*(r m$^+$)	(Casadaban et al., 1980)	N/A
Arabidopsis thaliana Col-0	NASC	N/A
Recombinant DNA		
pTB497.1	(van Gestel et al., 2014)	N/A
pTB498.1	(Dragoš et al., 2018b)	N/A

(*Continued on next page*)

Continued

REAGENT or RESOURCE	SOURCE	IDENTIFIER
Software and algorithms		
Zen 3.1 Software	Carl Zeiss, Oberkochen, Germany	https://www.zeiss.com/corporate/int/home.html
ImageJ	(Schindelin et al., 2012)	https://imagej.nih.gov/ij/
OriginPro 2020	OriginLab, Northampton, MA, USA	https://www.originlab.com/
R Studio	RStudio, Boston, MA, USA	https://www.rstudio.com/
bcl2fastq (v2.17.1.14)	Illumina, San Diego, CA, USA	https://www.illumina.com/
CLC Genomics Workbench	Qiagen, Hilden, Germany	https://digitalinsights.qiagen.com
SOAPnuke (v1.5.6)	(Chen et al., 2018)	https://github.com/BGI-flexlab/SOAPnuke
breseq (v0.35.7)	(Deatherage and Barrick, 2014)	https://barricklab.org/twiki/bin/view/Lab/ToolsBacterialGenomeResequencing
Others		
Glass beads Ø0.25-0.5 mm,	Carl Roth GmbH	Catalog # A553.1

RESOURCE AVAILABILITY

Lead contact

Further information and requests for resources and reagents should be directed to and will be fulfilled by the Lead Contact, Ákos T. Kovács (atkovacs@dtu.dk).

Materials availability

Bacterial isolates derived from the experimental evolution in this study are available upon request from Ákos T. Kovács (atkovacs@dtu.dk). This study did not generate new unique plasmids or reagents.

Data and code availability

The sequencing data for single evolved isolates has been deposited into the NCBI Sequence Read Archive (SRA) database under BioProject accession number: PRJNA705352, and sequencing data for endpoint populations into CNGB Sequence Archive (CNSA) (Guo et al., 2020) of China National GeneBank DataBase (CNGBdb) (Chen et al., 2020) with accession number CNP0002416.

Other data reported in this study is available from the lead contact upon reasonable request.

This study does not report any new, original code.

Any Additional information can be obtained upon request from Ákos T. Kovács (atkovacs@dtu.dk).

EXPERIMENTAL MODEL AND SUBJECT DETAILS

Bacterial strains and culture media

Bacillus subtilis DK1042 strain, an easily transformable derivative of the undomesticated *B. subtilis* NCBI 3610 (Konkol et al., 2013), was used as ancestor for the experimental evolution. For pairwise competitions between the ancestor and evolved isolates, and for root co-colonization with a synthetic, soil-derived community, TB500.1 and TB501.1, that were previously created by transforming DK1042 with pTB497.1 and pTB498.1 (Dragoš et al., 2018a; Mhatre et al., 2017), respectively, were used as the ancestor. In addition, selected evolved isolates derived from the ancestor were transformed with plasmids pTB497.1 and pTB498.1. These plasmids harbor the *gfp* and *mKATE* gene, respectively, under the control of the hyper-spank (constitutive) promoter and a spectinomycin resistance gene within the flanking regions of the *amyE* gene. Transformants were identified by selecting for spectinomycin resistance and double cross-overs were verified by the loss of amylase activity on LB agar + starch plates.

The four bacterial species, *Pedobacter* sp., *Rhodococcus globerulus*, *Stenotrophomas indicatrix* and *Chryseobacterium* sp., constituting a synthetic, soil-derived community were previously acquired in

Dyrehaven, Kongens Lyngby, Denmark (55° 47′ 19.68″ N, 12° 33′ 29.88″ E), as described (Lozano-Andrade et al., 2021). An overview of the strains used in this study is included in the Key Resources Table.

B. subtilis strains were routinely grown overnight (ON) in Lysogeny Broth (LB; LB-Lennox, Carl Roth, Germany; 10 g/L tryptone, 5 g/L yeast extract and 5 g/L NaCl) at 37°C while shaking at 220 rpm. When relevant, spectinomycin was added at a final concentration of 100 μg/mL. The bacterial species used for the synthetic, soil-derived community were grown for 48 h in 0.1% (w/v) Tryptic Soy Broth (TSB; Sigma-Aldrich, St. Louis, Missouri, USA) at room temperature. For the experimental evolution on plant roots and root colonization assays, a minimal salts nitrogen glycerol (MSNg) medium was used. MSNg was prepared as follows: The base was prepared by adding 0.026 g KH_2PO_4, 0.061 g K_2HPO_4, 2.09 g MOPS and 0.04 g $MgCl_2$ x $6H_2O$ per 100 mL dH_2O and adjusting the pH to 7.0 using KOH. The base was autoclaved, cooled down to room temperature and then supplemented with 0.05 mL of 100 mM $MnCl_2$, 0.1 mL of 1 mM $ZnCl_2$, 0.1 mL of 2 mM thiamine, 0.1 mL of 0.7 M $CaCl_2$, NH_4Cl_2 to a final 0.2% and glycerol to a final 0.05%. Growth of *B. subtilis* ancestor and evolved isolates alone or in co-culture with the synthetic, soil-derived community was monitored in MSNc + xylan, which was prepared similarly to MSNg except that instead of glycerol, cellobiose and xylan were added to a final concentration of 0.5%. Pellicle biofilm formation was assessed in LB medium with or without a supplementation of xylan (0.5%) (w/v). Pairwise competitions between the ancestor and evolved isolates were evaluated in LB + xylan (0.5%).

Plant material

Arabidopsis thaliana Col-0 seedings were used as plant host for the experimental evolution and root colonization assays. The seeds were surface sterilized in a 2% (v/v) sodium hypochlorite solution (VWR, Radnor, Pennsylvania, USA) and shaken on an orbital mixer for 12 minutes. The seeds were washed five times in sterile, distilled water. Approximately 15 sterilized seeds were carefully pipetted onto pre-dried MS agar plates (Murashige and Skoog basal salts mixture, Sigma-Aldrich) (2.2 g L^{-1}, pH = 5.6–5.8 supplemented with 1% agar). Plates were sealed with parafilm and stratified at 4°C for 3 days, and were then placed at an angle of 65°C in a plant chamber (cycles of 16 h light at 24°C, and 8 h dark at 20°C). The seedlings were grown in the plant chamber for 6-8 days before use.

METHOD DETAILS

Experimental evolution of *B. subtilis* on *A. thaliana* seedlings

To study the evolutionary adaptation of *B. subtilis* to *A. thaliana* roots, we employed an experimental evolution (EE) setup similar to the one established by Lin et al. (2021). This setup was inspired by a long-term EE on polystyrene beads (Poltak and Cooper, 2011), but instead of beads, *A. thaliana* roots were used for successive root colonization by *B. subtilis*. The EE on plant seedlings was carried out under axenic, hydroponic conditions optimized for *B. subtilis* (Beauregard et al., 2013; Dragoš et al., 2018a; Gallegos-Monterrosa et al., 2016; Nordgaard et al., 2021; Thérien et al., 2020). Seven parallel populations were initiated by inoculating *A. thaliana* seedlings, placed in 300 μL MSNg medium in 48-well plates, with *B. subtilis* DK1042 at a starting OD_{600} of 0.02. In addition, a replicate with a sterile root in MSNg without bacterial inoculation was included as a control. The 48-well plate was incubated in a plant chamber (cycles of 16 h light at 24°C/8 h dark at 20°C) at mild agitation (90 rpm). After 48 h, the colonized seedling was washed twice in MSNg and transferred to fresh medium containing a new, sterile seedling enabling re-colonization. Following this approach, the seven parallel populations were serially transferred every 48 h for a total of 32 transfers. At different time points during the ongoing EE, the old seedlings were washed twice in MSNg and vortexed with glass beads to disperse the biofilm. The resulting cell suspension was used for plating to follow the productivity of the evolving populations, i.e. colony-forming unit (CFU) per root, and also preserved as frozen (−80°C) stocks for later analysis.

Isolation of single evolved isolates and colony morphology assay

Frozen stocks of population 3, 4, 6 and 7 from three different time points during the EE (transfer 12, 18 and 30) were streaked on LB plates to obtain single colonies of evolved isolates. Transfer 30 (T30) was designated as the final transfer for the isolation of evolved isolates. From each population and time point, three colonies were randomly selected, prepared as ON cultures and saved as frozen stocks. Colony morphologies of evolved isolates were examined by spotting 2 μL ON cultures on LB agar (1.5%) and incubated at 30°C for 48 h. Importantly, by growing the ancestor and evolved isolates from frozen stocks in LB ON,

all isolates should be in a similar physiological state, so a potential difference in colony morphology should be attributed to genetic variation.

Root colonization assay

The evolved isolates were tested for root colonization under the same conditions applied during the EE. For individual root colonization, sterile *A. thaliana* seedlings in MSNg medium were inoculated with the ancestor or evolved isolates at a starting OD_{600} of 0.02. For pairwise competition experiments, sterile *A. thaliana* seedlings were inoculated with a 1:1 mix of the ancestor and evolved isolates with opposite, fluorescent labels. Importantly, to obtain a similar starting cell number for the competition experiment, ON cultures of the ancestor and isolate Ev6.1 were adjusted to an OD_{600} of 0.2, while Ev7.3 was adjusted to an OD_{600} of 1.0 corresponding to comparable total cell counts. For plant co-colonization by *B. subtilis* in the presence of a soil-derived synthetic community, cell suspensions of *Pedobacter* sp. D749 and *Rhodococcus globerulus* D757 were adjusted to an OD_{600} of 2.0, *Stenotrophomas indicatrix* D763 to an OD_{600} of 0.05 and *Chryseobacterium* sp. D764 to an OD_{600} of 0.1 and mixed by equal volumes (hereafter referred to as community). This mix was further adjusted to an OD_{600} of 0.2. OD-adjusted *B. subtilis* ancestor (OD_{600} of 0.2) or Ev7.3 (OD_{600} of 1.0) and community were co-inoculated in four different ratios (0.1:1, 1:1, 10:1, 100:1 of *B. subtilis* and community, respectively) into MSNg medium containing a sterile *A. thaliana* seedling. The 48-well plates of all root colonization assays were incubated in the plant chamber at mild agitation (90 rpm). After 48 h, the colonized seedling was washed twice in MSNg and either vortexed with glass beads, and the resulting cell suspension plated for CFU quantification, or transferred to a glass slide for imaging using confocal laser scanning microscopy (CLSM).

For root colonization competition between *B. subtilis* WT and the Δ*hag* mutant, ON cultures of the WT and Δ*hag* mutant with opposite fluorescent labels were mixed 1:1 and inoculated onto sterile *A. thaliana* seedlings in MSNg medium at a starting OD_{600} of 0.02. Plates were incubated in the plant chamber under static or shaking conditions (200 rpm) for 48 h. The seedlings were then washed in MSNg and transferred to fresh medium containing a new, sterile seedling and incubated under the same conditions as before (i.e. static or shaking conditions). This step was repeated once more, after which the third root was washed and vortexed with glass beads, and the resulting cell suspension was plated for CFU quantification.

Pairwise competition experiments in LB + xylan

ON cultures of the ancestor and selected evolved isolates were adjusted to an OD_{600} of 5.0. Ancestor was mixed 1:1 and 1:5 by volume with Ev6.1 and Ev7.3, respectively, to obtain a comparable number of starting cells. 80 μL of the mix was inoculated into 20 mL LB + xylan (0.5%) medium in 100 mL bottles, giving a starting OD_{600} of 0.02. Bottles were incubated at 37°C while shaking at 220 rpm for 48 h followed by plating for CFU quantification.

Biofilm formation in response to plant polysaccharides

To test for pellicle biofilm formation in response to plant polysaccharides, the ancestor or the evolved isolates were inoculated into 1.5 mL LB + xylan (0.5%) medium in 24-well plates to a starting OD_{600} of 0.05 and incubated under static conditions at 30°C for 48 h. In addition, the ancestor and evolved isolates were evaluated for biofilm formation in LB without supplementation.

Motility assays

Swimming motility was tested using soft agar plates (15 mL LB with 0.3% agar) dried for 5 minutes while swarming motility was evaluated on semi-soft agar plates (15 mL LB with 0.7% agar) dried for 20 minutes. 2 μL ON cultures of the ancestor or evolved isolates adjusted to an OD_{600} of 0.5 were spotted in the middle of a petri dish and incubated at 37°C. Multiple stacking was avoided in order to keep a similar humidity across all plates. Swimming and swarming motility were followed for 6 and 8 h, respectively. For each plate, motility was quantified as the averaged radius measured in four different directions.

Growth in the presence of xylan

To monitor the growth of ancestor and evolved isolates in the presence of plant compounds, two independent ON cultures of each isolate were independently inoculated into a 96-well plate containing 100 μL MSNc + xylan (0.5%) medium at a starting OD_{600} of 0.1. OD_{600} was monitored in a plate reader (BioTek Synergy HTX Multi-Mode Microplate Reader) every 15 min for 55 h at 24°C under continuous shaking (orbital).

To test for growth in co-culture with the community, two to three independent ON cultures of constitutively GFP-labelled *B. subtilis* ancestor and Ev7.3 were adjusted to an OD_{600} of 0.1 in MSNc + xylan (0.5%). Cell suspensions of the four community members were adjusted in MSNc + xylan (0.5%) to the same OD_{600} values used for the root colonization assay (see above), and the mixed community was adjusted to a final OD_{600} of 0.1. Ancestor or Ev7.3 was co-inoculated with the community in the same ratios as for the root colonization assay (0.1:1, 1:1, 10:1 and 100:1 of *B. subtilis* and community, respectively). OD_{600} and GFP were monitored in the plate reader every 15 minutes for 35 h at 24°C under continuous shaking (orbital). In both growth assays, each well was measured at 9 (OD_{600}) or 5 ($GFP_{485/20nm}$) different points to avoid artifacts due to aggregation.

Pairwise interactions of *B. subtilis* with community members

To study potential altered interactions with any of the four bacterial species of the community, 2 μL of ON cultures of *B. subtilis* ancestor or Ev7.3 adjusted to an OD_{600} of 0.5 was spotted on LB agar (1.5%). On the same plate, 2 μL of cell suspensions of *Pedobacter* sp. (OD_{600} of 2.0), *Rhodococcus globerulus* (OD_{600} of 2.0), *Stenotrophomas indicatrix* (OD_{600} of 0.1) or *Chryseobacterium* sp. (OD_{600} of 0.1) were spotted at a 0.7 cm distance from the *B. subtilis* inoculum. The plates were incubated at 30°C.

Microscopy/confocal laser scanning microscopy (CLSM)

Bright-field images of colonies, whole pellicle biofilms and pairwise interactions were acquired with an Axio Zoom V16 stereomicroscope (Carl Zeiss, Germany) equipped with a Zeiss CL 9000 LED light source and an AxioCam MRm monochrome camera (Carl Zeiss, Germany). Images of colonized seedlings were acquired using CLSM (Leica Microsystems Confocal Microscope SP8, Germany). The seedlings were washed twice in MSNg and placed onto glass slides. Images were obtained using the 63×/1.4 OIL objective. Fluorescent reporter excitation was performed with the argon laser at 488 nm while the emitted fluorescence of GFP and mKate was recorded at 484–536 nm and 567–654 nm, respectively. For each competition, three images from three independent seedlings were obtained. Representative images were used to visualize root colonization. Zen 3.1 Software (Carl Zeiss) and ImageJ was used for image visualization.

Genome re-sequencing and genome analysis of single isolates and endpoint populations

Genomic DNA of selected evolved isolates from different time points and whole populations from the final transfer (T30) of the EE was extracted from 2 mL ON cultures using the EURx Bacterial and Yeast Genomic DNA Kit. Resequencing of single evolved isolates was performed as previously described (Dragoš et al., 2018b, 2018c; Gallegos-Monterrosa et al., 2021; Martin et al., 2020; Thérien et al., 2020). Briefly, paired-end libraries were prepared using the NEBNext® Ultra™ II DNA Library Prep Kit for Illumina. Paired-end fragment reads were generated on an Illumina NextSeq sequencer using TG NextSeq® 500/550 High Output Kit v2 (300 cycles). Primary data analysis (base-calling) was carried out with "bcl2fastq" software (v2.17.1.14, Illumina). All further analysis steps were done in CLC Genomics Workbench. Reads were quality-trimmed using an error probability of 0.05 (Q13) as the threshold. In addition, the first ten bases of each read were removed. Reads that displayed ≥80% similarity to the reference over ≥80% of their read lengths were used in the mapping. Non-specific reads were randomly placed to one of their possible genomic locations. Quality-based SNP and small In/Del variant calling was carried out requiring ≥8 × read coverage with ≥25% variant frequency. Only variants supported by good quality bases (Q ≥ 20) were considered and only when they were supported by evidence from both DNA strands in comparison to the *B. subtilis* NCIB 3610 genome and pBS plasmid (GenBank accession no. NZ_CP020102 and NZ_CP020103, respectively).

For whole-population sequencing of the evolved populations from the final time point, acoustic fragmentation PCR-free libraries were prepared using MGIEasy PCR-free Library Prep Set (MGI Tech). Paired-end fragment reads (150bp x 2) were generated on a DNBSEQ-Tx sequencer (MGI Tech) following the manufacturer's procedures. All population samples were sequenced with >200 x coverage for polymorphism calling. Raw data were filtered using SOAPnuke (v1.5.6) (Chen et al., 2018) to remove low quality reads: reads including more than 50% of bases with quality lower than 12, reads including more than 10% of unknown base "N," and reads containing adaptor contamination. Mutations were called using *Breseq* (v0.35.7) with the default parameters and a -p option for population samples (Deatherage and Barrick, 2014). The default parameters called mutations only if they appeared at least 2 times from each strand and reached a frequency of at least 5% in the population. Similar to single evolved isolates, the *B. subtilis* NCIB 3610 genome and pBS plasmid were used as references for mutation calling. For both

single evolved isolates and whole populations, mutations were removed if they were also found in the ancestor to obtain the final mutation set. Identified mutations in the evolved isolates and whole populations are listed in Tables S1 and S2, respectively.

The sequencing data for single evolved isolates that support the findings of this study has been deposited into the NCBI Sequence Read Archive (SRA) database under BioProject accession number: PRJNA705352, and sequencing data for endpoint populations into CNGB Sequence Archive (CNSA) (Guo et al., 2020) of China National GeneBank DataBase (CNGBdb) (Chen et al., 2020) with accession number CNP0002416.

QUANTIFICATION AND STATISTICAL ANALYSIS

Data and statistical analysis

Data and statistical analysis were carried out in Excel, OriginPro and R Studio. Outliers were identified using Dixon's test for outliers. For all statistical tests, normality was evaluated with a Shapiro-Wilk test. Equal variance was tested using F-test (for two groups) or Levene's test (for more than two groups). In addition, p-values were corrected for multiple testing using the Benjamini & Hochberg (BH) procedure within each series of experiments. For all statistical tests, a significance level of 0.05 was used. No statistical methods were used to pre-estimate sample size and the experiments were not randomized.

For individual root colonization, the log10-transformed productivity (CFU/mm root) of the replicates were divided by the mean of the log10-transformed productivity of the ancestor from the same experimental setup. For competition between WT and the Δ*hag* mutant, the observed frequencies of the WT after 48 h (on the third root) were divided by 0.5 (the starting frequency in the inoculation mix). For these experiments, the resulting normalized values were subjected to a One-sample *t*-test to test whether the mean was significantly different from 1. For pairwise competitions between the ancestor and evolved isolates on the root or in LB + xylan, the relative fitness (r) of the evolved isolate was calculated by comparing the frequency of the evolved isolate at the beginning and the end of the competition experiment as shown in Equation 1 (Jousset et al., 2009; Li et al., 2021a; Ross-Gillespie et al., 2007), in which X_0 is the initial and X_1 is the final frequency of the evolved isolate. The relative fitness was log2-transformed, and these values were subjected to a One-sample *t*-test to test whether the mean was significantly different from 0.

$$\text{Relative fitness } (r) = \frac{X_1(1 - X_0)}{X_0(1 - X_1)} \qquad \text{(Equation 1)}$$

For root co-colonization of the ancestor and Ev7.3 with the community, within each inoculation ratio, statistical significance between *B. subtilis* ancestor and Ev7.3, and between the communities co-inoculated with the ancestor or with Ev7.3 was tested with a Two-sample *t*-test. If the groups had unequal variance, Welch's Two-sample *t*-test was applied.

For swimming and swarming motility, an ANOVA was performed on the log10-transformed data at each time point followed by a Dunnett's Multiple Comparison test using the ancestor as the control group.

For growth curve analysis of the ancestor and evolved isolates in monoculture, the carrying capacity (K) of individual replicates was calculated from the OD_{600} data using the Growthcurver-package in R (Sprouffske and Wagner, 2016). Significant difference in carrying capacity between ancestor and evolved isolates was tested by an ANOVA followed by a Dunnett's Multiple Comparison test. Similarly, for the growth profiles of *B. subtilis* ancestor and Ev7.3 in co-culture with the community, the carrying capacity (K) was calculated from the $GFP_{485/20nm}$ data. Significant difference between ancestor and Ev7.3 under the same inoculation ratio or alone was tested by a Two-sample *t*-test or Wilcoxon Unpaired Two-sample test (when data failed to meet parametric assumptions).

iScience, Volume *25*

Supplemental information

Experimental evolution of *Bacillus subtilis* on *Arabidopsis thaliana* roots reveals fast adaptation and improved root colonization

Mathilde Nordgaard, Christopher Blake, Gergely Maróti, Guohai Hu, Yue Wang, Mikael Lenz Strube, and Ákos T. Kovács

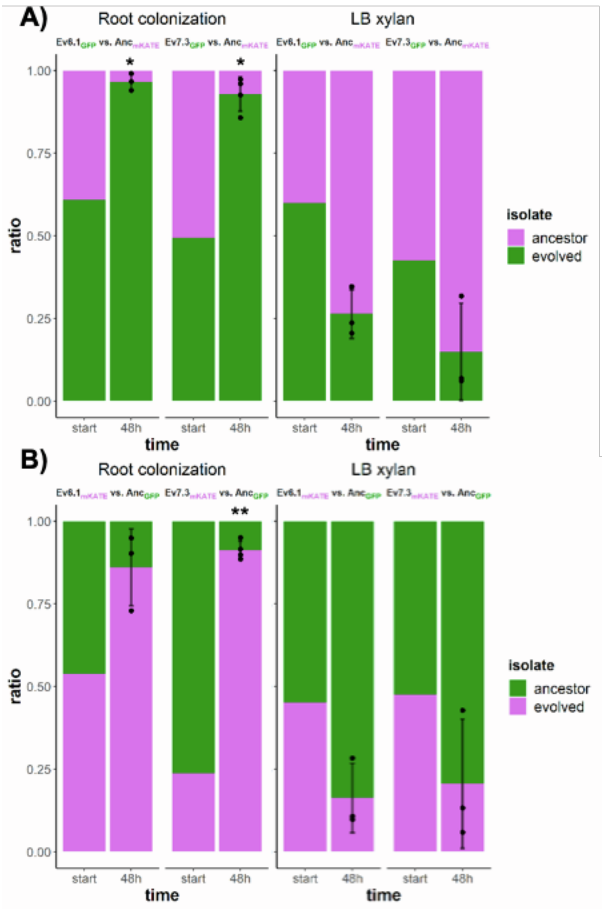

Figure S1: Competition between selected evolved isolates and the ancestor during root colonization and in LB xylan under shaking conditions. Related to Figure 4. (**A**) Competition between ancestor (magenta) and evolved isolates (green) during root colonization (left) and in LB xylan (0.5 %) under shaking conditions (right) for 48 h. (**B**) Same as in A, but with opposite fluorescent labels. The bar plots show the starting ratio of the evolved isolate and ancestor in the mix, and the observed ratios after 48 hours. Bars represent the mean (N=3-4) and the error bars represent standard deviation. The points show the replicates for the evolved (from below) and ancestor (from above). For statistical analysis, the relative fitness (r) of the evolved isolates was calculated by comparing the frequency of the evolved isolate at the beginning and at the end of the competition experiment. The log2-transformed relative fitness values were subjected to a One-sample *t*-test to test whether the mean was significantly different from 0. * and ** indicate P<0.05 and P<0.01, respectively.

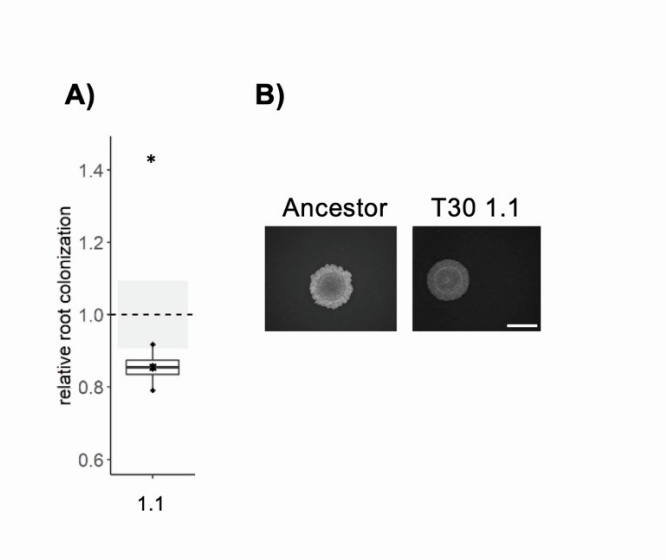

Figure S2: Relative root colonization and colony morphology of an evolved isolate from population 1 at the final transfer. Related to Figure 3. (**A**) Isolate Ev1.1 from transfer 30 was tested for individual root colonization. Relative root colonization was calculated by dividing the log10-transformed productivity (CFU/mm root) of each replicate by the mean of the log10-transformed productivity of the ancestor. The cross represents the mean relative root colonization (N=4). The dashed, horizontal line represents the mean of the ancestor (N=4), while the grey-shaded rectangles represent the standard deviation of the ancestor. The normalized values were subjected to a One-sample *t*-test to test whether the mean was significantly different from 1. * indicates $P<0.05$. (**B**) ON cultures of the ancestor and Ev1.1 were spotted on LB agar (1.5 %) and imaged after incubation for 48 h at 30 °C using the stereomicroscope. Ancestor represents *B. subtilis* DK1042. Each colony is representative of at least three replicates. Scale bar denotes 5 mm.

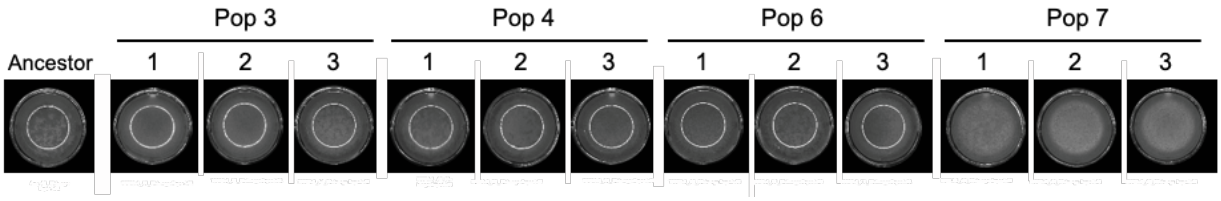

Figure S3: Pellicle biofilm formation in LB of the ancestor and evolved isolates from the final transfer. Related to Figure 5. *B. subtilis* ancestor and evolved isolates from transfer 30 were inoculated into LB medium at a starting OD_{600} of 0.05 in 24-well plates and incubated for 48 h at 30 °C. Each image is representative of 3-4 replicates. The wells are 16 mm width.

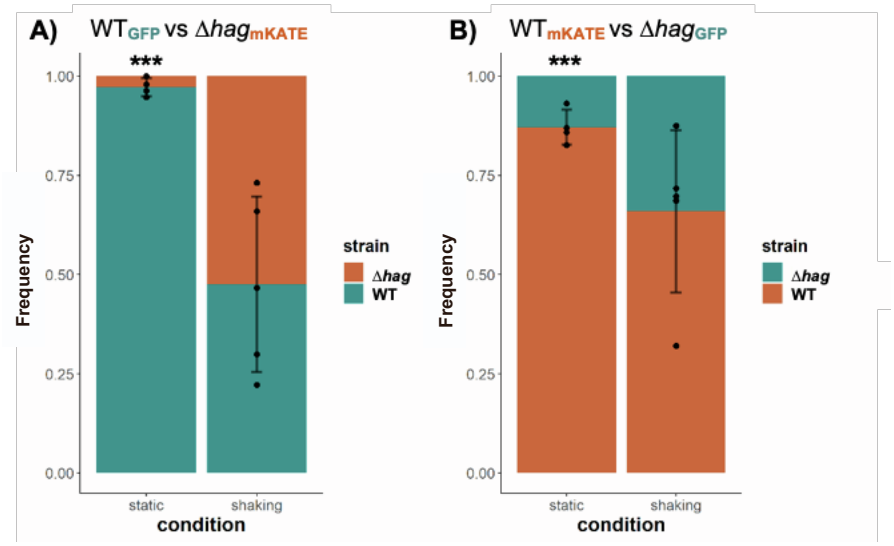

Figure S4: Motility is not important for root colonization under shaking conditions. Related to Figure 5. Competition between *B. subtilis* DK1042 (WT) and a Δ*hag* mutant during root colonization in MSNg medium. *A. thaliana* seedlings were inoculated with a 1:1 mix of WT and mutant with opposite fluorescent labels at a starting OD_{600}=0.02. Plates were incubated for 48 h in the plant chamber under static conditions or shaking conditions (200 rpm). After three successive rounds of root colonization, productivity on the third root was quantified as CFU per cm root. (**A**) Competition between WT (turquoise) and the Δ*hag* mutant (orange). (**B**) Same as in A, but with opposite fluorescent labels. Bars represent the mean ratio (N=4-5) and the error bars represent standard deviation. The points show the replicates for the WT (from below) and the Δ*hag* mutant (from above). The observed frequencies of the WT after 48 h (on the third root) were divided by 0.5 (the starting frequency in the inoculation mix), and the resulting normalized values were subjected to a One-sample *t*-test to test whether the mean was significantly different from 1. *** indicates P<0.001.

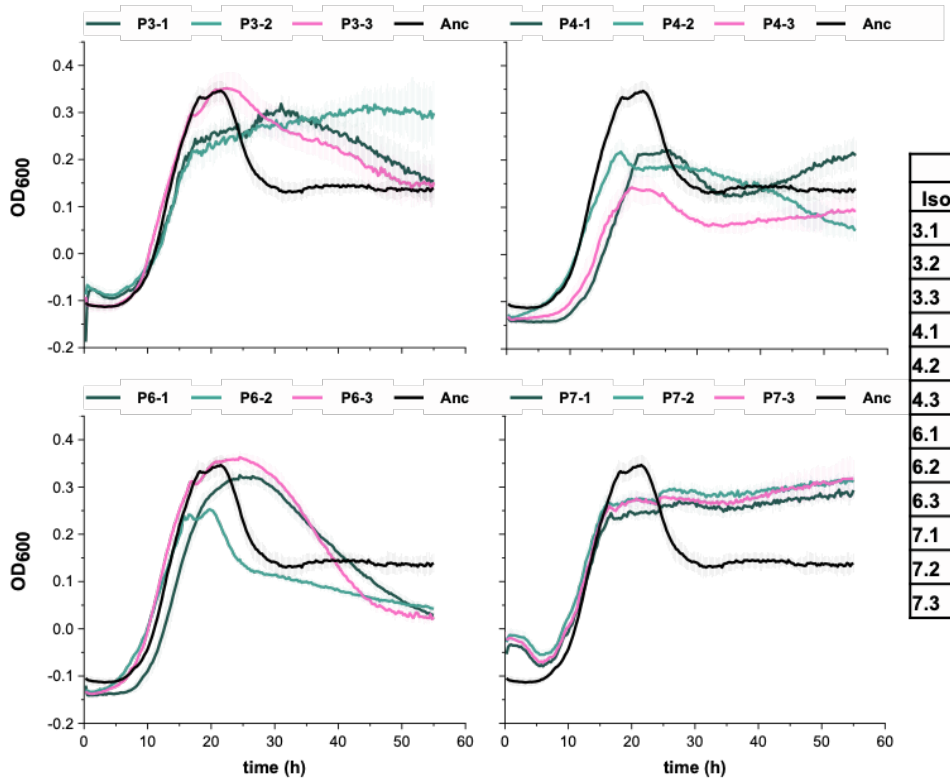

Carrying capacity (K)		
Isolate	**Estimate**	**P-value**
3.1	0.06171	<0.001 ***
3.2	0.1046	<0.001 ***
3.3	0.05412	<0.001 ***
4.1	-0.01126	0.868
4.2	-0.03859	<0.001 ***
4.3	-0.0955	<0.001 ***
6.1	0.01045	0.912
6.2	-0.06691	<0.001 ***
6.3	0.01917	0.254
7.1	0.07988	<0.001 ***
7.2	0.10695	<0.001 ***
7.3	0.09901	<0.001 ***

Figure S5: Growth of *B. subtilis* ancestor and evolved isolates in MSNc + xylan. Related to Figure 5. Growth of the ancestor and evolved isolates in MSNc + xylan (0.5 %) (starting OD_{600} = 0.1) was measured every 15 min at 24 °C under shaking conditions (orbital). Data represents mean and error bars represent standard deviation (N=6-12, 2 independent ON cultures with 3-6 technical replicates each). The carrying capacity (K) was calculated using “Growthcurver” in R. Significant difference between ancestor and evolved isolates was tested by an ANOVA followed by a Dunnett’s Multiple Comparison test. *** indicates P<0.001.

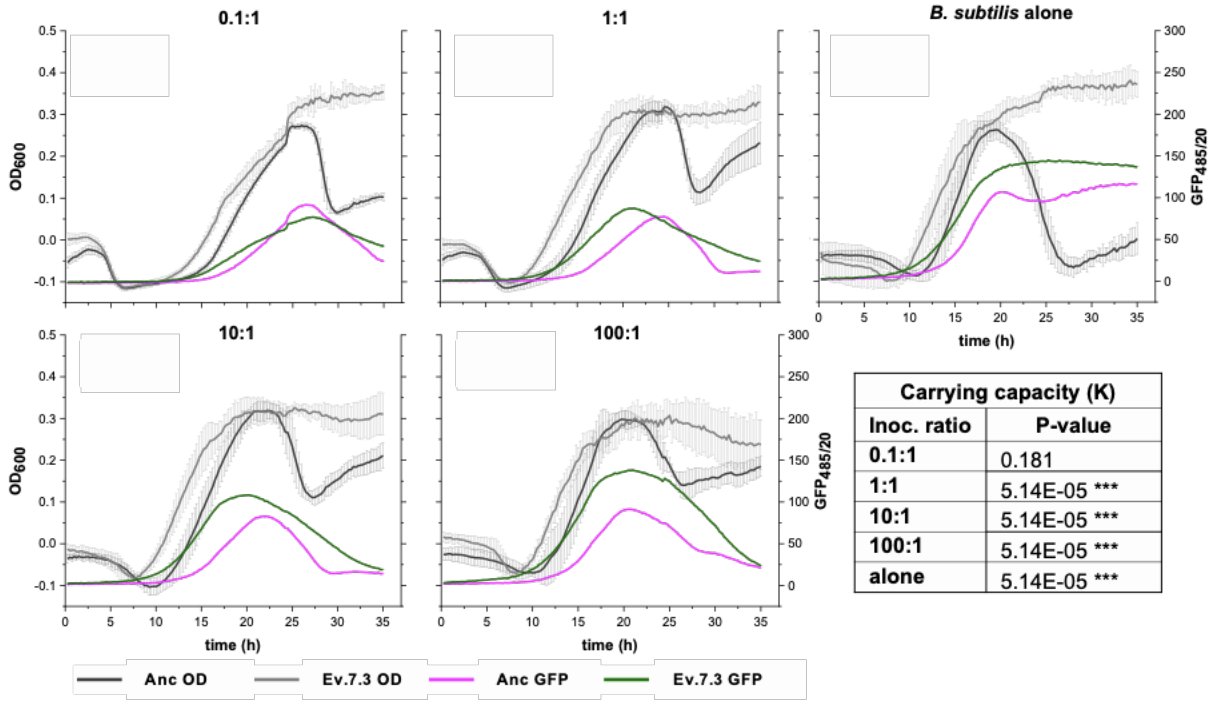

Carrying capacity (K)	
Inoc. ratio	P-value
0.1:1	0.181
1:1	5.14E-05 ***
10:1	5.14E-05 ***
100:1	5.14E-05 ***
alone	5.14E-05 ***

Figure S6: Ev7.3 shows enhanced carrying capacity in MSNc + xylan when co-cultured with a semi-synthetic, soil-derived community compared to the ancestor. Related to Figure 6. Growth of constitutively GFP-expressing *B. subtilis* ancestor or Ev7-3 in co-culture with the community in MSNc + xylan (0.5 %) was measured under four different inoculation ratios: 0.1:1, 1:1, 10:1 and 100:1 of *B. subtilis* and community, respectively. OD_{600} and $GFP_{485/20nm}$ were measured every 15 min for 35 h at 24 °C while shaking. Data represents mean and error bars represent standard deviation (N=6-9, 2-3 independent ON cultures with 3 technical replicates each). The carrying capacity (K) was calculated from the $GFP_{485/20nm}$ data. Significant difference in carrying capacity between the ancestor and Ev7.3 under the same inoculation ratio or alone was tested by a Two-sample *t*-test or Wilcoxon Unpaired Two-sample test (when data failed to meet parametric assumptions). *** indicates P<0.001.

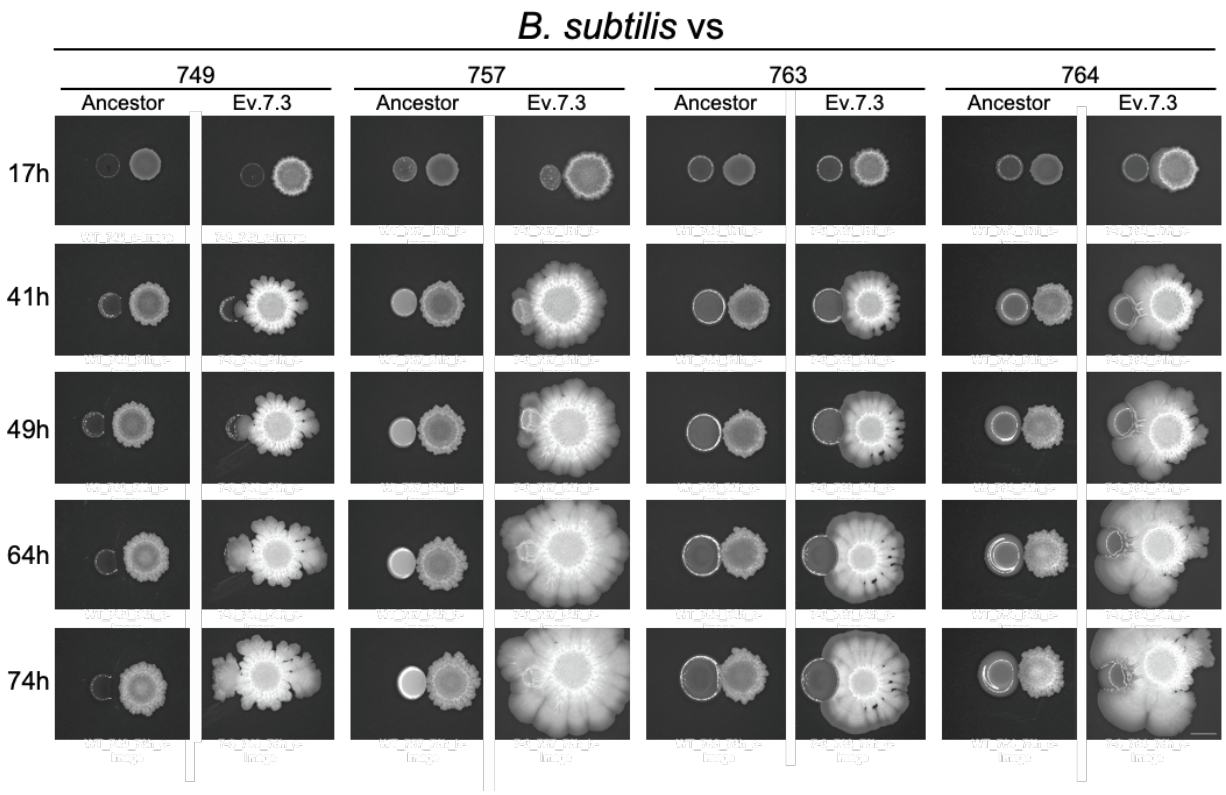

Figure S7: Pairwise interactions of *B. subtilis* ancestor or evolved isolate 7.3 with bacterial species. Related to Figure 6. Ancestor or Ev7.3 was spotted on LB agar (1.5 %) at 0.7 cm distance from bacterial species belonging to *Pedobacter sp.* D749, *Rhodococcus globerulus* D757, *Stenotrophomas indicatrix* D763 or *Chryseobacterium sp.* D764. Plates were incubated at 30 °C and images were captured at the given time points using the stereomicroscope. Ancestor represents *B. subtilis* DK1042. Each colony is a representative of three replicates. Scale bar denotes 5 mm.

Table S1: The table shows detected mutations in the re-sequenced genomes of evolved isolates. Related to Figure 5. The functions of the gene products were retrieved from the SubtiWiki Database (Zhu and Stülke, 2018). T = Transfer.

T12			T18			T30							Position	Gene	Mutation	Function
7.1	7.2	7.3	7.1	7.2	7.3	1.1	6.1	6.2	6.3	7.1	7.2	7.3				
								X					72039	*spoIIE*	Glu489*	protein serine phosphatase,
											X		84980	*pabC*	Leu24Val	aminodeoxychorismate lyase,
										X		X	235527	Intergenic (*glpT*/*ybeF*)	T>C	*glpT*: glycerol-3-phosphate permease. *ybeF*: unknown
	X												529455	*tRNA*	C>T	
		X											578493	*ydeS*	Ala39Val	unknown regulator (similar to transcriptional regulator (TetR family))
		X											961914	*ssuB*	483C>T	aliphatic sulfonate ABC transporter
						X							1002530	Intergenic (*glpP*/*glpF*)	G>T	*glpP*: transcriptional antiterminator, regulation of glycerol and glycerol-3-phosphate utilization. *glpF*: glycerol facilitator, glycerol uptake
							X	X	X				1002601	*glpF*	Cys22_Val25del	glycerol facilitator, glycerol uptake
		X				X							1073693	*scoC*	Ala21Asp	transition state regulator
							X						1221482	*oppA*	Thr534Asn	oligopeptide ABC transporter
							X		X				1471759	*kinA*	Gly568Val	two-component sensor kinase, initiation of sporulation
												X	1472932	*patA*	138G>A	aminotransferase, biosynthesis of lysine and peptidoglycan
		X											1528830	*pdhA*	474G>T	pyruvate dehydrogenase, links glycolysis and TCA cycle
X													1567847	*ylbD*	p.Glu56*	outer spore coat protein,
						X							1573820	*ddcP*	*342Leu	DNA damage checkpoint recovery protease
						X							1686014	*trmFO*	Arg58Ser	tRNA:m(5)U-54 methyltransferase, tRNA modification
							X		X				1702691	*fliM*	p.Arg326Ile	flagellar motor switch protein, movement and chemotaxis
							X		X				1947405	*galU*	672C>T	UTP--glucose-1-phosphate uridylyltransferase
										X			2026710	*yoaE*	p.Val427Leu	formate dehydrogenase

						X							2406541	*ypbD*	His116Asp	unknown
						X							2414116	*rsiX*	Lys200fs	anti-SigX, control of SigX activity
			X										2422584	*spmB*	p.Ala81Ser	spore maturation protein (spore core dehydratation)
									X				2434346	*ypuB*	p.Glu9*	hypothetical (unknown)
X			X	X	X					X	X	X	2552672	Intergenic (*sinI*/*sinR*)	C>G	sinI: antagonist of SinR sinR: transcriptional regulator, control of biofilm formation
										X			2759185	*sacC*	Arg304fs	levanase, degradation of levan to fructose
						X							2893562	*leuA*	150C>A	2-isopropylmalate synthase, biosynthesis of leucine
			X										3005087	*tcyN*	Gly19Val	cystine ABC transporter (ATP-binding protein), cystine uptake
												X	3070742	*ythQ*	Glu226Asp	*ythQ* = function unknown, similar to ABC transporter
										X		X	3141769	*ythB*	948G>A	cytochrome bd2, menaquinol oxidase, respiration
										X		X	3409591	*sigO*	Met139del	RNA polymerase sigma factor
			X	X									3498891	*yvfR*	Arg127Ile	ABC transporter (ATP-binding protein)
		X											3537728	*levB*	His70Tyr	endolevanase, levan degradation
				X									3547528	*pgmB (pgcM?)*	Asp14Tyr	beta-phosphoglucomutase, starch and maltodextrin utilization
		X											3570846	*glmR*	Pro223His	regulator of carbon partitioning between central metabolism and peptidoglycan biosynthesis
						X							3666013	*gtaB*	Cys116Phe	UTP-glucose-1-phosphate uridylyltransferase, biosynthesis of teichoic acid
						X							3666017	*gtaB*	A>G	
						X							3666019	*gtaB*	.Arg118Pro	
						X							3666048	*gtaB*	Val128Leu	
						X							3666050	*gtaB*	A>T	
						X							3666059	*gtaB*	T>A	
						X							3666080	*gtaB*	Glu138Asp	
						X							3672992	*yvzE*	Leu2Arg	

						X							3673014	*yvzE*	27T>C	putative UTP-glucose-1-phosphate uridylyltransferase
								X					3679471	*tagE*	His330Tyr	UDP-glucose:polyglycerol phosphate glucosyltransferase, biosynthesis of teichoic acid
			X	X									3679534	*tagE*	Glu309*	
					X					X	X	X	3679795	*tagE*	Glu222*	
							X		X				3679856	*tagE*	Trp202fs	
						X							4025538	*wapA*	Asn1683fs	cell wall-associated protein precursor, intercellular competition
						X							4151147	*walH*	Arg252Thr	negative effector of WalK, controls cell wall metabolism
		X											4152067	*walK*	Asp554Tyr	two-component sensor kinase, control of cell wall metabolism
							X	X	X				4152909	*walK*	Thr273Lys	

6.2 Study 2 (to be revised)

Species and condition shape the mutational spectrum in experimentally evolved biofilms

Guohai Hu, Yue Wang, Xin Liu, Mikael Lenz Strube, Bo Wang, Ákos T. Kovács

Note: supplementary figures and tables are attached at the end of the study, the **datasets** are available on GitHub:

https://github.com/GuohaiHu/Datasets-for-thesis

Species and condition shape the mutational spectrum in experimentally evolved biofilms

Guohai Hu[a,b,c], Yue Wang[a,b,d], Xin Liu[a,b,d], Mikael Lenz Strube[e], Bo Wang[a,b,#], Ákos T. Kovács[c,#]

[a]China National GeneBank, BGI-Shenzhen, 518120 Shenzhen, China

[b]BGI-Shenzhen, 518083 Shenzhen, China

[c]Bacterial Interactions and Evolution Group, DTU Bioengineering, Technical University of Denmark, 2800 Lyngby, Denmark

[d]BGI-Beijing, 102601 Beijing, China

[e]Bacterial Ecophysiology and Biotechnology Group, DTU Bioengineering, Technical University of Denmark, 2800 Lyngby, Denmark

Guohai Hu and Yue Wang contributed equally to this work.

#Address correspondence to: wangbo@cngb.org (Bo Wang), atkovacs@dtu.dk (Ákos T. Kovács)

Abstract

Laboratory experimental evolution provides a powerful tool for studying microbial adaptation to different environments. To understand the differences and similarities of the dynamic evolutionary landscapes of two model species from the *Bacillus* genus as they adapt to abiotic and biotic surfaces, we revived the archived population samples from our four previous experimental evolution studies and performed longitudinal whole-population genome sequencing. Surprisingly, higher number of mutations, higher genotypic diversity, and higher evolvability were detected in the biotic conditions with smaller population size. Different adaptation strategies were observed in different environments within each species, with more diversified mutational spectrum detected in biotic conditions. The insertion sequences of *Bacillus thuringiensis* are critical for its adaptation to the plastic bead-attached biofilm environment, but insertion sequence mobility was a general phenomenon in this species independent of the selection condition. Additionally, certain parallel evolution has been observed across species and environments, particularly when two species adapt to the same environment at the same time. Further, the higher degree of genetic diversification observed in biotic selective environments indicates an increased spatial niche heterogeneity and a nutritional source difference created by the plant host that provided a strong strength of selection during the adaptation process. Together, these results provide the first comprehensive mutational landscape of two bacterial species' biofilms that is adapted to an abiotic and biotic surface.

Importance

Biofilm formation is a vital factor for the survival and adaptation of bacteria in diverse environmental niches. Experimental evolution combined with the advancement of whole-population genome sequencing provides us a powerful tool to understand the genomic dynamic of evolutionary adaptation to different environments, such as during biofilm development. Previous studies described the genetic and phenotypic changes of selected clones from experimentally evolved *Bacillus thuringiensis* and *Bacillus subtilis* that were adapted under abiotic and biotic biofilm conditions. However, the full understanding of the dynamic evolutionary landscapes was lacking. Further, the differences and similarities of adaptive mechanisms in *B. thuringiensis* and *B. subtilis* were not identified. To overcome these limitations, we performed longitudinal whole-population genome sequencing to study the underlying genetic dynamics at high resolution. Our study provides the first comprehensive mutational landscape of two bacterial species' biofilms that is adapted to an abiotic and biotic surface.

Key words: experimental evolution, parallelism, population size, *Bacillus thuringiensis*, *Bacillus subtilis*

Introduction

Biofilms are matrix-enclosed microbial communities that adhere to biotic or abiotic surfaces. These complex assemblages confer emergent properties to their inhabitants and represent a much higher level of organization than free-living bacterial cells do(1, 2). The biofilm lifestyle not only protects bacteria to survive in harsh environments but also facilitates the colonization of new niches during dispersal from these microbial clusters. Bacteria form biofilms on almost all natural and artificial surfaces(2, 3), utilizing diverse mechanisms that depend on environmental conditions and specific species(4). Biofilms can be categorized into three models depending on the type of occupied niche, including pellicle biofilms at the air-liquid interface, colony biofilms at the air-solid interface, and submerged biofilms at the solid-liquid interface(5, 6). Regardless of the type, these biofilm types can be formed under either abiotic conditions or in connection with a host. Members of the Gram-positive *Bacillus* genus form various types of biofilms exhibiting either beneficial or pathogenic impact. Here, we focused on two model species from the *Bacillus* genus and experimental evolution of their biofilms.

Bacillus thuringiensis is commonly used as a biological pesticide belonging to the *Bacillus cereus sensu lato* group, and its spores can be isolated from diverse environments(7). *Bacillus subtilis* is a soil-dwelling, non-pathogenic bacterium that is commonly found in association with plants and their rhizosphere(6). Both species can form biofilms in diverse environments. They share a large number of transcriptional factors, including Spo0A, σ^B, SinI, and SinR(8), which play crucial roles in the intertwined regulation of sporulation and biofilm formation(9–

13). Between these two species, however, there are also some important differences in the regulatory pathways and transposable elements. For example, SigD, the motility-specific sigma factor, and the DegU/DegS two-component system, are absent from the species of the *B. cereus sensu lato* group; while the virulence regulator PlcR, which plays an important role in *B. cereus* and *B. thuringiensis* physiology(14, 15), is absent in *B. subtilis*. Besides, diverse Insertion Sequences (ISs) have been described in different *B. thuringiensis* isolates(16–19), while only limited number of ISs have been reported in *B. subtilis*(20). ISs are the simplest transposable elements and play important role in shaping their host genomes(21). Insertions of IS elements can results in both gene inactivation and activation, or alter the expression of neighboring genes(22). In addition, IS-mediated changes have been described to both promote and constrain evolvability of *Escherichia coli* in a long-term evolution experiment (LTEE)(23).

Experimental evolution has been widely used to study the evolutionary processes that occur in experimental populations in response to the surrounding environment(24–26). Experimental evolution provides a powerful tool to study microbial adaptation to different environments in real-time. Combined with the advancement of whole-population genome sequencing, it is possible to understand the genomic dynamic of evolutionary adaptation(27–30). Plenty of evolutionary studies have been performed on planktonic forms of bacteria and yeasts, under diverse environmental conditions(27, 30–35). In contrast, only a relatively limited number of evolution experiments have been performed with biofilm populations(28, 36–40). Most of the biofilm evolution studies have focused on the quick emergence of morphotypic, phenotypic and

genotypic variation within biofilms. In biofilms, astonishing parallelism has been observed at the different biological hierarchy levels, from fitness level to gene level and even nucleotide level, both between replicate lineages within the same evolution experiment and across different evolution experiments(24).

Previously, we have experimentally evolved *B. thuringiensis* and *B. subtilis* using generally comparable adaptation concepts. For *B. thuringiensis,* experimental evolution was performed using two approaches, a plastic bead attached biofilm model (Bth_bead)(41) and *Arabidopsis thaliana* root colonization model (Bth_root)(42). Similarly, *B. subtilis,* a static air-medium floating biofilm transfer mode (Bs_pellicle)(43) and an *A. thaliana* root colonization model (Bs_root)(44) were used. Thus, for each bacterial species, biofilm formation proceeded under abiotic conditions (plastic bead or air-liquid interface) and on biotic surfaces (*A. thaliana* root). In these laboratory evolution setups, 5 to 7 parallel lineages (i.e., subsequent populations with an individual evolutionary trajectory) were followed using 30 to 40 transfers. The detailed descriptions of each experiment were previously published(41–44).

In the Bth_bead study, all evolved lineages displayed significantly enhanced biofilm production accompanied by the appearance of a *B. thuringiensis* fuzzy spreader (FS) colony morphotype variant. This FS variant showed higher competitive ability in most multicellular traits compared to the ancestral strain, suggesting an important role for diversification during adaptation of *B. thuringiensis* to the abiotic surface biofilm lifestyle. Further, genetic characterization showed that the guanylyltransferase gene was disrupted by an IS element in the FS, which altered the

aggregation and hydrophobicity of this variant(41).

In the Bth_root experiments, bacterial lineages displayed enhanced root colonization ability compared with the ancestral strain. Single isolates from two of the evolved lineages showed higher recolonization efficiency of new roots compared with the other lineages, in addition to exhibiting altered bacterial differentiation and pathogenicity. Investigation of a key mutation in the gene encoding the Rho transcription termination factor in these lineages demonstrated how transcriptional rewiring alters cell fate decisions in *B. thuringiensis*(42).

In the case of Bs_pellicle approach, *B. subtilis* diversified into four distinct colony variants that dramatically differed in biofilm formation abilities and expression of biofilm-related genes. Genome comparison suggested that major phenotypic transformations between the morphotypes can be triggered by subtle genetic differences(43).

Finally, in the Bs_root study, *B. subtilis* was shown to rapidly adapt to the *A. thaliana* root environment, several evolved isolates displayed altered colony morphologies. Two selected evolved isolates from independent populations from the final transfer outcompeted the ancestor during root colonization. Re-sequencing of single evolved isolates from independent populations and different time points revealed mutations in genes related to different bacterial traits. The examined evolved isolates also displayed robust biofilm formation in response to plant polysaccharides, impaired motility, and altered growth on plant-derived compounds(44).

In each experiment of these four studies, the evolved clones diversified into distinct pheno- and/or genotypic colony variants in time, including dramatically increased biofilm development

of the isolated clones at the end of the experiments (**Fig. S1**). These findings provided novel insights into how *B. thuringiensis* and *B. subtilis* rapidly adapt to abiotic and biotic surface environment and revealed the evolutionary consequences. However, these four studies only studied the genomic changes of certain selected isolates at selected time points or only focused on certain lineages, while the full understanding of the dynamic evolutionary landscapes were lacking over the full experimental evolution setup. Further, the differences and similarities of adaptive mechanisms in *B. thuringiensis* and *B. subtilis* were not identified when these two species were adapted to the same environment and when one species is adapted to two distinct environments. To overcome these limitations, we revived the archived population samples from these four studies and performed longitudinal whole-population genome sequencing to study the underlying genetic dynamics at high resolution. Generally, parallel evolution was verified in *B. thuringiensis* and *B. subtilis* when adapted to respective selective environments (i.e., mutations were detected in overlapping genes), except in the Bth_root experimental evolution system. Interestingly, we found that transposable elements in *B. thuringiensis* possibly play a critical role in adaptive evolution. Our study provides the first comprehensive mutational landscape of two bacterial species' biofilms that is adapted to an abiotic and biotic surface.

Results

Mutation spectrum and genetic diversity. We performed longitudinal whole-population genome sequencing of 69 *B. thuringiensis* and 69 *B. subtilis* samples (subsequent time points of parallel lineages from two evolutionary conditions with each bacterium, see **Table S1**), as well as the ancestor of each strain, using the DNBSEQ-Tx platform(45, 46). We obtained >180× coverage depth raw data for each sample. The genetic alterations were detected compared with the respective ancestors, including SNPs, Indels (short insertions and deletions), and large fragment insert variants, using the *breseq* pipeline (version 0.35.7)(47, 48). The default parameters called mutations only if they appeared at least 2 times from each strand and reached a frequency of at least 5% in the population. Additionally, mutations that were detected in highly polymorphic regions were removed. This analysis revealed 119, 273, 158, and 350 mutations in the evolved lineages from the Bth_bead, Bth_root, Bs_pellicle, and Bs_root conditions, respectively (**Table 1** and **Dataset S1**). It is noteworthy that we detected relatively much more mutations in *B. subtilis* when we considering the genome size, which is 23.36% smaller than *B. thuringiensis* (4.2Mb vs 5.5Mb). Overall and in each lineage of both bacterial species, higher numbers of mutations were detected in the plant root evolved populations compared to the *in vitro* biofilm transfers. Additionally, large differences have been observed between each condition in the spectrum and the fraction of mutation types (**FIG 1a** and **b**, **Table 1** and **Fig. S2**), implying different adaptation strategies of these two species when adapting to these new selective environments. The detected mutations were not distributed uniformly across the

populations within each condition, and the large fluctuations in mutation numbers in many populations suggest a process where new mutations displaced older ones(40). Interestingly, a nonsynonymous mutation (A50D) was observed in the *mutL* gene reaching a frequency of 46.08% in lineage A of Bth_root at transfer 32 that suggested the potential evolution of a mutator strain. However, relative to other lineages and conditions, no dramatic increase in the number of mutations was observed in this lineage, suggesting that none of experimentally evolving lineages gained a mutator phenotype, at least above the detection limit.

Thirteen cases of transposable element rearrangements were identified in the evolving *B. thuringiensis* lineages (**Dataset S1**), in contrast to the lack of transposon activity in *B. subtilis*. Importantly, the genome of *B. subtilis* DK1042/NCIB 3610 contains only one incomplete transposase gene in contrast to the 39 transposase genes present in the *B. thuringiensis* 407 Cry- strain.

A large number of intergenic mutations were also detected (**Table 1**), accounting for 38.63% ± 8.32%, 25.57% ± 4.67%, 24.69% ± 3.46% and 16.32% ± 5.05% of total mutation in each lineage (Bth_bead, Bth_root, Bs_pellicle, and Bs_root, respectively), many of these likely located in promoter or terminator regions. Again, the relative frequencies of these intergenic region mutations were distinct between abiotic and biotic biofilms. The specific role of these numerous intergenic mutations remains vague in these two species; however, recent work has suggested certain intergenic regulatory regions to be critical in *B. subtilis* growth and adaptation in different environment(49–53). Adaptive changes in noncoding regions might possibly affect

the binding sites for regulatory proteins. For example, we found three intergenic point mutations in the region between operon *yhxA-glpP* and operon *glpFK* in four Bs_root lineages, one located at the terminator region of operon *yhxA-glpP* and two at the promoter region of operon *glpFK*(54, 55). These two operons encode proteins essential for growth on glycerol or glycerol 3-phosphate, which is possibly related to the adaptation to glycerol in the medium(56, 57). We also found one intergenic SNPs in the promoter and terminator region between gene *sinR*, respectively. The *sinR* gene encodes a DNA-binding transcription factor which is central to the determination of cell fate with respect to biofilm formation versus swimming motility(58). These results implicate adaptive changes in intergenic regions that presumably influence the binding sites for regulatory proteins.

The number of fixed mutations, which the frequency reach 100% and persisted to the end of the experiment, was higher in *B. thuringiensis* compared with *B. subtilis* (53 vs 10), and the overall mutation frequencies in the *B. thuringiensis* populations were also higher than that in the *B. subtilis* populations (**Dataset S1** and **S2**), which indicates that either the strength of selection on *B. thuringiensis* was possibly stronger than that on *B. subtilis*, or the population sizes or bottlenecks differed between these two species. The majority of fixed mutations were found in *B. thuringiensis* lineages evolved on the plant roots and most of them appeared as cohort, which refers to the appearance and fixation of several mutations in the same lineage at the same time, in contrast to the single fixed mutation identified in *B. subtilis* pellicle transfer approach that otherwise displayed a total of 158 mutations. In addition to the number of fixed

mutations and differences in mutation frequencies, the *dN/dS* ratio between each condition was determined. The total *dN/dS* ratio for Bth_bead, Bth_root, Bs_pellicle, and Bs_root conditions were 1.36, 1.25, 0.95 and 0.91, respectively (**FIG 1c** and **Table S2**), suggesting that majority of the observed mutations in *B. thuringiensis* are adaptive (even those driven extinct by clonal interference). By contrast, the *dN/dS* ratio near or below 1 in *B. subtilis* reflects that selection in favor of beneficial mutations (and presumably typically nonsynonymous) is balanced by hitchhiking of neutral mutations and purifying selection against deleterious mutations.

We hypothesized that biotic surface adaptation conditions would maintain higher genetic diversity than abiotic conditions due to potentially increased spatial niche heterogeneity and nutritional source difference created by the plant host. Although we detected more mutations in Bth_root than that in Bth_bead, the genotype alpha diversity (based on the genotype and frequency from genealogy analysis) of the last time point of Bth_root was only slightly higher than that in Bth_bead (genotype alpha diversity, $p = 0.7186$, t = -0.3731, df = 8.1641 via two-tailed t-test) (**FIG 1d** and **Fig. S3**). This non-significant difference was due to there was much more mutations in one genotype in Bth_root than in Bth_bead. The Bs_root diversity was higher than that in Bs_pellicle (genotype alpha diversity, $p = 0.008211$, t = -3.3897, df = 8.8412 via two-tailed t-test). We also compared the genotype alpha diversity between the last time point and the first time point sequenced of each condition, revealing a significant difference in all modes, except for in Bth_bead (genotype alpha diversity, $p = 0.0649$, t = 2.0776, df = 9.8394 via two-tailed t-test), this non-significant difference in Bth_bead was highly possibly due to

that the first time point sequenced in Bth_bead was from transfer 9, which was already much diversified in genotype. These results again support a process where new mutations were displacing older ones.

Mobilome activity in experimentally evolving *B. thuringiensis*. As highlighted above, transposition of insertion element in *B. thuringiensis* 407 contributes to adaptation to colonization of nylon beads and appearance of novel colony morphotypes(41), therefore we specifically explored potential mobile element rearrangements in the experimentally evolved lineages. We applied a two-round strategy using *breseq* pipeline (v0.35.7)(47, 48) to identify large size transposable element rearrangements (see **Materials and Methods**). While no IS transposition was exposed in *B. subtilis*, examination of the experimentally evolved lineages revealed 13 IS transposition cases in *B. thuringiensis* (**Table 2**). In line with higher frequency of IS transposition in experimentally evolved *B. thuringiensis*, closer examination of the genome sequences of the two species exposed 10 types of transposase genes, with 1~12 copies having lengths from 213~1,562 bp (four ISs smaller than 900bp are presumably truncated IS), giving a total of 39 copies in the *B. thuringiensis* 407 genome (**Table S3**), in contrast to only one incomplete transposase gene (186bp) was found in the genome of *B. subtilis* NCIB 3610/DK1042.

Among the 10 types of IS elements observed in *B. thuringiensis* 407, IS*110* family transposase was the most abundant IS with its 12 copies in the ancestor strain, while the IS*4*-like element

IS*231*A family transposase (IS*231*A for short below) was the most active element in the experimentally evolved lineages. We identified 12 IS*231*A and one IS*110* family transposition cases. Seven genes and three intergenic regions were disrupted by the inserted IS*231*A elements. We found that the cupin domain-containing protein (BTB_RS26870, *rfbM* gene) was disrupted by IS*231*A in 3 out of the 6 lineages in Bth_bead with max frequencies from 13.37% to 48.66%, which show high parallelism of adaptation to the plastic bead attached biofilm environment. We failed to find this mutation in the rest of three lineages in Bth_bead possibly due to low frequency (<5%) of this IS transposition. Importantly, when specifically sequencing FS colony morphotypes, IS*231*A insertion was detected within the *rfbM* gene in each of the 6 lineages(41). A loss-of-function *rfbM* mutant, Bt407Δ*rfbM*, constructed previously(41), could re-create the FS phenotype and the robust biofilm formation. Additionally, Bth_bead lineage A contained 4 IS transposition cases with max frequencies from 13.37% to 54.86%.

Genotype and genealogy analysis of evolving lineages. As mentioned above, hundreds of mutations rose to detectable frequencies (>5%) in these populations. To infer the genealogical structure of each lineages and visualize changes in lineage frequencies from shared, nested mutation trajectories over time, we utilized the *Lolipop* software package developed by Cooper and colleagues(40, 59). We obtained average of 13.83 ± 2.27, 24 ± 4.29, 17.33 ± 3.25, and 27.43 ± 5.1 genotypes in the Bth_bead, Bth_root, Bs_pellicle, and Bs_root experimental setups, respectively, each with multiple mutations, rose to a detectable frequency. The number of

genotypes in each condition is consistent with the mutation number and diversity within each condition.

Clonal interference. It is generally expected that a genotype with one or a combination of several beneficial mutations whose combined fitness is superior, may outcompete the other, less fit genotypes. However, due to the numerous possible routes for one bacterium to adapt to a new environment, competition between different genotypes that contain beneficial mutations, the rate at which any one of these genotypes spreads through the population is slowed because it must displace other fitter competitors rather than only its ancestor. Such dynamic population process is called as clonal interference(33, 60–62). In our experiments, we frequently observed clonal interference in all experimentally evolving lineages (**FIG 2**). Numerous mutations or groups of mutations rose to high frequency and then fall to extinction, while outcompeted by another group, and therefore many distinct mutations existed at a very low frequency (below 5%) during the earlier period of experiment and then rose to high frequency in the later period.

We observed nested fixations(63) in lineage F of Bth_bead, lineage A, C, D, and E of Bth_root, lineage 1 of Bs_root, where beneficial mutation or mutations cohorts fix sequentially in the background of the previous fixed mutation(s) (**FIG 2**). The clonal interference was obviously much stronger in biotic surface environments than that in abiotic surface: we observed more mutations or genotypes appear and disappear in biotic surface environments, which is consistent with the mutation spectrum and genotype dynamic. Although we observed most nested fixations events in Bth_root, the clonal interference was still very strong in these lineages, especially in

the late stage of the experiment.

Evolvability. During the adaptation experiment of evolving lineages, the selection not only had immediate effects on new mutations or new combinations of alleles but also on those new genotypes differ in their capability to further evolve(26). The evolvability of the new genotypes may be affected in at least two main ways: changed mutation rates or differences in epistatic interactions with potential further mutations. From the lineage diagram figures (**Fig. S4**), we observed that there were much more first-order and less second-order genotypes (nested genotypes) in abiotic adaptation conditions than that in biotic adaptation conditions in both bacterial species, while many genotypes persisted along the experiments in the two abiotic adaptation conditions. To better compare the evolvability among different models, we calculate the accumulated mutation numbers of each genotype in each condition at the last time point. The average accumulated mutation number is 2.58, 8.94, 1.75 and 3.1 in Bth_bead, Bth_root, Bs_pellicle, and Bs_root, respectively (**FIG 3**). We observed obvious nested fixations in Bth_root, in which the new beneficial mutations accumulated and fixed in the background of the previous ones. Bs_pellicle contained least accumulated mutations, this is possibly caused by the transfer model that pellicle transfer contained a more homogeneous mix of the biofilm bacterial cells than bead or root biofilm transfer model. These results showed that evolvability and biofilm surface type, selective conditions have a strong effect on the evolutionary history of bacteria.

More shared dominance mutated genes or genotypes in abiotic environments. In the Muller

plots, which show how diversity emerges and how changes over time, an obvious pattern could be observed, namely, abiotic environment resulted in a more consistent mutation profile compared with the biotic environment (**FIG 2**), which is consistent with the Jaccard index of each environment.

Parallelism and genetic targets of selection

Next, we quantified parallel evolution by testing whether mutations in certain genes appeared more frequently than expected by chance and calculated the proportion of mutations shared between two evolved lineages within each condition.

We defined 'multiplicity' of a gene as the number of mutations in that gene across all sequenced lineages in each condition, scaled by its gene length(27, 30). To exam whether there was parallelism within each species, we also performed this analysis by applying it to both conditions in each species as a whole. Similar to many other laboratory adaptation experiments(30, 33, 59, 64), we observed more high multiplicity genes than expected by chance in each condition and species, relative to a null hypothesis in which mutations are distributed randomly across all genes (**FIG 4a**). We also observed that excess, the degree of observed multiplicity related to the null distribution, was more pronounced in *B. subtilis* than that in *B. thuringiensis*, which is consistent with the number of shared mutated genes in each species. Four genes were detected to be mutated in both *B. thuringiensis* adaptation conditions, while Thirteen genes were identified in both *B. subtilis* adaptation conditions. Extraordinarily, in

Bth_root, we found that the fraction of genes with multiplicity more than the number of lineages in each condition was much lower relative to other conditions (**FIG 4a)**, the number of lineages in Bth_bead, Bth_root, Bs_pellicle, and Bs_root, is 6, 5, 6 and 7, respectively. This was because the five lineages of this experiments could be categorized into three types, each type contained different mutated genes (**FIG 5a** and **Dataset S2**). When studying the divergence evolution in Bth_root among lineages, we observed three starkly different adaptive strategies lead to marked divergence.

The Jaccard Index (*J*) of all pair of lineages (two evolved lineages with sets of accumulated mutated genes G1 and G2) from each evolved condition was calculated. The Jaccard Index is a common measure of similarity, which describes the likelihood that the same gene is mutated in two independent lineages(65, 66), ranges from 0 (no mutated genes in the two lineages are shared, $G1 \cap G2 = 0$) to 1 (the two lineages have exactly the same set of mutated genes, G1 = G2). The *J* values of abiotic conditions were significantly higher than that of biotic conditions in both species ($p < 0.001$) (**FIG 4b**), averaged at 0.22, 0.057, 0.23 and 0.11 for Bth_bead, Bth_root, Bs_pellicle, and Bs_root, respectively, which agrees with the consistency in mutated genes observed previously (**FIG 2**). To test whether population size contribute to this parallelism difference(66), we estimate the approximate population size (here we calculate the biofilm production for comparison) of each condition from the previous data(41–44), range 8.40E+05 to 3.29E+07, 1.13E+03 to 1.05E+06, 3.33E+08 to 1.99E+10, and 6.00E+04 to 4.68E+06 for Bth_bead, Bth_root, Bs_pellicle, and Bs_root, respectively (**Fig. S5**). The

population size of abiotic environments is much larger than that of biotic environments, demonstrated the positive relationship between population size and the probability of parallelism, e.g. that the probability of parallelism is increased with population size(66). The small population size of Bth_root also helps to explain why lineage B disappeared only after five transfers during the experimental evolution experiment and the remaining five lineages of this experiments could be categorized into three evolutionary trajectory types. The strong bottleneck and genetic drift may therefore greatly influence the evolutionary landscape of these evolving lineages.

Next, we quantified how signatures of each mutated gene were greater than expected by chance. For this, we focused on genes mutated two or more times in each species. We found that 35 genes in *B. thuringiensis* and 48 genes in *B. subtilis* mutated two or more times, but these genes constituted only 0.88% and 1.89% of the coding genome of *B. thuringiensis* and *B. subtilis*, respectively. Almost all mutations in these genes (except for one gene for each species) were distributed non-randomly (Fisher's exact test and corrected with Benjamini-Hochberg method, $q < 0.05$), accounting for 54 mutations (45.38% of all mutations, **Table 1**), 57 mutations (20.88%), 81 mutations (51.27%), and 150 mutations (42.86%) in each condition (Bth_bead, Bth_root, Bs_pellicle, and Bs_root, respectively). Most mutations are nonsynonymous mutations and indels.

To understand the functional basis of this parallelism, we categorized function of these genes based on KEGG pathway, and then focused on the genes that contains nonsynonymous and

indel mutations which occurred in at least half of the populations in each condition. Mutated genes or genotypes were shared more frequently in abiotic adaptation environments than that in biotic adaptation environments (**FIG 5** and **Dataset S2**).

Cell fate decision related genes are most targeted in Bth_bead. In Bth_bead, four quorum sensing and sporulation regulation related genes (e.g. *spo0F*, *nprR*, *spo0A* and *spo0B*) were mutated more frequently and reach high frequencies and were even fixed in more than one lineage, *spo0F*(A82T) fixed in lineage C and F, and *spo0F* (Y12*) fixed in lineage D. In addition, *rfbM* gene was disrupted by IS*231*A in 4 out of the 6 lineages with max frequencies from 12% to 49.79%, the variants contain this mutation displayed higher competitive ability versus the ancestral strain(41).

Different gene target range observed in Bth_root. In Bth_root, there were total 47 fixed mutations across all lineages. Transporter and ribosome related genetic information processing genes are the frequently targets of selection in Bth_root, motility, metabolism related genes are also selected. As we could observe clearly three different routes of *B. thuringiensis* adapting to the *A. thaliana* root environment, the shared mutated genes could be also separated. Lineage C had no shared mutated genes with other four lineages, except for two shared mutations in very low frequencies with other lineages. Lineage D also had no shared mutated genes with other four lineages, except for four shared mutations in very low frequencies with other lineages. Lineage A, E and F could be categorized into an independent group of adaptation. Within the lineage A, E, and F groups, lineages E and F shared most of the high parallelism genes, whereas

lineage A only shared 5 genes with lineages E or F. Lineages E and F also contained a *rho* (E54*) mutation that was studied thoroughly by Lin et al, which demonstrated that the nonsense mutation in *rho* gene impaired the swimming motility of Bt407, but increased robust pellicle formation, and this nonsense mutation in *rho* reshapes the transcriptional landscape of *B. thuringiensis*(42).

Motility, chemotaxis and aerotaxis contribute to adaption in pellicle evolution in Bs_pellicle. In Bs_pellicle, three bacterial motility protein and flagellar motility related genes, *hemAT*, *fliY* and *mcpC*, were mutated more frequently than expected and reached to high frequencies or even fixed, supporting a role of these mutations in the adaptation of *B. subtilis* to air-liquid interface environment. We also found mutations in the *kinA* gene, a protein product of which gene was directly linked to modulating the phosphorylation level of Spo0A, influencing both matrix production and sporulation.

Multiple adaptation routes of B. subtilis to A. thaliana roots in Bs_root. In Bs_root, we could observe *tagE*, *hpr (scoC)*, *glpF* and *walK* were mutated more frequently and reach to high frequencies then other genes. Unlike in other conditions, the functions of these gene are not focused on certain biological function, but more dispersed, which imply the complexity and multiple adaptation routes of *B. subtilis* to *A. thaliana* roots.

Parallel Evolution across Species and Environments. Besides functional parallel evolution within each model, we also observed certain parallel evolution across species and environments, especially when two species adapt to the same environment. *B. subtilis* shared more mutated

genes in similar KEGG functions than that in *B. thuringiensis* between abiotic and biotic models, which might suggest that the two models in *B. subtilis* are more similar than in *B. thuringiensis*. Additionally, the shared mutated genes in similar KEGG functions are higher for the biotic model of the two microorganisms compared with the abiotic models, suggesting that the functional mechanism for the two species to adapt to the same selection stress is similar, compared to the distinct adaption to two different abiotic environments (i.e., cyclic colonization of beads by *B. thuringiensis* compared with the artificial disruption of pellicle biofilms to start a new cycle in *B. subtilis*).

Discussion

We used longitudinal whole-population genome sequencing(27, 28, 30) to study the underlying genetic dynamics of the two species adapt to abiotic and biotic environment at high resolution, this method allowed us to capture the mutations with a frequency of 5%. We observed hundreds of mutations in each evolved condition: there were higher number of mutations, relatively few intergenic mutations, higher fixed mutation rate and higher genetic diversity in biotic conditions compare with abiotic conditions in both species. The higher genetic diversity in biotic conditions was possibly due to potentially increased spatial niche heterogeneity and nutritional source difference created by the plant host. In addition, there were more fixed mutations in biotic conditions in both species, and extremely more fixed cases were found in Bth_root which possibly related with the small population size. The *dN/dS* ratio is slightly higher in *B. thuringiensis* and we only detected IS mediated mutations in *B. thuringiensis*.

IS elements are small and autonomous transposable elements with variable numbers and copies found in most bacterial genomes, and have been reported to play important roles in shaping the genomes of their hosts(23, 67). These simplest transposable elements usually contain only the genes responsible for their transposition(17). The IS mediated transpositions could lead to gene inactivation or to the activation or alteration of the expression of neighboring genes(22), and consequently, the effect could be either beneficial, deleterious, or neutral. Both the number and activity of the IS elements of a given bacterium will influence the genome structure and gene expression, which will further impact the fitness of the bacterium in certain environments(22,

67). IS-mediated changes have been described to both promote and constrain evolvability of *Escherichia coli* in a long-term evolution experiment (LTEE)(23), and an experimental evolution using cyanobacterium *Acaryochloris marina* revealed that the vast majority of beneficial mutations during laboratory evolution are due to transposition of a single IS element(21). ISs play a critical role in *B. thuringiensis* adapt to the plastic bead attached biofilm environment(41). In fact, we identified a total of 14 IS transposition cases in *B. thuringiensis* of which, *rfbM* gene was disrupted by IS*231*A in 3 out of 6 lineages in Bth_bead. The FS variant that was identified previously to harbor this insertion showed altered aggregation and hydrophobicity. Interestingly, this ISs rearrangement in the genomes of the evolved lineages and final populations' isolates showed high parallelism of adaptation. We also observed four IS mediated mutations in Bth_root (three mediated by IS*231*A, and one mediated IS*110*), while insert positions were distributed in different area of the genome, which imply that these ISs may only contribute little in adapt to the *A. thaliana*. Our study has important implications for understanding the contribution of how IS elements in the *B. thuringiensis* genome affects the fitness, biofilm formation, and adaptation.

We frequently observed clonal interference in all experimentally evolving lineages. The frequency of mutations fixation rate was different among the four conditions, and mutations seemed to be more frequent in biotic conditions, while also negatively correlated with the population size. When we reviewed the population size of four experiments, we found that the biotic conditions harbored much lower population size than abiotic conditions at the end of each

timepoints and each transfer. Our results suggest that a stronger population bottleneck will lead to a more frequent fixation of specific genotypes due to genetic drift. Further, the difference in the frequency of fixed mutations might be explained by the different population sizes, the strong effect of competing beneficial mutations in the abiotic populations, and the strong impact of genetic drift in the biotic populations(68). We also observed nested fixations in some of the evolving lineages and some even fixed simultaneously as cohort(33, 63), especially in Bth_root (4 of 5 lineages), in which the size of the fixation cohorts was the largest among all conditions (up to seven mutations fixed simultaneously). However, it is very unlikely that these mutations occurred simultaneously when considering the typical mutation rates in bacteria. One possible explanation is that the beneficial mutation(s) occurs in a background that already has a certain sets of neutral or deleterious mutation, and therefore the hitchhiker and beneficial driver mutations fix at the same time(63). We found this possible phenomenon frequently in Bth_root, in lineage D, the *ywdH*: T186T mutation is possibly a neutral mutation as a background and the later beneficial co-drivers occurred sequentially and led the genotype contains the cohort to fix. Although there are differences in *dN/dS* among four conditions, the total ratio are all near 1, which is relatively low compared with the high *dN/dS* ratio observed in previous studies(27, 40). This implies that neutral or weakly deleterious hitchhikers occurred frequently in our experimental evolution models. Thus, the higher mutations (or cohort) fixation rate were possibly caused by the smaller population size and strong population bottleneck (genetic drift) under the biotic conditions. While we still need to explain why the mutation cohort occurrence and fixation rate were higher in biotic conditions.

We observed obvious parallelism at genotype level in Bth_bead, Bs_pellicle, and Bs_root conditions, but not in Bth_root, which is consistent with the parallelism at phenotype level. In Bth_root, isolate from lineage E and F displayed improved iterative ecesis on roots and increased virulence against insect larvae, the motility ability, sporulation kinetics and cell morphologies were also different from other lineages(42). When we reviewed the population size of four experiments, we found that the Bth_root contains the smallest population size, only contains from 1.13E+03 to 1.05E+06 cells at the end of each timepoints and each transfer. Theory and empirical studies suggest that strong selection and large population sizes increase the probability for parallel evolution at the phenotypic and genotypic levels(33, 66, 69–71). Differences in population sizes between populations exposed to similar conditions can affect the degree of parallelism(69). The use of different-sized experimental populations of the unicellular alga *Chlamydomonas reinhardtii* adapting to a high salt environment demonstrated that adaptation to salt was repeatable at the fitness level in medium and large populations, but was not in small populations(70). Similarly, evolution experiments with large and small yeast populations revealed that beneficial mutations occur more consistently in larger populations(33). Further, smaller population size generally led to a greater among-population variation than large population sizes do in a viral adaptation model(72). As we shown above, the abiotic conditions contain much larger population size than that in biotic conditions, consistently with the Jaccard Index (*J*) and the muller plots; thus, higher degree of parallelisms observed in the large population size conditions in each species.

Generally, as larger population size permits higher number of mutations, we would expect to detect more mutations, higher diversity, and more intense clonal interference in larger populations for both *B. thuringiensis* and *B. subtilis* in the same environment. In contrast, higher number of mutations could be detected in total and at the end of the experiment of each lineage in biotic condition in each species in spite of the lower population size under these conditions compared to the abiotic environment. Additionally, the alpha diversity and clonal interference was also higher in biotic conditions. We found that the overall frequency of specific mutations of the populations evolved in the biotic conditions is lower than that in abiotic conditions, accompanied low frequency of mutations observed in the biotic conditions. The four experimental evolution setups used here differed in several parameters, e.g. cultivation temperature and volume, from which the biofilm surface, growth temperature and cultural volume (which would affect nutrition supply) together may play a pivotal role in the adaptation and also possibly affected the population size. Furthermore, we speculate that the population bottleneck size correlated with the population size, although it was not possible to calculate the exact cells numbers transferred from one round to another in these experimental setups. While the *B. subtilis* pellicle population was consecutively diluted 100-fold each time, thus the generation number could be calculated, we could not determine the exact number of cells colonizing the new root or beads in the other three experimental evolution setups. The strong bottleneck imposed during the transfer process possibly influenced the selection effectiveness and genetic drift was more robust, especially in Bth_root, which showed the lowest parallelism among four conditions in both phenotypic and genotypic level. This observation suggests that

the selective conditions have a stronger effect on the evolutionary history of bacteria in comparison to population size(73). In addition, a sharper fluctuation of mutation number was also observed in biotic conditions, which suggests that a lot of mutations were lost during transfer process due to the small population bottleneck size in these conditions. The higher number of mutations, higher genotypic diversity, and higher evolvability (accumulated mutations in each genotype at the last timepoint) are puzzling in the populations evolved in the biotic conditions. The averaged mutation number per transfer in each lineage was calculated to be 0.60, 1.20, 0.90, and 1.67 for Bth_bead, Bth_root, Bs_pellicle, and Bs_root, respectively, nearly twice as much in biotic conditions than in abiotic. We speculate that this is possibly caused by the heterogeneity in selection under biotic conditions, where the mutation number increased much sharper at the first few transfers of the experiments caused by the increased spatial niche heterogeneity and nutritional source difference created by the plant host and possibly also due to the periodic exudate ingredient changes caused by the recurrent exposure to light and different temperature, which needs to be further confirmed. These results indicate that the increased spatial niche heterogeneity and nutritional source difference created by the plant host provided a strong strength of selection during the adaptation process.

Materials and Methods

Materials. Ancestor bacterial strains and evolved population samples used in this study are from previous studies(41–44). Frozen samples from each adaptation model were revived via cultivation in Lysogeny broth (LB; Lennox, Carl Roth; 10 $g \cdot L^{-1}$ tryptone, 5 $g \cdot L^{-1}$ yeast extract, and 5 $g \cdot L^{-1}$ NaCl) medium for 16 hours at 30℃ and 37℃ for *B. thuringiensis* and *B. subtilis*, respectively, before harvesting the cells for genomic DNA extraction. Genomic DNA was extracted from each culture using EURx Bacterial and Yeast Genomic DNA kit.

Sequencing and variant calling. For whole-population sequencing of the evolved populations and ancestor strain samples, acoustic fragmentation PCR-free libraries were prepared using MGIEasy PCR-free Library Prep Set (MGI Tech). Paired-end fragment reads (150bp × 2) were generated on a DNBSEQ-Tx sequencer (MGI Tech) following the manufacturer's procedures(45, 46). All population samples were sequenced with >180× depth coverage for polymorphism calling.

Raw data were filtered using SOAPnuke (version 1.5.6)(74) to remove low quality reads: reads including more than 50% of bases with quality lower than 12, reads including more than 10% of unknown base "N", and reads containing adaptor contamination. To ensure the similar variants calling sensitivity, we normalized the clean data to 200× depth except for two *B. thuringiensis* populations with 186.42× and 193.86× depth. Mutations were called using *breseq* (version 0.35.7) with the default parameters and a -p option for population samples(47, 48).

The default parameters called mutations only if they appeared at least 2 times from each strand and reached a frequency of at least 5% in the population. To call large size IS mutations in *B. thuringiensis*, we performed a two-round strategy. First, we ran *breseq* using the default parameters and then annotated the insert sequence (**Table S4**) into the reference file manually using the information from unassigned new junction and missing coverage evidence in the first-round *breseq* output(47). Then we performed *breseq* using the new reference again to obtain the IS mutations. The reference genome used in our analysis are *B. thuringiensis* 407 Cry$^-$ (Bt407) (GenBank accession number CP003889.1) and *B. subtilis* NCIB 3610 genome and pBS plasmid (GenBank accession no. NZ_CP020102 and NZ_CP020103, respectively) for *B. thuringiensis* and *B. subtilis*, respectively. We then remove the mutations that also found in the ancestor strains and in regions of high polymorphism to obtain the final mutation set for each model.

***dN/dS* calculation.** The neutral ratio of nonsynonymous to synonymous substitutions (*dN/dS* ratio) of the ancestral *B. thuringiensis* and *B. subtilis* were estimated by using the codon usage table of each species from Genome2D (http://genome2d.molgenrug.nl/), calculated as 3.69 and 3.51, respectively. All reported *dN/dS* ratios of each adaptation model are normalized by the neutral ratio of synonymous and nonsynonymous sites of *B. thuringiensis* and *B. subtilis*, respectively.

$$dN/dS = \frac{\#\ nonsynonymous\ mutations}{\#\ synonymous\ mutations} \times neutral\ ratio \quad (1)$$

Genotype and genealogy analysis. Muller plots were generated using the *Lolipop* package (https://github .com/cdeitrick/lolipop) (version 0.6) using default parameters(40, 59). Then Muller plots were manually colored by the presence of shared dominance mutated genes or genotypes.

Parallelism analysis. We defined 'multiplicity' (m_i) of gene I as the number of mutations of gene i (n_i), multiplied by the mean gene length across all genes (L_{mean}), scaled by gene length (L_i)(27, 30).

$$m_i = n_i \frac{L_{mean}}{L_i} \quad (2)$$

In our null model, the mutations for each model or species were randomly assigned to genes from the complete set annotated genes and weighted by gene length of each gene. We simulate these random draws 1000 times to generate null distributions for gene multiplicity.

To further quantify how signatures of each mutated gene were greater than expected by chance, we focused on genes mutated two or more times in each species. Fisher's exact test was performed using this compiled list: the numbers of mutations per gene, the total number of mutations observed in each species, the gene length and the genome length of each species. Testing was performed for each gene, and false positives were reduced using the Benjamini-Hochberg correction to adjust the p_value(40).

Jaccard Index (*J*) for two evolved lineages with sets of accumulated mutated genes G1 and G2 was calculated using the formula (3). In words, the number of mutated genes shared by both lineages divided by the total number of genes mutated in both lineages.

$$J_{G1,G2} = \frac{|G1 \cap G2|}{|G1 \cup G2|} \quad (3)$$

Population size estimation. It is impossible to calculate the exact population size of each population for we only tested the biofilm production in our previous studies, so we calculated the biofilm production as reference. The experimental evolution setup of Bth_bead contains one old, colonized bead from last transfer and two new colonized beads, and the cell number of the new colonized bead was analyzed, then we use the cell number multiply by three as the population size of Bth_bead from each lineage and timepoint. This method underestimates the population size as it does not count the planktonic cells. We count the biofilm production of each population from transfer 6 to transfer 40.

In Bth_root and Bs_root, each contains one old, colonized root from last transfer and one new colonized root, and the cell number of the old, colonized root was analyzed, then we use the cell number multiply by two as the population size of Bth_root and Bs_root from each lineage and timepoint. This method may overestimate the population size since the old, colonized root contains more cells than the new one. We count the biofilm production of each population from transfer 5 to transfer 38 and transfer 4 to transfer 32 for Bth_root and Bs_root, respectively.

In Bs_pellicle, we use the pellicle production directly. This method also underestimates the population size for it didn't count the planktonic cells. We count the biofilm production of each population from transfer 5 to transfer 35.

Data availability. The sequencing data that support the findings of this study has been deposited into CNGB Sequence Archive (CNSA)(75) of China National GeneBank DataBase (CNGBdb)(76) with accession number CNP0002416 and CNP0002735.

Acknowledgements

We thank Anna Dragos, Mathilde Nordgaard, Yicen Lin for providing the genomic DNA samples from the evolved populations. We thank Jeff Barrick for valuable suggestions on the data analysis method. This project was supported by China National GeneBank (CNGB), Danish National Research Foundation (DNRF137) for the Center for Microbial Secondary Metabolites, and Novo Nordisk Foundation within the INTERACT project of the Collaborative Crop Resiliency Program (NNF19SA0059360).

References

1. Flemming HC, Wuertz S. 2019. Bacteria and archaea on Earth and their abundance in biofilms. Nat Rev Microbiol 17:247–260.

2. Hall-Stoodley L, Costerton JW, Stoodley P. 2004. Bacterial biofilms: From the natural environment to infectious diseases. Nat Rev Microbiol. Nature Publishing Group https://doi.org/10.1038/nrmicro821.

3. Stewart PS, Franklin MJ. 2008. Physiological heterogeneity in biofilms. Nat Rev Microbiol 6:199–210.

4. López D, Vlamakis H, Kolter R. 2010. Biofilms. Cold Spring Harb Perspect Biol 2:a000398.

5. Kovács ÁT, Dragoš A. 2019. Evolved Biofilm: Review on the Experimental Evolution Studies of *Bacillus subtilis* Pellicles. J Mol Biol https://doi.org/10.1016/j.jmb.2019.02.005.

6. Arnaouteli S, Bamford NC, Stanley-Wall NR, Kovács ÁT. 2021. *Bacillus subtilis* biofilm formation and social interactions. Nat Rev Microbiol 19:600–614.

7. Raymond B, Johnston PR, Nielsen-LeRoux C, Lereclus D, Crickmore N. 2010. Bacillus thuringiensis: An impotent pathogen? Trends Microbiol 18:189–194.

8. Ivanova N, Sorokin A, Anderson I, Galleron N, Candelon B, Kapatral V, Bhattacharyya A, Reznik G, Mikhailova N, Lapidus A, Chu L, Mazur M, Goltsman E, Larsen N, D'Souza M, Walunas T, Grechkin Y, Pusch G, Haselkorn R, Fonstein M, Ehrlich SD, Overbeek R, Kyrpides N. 2003. Genome sequence of Bacillus cereus and comparative analysis with *Bacillus anthracis*. Nature 423:87–91.

9. Cairns LS, Hobley L, Stanley-Wall NR. 2014. Biofilm formation by *Bacillus subtilis*: new insights into regulatory strategies and assembly mechanisms. Mol Microbiol 93:587–598.

10. Slamti L, Perchat S, Huillet E, Lereclus D. 2014. Quorum sensing in *Bacillus thuringiensis* is required for completion of a full infectious cycle in the insect. Toxins (Basel) 6:2239–2255.

11. Fagerlund A, Dubois T, Økstad OA, Verplaetse E, Gilois N, Bennaceur I, Perchat S, Gominet M, Aymerich S, Kolstø AB, Lereclus D, Gohar M. 2014. SinR controls enterotoxin expression in *Bacillus thuringiensis* biofilms. PLoS One 9:e87532.

12. Tan SJ and T. 2008. Spore Formation in *Bacillus subtilis*. Bone 23:212–225.

13. Hamon MA, Lazazzera BA. 2001. The sporulation transcription factor Spo0A is required for biofilm development in *Bacillus subtilis*. Mol Microbiol 42:1199–1209.

14. Verplaetse E, Slamti L, Gohar M, Lereclus D. 2017. Two distinct pathways lead *Bacillus thuringiensis* to commit to sporulation in biofilm. Res Microbiol 168:388–393.

15. Gohar M, Faegri K, Perchat S, Ravnum S, Økstad OA, Gominet M, Kolstø AB, Lereclus D. 2008. The PlcR Virulence Regulon of *Bacillus cereus*. PLoS One 3:e2793.

16. Mahillon J, Rezsöhazy R, Hallet B, Delcour J. 1994. IS*231* and other *Bacillus thuringiensis* transposable elements: A review. Genetica 93:13–26.

17. Joung KB, Côté JC. 2003. Distribution analysis of IS*231*-like sequences among *Bacillus thuringiensis* serovars inferred from restriction fragment length polymorphisms. Curr Microbiol 47:417–424.

18. Mahillon J, Seurinck J, van Rompuy L, Delcour J, Zabeau M. 1985. Nucleotide sequence and structural organization of an insertion sequence element (IS*231*) from *Bacillus thuringiensis* strain berliner 1715. EMBO J 4:3895–3899.

19. Qiu N, He J, Wang Y, Cheng G, Li M, Sun M, Yu Z. 2010. Prevalence and diversity of insertion sequences in the genome of *Bacillus thuringiensis* YBT-1520 and comparison with other *Bacillus cereus* group members. FEMS Microbiol Lett 310:9–16.

20. Nagai T, Tran LSP, Inatsu Y, Itoh Y. 2000. A new IS4 family insertion sequence, IS4Bsu1, responsible for genetic instability of poly-γ-glutamic acid production in *Bacillus subtilis*. J Bacteriol 182:2387–2392.

21. Miller SR, Abresch HE, Ulrich NJ, Sano EB, Demaree AH, Oman AR, Garber AI. 2021. Bacterial Adaptation by a Transposition Burst of an Invading IS Element. Genome Biol Evol 13:evab245.

22. Schneider D, Lenski RE. 2004. Dynamics of insertion sequence elements during experimental evolution of bacteria. Res Microbiol 155:319–327.

23. Consuegra J, Gaffé J, Lenski RE, Hindré T, Barrick JE, Tenaillon O, Schneider D. 2021. Insertion-sequence-mediated mutations both promote and constrain evolvability during a long-term experiment with bacteria. Nat Commun 12:980.

24. Steenackers HP, Parijs I, Foster KR, Vanderleyden J. 2016. Experimental evolution in biofilm populations. FEMS Microbiol Rev 40:373–397.

25. Kawecki TJ, Lenski RE, Ebert D, Hollis B, Olivieri I, Whitlock MC. 2012. Experimental evolution. Trends Ecol Evol 27:547–560.

26. Barrick JE, Lenski RE. 2013. Genome dynamics during experimental evolution. Nat Rev Genet 14:827–839.

27. Good BH, McDonald MJ, Barrick JE, Lenski RE, Desai MM. 2017. The dynamics of molecular evolution over 60,000 generations. Nature 551:45–50.

28. Cooper VS, Honsa E, Rowe H, Deitrick C, Iverson AR, Whittall JJ, Neville SL, McDevitt CA, Kietzman C, Rosch JW. 2020. Experimental Evolution In Vivo To Identify Selective Pressures during *Pneumococcal Colonization*. mSystems 5:e00352-20.

29. Nguyen Ba AN, Cvijović I, Rojas Echenique JI, Lawrence KR, Rego-Costa A, Liu X, Levy SF, Desai MM. 2019. High-resolution lineage tracking reveals travelling wave of adaptation in laboratory yeast. Nature 575:494–499.

30. Johnson MS, Gopalakrishnan S, Goyal J, Dillingham ME, Bakerlee CW, Humphrey PT, Jagdish T, Jerison ER, Kosheleva K, Lawrence KR, Min J, Moulana A, Phillips AM, Piper JC, Purkanti R, Rego-Costa A, McDonald MJ, Ba ANN, Desai MM. 2021. Phenotypic and molecular evolution across 10,000 generations in laboratory budding yeast populations. Elife 10:e63910.

31. Nilsson AI, Koskiniemi S, Eriksson S, Kugelberg E, Hinton JCD, Andersson DI. 2005. Bacterial genome size reduction by experimental evolution. Proc Natl Acad Sci U S A 102:12112–12116.

32. Ackermann M, Schauerte A, Stearns SC, Jenal U. 2007. Experimental evolution of aging in a bacterium. BMC Evol Biol 7:126.

33. Lang GI, Rice DP, Hickman MJ, Sodergren E, Weinstock GM, Botstein D, Desai MM. 2013. Pervasive genetic hitchhiking and clonal interference in forty evolving yeast

populations. Nature 500:571–574.

34. Koeppel AF, Wertheim JO, Barone L, Gentile N, Krizanc D, Cohan FM. 2013. Speedy speciation in a bacterial microcosm: new species can arise as frequently as adaptations within a species. ISME J 7:1080–1091.

35. Lenski RE, Rose MR, Simpson SC, Tadler SC. 1991. Long-Term Experimental Evolution in *Escherichia coli*. I. Adaptation and Divergence During 2,000 Generations. Am Nat 138:1315–1341.

36. Poltak SR, Cooper VS. 2011. Ecological succession in long-term experimentally evolved biofilms produces synergistic communities. ISME Journal 5:369–378.

37. Zhang Q, Lambert G, Liao D, Kim H, Robin K, Tung CK, Pourmand N, Austin RH. 2011. Acceleration of emergence of bacterial antibiotic resistance in connected microenvironments. Science (1979) 333:1764–1767.

38. Traverse CC, Mayo-Smith LM, Poltak SR, Cooper VS. 2013. Tangled bank of experimentally evolved *Burkholderia* biofilms reflects selection during chronic infections. Proceedings of the National Academy of Sciences 110:E250–E259.

39. Li E, Zhang H, Jiang H, Pieterse CMJ, Jousset A, Bakker PAHM, de Jonge R. 2021. Experimental-evolution-driven identification of arabidopsis rhizosphere competence genes in pseudomonas protegens. mBio 12:e00927-21.

40. Harris KB, Flynn KM, Cooper VS. 2021. Polygenic Adaptation and Clonal Interference Enable Sustained Diversity in Experimental Pseudomonas aeruginosa Populations. Mol Biol Evol 38:5359–5375.

41. Lin Y, Xu X, Maróti G, Strube ML, Kovács ÁT. 2022. Adaptation and phenotypic diversification of Bacillus thuringiensis biofilm are accompanied by fuzzy spreader morphotypes. NPJ Biofilms Microbiomes 8:27.

42. Lin Y, Alstrup M, Pang JKY, Maróti G, Er-Rafik M, Tourasse N, Økstad OA, Kovács ÁT. 2021. Adaptation of Bacillus thuringiensis to Plant Colonization Affects Differentiation and Toxicity. mSystems 6:e00864-21.

43. Dragoš A, Lakshmanan N, Martin M, Horváth B, Maróti G, Falcón García C, Lieleg O, Kovács ÁT. 2018. Evolution of exploitative interactions during diversification in

Bacillus subtilis biofilms. FEMS Microbiol Ecol 94:fix155.

44. Nordgaard M, Blake C, Maróti G, Hu G, Wang Y, Strube ML, Kovács ÁT. 2022. Experimental evolution of Bacillus subtilis on Arabidopsis thaliana roots reveals fast adaptation and improved root colonization. iScience 25:104406.

45. Chen A, Liao S, Cheng M, Ma K, Wu L, Lai Y, Qiu X, Yang J, Xu J, Hao S, Wang X, Lu H, Chen X, Liu X, Huang X, Li Z, Hong Y, Jiang Y, Peng J, Liu S, Shen M, Liu C, Li Q, Yuan Y, Wei X, Zheng H, Feng W, Wang Z, Liu Y, Wang Z, Yang Y, Xiang H, Han L, Qin B, Guo P, Lai G, Muñoz-Cánoves P, Maxwell PH, Thiery JP, Wu Q-F, Zhao F, Chen B, Li M, Dai X, Wang S, Kuang H, Hui J, Wang L, Fei J-F, Wang O, Wei X, Lu H, Wang B, Liu S, Gu Y, Ni M, Zhang W, Mu F, Yin Y, Yang H, Lisby M, Cornall RJ, Mulder J, Uhlén M, Esteban MA, Li Y, Liu L, Xu X, Wang J. 2022. Spatiotemporal transcriptomic atlas of mouse organogenesis using DNA nanoball-patterned arrays. Cell 185:1777-1792.e21.

46. Han L, Wei X, Liu C, Volpe G, Zhuang Z, Zou X, Wang Z, Pan T, Yuan Y, Zhang X, Fan P, Guo P, Lai Y, Lei Y, Liu X, Yu F, Shangguan S, Lai G, Deng Q, Liu Y, Wu L, Shi Q, Yu H, Huang Y, Cheng M, Xu J, Liu Y, Wang M, Wang C, Zhang Y, Xie D, Yang Y, Yu Y, Zheng H, Wei Y, Huang F, Lei J, Huang W, Zhu Z, Lu H, Wang B, Wei X, Chen F, Yang T, Du W, Chen J, Xu S, An J, Ward C, Wang Z, Pei Z, Wong C-W, Liu X, Zhang H, Liu M, Qin B, Schambach A, Isern J, Feng L, Liu Y, Guo X, Liu Z, Sun Q, Maxwell PH, Barker N, Muñoz-Cánoves P, Gu Y, Mulder J, Uhlen M, Tan T, Liu S, Yang H, Wang J, Hou Y, Xu X, Esteban MA, Liu L. 2022. Cell transcriptomic atlas of the non-human primate *Macaca fascicularis*. Nature 604:723–731.

47. Barrick JE, Colburn G, Deatherage DE, Traverse CC, Strand MD, Borges JJ, Knoester DB, Reba A, Meyer AG. 2014. Identifying structural variation in haploid microbial genomes from short-read resequencing data using breseq. BMC Genomics 15:1039.

48. Deatherage DE, Barrick JE. 2014. Identification of Mutations in Laboratory-Evolved Microbes from Next-Generation Sequencing Data Using breseq. Methods Mol Biol 1151:165–188.

49. Howell A, Dubrac S, Andersen KK, Noone D, Fert J, Msadek T, Devine K. 2003. Genes controlled by the essential YycG/YycF two-component system of Bacillus subtilis revealed through a novel hybrid regulator approach. Mol Microbiol 49:1639–1655.

50. Lewandoski M, Dubnau E, Smith I. 1986. Transcriptional regulation of the spo0F gene of Bacillus subtilis. J Bacteriol 168:870–877.

51. Estacio W, Santa Anna-Arriola S, Adedipe M, Márquez-Magaña LM. 1998. Dual promoters are responsible for transcription initiation of the fla/che operon in Bacillus subtilis. J Bacteriol 180:3548–3555.

52. Kobayashi K. 2007. Gradual activation of the response regulator DegU controls serial expression of genes for flagellum formation and biofilm formation in Bacillus subtilis. Mol Microbiol 66:395–409.

53. Shafikhani SH, Mandic-Mulec I, Strauch MA, Smith I, Leighton T. 2002. Postexponential Regulation of sin Operon Expression in Bacillus subtilis. J Bacteriol 184:564–571.

54. Beijer L, Nilsson RP, Holmberg C, Rutberg L. 1993. The glpP and glpF genes of the glycerol regulon in Bacillus subtilis. J Gen Microbiol 139:349–359.

55. Holmberg C, Beijer L, Rutberg B, Rutberg L. 1990. Glycerol catabolism in Bacillus subtilis: nucleotide sequence of the genes encoding glycerol kinase (glpK) and glycerol-3-phosphate dehydrogenase (glpD). J Gen Microbiol 136:2367–2375.

56. Herring CD, Raghunathan A, Honisch C, Patel T, Applebee MK, Joyce AR, Albert TJ, Blattner FR, Van Den Boom D, Cantor CR, Palsson B. 2006. Comparative genome sequencing of Escherichia coli allows observation of bacterial evolution on a laboratory timescale. Nat Genet 38:1406–1412.

57. Bram Van den Bergh, Toon Swings, Maarten Fauvart JM. 2018. Experimental Design, Population Dynamics, and Diversity in Microbial Experimental Evolution. Microbiology and Molecular Biology Reviews 82:e00008-18.

58. Kampf J, Gerwig J, Kruse K, Cleverley R, Dormeyer M, Grünberger A, Kohlheyer D, Commichau FM, Lewis RJ, Stülke J. 2018. Selective pressure for biofilm formation in Bacillus subtilis: Differential effect of mutations in the master regulator sinR on bistability. mBio 9:e01464-18.

59. Scribner MR, Santos-Lopez A, Marshall CW, Deitrick C, Coopera VS, Hogan DA. 2020. Parallel evolution of tobramycin resistance across species and environments. mBio 11:e00932-20.

60. Kao KC, Sherlock G. 2008. Molecular characterization of clonal interference during adaptive evolution in asexual populations of Saccharomyces cerevisiae. Nat Genet 40:1499–1504.

61. Birky CW, Walsh JB. 1988. Effects of linkage on rates of molecular evolution. Proceedings of the National Academy of Sciences 85:6414–6418.

62. Comeron JM, Williford A, Kliman RM. 2008. The Hill-Robertson effect: Evolutionary consequences of weak selection and linkage in finite populations. Heredity (Edinb). Nature Publishing Group https://doi.org/10.1038/sj.hdy.6801059.

63. Maddamsetti R, Lenski RE, Barrick JE. 2015. Adaptation, clonal interference, and frequency-dependent interactions in a long-term evolution experiment with *Escherichia coli*. Genetics 200:619–631.

64. Tenaillon O, Barrick JE, Ribeck N, Deatherage DE, Blanchard JL, Dasgupta A, Wu GC, Wielgoss S, Cruveiller S, Médigue C, Schneider D, Lenski RE. 2016. Tempo and mode of genome evolution in a 50,000-generation experiment. Nature 536:165–170.

65. Bailey SF, Rodrigue N, Kassen R. 2015. The Effect of Selection Environment on the Probability of Parallel Evolution. Mol Biol Evol 32:1436–1448.

66. Bailey SF, Blanquart F, Bataillon T, Kassen R. 2017. What drives parallel evolution?: How population size and mutational variation contribute to repeated evolution. BioEssays 39:1600176.

67. Siguier P, Gourbeyre E, Chandler M. 2014. Bacterial insertion sequences: their genomic impact and diversity. FEMS Microbiol Rev 38:865–891.

68. Wein T, Dagan T. 2019. The Effect of Population Bottleneck Size and Selective Regime on Genetic Diversity and Evolvability in Bacteria. Genome Biol Evol 11:3283–3290.

69. Frickel J, Feulner PGD, Karakoc E, Becks L. 2018. Population size changes and selection drive patterns of parallel evolution in a host-virus system. Nat Commun 9:1706.

70. Lachapelle J, Reid J, Colegrave N. 2015. Repeatability of adaptation in experimental populations of different sizes. Proceedings of the Royal Society B: Biological Sciences 282:20143033.

71. Schenk MF, Zwart MP, Hwang S, Ruelens P, Severing E, Krug J, de Visser JAGM. 2022.

Population size mediates the contribution of high-rate and large-benefit mutations to parallel evolution. Nat Ecol Evol 6:439–447.

72. Miller CR, Joyce P, Wichman HA. 2011. Mutational Effects and Population Dynamics During Viral Adaptation Challenge Current Models. Genetics 187:185–202.

73. Wein T, Dagan T. 2019. The effect of population bottleneck size and selective regime on genetic diversity and evolvability in bacteria. Genome Biol Evol 11:3283–3290.

74. Chen Y, Chen Y, Shi C, Huang Z, Zhang Y, Li S, Li Y, Ye J, Yu C, Li Z, Zhang X, Wang J, Yang H, Fang L, Chen Q. 2018. SOAPnuke: A MapReduce acceleration-supported software for integrated quality control and preprocessing of high-throughput sequencing data. Gigascience 7:gix120.

75. Guo X, Chen F, Gao F, Li L, Liu K, You L, Hua C, Yang F, Liu W, Peng C, Wang L, Yang X, Zhou F, Tong J, Cai J, Li Z, Wan B, Zhang L, Yang T, Zhang M, Yang L, Yang Y, Zeng W, Wang B, Wei X, Xu X. 2020. CNSA: A data repository for archiving omics data. Database 2020:baaa055.

76. Chen FZ, You LJ, Yang F, Wang LN, Guo XQ, Gao F, Hua C, Tan C, Fang L, Shan RQ, Zeng WJ, Wang B, Wang R, Xu X, Wei XF. 2020. CNGBdb: China National GeneBank DataBase. Hereditas 42:799–809.

Tables and figures

Table 1. Mutation type and number

Category	Bth_bead	Bth_root	Bs_pellicle	Bs_root
Pseudogene	5	9	0	7
Non-coding gene*	0	3	0	1
Coding gene	69	184	119	286
Synonymous	8	27	22	62
Non-synonymous	33	113	69	160
Nonsense	7	12	4	37
InDel **	21	32	24	27
Intergenic ***	45	77	39	56
Total number	**119**	**273**	**158**	**350**
Fixed	6	47	1	9
Fixed rate	5.04%	17.22%	0.63%	2.57%

Notes: there is no overlap between each category. * Non-coding gene includes tRNA gene, ncRNA gene, and repeat region (IS); ** InDel here only refers to the insertion and deletion mutations in coding gene regions; *** intergenic mutations includes all kinds of mutations in intergenic region.

Table 2. IS transposition cases detected in the experimentally evolved *B. thuringiensis* lineages

Position	Insertion sequence*	Gene	Description	Condition	Lineage	Highest frequency in lineage
397,547	I1(+) + 12bp	*glnP*	Glutamine transport system permease protein GlnP	Bth_bead	B	6.12%
607,087	I1(-) + 11bp	*npr*	Bacillolysin	Bth_bead	E	5.23%
985,569	I1(+) + 11bp	BTB_RS05005/ BTB_RS34715	---/---	Bth_bead	A	34.73%
1,233,591	I1(-) + 11bp	*rfbB*	dTDP-glucose 4,6-dehydratase	Bth_bead	A	54.86%
2,650,349	I3(+) + 11bp	BTB_RS13370	RNaseH domain-containing protein	Bth_bead	D	8.36%
5,263,506	I3(+) + 12bp	*rfbM*	cupin domain-containing protein	Bth_bead	A	13.37%
5,263,506	I3(+) + 12bp	*rfbM*	cupin domain-containing protein	Bth_bead	B	48.66%
5,263,506	I3(+) + 12bp	*rfbM*	cupin domain-containing protein	Bth_bead	F	26.13%
5,289,559	I3(-) + 12bp	*nuoN*	NADH-quinone oxidoreductase subunit N	Bth_bead	A	29.23%
493,064	I2(+) + 3bp	*wbpA*	UDP-N-acetyl-D-glucosamine 6-dehydrogenase	Bth_root	F	8.59%
524,134	I1(+) + 11bp	BTB_RS02650	GNAT family N-acetyltransferase	Bth_root	C	100.00%
1,915,321	I1(-) + 11bp	*braD*	High-affinity branched-chain amino acid transport system permease protein BraD	Bth_root	F	18.75%
3,677,033	I3(+) + 12bp	*glnR/ynbB*	HTH-type transcriptional regulator GlnR/Uncharacterized protein YnbB	Bth_root	E	12.46%

*The Insertion sequence definition can be found in Table S4.

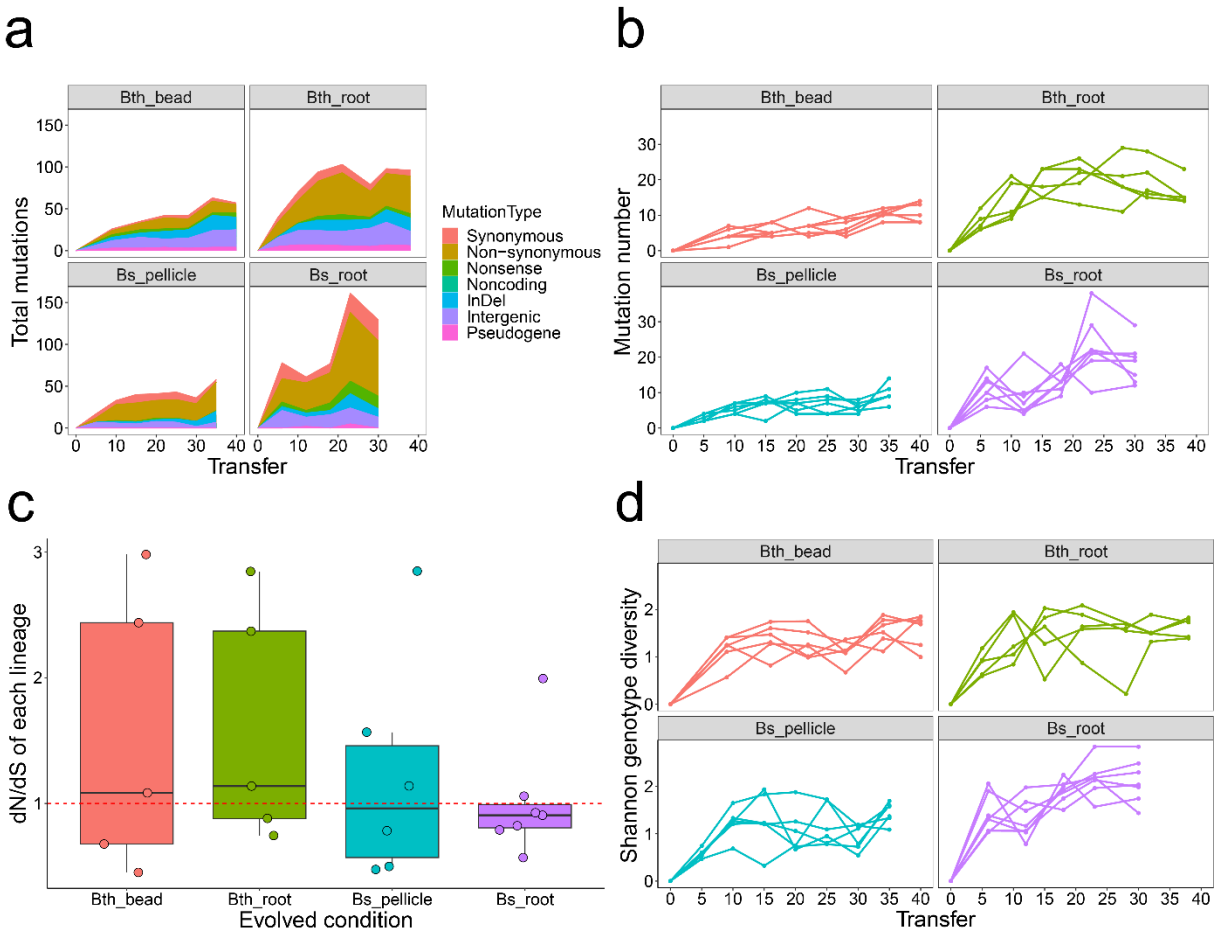

FIG 1 Mutation spectrum, dynamics and diversity. a, Distribution of detected mutations of each type in four adaptation models over time. Shaded bars show the distribution of different mutation types in each time point or total. **b**, Dynamic distribution of detected mutations in each lineage over time. **c**, *dN/dS* ratio. The ratio of nonsynonymous to synonymous mutations (*dN/dS*) in the entire pool of detected mutations of each condition, this ratio is normalized by the relative number of synonymous and nonsynonymous sites of *B. thuringiensis* and *B. subtilis*, respectively. Boxes indicate Q1–Q3, lines indicate the median, black circles filling with different color indicate the ratio of each lineage. **d**, Genotype diversity**.** Dynamic distribution of genotype alpha diversity in each population of four adaptation models over time calculated using Shannon method. Genotypes and frequencies were generated by *Lolipop* software package in Genotype and genealogy analysis.

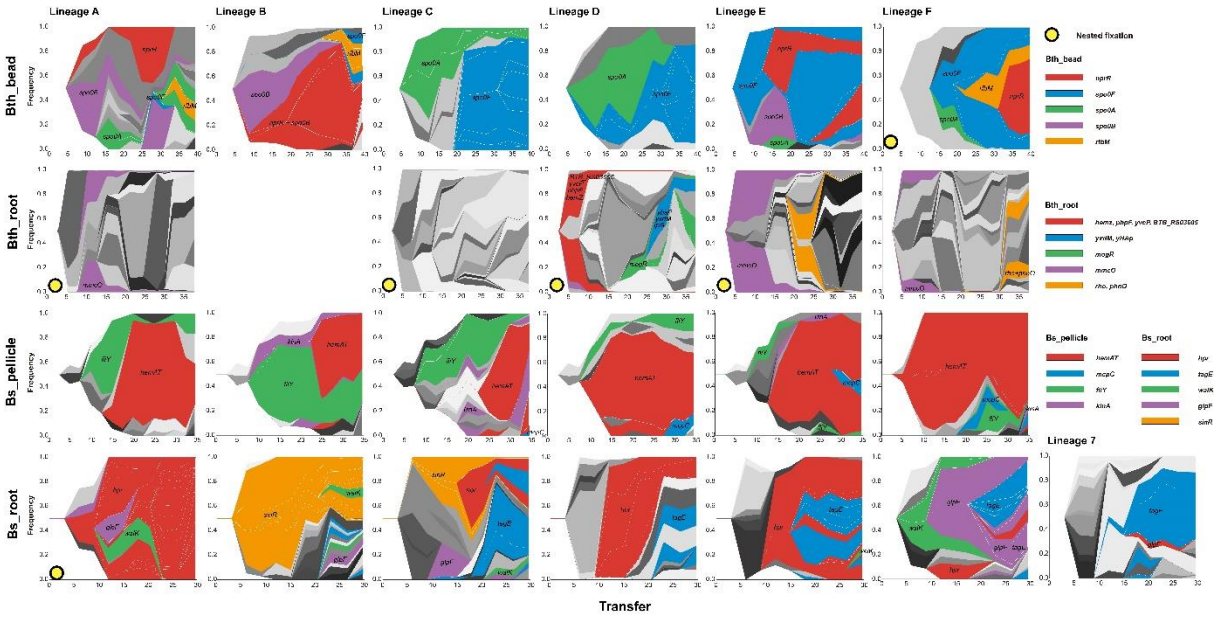

FIG 2 Genealogy and genotype frequencies over time. Each shade or color represents a different genotype and vertical area corresponds to genotype frequency, inferred by *Lolipop*. Dominant genotypes that contain the high frequency mutated genes, which are shared in different populations, are highlighted in certain colors within each adaptation model. The nested genotypes of the dominant genotype are highlighted with the same color in in Bth_bead, Bs_pellicle, and Bs_root, except for the nested genotypes which also belong to the dominant genotypes. In Bth_root, for the complex combination of mutations among different lineages and early fix of new mutations, nested genotypes are not highlighted. Other genotypes are in gray.

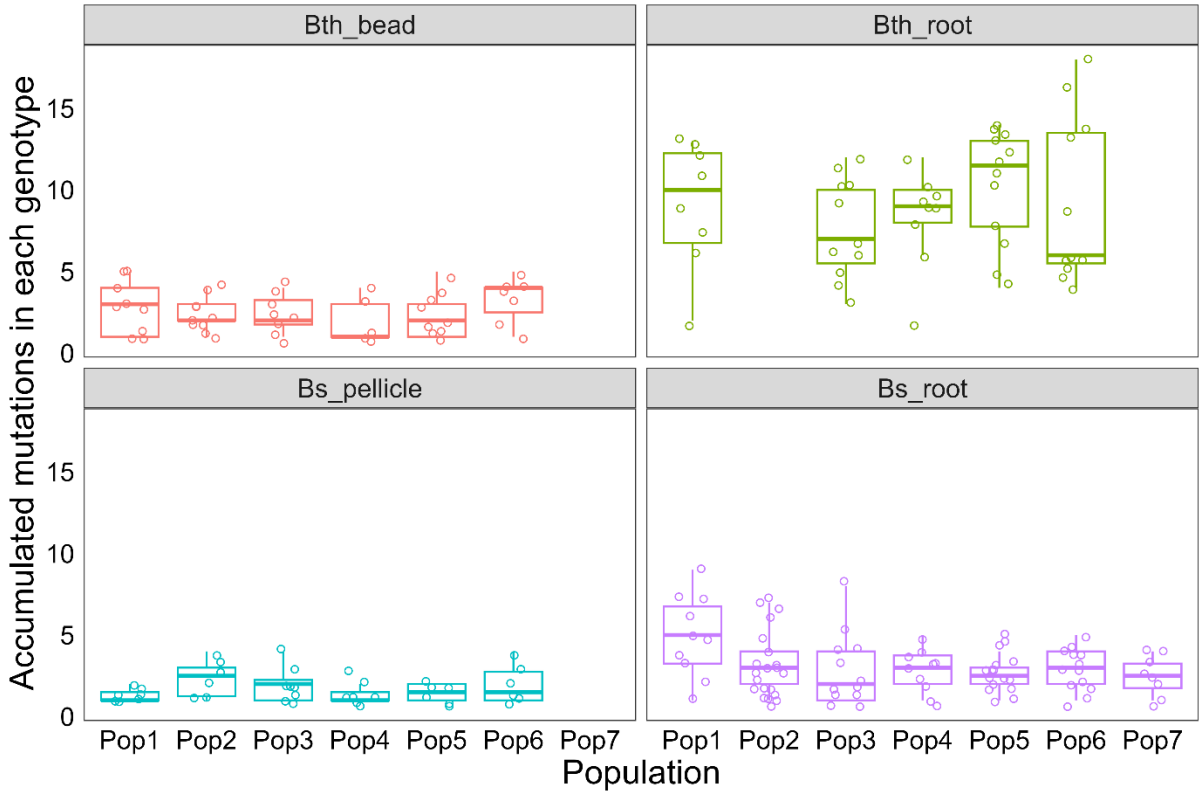

FIG 3 Evolvability. The number of accumulated mutations in each genotype at the last time point in each condition. Each circle represents one genotype. Boxes indicate Q1–Q3, lines indicate the median, circles with no filling indicate the accumulated mutation number of each genotype.

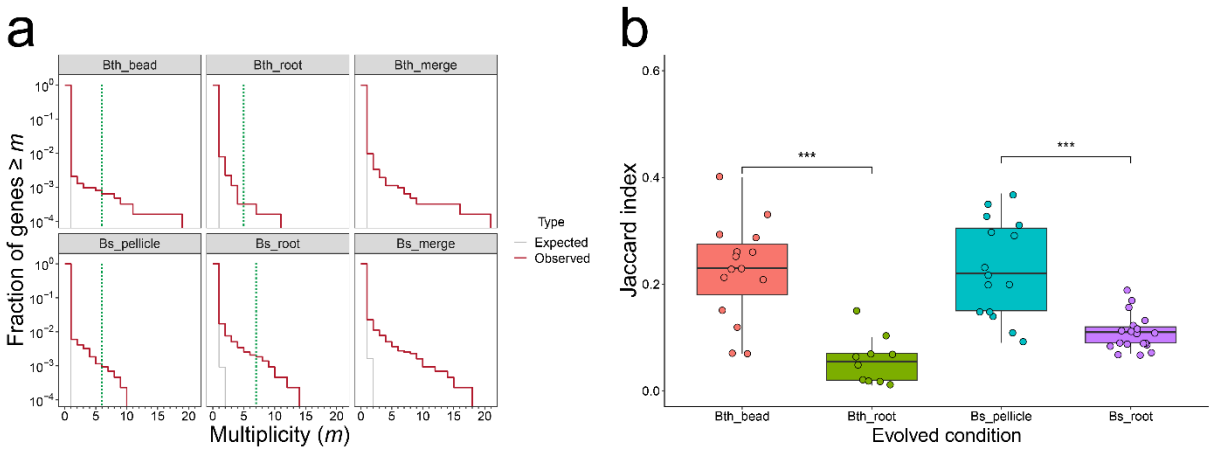

FIG 4 Parallelism. a, parallelism in each adaptation model and species. For all plots, the null distribution (shown in gray) was obtained by simulating random mutations to genes, considering the number of mutations in each model and species in our data and the relative length of each gene. The green dotted line indicates the number of lineages in each condition **b,** Degree of parallelism within each condition estimated by Jaccard index. Asterisks at the top indicate significant differences between biotic and abiotic evolved conditions of each species (***$p < 0.001$, Student's unpaired two-tailed t-test was performed). Boxes indicate Q1–Q3, lines indicate the median, black circles filling with different color indicate the *J* value of each combination, gray dots indicate the outliers.

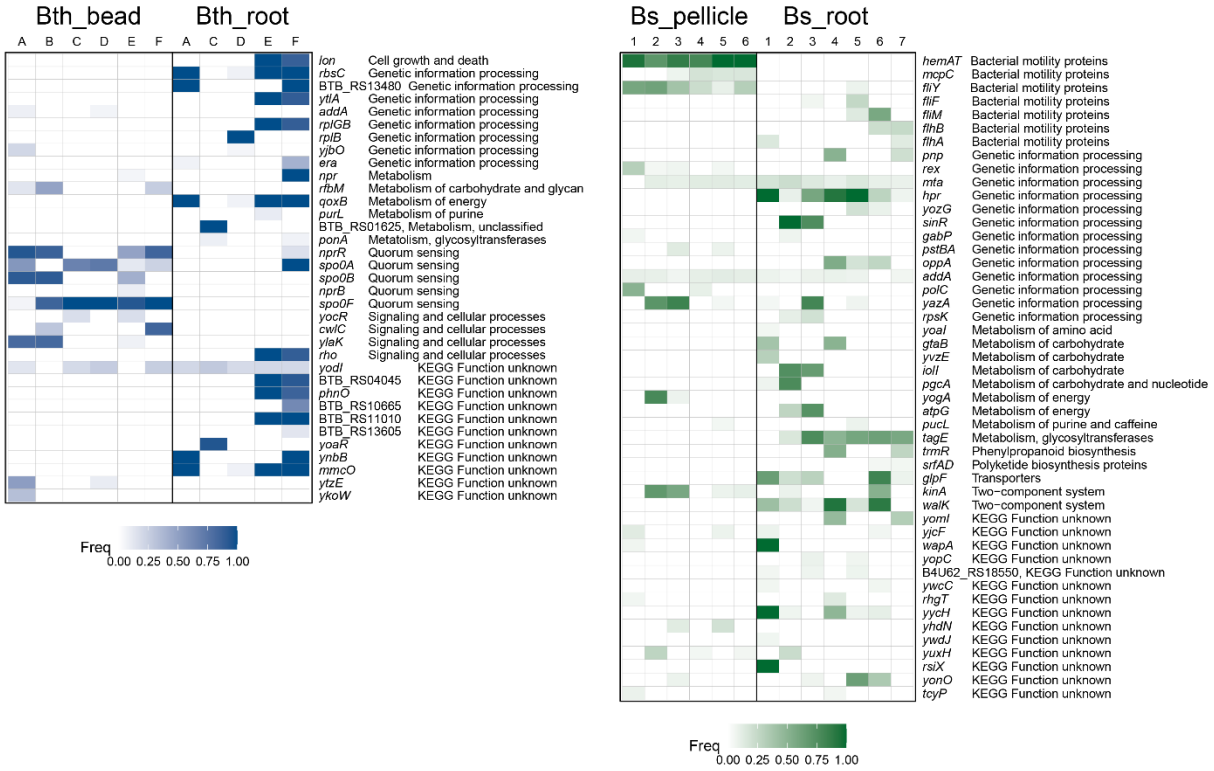

FIG 5 Genes mutated more than one time in *B. thuringiensis* and *B. subtilis*. Each column represents one replicate lineage. Forty-six genes and fifty genes mutated more than one time in *B. thuringiensis* (**a**) and *B. subtilis* (**b**), respectively, were distributed non-randomly. Color indicates the highest frequency of mutations in that gene in that lineage. Detailed information of these genes can be found in Dataset S2.

Table S1 Laboratory evolution setups of four experiments

Group	**Bth_bead**	**Bth_root**	**Bs_pellicle**	**Bs_root**
Species	*B. thuringiensis*	*B. thuringiensis*	*B. subtilis*	*B. subtilis*
Adaptation condition	Nylon beads floating in the medium	*A. thaliana* root	Pellicle biofilm at the air-medium interface	*A. thaliana* root
Medium	EPS medium	MSNg medium	MSgg medium	MSNg medium
Medium volume	1000 μL	300 μL	2000 μL	300 μL
Temperature	30C	16 h light at 24 °C/8 h dark at 20 °C	30C	16 h light at 24 °C/8 h dark at 20 °C
Transfer interval time	24h	48h	48h	48h
Number of transfers	40	38	35	30
Number of parallel linages	5	6	5	7
Timepoints	7	6	7	5
Total population samples sequenced	35	36	35	35
Adaptation model	one colonized bead to **two** new beads	one colonized root to one new root	static floating biofilm disrupted by glass beads and vortexing for 1:100 reinoculation	one colonized root to one new root
Shaking condition	90 rpm	90 rpm	static	90 rpm

Table S2 *dN/dS* ratio

Replicate	**Bth_bead**	**Bth_root**	**Bs_pellicle**	**Bs_root**
R1	2.98	2.85	0.50	0.79
R2	*	1.14	1.57	0.91
R3	0.68	0.88	2.85	0.57
R4	0.45	0.75	0.47	0.82
R5	2.44	2.37	1.14	1.06
R6	1.08		0.78	1.99
R7				0.93
Total ratio	1.36	1.25	0.95	0.91
Average	1.53	1.60	1.22	1.01
SD	1.00	0.85	0.82	0.43

* no synonymous mutation detected in this lineage

Table S3 Transposase gene in the *B. thuringiensis* 407 genome

Transposase gene	**Copies**
IS*110* family transposase	12
IS*110*-like element ISBth13 family transposase	5
IS*21*-like element IS*232* family transposase	5
IS*3* family transposase	5
transposase	5
IS*4* family transposase	2
IS*4*-like element IS*231*A family transposase	2
IS*4*-like element IS*231*C family transposase	1
IS*607* family transposase	1
IS*66* family transposase	1

Table S4 Insertion sequence definition in the second-round analysis using *breseq*

IS no.	Position	Length	Tag	Gene name
IS1	1903509~1905263	1755	BTB_RS09780	IS*4* like element IS*231*A family transposase
IS2	2497927~2499656	1730	BTB_RS12605	IS*110* family transposase
IS3	2615786~2617440	1655	BTB_RS13165	IS*4* like element IS*231*A family transposase

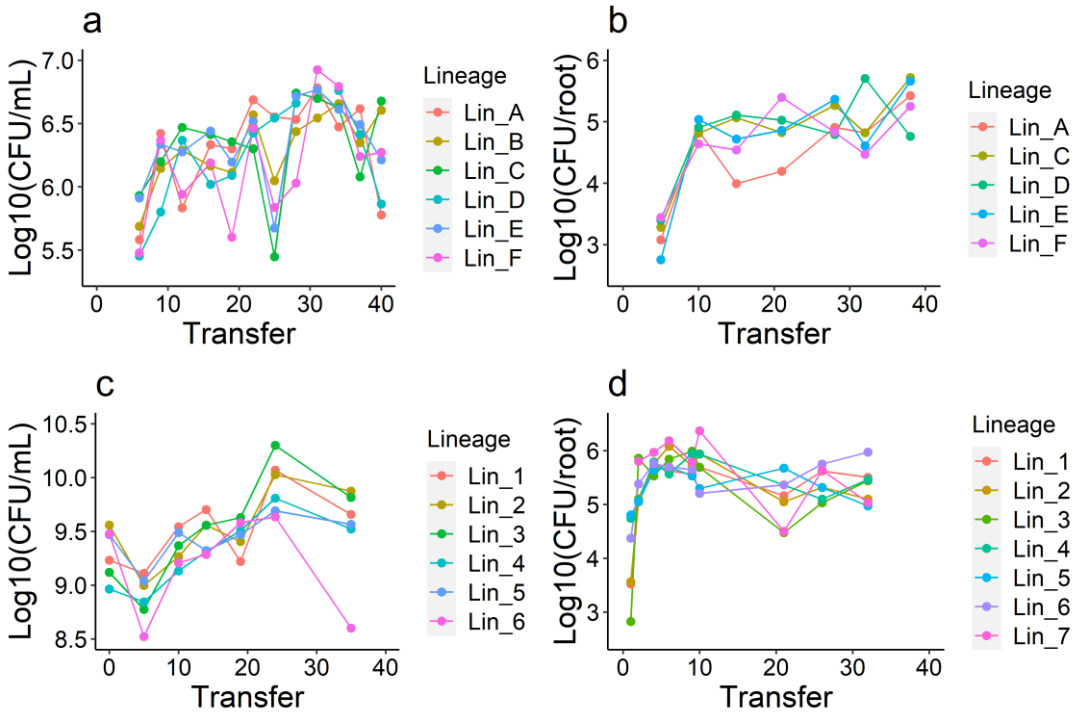

Fig S1 Biofilm productivity of four experiments. Data are from previous studies and replotted for better comparison

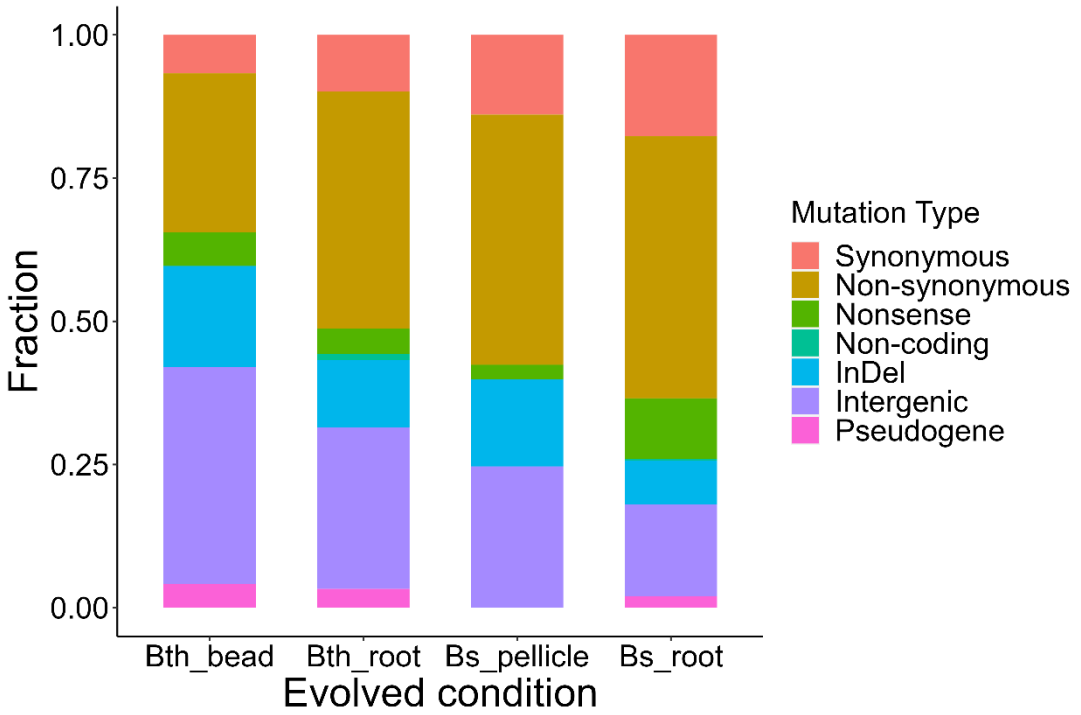

Fig S2 Mutation spectrum. Summary of mutational spectrum of the four adaptation models from all time points.

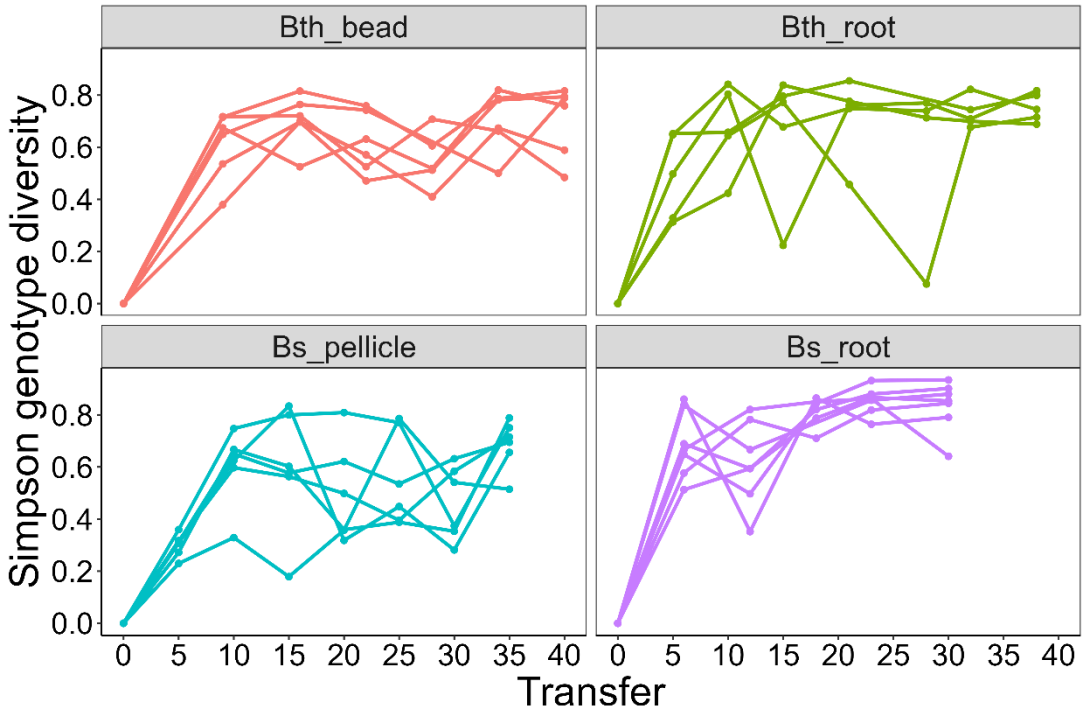

Fig S3 Genotype diversity. Dynamic distribution of genotype alpha diversity in each population of four adaptation models over time calculated using Simpson method.

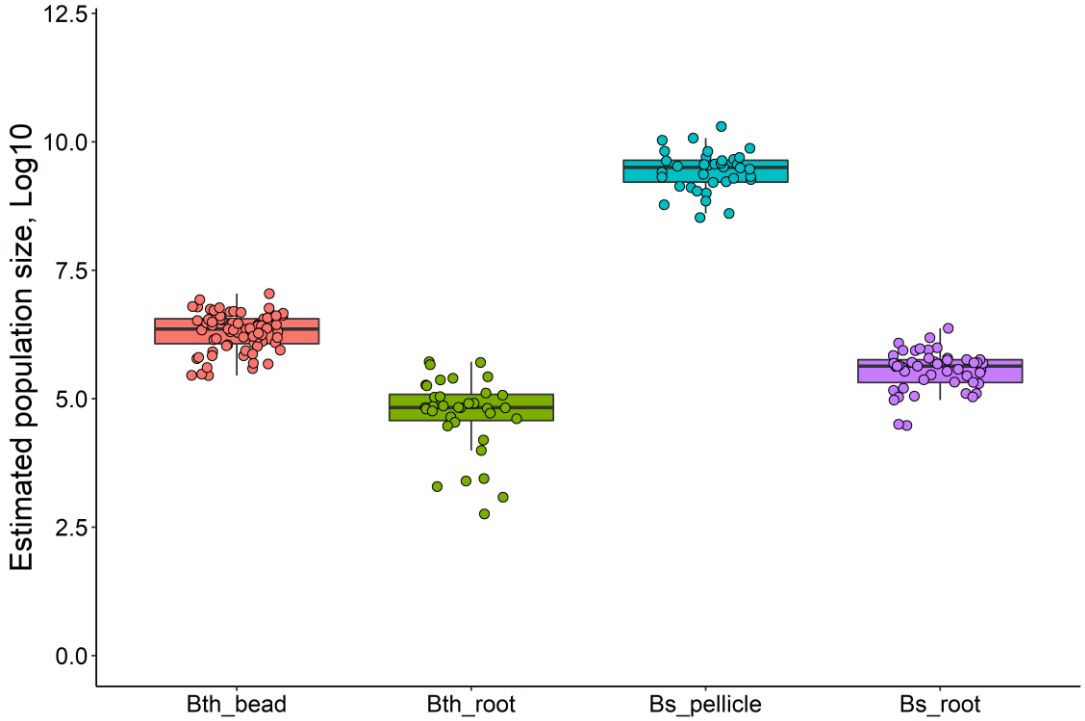

Fig S5 Estimated population size of each population and timepoints calculated from biofilm productivity data. Boxes indicate Q1–Q3, lines indicate the median, black circles filled with different color indicate the population size of each population.

Supplementary Fig. 4A, Bth_bead lineage diagram

Lineage A

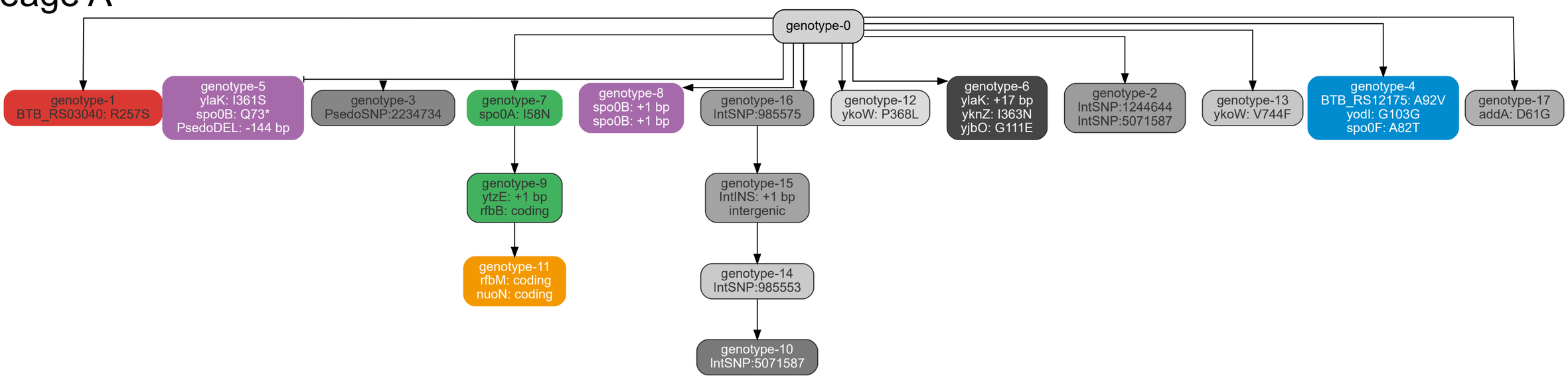

Lineage B

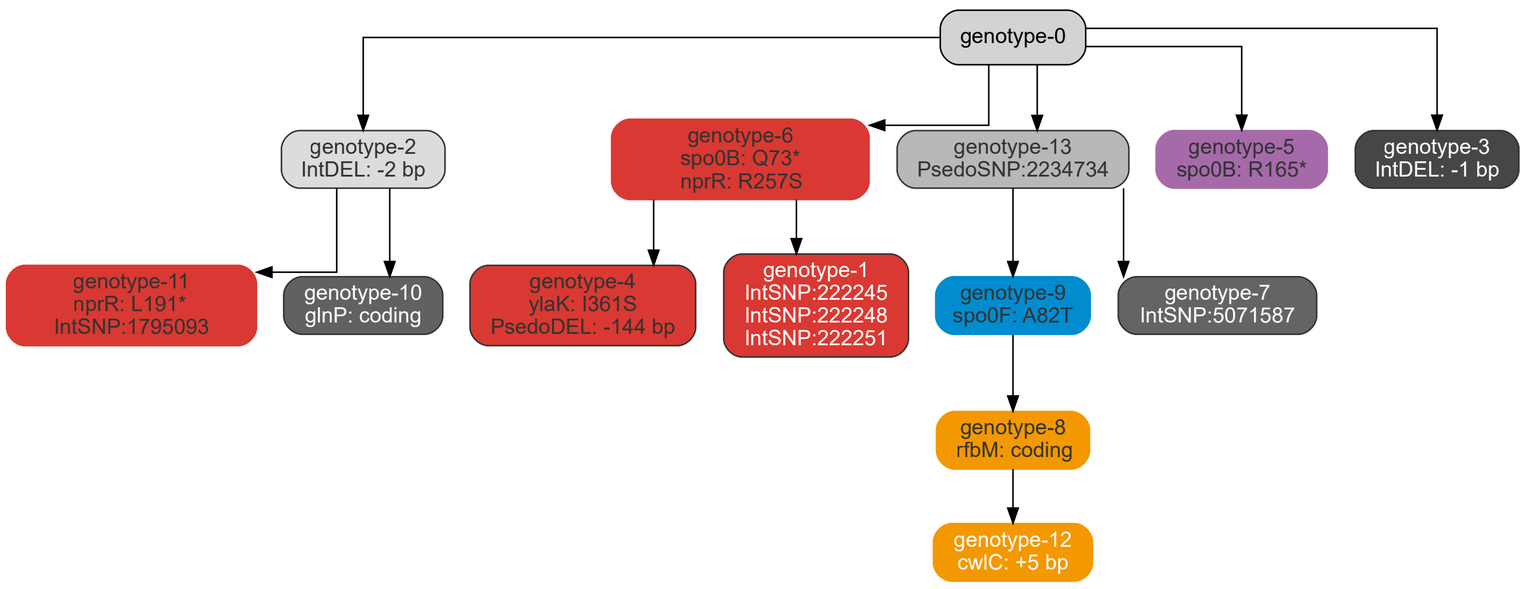

Lineage C

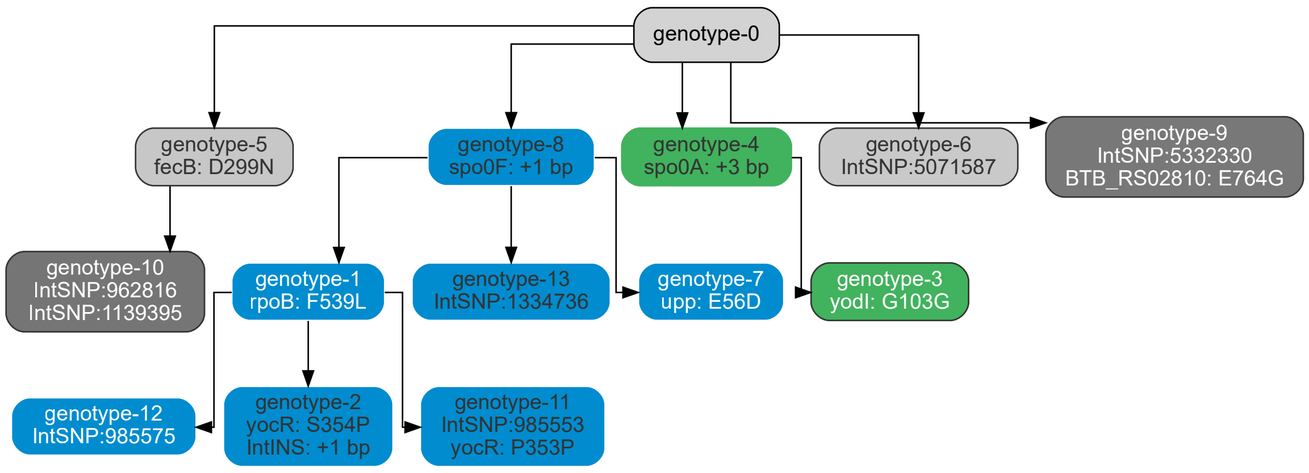

Lineage D

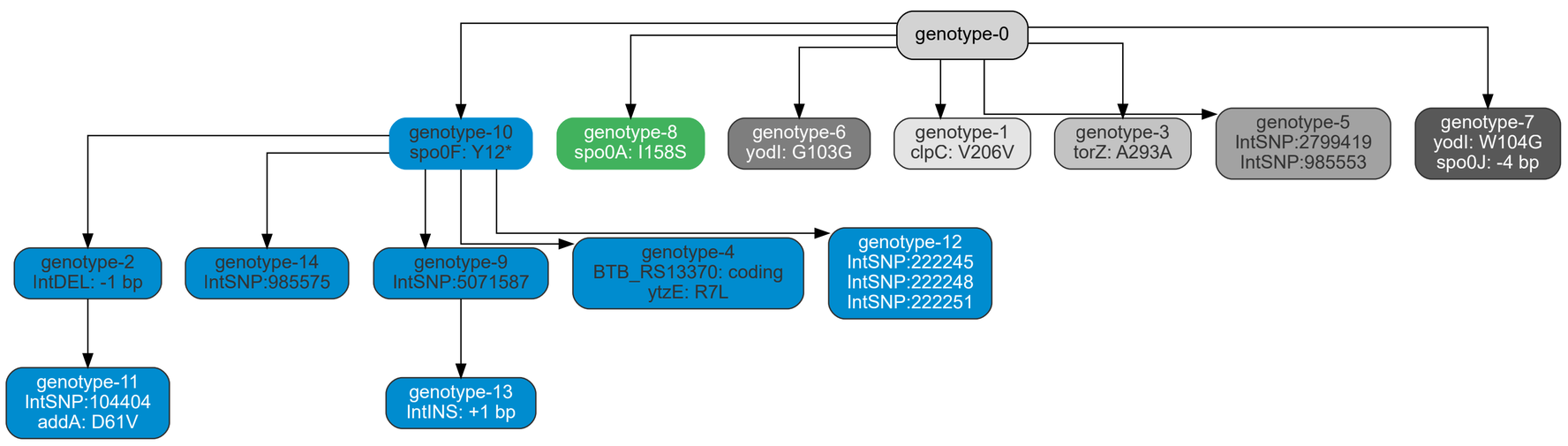

Lineage E

Lineage F

Supplementary Fig. 4B, Bth_root lineage diagram

Lineage A

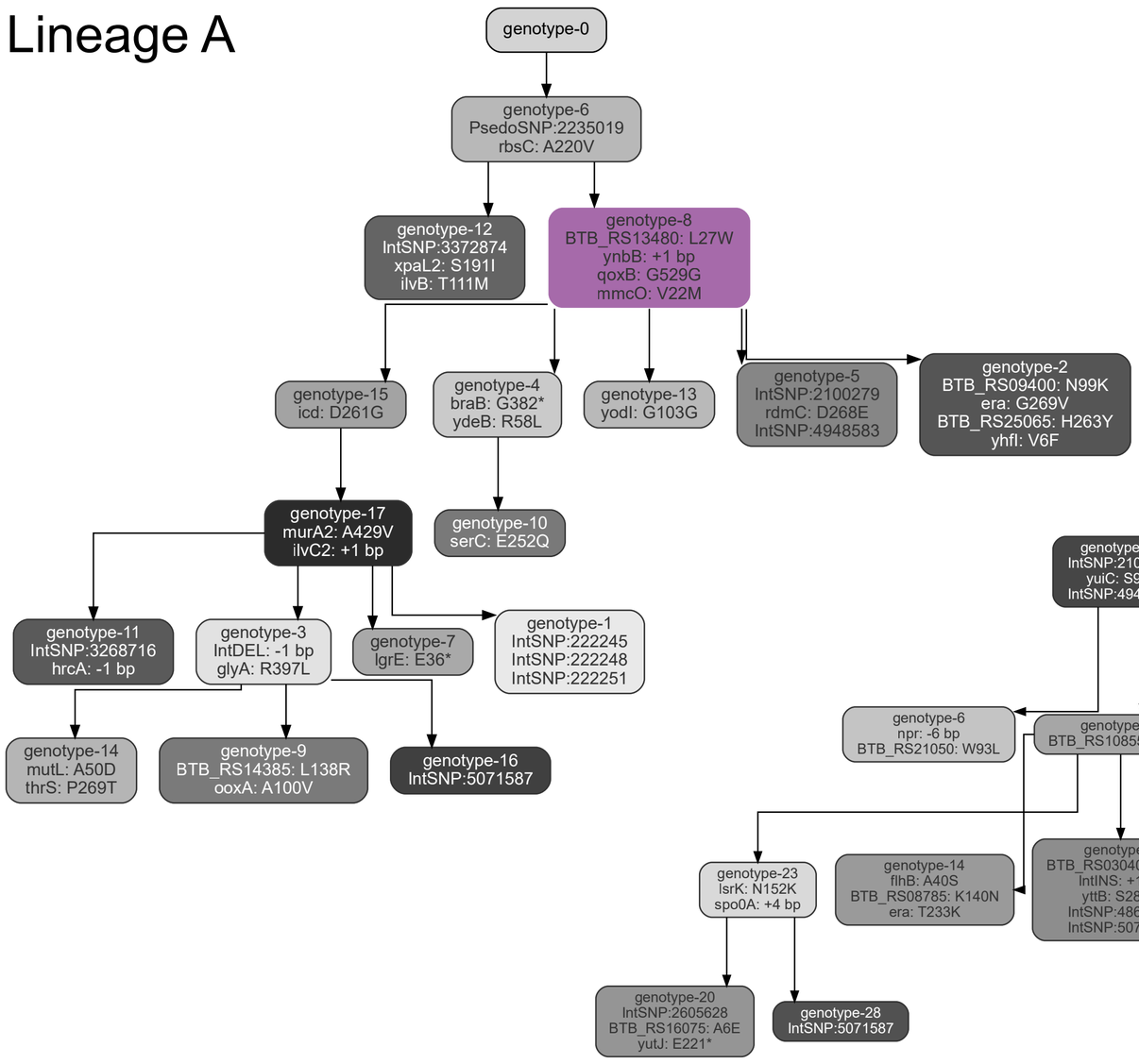

Lineage F

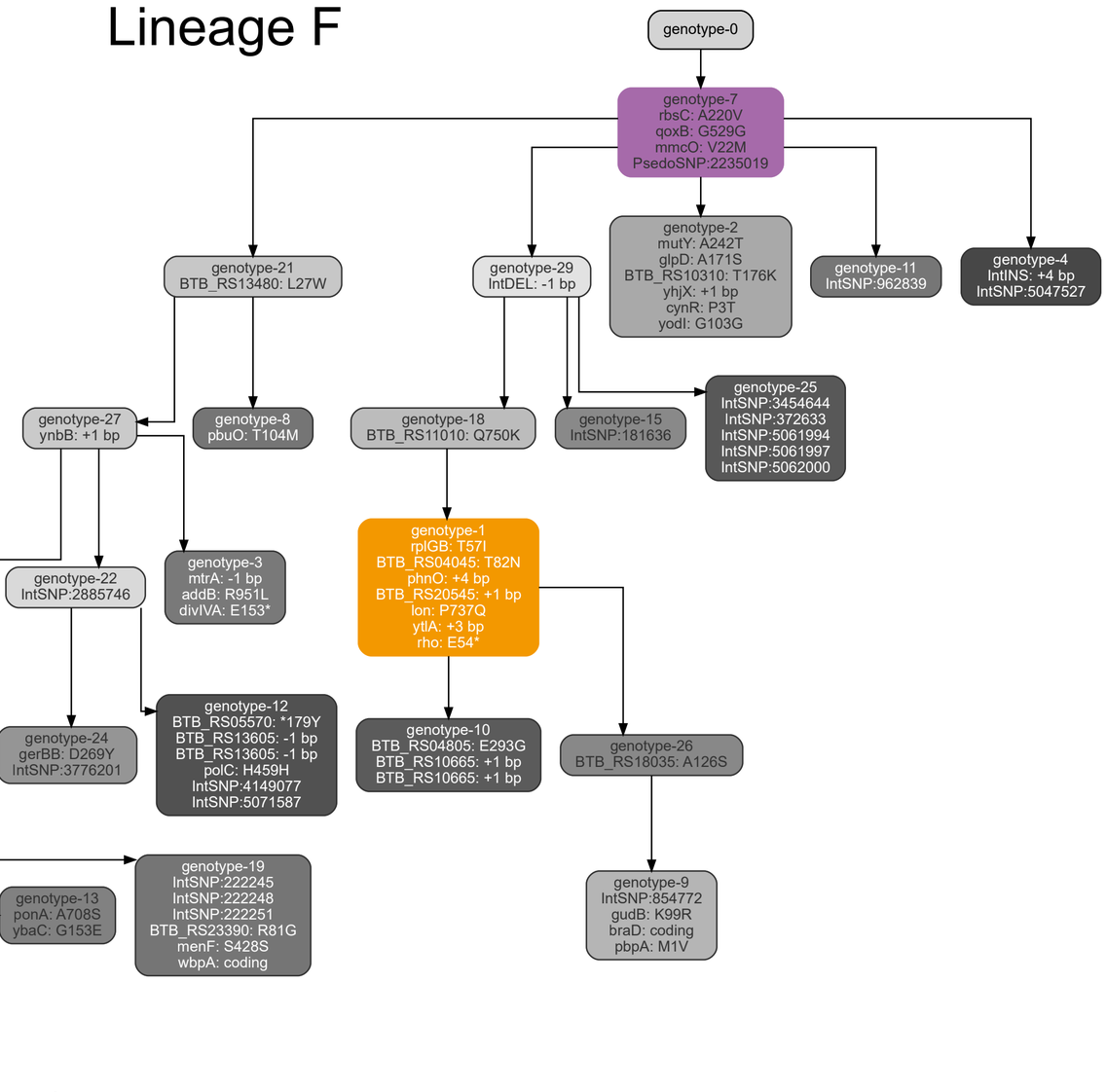

Lineage C

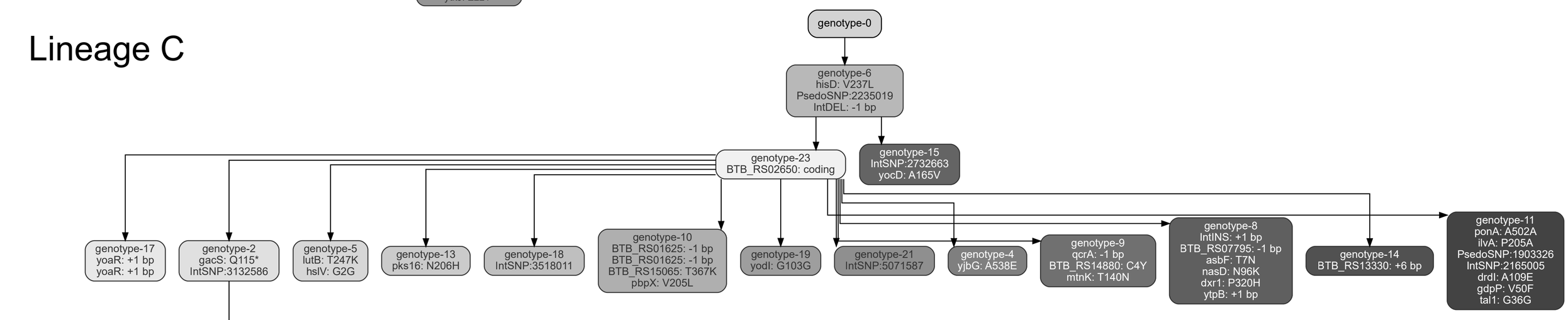

Lineage D

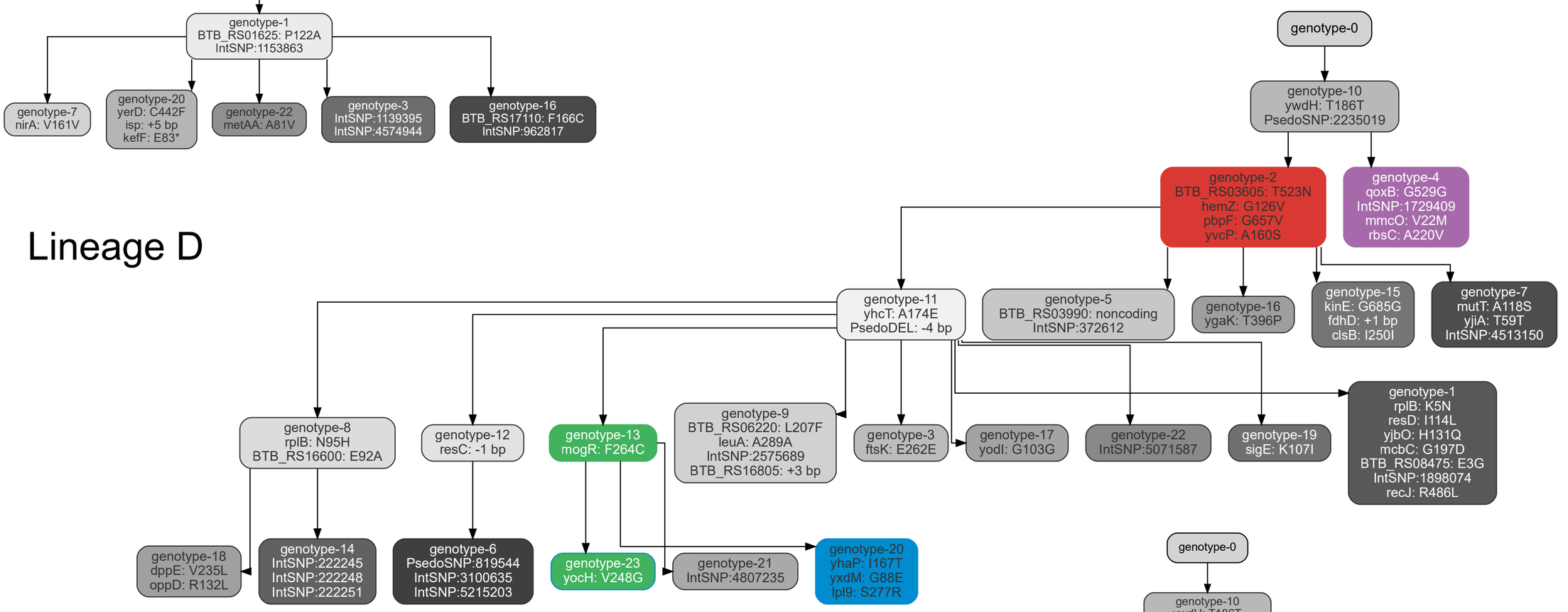

Lineage E

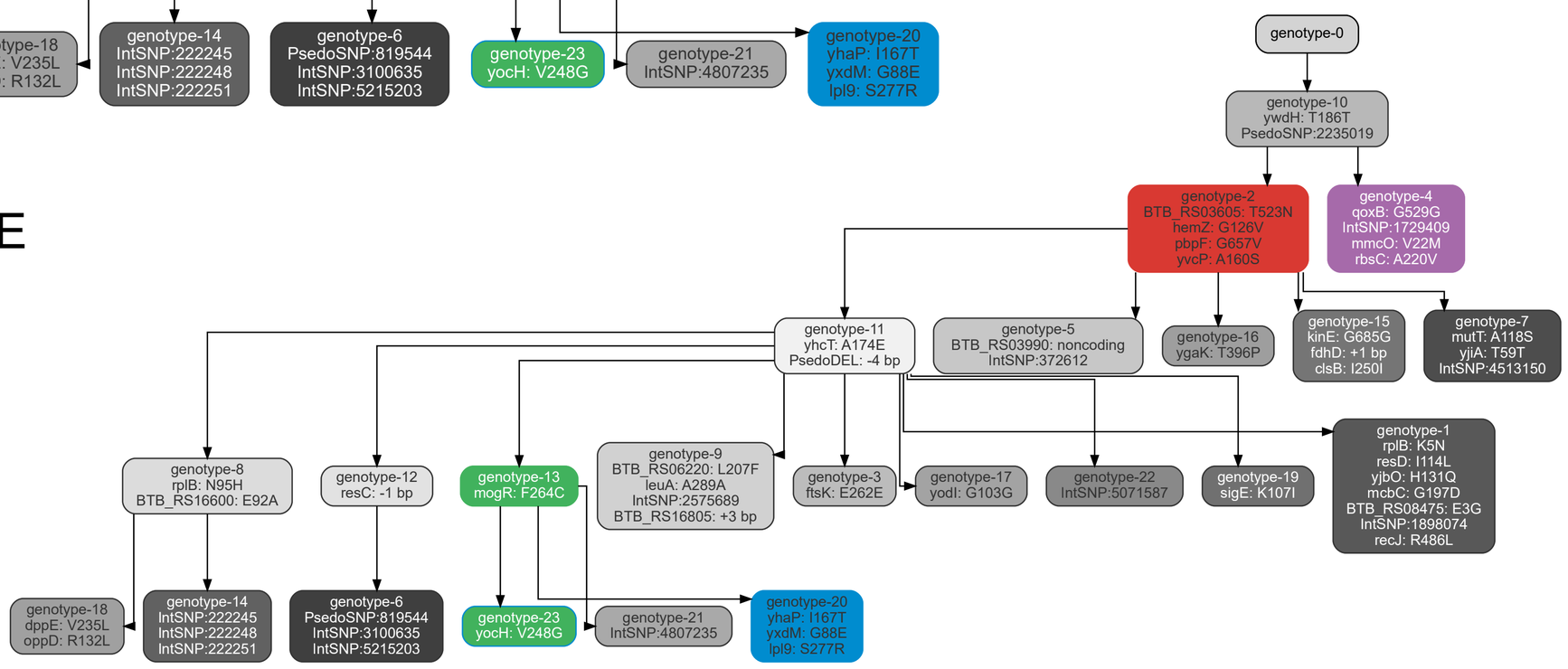

Supplementary Fig. 4C, Bs_pellicle lineage diagram

Lineage 1

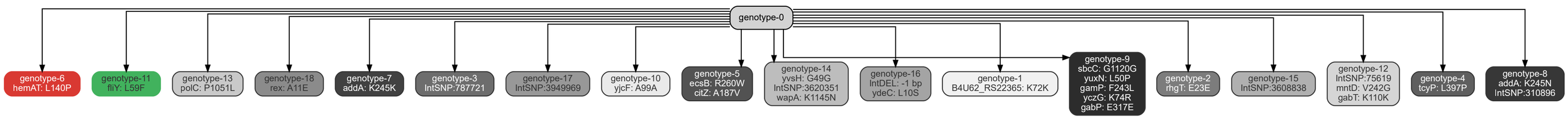

Lineage 2

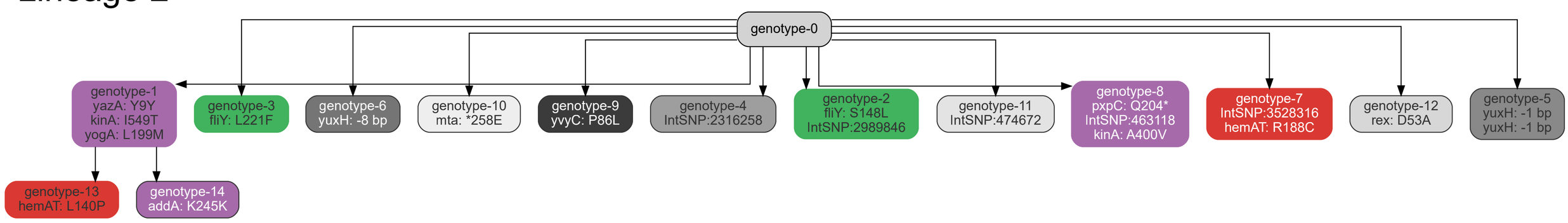

Lineage 3

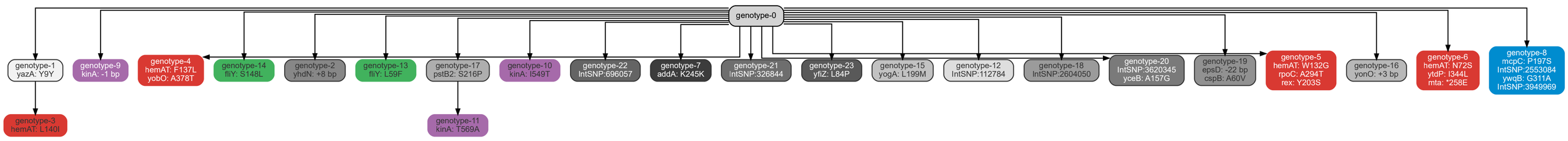

Lineage 4

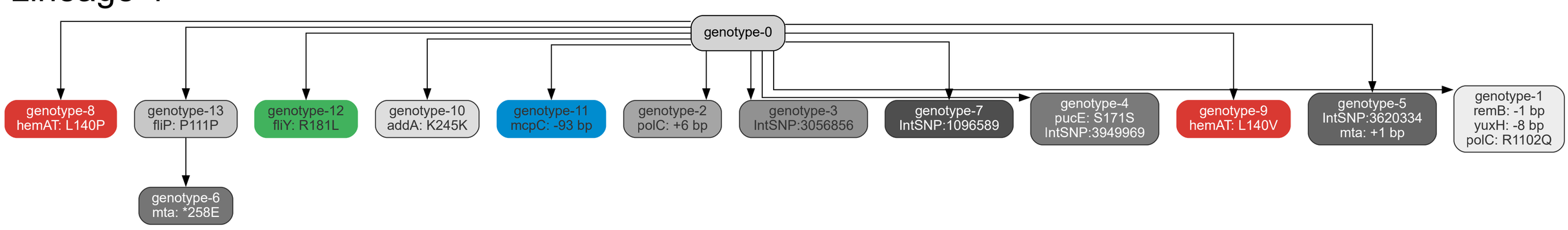

Lineage 5

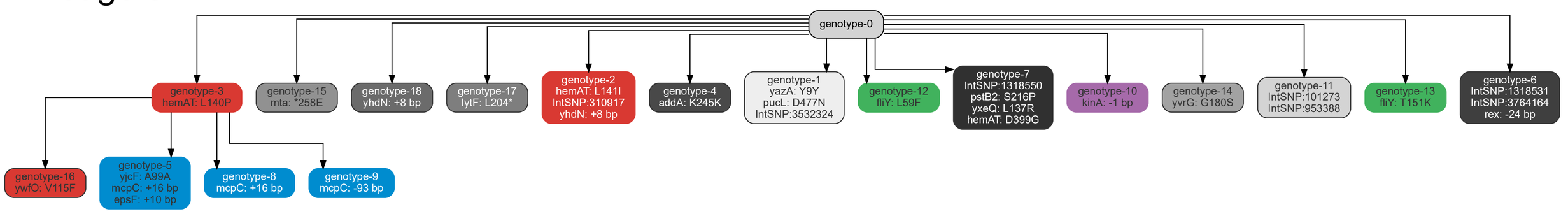

Lineage 6

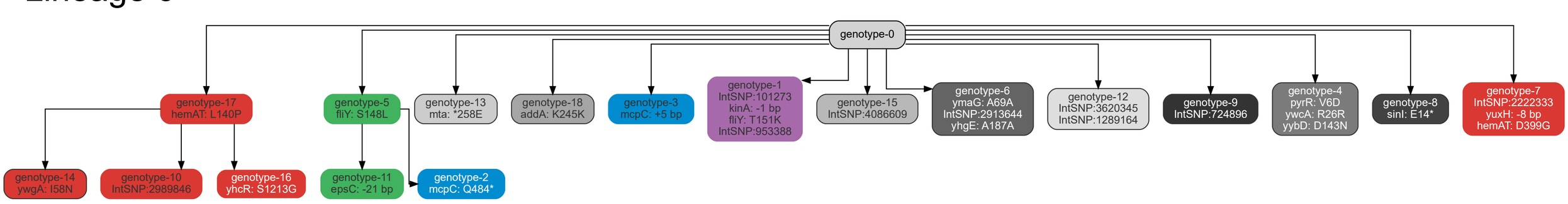

Supplementary Fig. 4D, Bs_root lineage diagram

Lineage 1

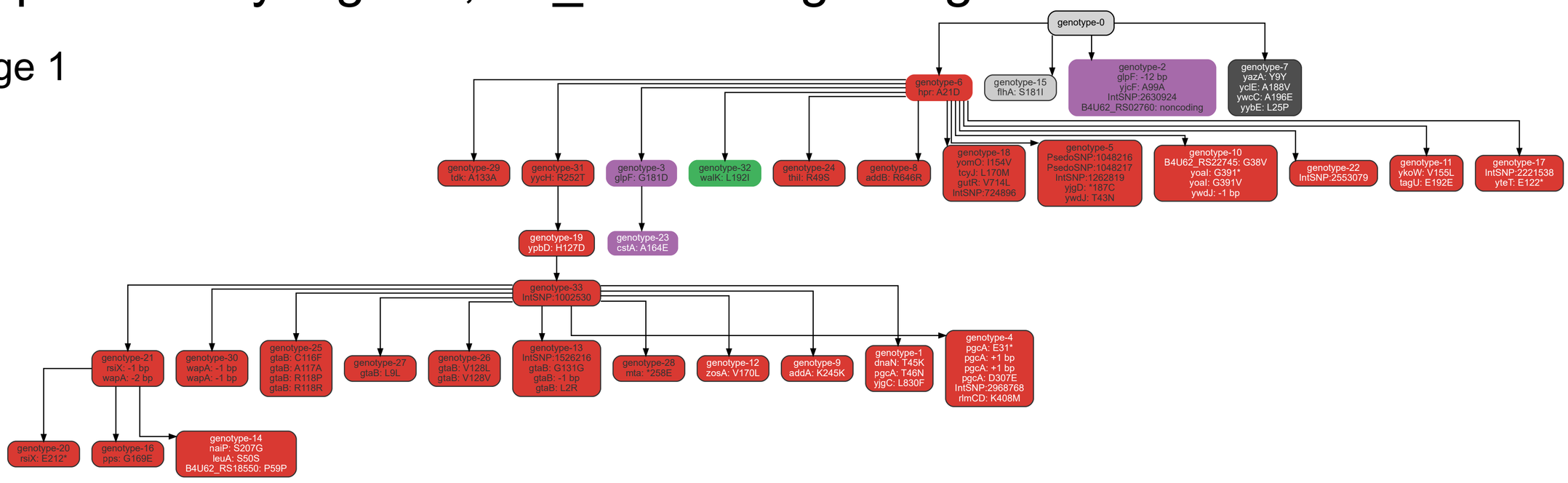

Lineage 2

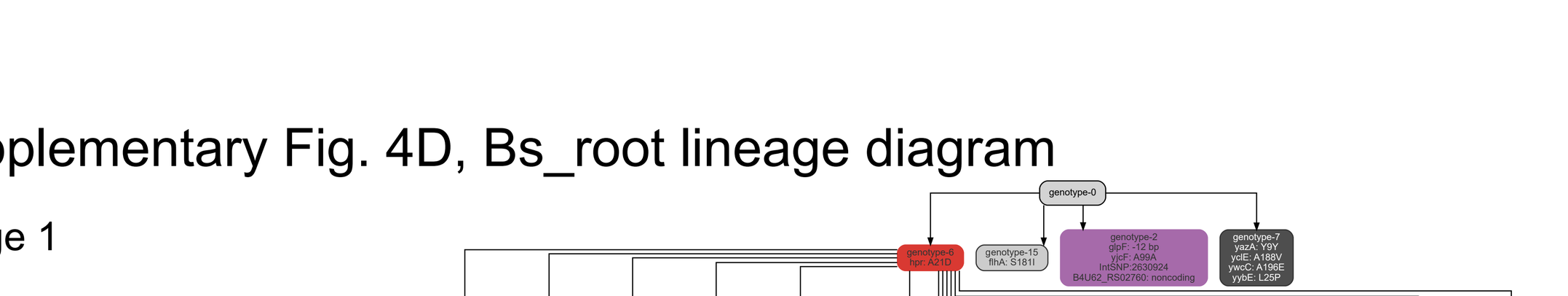

Lineage 3

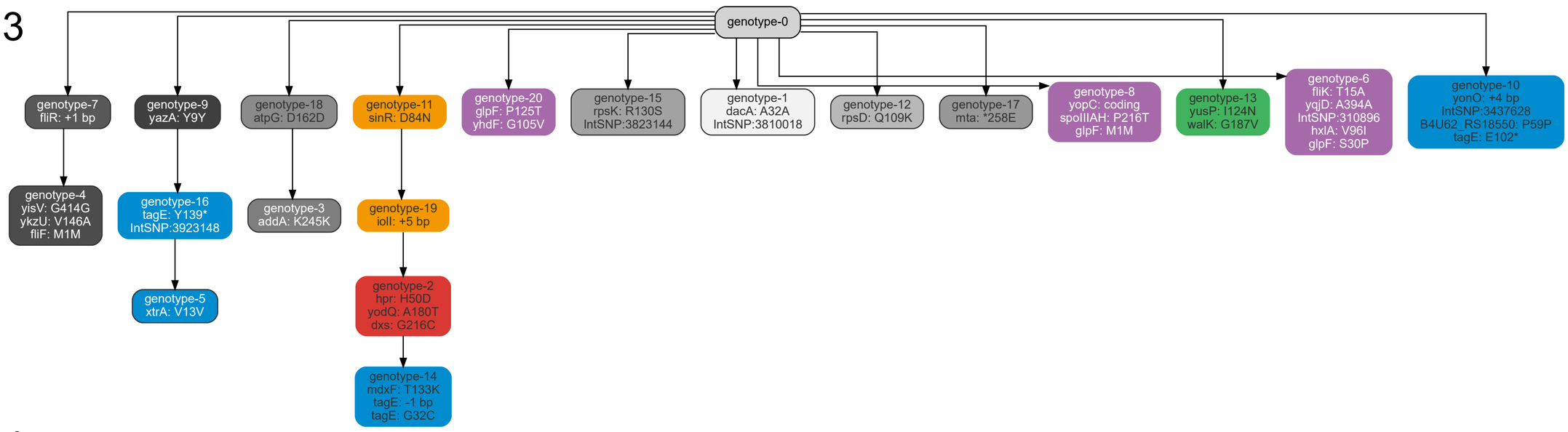

Lineage 4

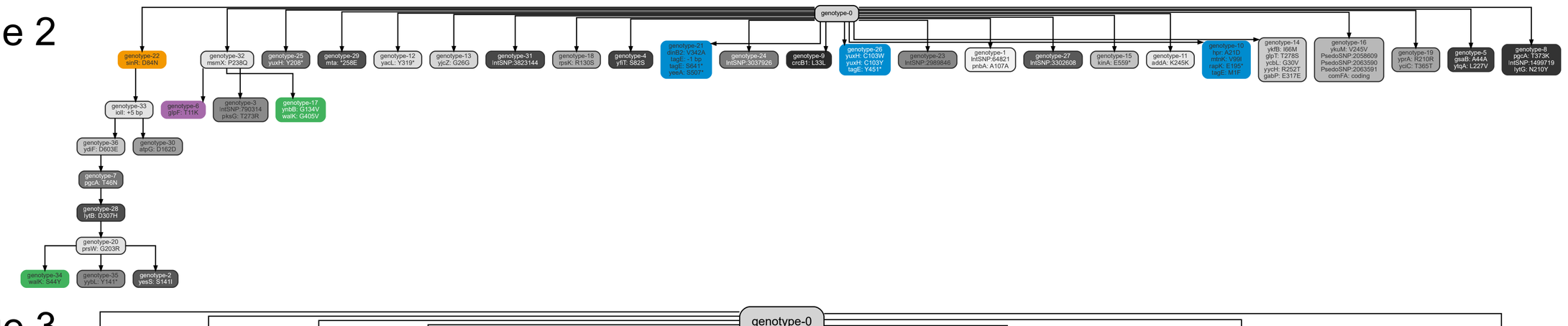

Lineage 5

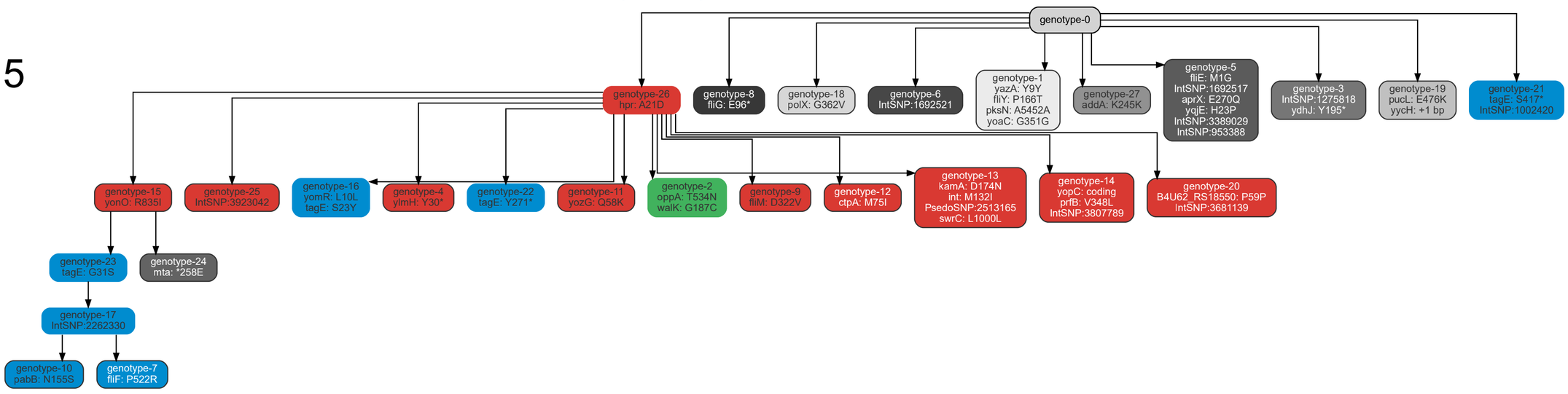

Lineage 6

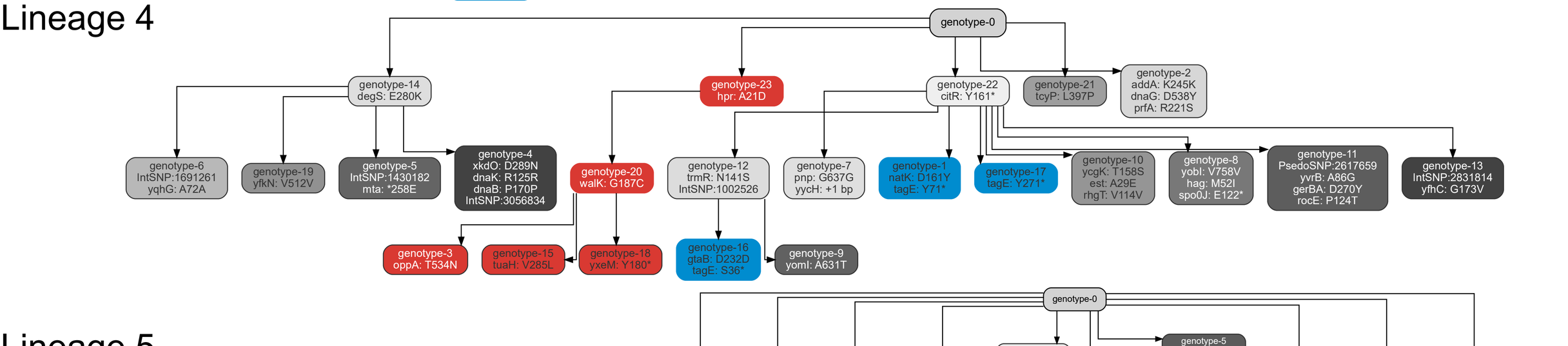

Lineage 7

6.3 Study 3 (submitted manuscript)

Parallel genetic adaptation of *Bacillus subtilis* to different plant species

Guohai Hu, Yue Wang, Christopher Blake, Mathilde Nordgaard, Xin Liu, Bo Wang, Ákos T. Kovács

Note: supplementary figures and tables are attached at the end of the study, the **datasets** are available on bioRxiv:

https://www.biorxiv.org/content/10.1101/2023.03.17.533125v1

Parallel genetic adaptation of *Bacillus subtilis* to different plant species

Guohai Hu[1,2,3,6], Yue Wang[1,2,4,6], Christopher Blake[3], Mathilde Nordgaard[3], Xin Liu[1,2,4], Bo Wang[1,2,5,*], Ákos T. Kovács[3,7*]

[1] China National GeneBank, BGI-Shenzhen, 518120 Shenzhen, China

[2] BGI-Shenzhen, 518083 Shenzhen, China

[3] Bacterial Interactions and Evolution Group, DTU Bioengineering, Technical University of Denmark, 2800 Lyngby, Denmark

[4] BGI-Beijing, Beijing, 102601, China

[5] Shenzhen Key Laboratory of Environmental Microbial Genomics and Application, BGI-Shenzhen, 518083 Shenzhen, China

[6] These authors contributed equally

[7] New position: Institute of Biology, Leiden University, 2333BE Leiden, The Netherlands

[*]Corresponding authors: a.t.kovacs@biology.leidenuniv.nl (Ákos T. Kovács), wangbo@cngb.org (Bo Wang)

Abstract

Plant growth-promoting rhizobacteria are known to benefit plants by stimulating their growth or protecting them against phytopathogens. Rhizobacteria must colonize and persist on plant roots effectively to exert their benefits. However, little is known regarding the process of rhizobacteria adapting to different plant species or in alternating host regime in long-term. Here we used experimental evolution and whole-population WGS sequencing to analysis how *Bacillus subtilis* evolves on *Arabidopsis thaliana* and tomato seedlings, as well as in an alternating host regime of the two plants in a static hydroponic setup. We identified parallel evolution across multiple levels of biological organization in all conditions, and highest in two heterogeneous, multi-resource spatially structured environments in gene level. Species-specific adaptation in genetic level was also observed, possibly caused by the selection stress imposed by different host plants. Further, the trade-off between motility and biofilm development was supported by the mutational changes in motility- and biofilm-related genes. Finally, we identified several condition-specific and common targeted genes in different environments by comparing three different *B. subtilis* biofilm adaptation settings. These results demonstrate a common strategy used by *B. subtilis* when adapting to the plant rhizosphere in similar conditions and also reveal the differences of genetic mechanism between the two different host plants, both will likely support strain improvements for sustainable agriculture.

Key words: adaptation, experimental evolution, plant-bacteria interaction, trade-off

Data summary

The sequencing data underlying this article are available in CNGB Sequence Archive (CNSA) [1] of China National GeneBank DataBase (CNGBdb) [2] with accession number CNP0002416 and CNP0003952. Note, the ancestor DK1042 strain data are available in project CNP0002416.

Impact Statement

To exert the benefits of rhizobacteria on plant growth and protection against phytopathogens, bacteria must colonize and persist on plant roots effectively. Understanding how rhizobacteria adapt to different plants species will assist strain development in sustainable agriculture. To explore the rhizobacterial adaptation process to different plant species or in alternating host regimes, *B. subtilis* was experimentally evolved on *A. thaliana* or tomato roots, or alternating these plants. Both parallel and species-specific adaptation is revealed at genetic level. Further, the trade-off between motility and biofilm formation was explored. Our results reveal several condition-specific and commonly targeted genes from our experiments and those performed previously with experimentally evolving *B. subtilis* biofilms.

Introduction

In natural environments, plant growth and yield depend on a plethora of interactions within the complex and dynamic communities of bacteria and fungi [3]. The rhizosphere plays an important niche for the mutualistic relationships between plants and the microorganisms in the surrounding soil. Overall, plants exude up to 20% of fixed carbon and 15% of nitrogen into their environment [4, 5], and these exudates shape the microbiome. Importantly, the amount and composition of exudates vary depending on the plant species, the stage of development, and the environmental stresses [6]. The exudates contribute a rhizobiome formation by recruiting plant-growth-promoting rhizobacterium (PGPR) and serving as nutrients [7], while PGPRs benefit plant growth and enhance plant tolerance to different abiotic and biotic stresses[8]. *Bacillus subtilis* is a soil-dwelling, biofilm forming, Gram-positive PGPR that is commonly found in association with plants and their rhizosphere [9]. It has been widely recognized that this bacterial species aids plants in several direct and indirect ways[10]. Some *B. subtilis* strains have been applied as biocontrol agents within agriculture, but the effects vary immensely under field conditions [11, 12]. To exert their beneficial effects, PGPR usually must colonize and persist on the root surface efficiently, which mainly depends on their ability to form biofilms.

Each plant species has a distinct effect on its rhizobiome that is partly driven by plant-secreted exudates. Root exudates not only provide nutritional source for soil microorganisms, but also serve as a signal to attract or repel specific groups of microbes [13]. For example, diverse sugars and organic acids induce biofilm formation of *B. subtilis in vitro* or directly on

the plant via different molecular mechanisms. Spo0A is a central transcriptional regulator in *B. subtilis* involved in biofilm development [14]. Biofilm formation is triggered when moderate level of phosphorylated Spo0A (Spo0A-P) is established within a cell. The level of Spo0A-P is controlled by five histidine kinases (KinA-E), which respond to different environmental signals [15]. Chen et al. described *B. subtilis* biofilm formation on tomato roots to be dependent on KinD and small signaling molecules, possibly L-malic acid, released by the roots to stimulate *B. subtilis* biofilm *in vitro* [16]. In contrast to the observation with tomato, deletion of *kinCD* has only a moderate effect on biofilm formation on *Arabidopsis thaliana* roots [17], suggesting that the kinase requirement of *B. subtilis* for root colonization differs from one plant to another. In the case of *A. thaliana*, biofilm formation by *B. subtilis* is triggered by plant polysaccharides pectin, arabinogalactan, and xylan, which act both as environmental cues and substrates for matrix synthesis [17]. Moreover, the disaccharide sucrose that is abundantly secreted from plant roots, activates a signaling cascade to trigger solid surface motility and promotes rhizosphere colonization by *B. subtilis* [18].

Interestingly, a *B. subtilis* strain isolated from the banana rhizosphere and a *Bacillus amylolicefaciens* strain isolated from the cucumber rhizosphere colonize their original plant hosts more efficiently than the non-host plant [19], demonstrating a species-specific colonization pattern. Additionally, organic acids detected exclusively in one of the plant species induce the chemotaxis and biofilm formation of the corresponding bacterial isolate from that given host [19]. Chemotaxis and swarming motility are important for plant colonization [19, 20]. Defect in chemotaxis or swarming reduce the ability of *B. subtilis* to efficiently colonize

tomato seedlings in a gnotobiotic system [20]. Similarly, mutants lacking flagellum production are unable to colonize the roots of *A. thaliana* in a static hydroponic setup and tomato in a gnotobiotic system [20, 21]. In addition to testing specific mutants, experimental evolution provides a powerful tool to reveal the molecular mechanisms related to interaction with a plant, as microbes adapt to the plant root niche [22]. Experimentally evolved clones of *Bacillus thuringiensis* from *A. thaliana* roots displayed improved root colonization ability and enhanced swarming, while those were impaired in swimming, in addition to altered bacterial differentiation and pathogenicity [23]. In a similar setup, when *B. subtilis* was adapted to *A. thaliana* roots, evolved isolates demonstrated elevated root colonization and impaired swimming and swarming motility [24], indicating a possible biofilm-motility trade-off. *Pseudomonas protegens*, adapted to *A. thaliana* rhizosphere in an axenic sandy condition, exhibited enhanced swimming motility and impaired swarming motility [25]. These results all highlight the existence of an evolutionary trade-off between biofilm development and motility. However, it remains largely unknown how such mechanisms supervene from an evolutionary perspective.

Since crop rotation regime has great influence on soil multifunctionality and bacterial community in agroecosystems [26], we asked whether a plant colonizing bacterium adapts differently in an alternating host regime compared with using the same plant throughout the experiment. In addition, we questioned what portion of bacterial adaptation on a plant root will be host specific. To explore these questions, we employed experimental evolution combined with whole-population metagenome sequencing method to analyze how *B. subtilis* evolves on

A. thaliana and tomato seedlings, as well as in an alternating host regime of these two species in a static hydroponic setup. We identified parallel evolution across multiple levels of biological organization and a higher gene-level parallelism in populations evolved in an alternating host regime. We also observed species-specific adaptation at genetic level, which was potentially provoked by specific host plant-imposed selection, either due to root exudates, plant polysaccharides, or certain stress conditions. Additionally, motility-biofilm trade-off was revealed in the mutational landscape of related genes, in addition to reduced swimming and swarming motility. Finally, we identified several condition-specific and shared list of mutated genes of *B. subtilis* when evolved in different biofilm environments.

Methods

Bacterial strains and experimental methods

We used identical materials and methods for the tomato and two host-cycling evolution setups as described in detail previously for the *A. thaliana* selection approach [27], including the bacterial strain and the culture conditions, the seedling preparation, the experimental evolution, and the morphological diversification experiments.

Motility assays

20 mL of either 0.3% or 0.7% lysogeny broth (LB)-agar plates were used to test swimming and swarming motility. In both cases, the plates were dried for exactly 20 minutes before the bacterial cultures were applied to the center of the plates. 2 µL overnight cultures of the ancestor or evolved isolates adjusted to an OD_{600} of 5.0 were spotted in the middle of the plate. To keep a similar humidity across all plates, multiple stacking was avoided. Plates were incubated at 30°C and images were taken for swimming after 6h, 8h and 24h and for swarming after 8h, 10h and 24h with a camera (Lumix DC T290, Panasonic equipped with lens DC Vario-ELMAR, Leica). The area the bacterial cells covered at a given time point as well as the area of the whole agar plate were measured using ImageJ (Fiji ImageJ 1.52p). The capacity in swimming and swarming motility was calculated by dividing the covered area by the total area.

Sequencing and variant calling

Archived samples from each experimental evolution environment were revived via cultivation in lysogeny broth (LB; Lennox, Carl Roth; 10 g/L tryptone, 5 g/L yeast extract, and 5 g/L NaCl)

medium at 37℃ for 16 hours. Then the genomic DNA was extracted from the harvested cells from each culture using EURx Bacterial and Yeast Genomic DNA kit.

For whole-population genome sequencing of the evolved populations and ancestor strain samples, the MGIEasy PCR-free Library Prep Set (MGI Tech) was used for libraries preparation. 150bp × 2 pair-end sequencing were performed on a DNBSEQ-Tx sequencer (MGI Tech) following the manufacturer's procedures[28, 29]. More than 200× depth coverage raw data were generated for All population samples for further polymorphism calling.

To remove low quality data, filtering was performed using SOAPnuke (version 1.5.6) [30]. Therefore, reads including more than 50% of bases with quality lower than 12, reads including more than 10% of unknown base "N", and reads containing adaptor contamination were removed. Subsequently, the derived data was normalized to 200× depth for all sample to ensure a similar variants calling sensitivity. Mutations were reported by using *breseq* (version 0.35.7) with the default parameters and a -p option for population samples [31, 32]. The default parameters reported mutations only if they appeared at least two reads from each strand and reached a frequency of at least 5% in the population. Mutations that also found in the ancestor strains were removed for further analysis.

Genotype inferences from populations and Muller plots

To generate the muller plots, the *Lolipop* package (https://github.com/cdeitrick/lolipop) (version 0.6) was used with default parameters [33, 34]. These methods predict genotypes and lineages based on the shared trajectories of mutations over time test their probability of

nonrandom genetic linkage. Muller plots were then manually colored by the presence of shared mutated genes or genotypes. The genotypes and their frequencies were used for genotype diversity calculation in R (version 4.2.2) with the package vegan (version 2.6-4).

Jaccard Index calculation

Jaccard Index (*J*) for two evolved lineages was calculated using formula (1), given two lineage, each contains mutated gene set G1 and G2, respectively. In words, *J* is the number of genes mutated genes in both lineages divided by the total number of genes mutated in both lineages. *J* ranges from 0 to 1, with 1 indicating two lineages have exactly the same set of mutated genes and 0 indicating no mutated genes in two lineages are shared. This value was calculated for all pairs of evolved lineages, both within and between evolved environments.

$$J_{G1,G2} = \frac{|G1 \cap G2|}{|G1 \cup G2|} \quad (1)$$

Results

B. subtilis shows rapid improvement and diversification during evolution on plant roots

Do plant colonizing bacteria adapt differently in an alternating host regime compared with a setup where the same plant is used throughout the experiment? To investigate this, we tested adaptation of *B. subtilis* to the roots of two different plant species and compared those with a condition where plants were sequentially alternated. Therefore, starting from a clonal *B. subtilis* DK1042 strain, four different evolution experiments each with five parallel lineages (from A to E), were passaged on both *A. thaliana* and tomato seedlings for 20 transfers, spanning over a total of 40 days (**Fig. 1a,** and **1b**). We conducted two mono-host evolution experiments, one using only ***A****. thaliana* (Bs_root_**A**) and another with **T**omato (Bs_root_**T**), as well as two host-cycling evolution experiments, which either started on ***A****. thaliana* (Bs_root_**A**T) or **T**omato (Bs_root_**T**A) and switched the plant species after every third transfers. Evolved clones from Bs_root_A setup have been examined in details previously [27]. To evaluate the improvements in root colonization during the experimental evolution, colony forming unit (CFU) per gram of roots was measured after transfer 1, 5, 10, 17, and 20 (T1, T5, T10, T17, and T20 respectively). As expected [23, 24, 27], root colonization ability improved significantly in all evolving lineages and conditions, on average 9.10-fold, 7.41-fold, 25.29-fold, and 11.98-fold after 20 transfers in Bs_root_A, Bs_root_T, Bs_root_AT, and Bs_root_TA, respectively (**Fig. 1c**). Furthermore, morphological diversification was also observed in all evolving lineages and conditions in the CFU assays with morphotypes termed as Wrinkle (WR), Snow (SN) and Smooth (SM) [27], where colony morphology of WR variant was comparable with the ancestor.

To investigate how the distribution of the distinct morphotypes developed during the experimental evolution, overnight-grown cultures of the frozen stocks of evolved populations from root 5, 10, 17 and 20 as well as from the ancestral strain ("transfer 0") were prepared and plated on LB-agar. Different morphological variants were identified and counted to calculate the ratio of a given morphotype at each time point for each lineage. In all four conditions, WR was the most abundant in all lineages through the experiment (**Fig. 1d**). SN appeared in all lineages at T5 reaching an average frequency of 21.78%, 15.48%, 23.81%, and 21.28% in Bs_root_A, Bs_root_T, Bs_root_AT, and Bs_root_TA, respectively (**Fig. 1d**), however was below detection limit in some of the lineages at T10 and T17, and raised again in all lineages at T20. SM was observable in 11 of the 20 lineages at T10 and only absent in one lineage at T17 and T20 (**Fig. 1d**). The three distinct morphotypes coexisted until the end of the evolution experiment, reaching on average highly similar ratios of approximately 80% WR, 17% SN and 3% SM in all four evolution experiments, which showed astounding degree of parallelism at morphotypic level.

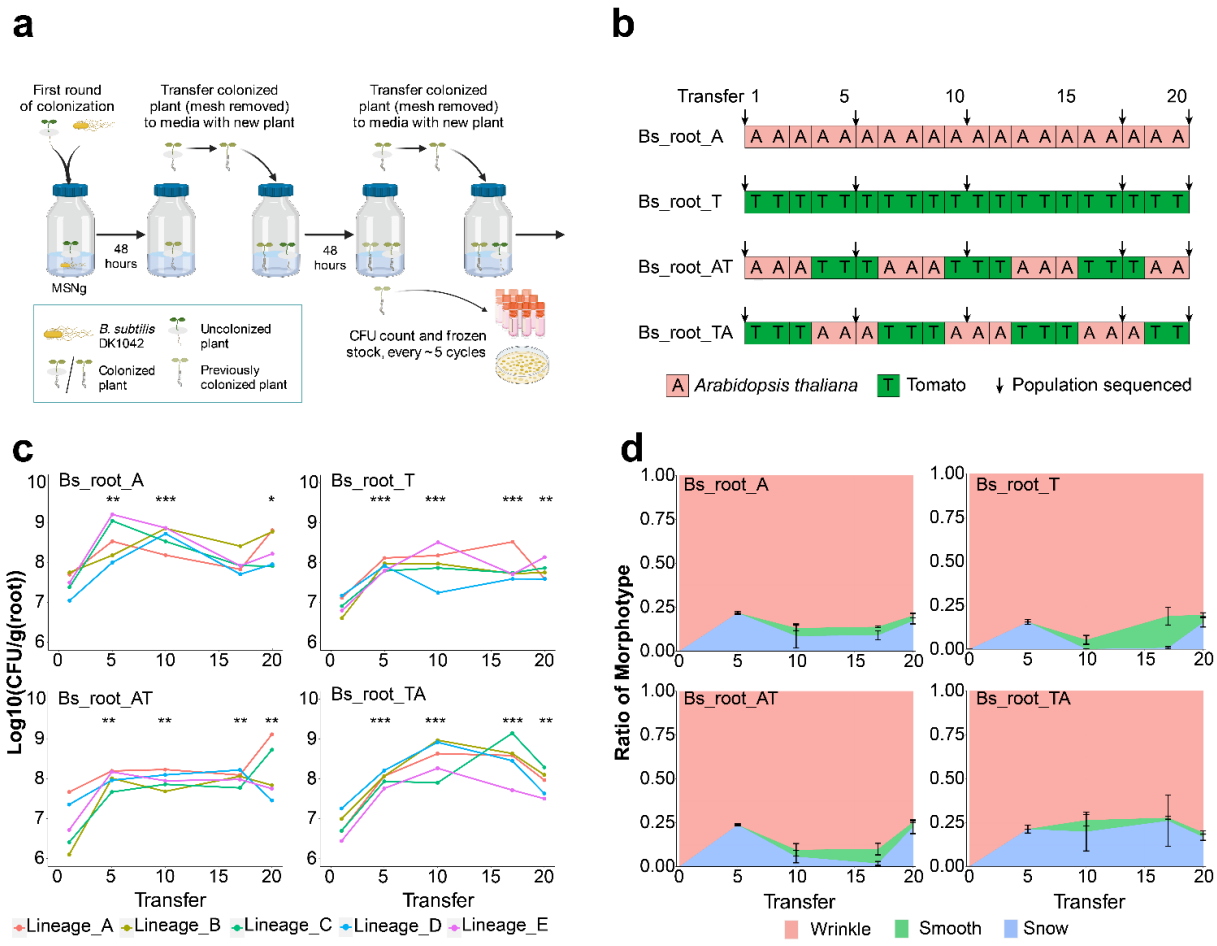

Fig. 1 Evolution of *B. subtilis* on different plant roots. a. Experimental evolution scheme of *B. subtilis* adapting to plant seedling (Created with BioRender.com), **b.** In total four evolution experiments were conducted, either as mono evolution experiments, with only *A. thaliana* or tomato seedlings, or cycling evolution experiments, where the plant species was switched after every third transfer. Sequenced population samples are indicated with an arrow. **c.** root colonization ability was detected during the experiment as CFU per gram root for T1, T5, T10, T17, and T20 in all lineages. (*: $P < 0.05$, **: $P < 0.01$, ***: $P < 0.001$). **d.** the dynamic frequency changes of different morphotypes along the evolution experiment in average of all five populations in each condition ($n = 5$), data represent mean and error bars represent standard error.

Evolved isolates showed impaired motility

In a soil environment, bacterial cells need to actively move towards the plant roots during the initial phase of root colonization, as well as when recolonizing [21]. We hypothesized that, in the static hydroponic setup, which select for a regular root recolonization, including chemotaxis, biofilm formation and dispersal, the motility would improve significantly during the evolution experiment, resulting in better root colonization. To examine this, evolved end-point isolates from Bs_root_A and Bs_root_T were tested for swimming and swarming motility, by spotting 2μL of an overnight culture on 0.3% and 0.7% LB-agar, respectively. Contrary to our expectations, none of the tested seven isolates evolved on *A. thaliana*, as well as none of the tested five isolates evolved on tomato, showed improvements in either swimming or swarming (**Fig. 2**). Instead, most isolates displayed significantly smaller swimming radius after 6h and 8h compared with the ancestor, although all isolates colonized the entire plate after 24h, thus mobility was preserved. Importantly, other form of motility, e.g. sliding [35, 36], might mask the effect of swimming after 24h. Moreover, all isolates exhibited either delayed, reduced or even impaired swarming abilities.

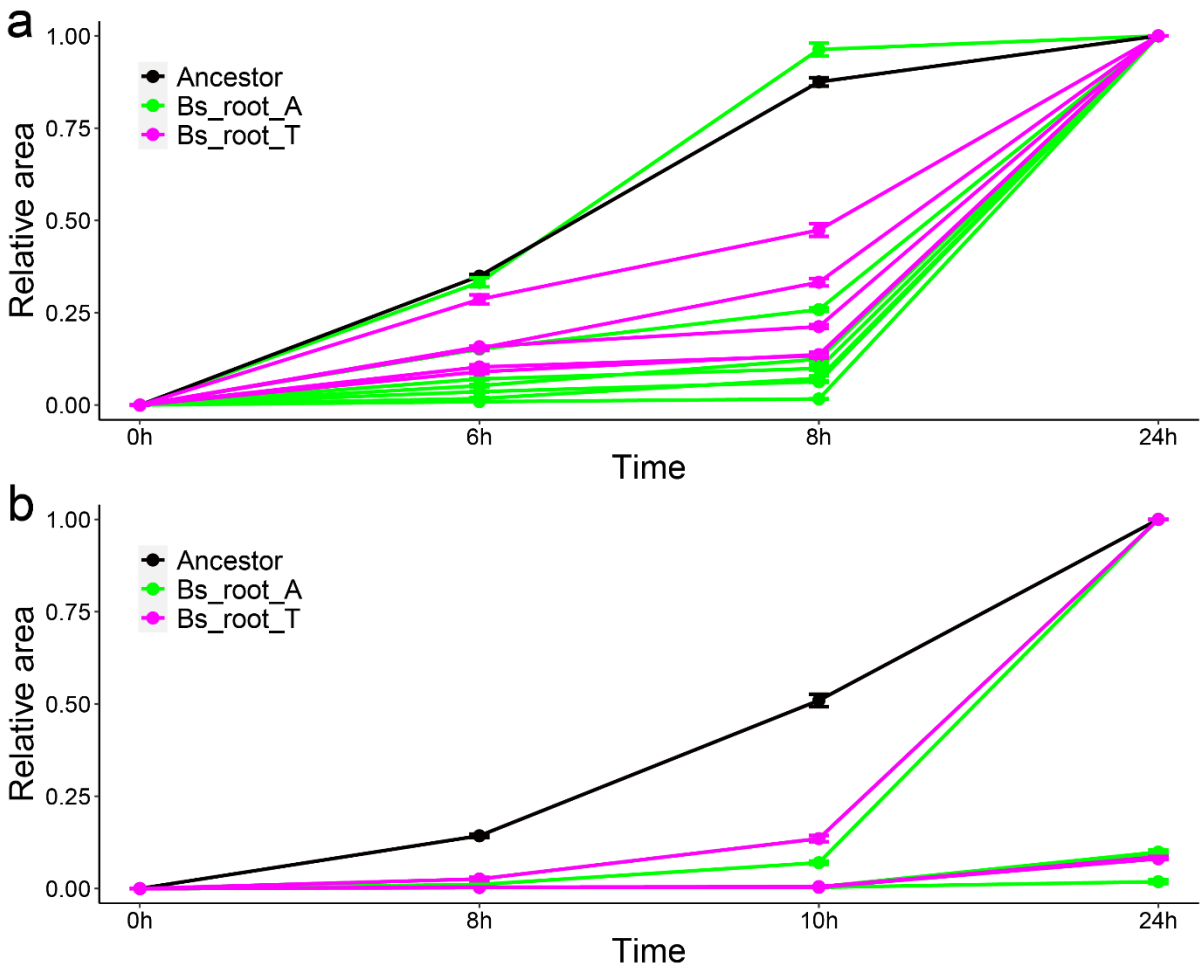

Fig. 2 Evolved isolates showed impaired motility. Swimming (a) and **Swarming (b)** motility of evolved isolates from Bs_root_A (green, 7 isolates) and Bs_root_T (magenta, 5 isolates) in comparison to the ancestor (**Black**). Notably, swarming motility of several isolates are similar and low, thus indistinguishable from each other in panel b. Data represent mean and error bars represent standard error, each isolate repeated for 3 times, the ancestor repeated for 9 times. Tested isolates include two SN from lineage A and E of Bs_root_A, two SM from lineage A and E of Bs_root_A, three WR from lineage A, D and E of Bs_root_A, and five WR from lineage A (1), B (2) and C (2) of Bs_root_T, respectively.

Mutation spectrum and genetic diversity

Mutations provide the ultimate source of diversity, allowing selection to act and evolution to take place. To understand the genetic basis behind the observed phenotypic diversification, impaired motility, and the dynamic landscape of evolution, we employed a longitudinal whole-population genome sequencing approach of 79 B. subtilis population samples (one population sample was lost during freezer maintenance) and the ancestor strain, using the DNBSEQ-Tx platform [28, 29]. More than >200× coverage depth raw data were generated for each sample. Mutation of SNPs, Indels (short insertions and deletions) were detected compared with the ancestor, using breseq pipeline (version 0.35.7) [31, 32]. As default parameter, mutations were reported only if those appeared at least two reads from each strand and reached a frequency of at least 5% in the population. This analysis revealed 117, 106, 104, and 134 mutations in the evolved lineages from the Bs_root_A, Bs_root_T, Bs_root_AT, and Bs_root_TA conditions (

Table 1), respectively. No significant difference in mutation numbers were detected between the evolution conditions (Kruskal–Wallis test, $p = 0.1277$), though the mutation spectra were slightly different between the selection setups (

Table 1). When the filtering step excluded the mutations below 10% frequency, the cyclic evolving conditions were found to contain more mutations than the mono-evolved conditions ($p = 0.0005162$, $t = -4.2419$, $df = 17.542$ via two-tailed t-test), suggesting that the mono-evolved conditions contained several low frequency mutations, especially the Bs_root_A setup. Only 4 fixed mutations were present parallel in all 20 lineages, possibly due to the short transfer times used in the experiment.

Table 1. mutation type and number

Category	Bs_root_A	Bs_root_T	Bs_root_AT	Bs_root_TA
Pseudogene	0	1	0	0
Non-coding gene*	0	1	0	0
Coding gene	81	91	88	104
Synonymous	15	15	19	19
Non-synonymous	57	58	47	58
Nonsense	0	1	3	6
InDel**	9	17	19	21
Intergenic***	36	13	16	30
Total mutation number	117	106	104	134
Total mutation number (>10%)	50	69	80	92
Fixed	1	0	2	1

Notes: there is no overlap between each mutation type. * Non-coding gene includes tRNA gene, ncRNA gene, and repeat region (IS); ** InDel indicates small insertions or deletions in coding gene regions; *** Intergenic refers to all kinds of mutations occurred in intergenic regions.

Though there was no significant difference in mutation numbers between the evolution

conditions, we expected that the population samples evolved in cyclic evolved conditions would increase the genetic diversity compared with the mono-evolved conditions at the end of the experiment due to the higher complexity and fluctuating nutrient composition caused by the alternating host plants. Therefore, the genotype diversities of the endpoint samples were compared between each condition. Indeed, the genotype diversity was significantly lower in mono-evolved conditions than cyclic evolving conditions (p = 0.01133, t = -2.9044, df = 14.315 via two-tailed t-test), being lowest in Bs_root_A condition (**Fig. 3**).

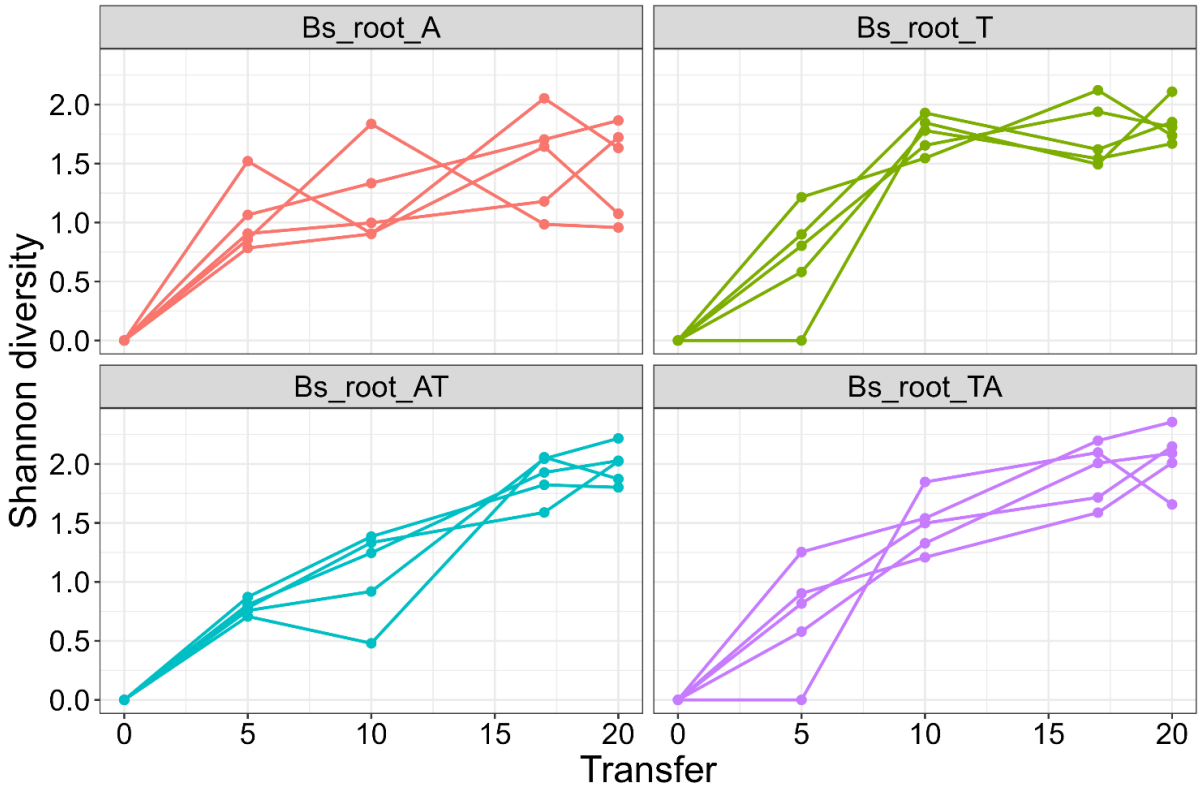

Fig. 3 Genotype diversity. Dynamic distribution of genotype alpha diversity (Shannon method) in each population of four adaptation models over time. Genotype and their frequencies were from genotype and genealogy analysis using *Lolipop*.

Ecological differentiation and parallel evolution

To infer the ecological differentiation in each lineage and visualize the changes in lineage frequencies from shared, nested mutation trajectories over time, we utilized the *Lolipop* software package developed by Cooper and colleagues [33, 34]. An average of 16 ± 1.10, 15.6 ± 2.15, 14.6 ± 1.85, and 17.4 ± 2.15 genotypes were obtained in Bs_root_A, Bs_root_T, Bs_root_AT, and Bs_root_TA conditions, respectively, with multiple mutations in each genotype. Consistent with mutation number, there was no significant difference in genotype numbers between evolved conditions (Kruskal–Wallis test, $p = 0.3129$). Overall, the number of genotypes continuously increased in all conditions, consistently with the detected genotype diversity in each condition. Notably, the genotype number or diversity didn't reach a peak within the time frame of the experiment (**Fig. 3**).

Each of the lineage was dominated by a few genotypes which contain one or more mutations in certain genes. In general, *sinR*, *pstBA*, *yuxH*, *sigD* and eight flagellum-related genes were the most selected, demonstrating a high parallel evolution in gene and function-level within and between different evolved conditions (**Fig. 4**). Diverse functional genes were mutated, among which, the bacterial motility related genes were targeted most frequently, which show high parallelism in functional level across all environments. To further compare the genetic similarity between conditions, we determined the Jaccard Index (J) of all pairs of lineages within each condition. The Jaccard Index is commonly used in measuring similarity, indicating how likely it is for the same gene to be mutated in two separate lineages [37, 38], ranging from 0 to 1. Again, we observed relatively lower genetic similarity in mono-evolved

conditions than that of cyclic evolved conditions, and lowest genetic similarity within condition in the Bs_root_A, in which is significantly lower than that in Bs_root_T ($p = 0.0249$, t = -2.4471, df = 17.998 via two-tailed t-test) and the other two cyclic evolved conditions ($p < 0.001$ and < 0.05, respectively) (**Fig. 5**).

Subsequently, we compared the genetic similarity between different evolved conditions. The similarity between the two cyclic evolved conditions was much higher than the two mono-evolved conditions (p = 2.628e-12, t = -10.022, df = 38.695 via two-tailed t-test), and the similarity between Bs_root_A and two cyclic conditions were also much lower than the similarity between Bs_root_T and two cyclic conditions (**Fig. 5**). These results strongly indicated that the selection pressure imposed by the *A. thaliana* was much weaker than observed with tomato, and the tomato root was potentially the main selective factor in the two cyclic evolution conditions.

We observed high parallelism from root colonization ability and morphotype, to functional pathway and gene level, additionally, extensive parallelism at the level of individual nucleotides was also observed (**Dataset S1**). One of the most striking examples, 18 out of the 20 lineages contained a frameshift in gene *flhB*, which is required for flagellum and nanotube assembly [39]. Another 8bp deletion found in gene *yuxH*, which is involved in c-di-GMP regulation in *B. subtilis* [40, 41], was detected in 15 lineages. Additional high parallelism mutations at nucleotide level, which occurred in more than 10 lineages and belong to nonsynonymous mutations, occurred in *hag* and *sigD* genes. Notably, all mutations mentioned above reach high frequency from 12.9% to 68.53% in the evolution conditions.

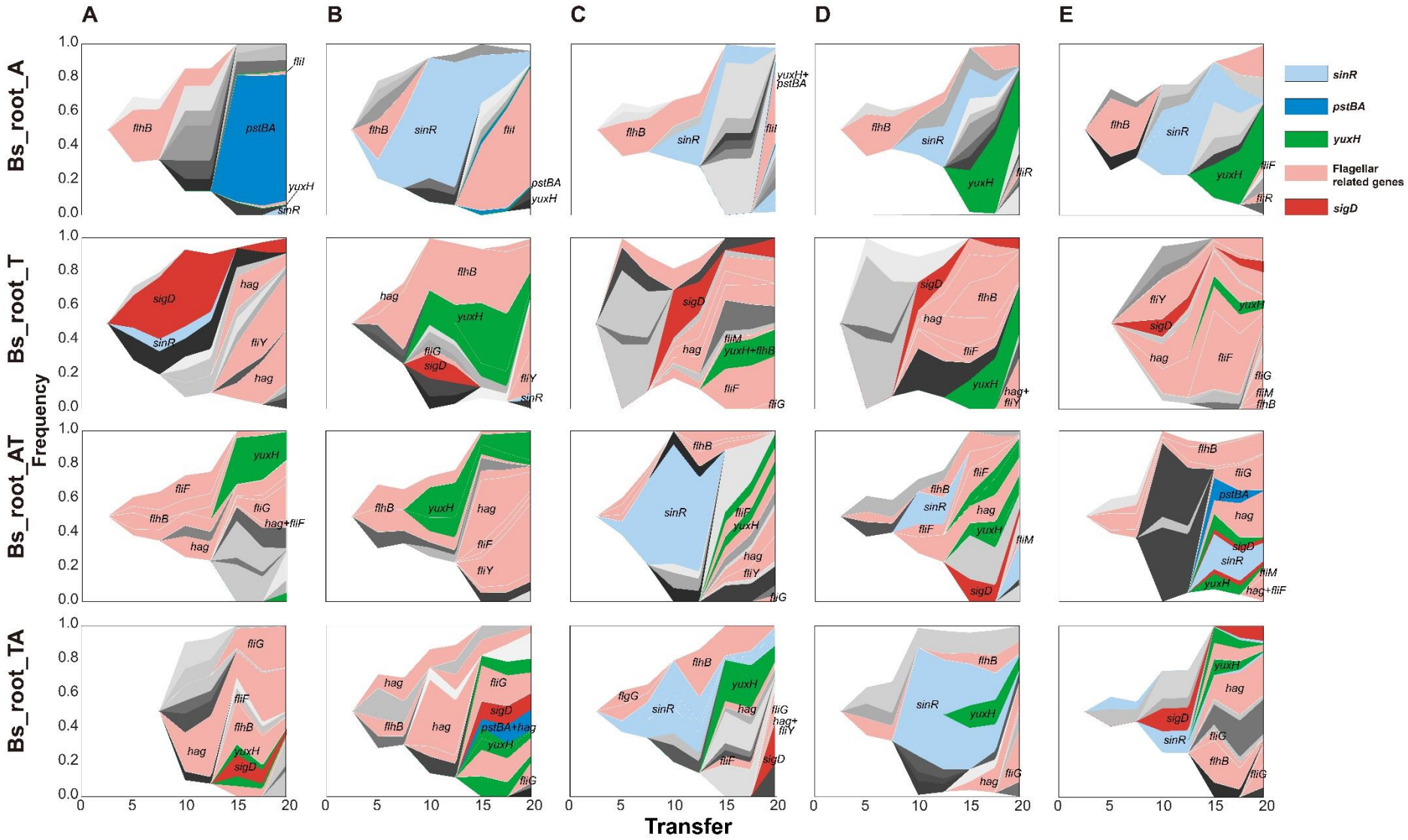
A
B
C
D
E
Bs_root_A
Bs_root_T
Bs_root_AT
Bs_root_TA
Frequency
Transfer
sinR
pstBA
yuxH
Flagellar related genes
sigD

Fig. 4 Evolutionary dynamics of *B. subtilis* during plant root colonization. Each shade or color represents a different genotype and vertical area corresponds to genotype frequency, inferred by *Lolipop*. Genotypes under selective pressure in certain condition(s) are highlighted in different colors and with annotates within or near the shadows, while the other genotypes are in different levels of gray without annotation. The nested genotypes of the highlighted genotype are highlighted with the same color, except for the nested genotypes which also contain the genes under selective pressure. Notably, some genotypes are less presented in the figure due to their frequencies are similar to their nested genotypes, like *fliI* and *yuxH* in lineage A of Bs_root_A, *pstBA* and *yuxH* in lineage B and C of Bs_root_A. Different colors represent different genotypes contain certain targeted genes, flagellar related genes include *fliF*, *fliI*, *fliR*, *flhB*, *fliG*, *fliM*, *fliY*, and *hag*. Genotypes containing more than one targeted gene are colored with the color of the gene displayed in the front.

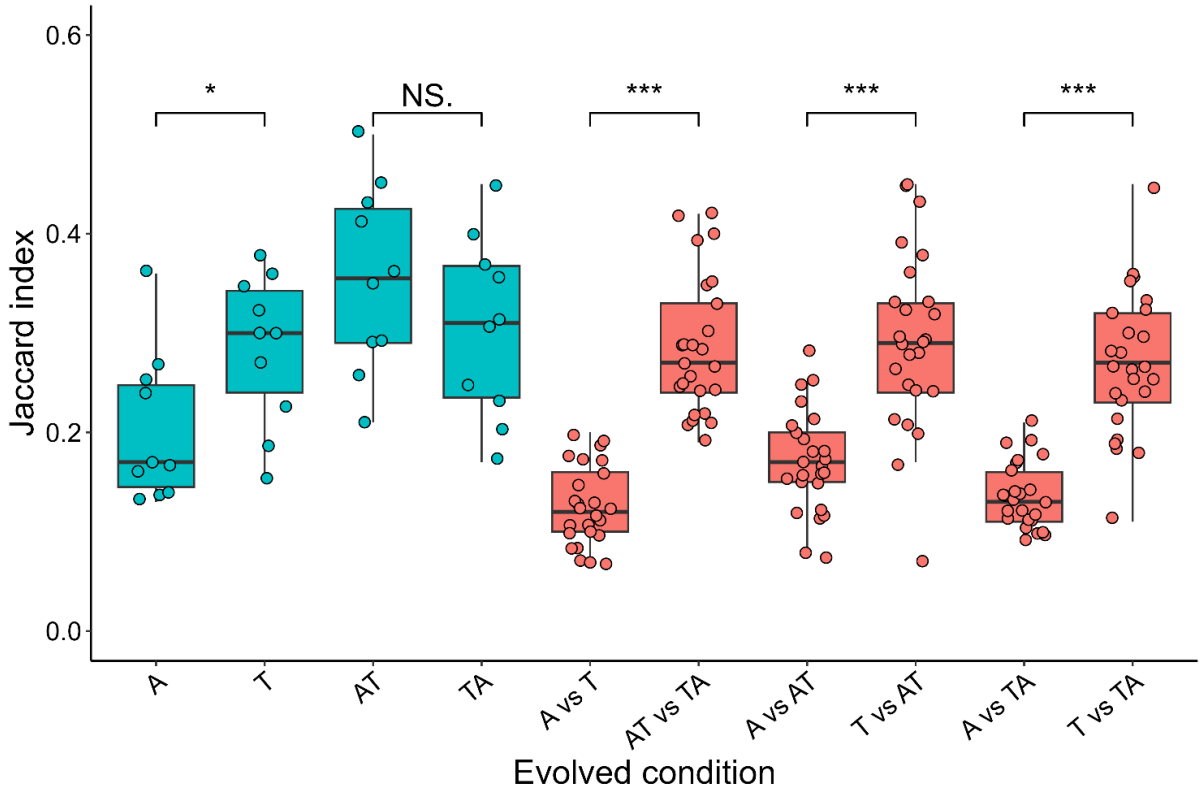

Fig. 5 Parallelism. Degree of parallelism within and between each evolved environment was estimated using the Jaccard index. Asterisks at the top indicate significant differences between different environment combinations (*$p < 0.05$, ***$p < 0.001$, by student's unpaired two-tailed t-test). Boxes indicate Q1–Q3, lines indicate the median, circles indicate the *J* value of each pair within (blue) or between (soft red) evolved conditions.

B. subtilis adapt specifically towards the plant species

The lower mutation number (frequency >10%), lower genotype diversity, and lower genetic similarity of Bs_root_A strongly imply that the adaptation strategy between Bs_root_A and other three conditions were different. Therefore, we focused on the genes with a mutation frequency higher than 10% and categorized them based on KEGG pathway. Overall, bacterial

motility proteins, genetic information processing and metabolism related genes were mutated more frequently and reached high frequencies, account for 61.36% mutated genes (frequency >10%).

As mentioned above, bacterial motility proteins were the most selected in our experiment. Among the revealed motility protein genes, eight out of the eleven bacterial motility protein genes are flagellar structure protein coding genes (**Fig. 6**) [42], and could be categorized into filament coding genes (flagellin, *hag*), basal body coding genes (*fliF*, *fliG*, *fliM*, and *fliY*), and flagellar type III secretion (T3S) apparatus protein genes (*fliI*, *fliR*, and *flhB*) [42]. Although bacterial motility genes were targeted frequently in all conditions, *fliI* and *fliR* were only mutated in Bs_root_A and mutations in *fliG*, *fliY* and *hag* were only absent in Bs_root_A. FliI is a flagellar-specific ATPase for the export of flagellar proteins [43], and FliR is the part of the T3S apparatus [44], which required for flagellum and nanotube assembly. Another gene required for flagellum and nanotube assembly, *flhB* [39], was mutated in all evolved conditions. FliG involved directly in flagellar rotation[45], while FliY interacts with the chemotaxis system and control the direction of flagellar rotation [42, 46], and *hag* encoding the flagellin monomer protein Hag, which is also essential for flagellar assembly [47, 48]. A sigma factor encoding gene, *sigD*, which regulates flagella, motility, chemotaxis and autolysis in *B. subtilis* [48–50], was solely not mutated in the Bs_root_A samples, while gene *yuxH* (*pdeH*), encoding for c-di-GMP degrading phosphodiesterase, was mutated in all conditions and relatively high frequencies. c-di-GMP is a second messenger that regulates diverse cellular processes in bacteria, including bacterial motility, biofilm formation, cell-cell signaling, and host

colonization [40, 41]. Overall, species-specific and common mutations in both flagellar structure proteins and motility regulator proteins were identified, which were possibly caused by the species-specific evolution stress imposed by different plant species and the same static hydroponic setup.

Mutation in a relevant gene for biofilm development, *sinR*, which codes for a DNA-binding protein that regulate the expression of the operons involved in matrix production, *epsA-O* and *tapA-sipW-tasA* [51, 52], was only detected transiently with low frequency (max at 7.19%) in Bs_root_T (**Fig. 4**, **Fig. 6** and **Dataset S2**), while it was observed more frequently and with higher frequency in the other conditions, suggesting an *A. thaliana* specific mutation.

Another suspected *A. thaliana* specific mutated gene, *pstBA*, which encoding phosphate transport system ATP-binding protein, was only absent in the Bs_root_T sample, and transiently with low frequency in two cyclic evolved condition, while detected at high frequency in three out of five lineages in Bs_root_A. *pstBA* belongs to the five genes containing *pst* operon, a member of the PhoP-PhoR two-component signal transduction system [53–55]. The encoded proteins are responsible for phosphate uptake under nutrient stress in *B. subtilis* [55], while the *pst* operon is alkali inducible [53].

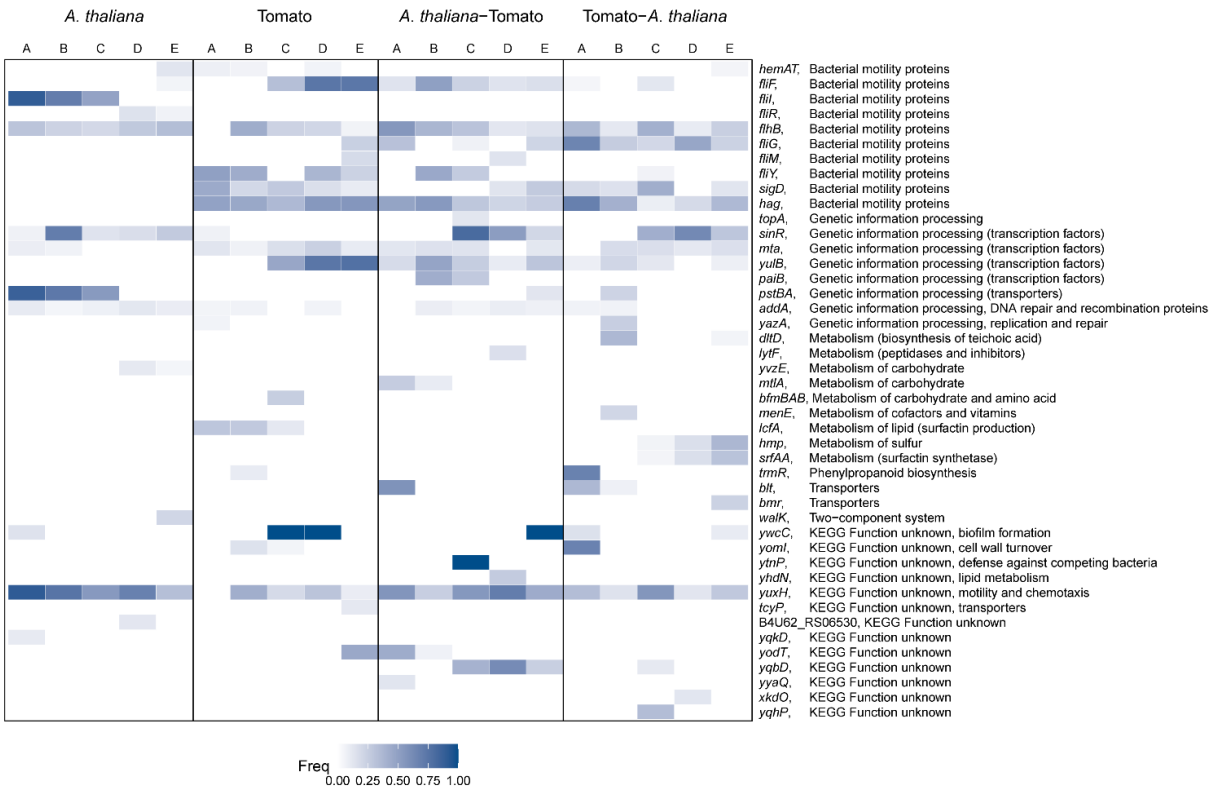

Fig. 6 Genes with mutation frequency > 10%. Each column represents one replicate lineage. In each lineage, the color represents the highest frequency of mutations in that certain gene. Detailed information of these genes and mutations can be found in **Dataset S2**.

DISCUSSION

Do plant colonizing bacteria adapt differently in an alternating host regime in comparison with using the same plant throughout the experiment? Does a bacterial species adapt differently to different plant hosts? To explore these questions, experimental evolution and whole-population WGS sequencing method were exploited to analyze how *B. subtilis* evolves on *A. thaliana* and tomato seedlings, as well as when these two plant hosts were alternating in a static hydroponic setup [27]. The observed data does not offer a simple binary answer for the initial questions.

Similar to several previous studies [23, 24, 27], *B. subtilis* showed rapid improvement on root colonization ability, albeit at varying rates, and diversified to three distinct morphotypes during adaptation in all evolved lineages and conditions. Additionally, the three distinct morphotypes coexisted until the end of the evolution experiment, reaching on average highly similar ratios in all four evolution experiments. Both the root colonization improvement and morphotypic diversification displayed remarkable degree of parallelism across all evolved conditions. Furthermore, all but one randomly selected isolate from Bs_root_A and Bs_root_T showed impaired swimming and swarming motility. The populations from two host-cyclic evolved conditions share numerous mutated genes with Bs_root_T suggesting similar trade-offs being present in the alternating plant setup also. Analysis of the genetic basis behind the two levels of parallelism (morphotypes and altered motility) revealed bacterial motility proteins, genetic information processing, and metabolism related genes to be mutated more frequently and reaching high frequencies in all evolved conditions. Besides the parallelism on phenotypic and functional level, mutational resemblance was observed in certain genes and even at

individual nucleotide level. Two genes, *flhB* and *yuxH*, showed striking parallelism on both gene and at individual nucleotide level, 18 out of the 20 lineages contained a frameshift in gene *flhB* and 15 lineages contained an 8bp deletion in *yuxH*. *flhB* is required for flagellum and nanotube assembly and *yuxH* is involved in c-di-GMP regulation in *B. subtilis* [40, 41], both may contribute to the adaptation of *B. subtilis* to the plant roots related to motility. However, reintroduction of single mutations alone or in combination will be necessary in the future to precisely measure the influence of these mutations on fitness. Hereto, we identified repeated changes across multiple levels of biological organization from phenotypic, functional pathways, genes, and even to individual nucleotide [37], demonstrating the overlapping strategies employed by *B. subtilis* when adapting to *A. thaliana* and tomato roots as well as roots in an alternating regime.

The static hydroponic setup used in our study selects for a regular root recolonization by the bacterial cells on different plant species, that includes bacterial traits of chemotaxis, biofilm formation and dispersal [27]. Different histidine kinases influence the phosphorylation level of the global regulator, Spo0A [15] when *B. subtilis* forms a biofilm on the roots of *A. thaliana* [16] and tomato [17], and different Bacillus species have distinct host plant colonization [19]. These previous results motivated the hypothesis that *B. subtilis* adaptation to *A. thaliana* or tomato will display distinct gene-level attributes behind the species-specific adaptation. Although parallelism was identified at phenotypic and nucleotide change levels, obvious differences were detected in the number of mutation (at a frequency >10%), the genotype diversity, the mutated gene, and the genetic similarity between and among the different

conditions.

Less mutations (at a frequency >10%), lower genotype diversity, and lower within condition genetic similarity were observed in mono-evolved conditions, especially in Bs_root_A. The difference between mono-evolved condition and cyclic evolved conditions could be explained by a more heterogeneous, multi-resource spatially structured environment created by the host-cycling environment, suggesting that environmental heterogeneity might have an important influence on adaptation [34, 37, 56]. When *Pseudomonas fluorescens* is evolved in five different environments that varied in resource type and arrangement, higher number of mutations and higher degree of parallelism can be observed at gene level in the most heterogeneous environment [37]. Similarly, evolution of *Pseudomonas aeruginosa* populations on plastic beads that favors a biofilm lifestyle exhibits higher morphologic diversity and mutation rates compared with planktonic cultures [57]. Consistent with previous studies, the degree of parallel evolution was significantly higher in the here described *B. subtilis* populations evolved in a heterogeneous, multi-resource spatially structured environment.

Bs_root_A populations harbored the lowest number of mutations and the least similarity among these, even lower than that of the Bs_root_T samples. Additionally, the genetic similarity between the two mono-evolved conditions was much lower than between the two cyclic evolved conditions, and the similarity between Bs_root_A and the two cyclic conditions were also much lower than the similarity between Bs_root_T and the two cyclic conditions. Furthermore, several specific mutated genes were also observed, which were present or absent exclusively in one of the plant species. These results imply that the adaptation pattern of *B.*

subtilis to the root of *A. thaliana* and tomato was different, and *A. thaliana* exerted less influence on the adaptation process in the two cyclic evolved conditions. A potential key difference between *A. thaliana* and tomato that might alter bacterial evolution is the composition and amounts of exudates. In our experimental system, *B. subtilis* was evolved in a minimal salt medium (MSM; see **Materials and Methods**), where bacterial cells are dependent on carbon sources provided by the plant for their growth. The composition and amount of exudates in and between *A. thaliana* [58] and tomato [59] plants varies depending on the growth stage.

We found the most targeted genes to be related to motility, while all lineages displayed improved root colonization. Motility and biofilm formation are considered to be inversely regulated lifestyles with bacteria expressing genes necessary for either motility or biofilm matrix production but not both simultaneously [60, 61]. Motility is vital for many bacteria, as this process enables them to explore resources and supports the dispersal of progeny [62]. Motility has been shown to be important for the effective root colonization of different plant species by *B subtilis* under different conditions [18–21]. It is not surprising that the loss of motility is repeatedly evolved in populations growing in well-mixed liquid media where motility is not essential [37] and where the production of proteins for motility, primarily for flagella, is energy and resources costly [63]. A biofilm-motility trade-off was previous also suggested where *B. subtilis* evolved on *A. thaliana* roots under shaking condition [24]. Surprisingly, all mutations in flagellar structure protein coding genes were nonsynonymous SNPs or InDels, suggesting these mutations to cause loss-of-function of flagella. Notably, a 78bp duplication (23 amino acids, 133~155) occurred in *hag* in three evolved conditions (in 12

lineages) and reached high frequency, which would strongly affect the structure and function of flagellin, i.e. cell motility. Additionally, widespread and high frequency mutations in *sinR*, which encoding biofilm master regulator [64], *sigD*, encoding sigma factor D [48–50], which regulates flagella, motility, chemotaxis and autolysis of *B. subtilis*, *yuxH*, which is involved in c-di-GMP regulation in *B. subtilis* [40, 41], and *pstBA*, which responsible for phosphate uptake under nutrient stress in *B. subtilis* [55], were all predicted to regulate the motility-biofilm balance in *B. subtilis*.

Finally, we compared the genetic similarities and differences in certain biological functions, e.g. aerotaxis, chemotaxis, motility (regulation) and biofilm development, when *B. subtilis* was evolved under different experimental conditions, including a static air-medium pellicle biofilm transfer mode (Bs_pellicle) [65], an *A. thaliana* root colonization study under shaking hydroponic setup (Bs_root) [24] and the here reported plant root colonization under static hydroponic setup (Bs_root_ATTA) (**Fig. S1**). Both common and condition-specific genes were identified to carry mutations. We found *hemAT* to be mutated in both Bs_pellicle and Bs_root_ATTA systems, although less frequently in Bs_root_ATTA. Importantly, both experiments were performed under static condition, where an oxygen gradient is generated in the culture and HemAT is a key oxygen sensor important during pellicle formation [50]. The lower frequency of mutation in *hemAT* detected in Bs_root_ATTA suggests lower selection for aerotaxis in the cells that colonize the submerged part of the plant roots compared with the cells that localized the medium-air interface. Interestingly, the sigma factor encoding gene, *sigD*, was mutated only in conditions where tomato was used as host in Bs_root_ATTA, suggesting that it

is a tomato-specific mutational target gene. Flagella related genes were identified to be mutated in all three conditions, although mutations were detected in different genes and with different frequency. Further, the c-di-GMP degrading phosphodiesterase-encoding *pdeH* was mutated in all three conditions and more frequently and with high frequencies in Bs_root_ATTA. c-di-GMP is a second messenger that modulates diverse cellular activities in bacteria, including bacterial motility, biofilm formation, cell-cell signaling, and host colonization [40, 41], however, studies c-di-GMP signaling have mostly focused on Gram-negative bacteria until recently. *sinR*, seems to be a target in plant specific conditions as it solely lacked mutations in the Bs_pellicle samples. Another possible static condition specific target similar to *hemAT* is *pstBA*, which involved in high-affinity phosphate uptake in *B. subtilis* [55].

In conclusion, our study identified parallel evolution across multiple levels of biological organization from phenotypic to individual nucleotide level, while the degree of parallel evolution in gene level was significantly higher in populations evolved in a heterogeneous, multi-resource spatially structured environment. We also observed species-specific adaptation at genetic level, which was possibly caused by the selection stress imposed by different host plants. Additionally, a strong trade-off between motility and growth as well as biofilm formation was observed under the here applied static selection condition. Finally, we identified several condition-specific and common mutated genes by comparing the genetic similarities and differences between three studies.

Funding information

This project was supported by China National GeneBank (CNGB), Danish National Research Foundation (DNRF137) for the Center for Microbial Secondary Metabolites, and Novo Nordisk Foundation within the INTERACT project of the Collaborative Crop Resiliency Program (NNF19SA0059360).

Conflicts of interest

The authors declare that there are no conflicts of interest.

References

1. **Guo X, Chen F, Gao F, Li L, Liu K, *et al.*** CNSA: A data repository for archiving omics data. *Database* 2020;2020:baaa055.

2. **Chen FZ, You LJ, Yang F, Wang LN, Guo XQ, *et al.*** CNGBdb: China National GeneBank DataBase. *Hereditas* 2020;42:799–809.

3. **Schmidt JE, Bowles TM, Gaudin ACM**. Using ancient traits to convert soil health into crop yield: Impact of selection on maize root and rhizosphere function. *Front Plant Sci* 2016;7:373.

4. **Haichar F el Z, Heulin T, Guyonnet JP, Achouak W**. Stable isotope probing of carbon flow in the plant holobiont. *Curr Opin Biotechnol* 2016;41:9–13.

5. **Venturi V, Keel C**. Signaling in the Rhizosphere. *Trends Plant Sci* 2016;21:187–198.

6. **Sasse J, Martinoia E, Northen T**. Feed Your Friends: Do Plant Exudates Shape the Root Microbiome? *Trends Plant Sci* 2018;23:25–41.

7. **Lareen A, Burton F, Schäfer P**. Plant root-microbe communication in shaping root microbiomes. *Plant Mol Biol* 2016;90:575–587.

8. **Vives-Peris V, de Ollas C, Gómez-Cadenas A, Pérez-Clemente RM**. Root exudates: from plant to rhizosphere and beyond. *Plant Cell Rep* 2020;39:3–17.

9. **Arnaouteli S, Bamford NC, Stanley-Wall NR, Kovács ÁT**. *Bacillus subtilis* biofilm formation and social interactions. *Nat Rev Microbiol* 2021;19:600–614.

10. **Blake C, Christensen MN, Kovács ÁT**. Molecular Aspects of Plant Growth Promotion and Protection by *Bacillus subtilis*. *Molecular Plant-Microbe Interactions* 2021;34:15–25.

11. **Peng G, Mcgregor L, Lahlali R, Gossen BD, Hwang SF, *et al.*** Potential biological control of clubroot on canola and crucifer vegetable crops. *Plant Pathol* 2011;60:566–574.

12. **Wei F, Hu X, Xu X**. Dispersal of Bacillus subtilis and its effect on strawberry phyllosphere microbiota under open field and protection conditions. *Scientific Reports 2016 6:1* 2016;6:1–9.

13. **Badri D v., Weir TL, van der Lelie D, Vivanco JM**. Rhizosphere chemical dialogues: plant–microbe interactions. *Curr Opin Biotechnol* 2009;20:642–650.

14. **Hamon MA, Lazazzera BA**. The sporulation transcription factor Spo0A is required for biofilm development in *Bacillus subtilis*. *Mol Microbiol* 2001;42:1199–1209.

15. **Jiang M, Shao W, Perego M, Hoch JA**. Multiple histidine kinases regulate entry into stationary phase and sporulation in *Bacillus subtilis*. *Mol Microbiol* 2000;38:535–542.

16. **Chen Y, Cao S, Chai Y, Clardy J, Kolter R, *et al.*** A *Bacillus subtilis* sensor kinase involved in triggering biofilm formation on the roots of tomato plants. *Mol Microbiol* 2012;85:418–430.

17. **Beauregard PB, Chai Y, Vlamakis H, Losick R, Kolter R**. *Bacillus subtilis* biofilm induction by plant polysaccharides. *Proc Natl Acad Sci U S A* 2013;110:1621–1630.

18. **Tian T, Sun B, Shi H, Gao T, He Y, *et al.*** Sucrose triggers a novel signaling cascade promoting *Bacillus subtilis* rhizosphere colonization. *ISME J* 2021;15:2723–2737.

19. **Zhang N, Wang D, Liu Y, Li S, Shen Q, *et al.*** Effects of different plant root exudates and their organic acid components on chemotaxis, biofilm formation and colonization by beneficial rhizosphere-associated bacterial strains. *Plant Soil* 2014;374:689–700.

20. **Gao S, Wu H, Yu X, Qian L, Gao X**. Swarming motility plays the major role in migration during tomato root colonization by *Bacillus subtilis* SWR01. *Biological Control* 2016;98:11–17.

21. **Allard-Massicotte R, Tessier L, Lécuyer F, Lakshmanan V, Lucier JF, *et al.*** *Bacillus subtilis* Early Colonization of *Arabidopsis thaliana* Roots involves multiple chemotaxis receptors. *mBio* 2016;7:e01664-16.

22. **Lenski RE**. What is adaptation by natural selection? Perspectives of an experimental microbiologist. *PLoS Genet* 2017;13:e1006668.

23. **Lin Y, Alstrup M, Pang JKY, Maróti G, Er-Rafik M, *et al.*** Adaptation of *Bacillus thuringiensis* to Plant Colonization Affects Differentiation and Toxicity. *mSystems* 2021;6:e00864-21.

24. **Nordgaard M, Blake C, Maróti G, Hu G, Wang Y, *et al.*** Experimental evolution of *Bacillus subtilis* on *Arabidopsis thaliana* roots reveals fast adaptation and improved root colonization. *iScience* 2022;25:104406.

25. **Li E, Zhang H, Jiang H, Pieterse CMJ, Jousset A, *et al.*** Experimental-evolution-driven identification of arabidopsis rhizosphere competence genes in *pseudomonas protegens*. *mBio* 2021;12:e00927-21.

26. **Li M, Guo J, Ren T, Luo G, Shen Q, *et al.*** Crop rotation history constrains soil biodiversity and multifunctionality relationships. *Agric Ecosyst Environ* 2021;319:107550.

27. **Blake C, Nordgaard M, Maróti G, Kovács ÁT**. Diversification of *Bacillus subtilis* during experimental evolution on *Arabidopsis thaliana* and the complementarity in root colonization of evolved subpopulations. *Environ Microbiol* 2021;23:6122–6136.

28. **Chen A, Liao S, Cheng M, Ma K, Wu L, *et al.*** Spatiotemporal transcriptomic atlas of mouse organogenesis using DNA nanoball-patterned arrays. *Cell* 2022;185:1777-1792.e21.

29. **Han L, Wei X, Liu C, Volpe G, Zhuang Z, *et al.*** Cell transcriptomic atlas of the non-human primate *Macaca fascicularis*. *Nature* 2022;604:723–731.

30. **Chen Y, Chen Y, Shi C, Huang Z, Zhang Y, *et al.*** SOAPnuke: A MapReduce acceleration-supported software for integrated quality control and preprocessing of high-throughput sequencing data. *Gigascience* 2018;7:gix120.

31. **Deatherage DE, Barrick JE**. Identification of Mutations in Laboratory-Evolved Microbes from Next-Generation Sequencing Data Using *breseq*. *Methods Mol Biol* 2014;1151:165–188.

32. **Barrick JE, Colburn G, Deatherage DE, Traverse CC, Strand MD, *et al.*** Identifying structural variation in haploid microbial genomes from short-read resequencing data using *breseq*. *BMC Genomics* 2014;15:1039.

33. **Scribner MR, Santos-Lopez A, Marshall CW, Deitrick C, Coopera VS, *et al.*** Parallel evolution of tobramycin resistance across species and environments. *mBio* 2020;11:e00932-20.

34. **Harris KB, Flynn KM, Cooper VS**. Polygenic Adaptation and Clonal Interference Enable Sustained Diversity in Experimental *Pseudomonas aeruginosa* Populations. *Mol Biol Evol* 2021;38:5359–5375.

35. **Kovács ÁT, Grau R, Pollitt EJG**. Surfing of bacterial droplets: Bacillus subtilis sliding

revisited. *Proceedings of the National Academy of Sciences* 2017;114:E8802.

36. **Hölscher T, Kovács ÁT**. Sliding on the surface: bacterial spreading without an active motor. *Environ Microbiol* 2017;19:2537–2545.

37. **Bailey SF, Rodrigue N, Kassen R**. The Effect of Selection Environment on the Probability of Parallel Evolution. *Mol Biol Evol* 2015;32:1436–1448.

38. **Bailey SF, Blanquart F, Bataillon T, Kassen R**. What drives parallel evolution?: How population size and mutational variation contribute to repeated evolution. *BioEssays* 2017;39:1600176.

39. **Kuhlen L, Johnson S, Zeitler A, Bäurle S, Deme JC, *et al.*** The substrate specificity switch FlhB assembles onto the export gate to regulate type three secretion. *Nat Commun* 2020;11:1296.

40. **Chen Y, Chai Y, Guo J-H, Losick R**. Evidence for Cyclic Di-GMP-Mediated Signaling in *Bacillus subtilis*. *J Bacteriol* 2012;194:5080–5090.

41. **Gao X, Mukherjee S, Matthews PM, Hammad LA, Kearns DB, *et al.*** Functional Characterization of Core Components of the Bacillus subtilis Cyclic-Di-GMP Signaling Pathway. *J Bacteriol* 2013;195:4782–4792.

42. **Mukherjee S, Kearns DB**. The structure and regulation of flagella in *Bacillus subtilis*. *Annu Rev Genet* 2014;48:319–340.

43. **Ibuki T, Imada K, Minamino T, Kato T, Miyata T, *et al.*** Common architecture of the flagellar type III protein export apparatus and F- and V-type ATPases. *Nat Struct Mol Biol* 2011;18:277–282.

44. **Kuhlen L, Abrusci P, Johnson S, Gault J, Deme J, *et al.*** Structure of the Core of the Type Three Secretion System Export Apparatus. *Nat Struct Mol Biol* 2018;25:583.

45. **Ward E, Kim EA, Panushka J, Botelho T, Meyer T, *et al.*** Organization of the flagellar switch complex of *Bacillus subtilis*. *J Bacteriol* 2019;201:e00626-18.

46. **Sircar R, Greenswag AR, Bilwes AM, Gonzalez-Bonet G, Crane BR**. Structure and activity of the flagellar rotor protein FliY: A member of the CheC phosphatase family. *Journal of Biological Chemistry* 2013;288:13493–13502.

47. **LaVallie ER, Stahl ML**. Cloning of the flagellin gene from *Bacillus subtilis* and

complementation studies of an in vitro-derived deletion mutation. *J Bacteriol* 1989;171:3085–3094.

48. **Hölscher T, Schiklang T, Dragoš A, Dietel AK, Kost C, *et al.*** Impaired competence in flagellar mutants of *Bacillus subtilis* is connected to the regulatory network governed by DegU. *Environ Microbiol Rep* 2018;10:23–32.

49. **Marquez LM, Helmann JD, Ferrari E, Parker HM, Ordal GW, *et al.*** Studies of σ^D-dependent functions in *Bacillus subtilis*. *J Bacteriol* 1990;172:3435–3443.

50. **Hölscher T, Bartels B, Lin YC, Gallegos-Monterrosa R, Price-Whelan A, *et al.*** Motility, Chemotaxis and Aerotaxis Contribute to Competitiveness during Bacterial Pellicle Biofilm Development. *J Mol Biol* 2015;427:3695–3708.

51. **Kearns DB**. A field guide to bacterial swarming motility. *Nature Reviews Microbiology* 2010;8:634–644.

52. **Chu F, Kearns DB, Branda SS, Kolter R, Losick R**. Targets of the master regulator of biofilm formation in *Bacillus subtilis*. *Mol Microbiol* 2006;59:1216–1228.

53. **Atalla A, Schumann W**. The *pst* Operon of *Bacillus subtilis* Is Specifically Induced by Alkali Stress. *J Bacteriol* 2003;185:5019–5022.

54. **Allenby NEE, O'Connor N, Prágai Z, Carter NM, Miethke M, *et al.*** Post-transcriptional regulation of the *Bacillus subtilis pst operon* encoding a phosphate-specific ABC transporter. *Microbiology (N Y)* 2004;150:2619–2628.

55. **Moreno-Letelier A, Olmedo G, Eguiarte LE, Martinez-Castilla L, Souza V**. Parallel Evolution and Horizontal Gene Transfer of the *pst* Operon in Firmicutes from Oligotrophic Environments. *Int J Evol Biol* 2011;2011:781642.

56. **Bram Van den Bergh, Toon Swings, Maarten Fauvart JM**. Experimental Design, Population Dynamics, and Diversity in Microbial Experimental Evolution. *Microbiology and Molecular Biology Reviews* 2018;82:e00008-18.

57. **Flynn KM, Dowell G, Johnson TM, Koestler BJ, Waters CM, *et al.*** Evolution of ecological diversity in biofilms of Pseudomonas aeruginosa by altered cyclic diguanylate signaling. *J Bacteriol* 2016;198:2608–2618.

58. **Chaparro JM, Badri D V, Bakker MG, Sugiyama A, Manter DK, *et al.*** Root Exudation of Phytochemicals in Arabidopsis Follows Specific Patterns That Are

Developmentally Programmed and Correlate with Soil Microbial Functions. *PLoS One* 2013;8:e55731.

59. **Kravchenko L V., Azarova TS, Leonova-Erko EI, Shaposhnikov AI, Makarova NM, *et al.*** Root exudates of tomato plants and their effect on the growth and antifungal activity of *Pseudomonas* strains. *Microbiology (N Y)* 2003;72:37–41.

60. **Guttenplan SB, Kearns DB**. Regulation of flagellar motility during biofilm formation. *FEMS Microbiol Rev* 2013;37:849–871.

61. **van Ditmarsch D, Boyle KE, Sakhtah H, Oyler JE, Nadell CD, *et al.*** Convergent evolution of hyperswarming leads to impaired biofilm formation in pathogenic bacteria. *Cell Rep* 2013;4:697–708.

62. **Wadhwa N, Berg HC**. Bacterial motility: machinery and mechanisms. *Nat Rev Microbiol* 2022;20:161–173.

63. **Keegstra JM, Carrara F, Stocker R**. The ecological roles of bacterial chemotaxis. *Nat Rev Microbiol* 2022;20:491–504.

64. **Kearns DB, Chu F, Branda SS, Kolter R, Losick R**. A master regulator for biofilm formation by *Bacillus subtilis*. *Mol Microbiol* 2005;55:739–749.

65. **Dragoš A, Lakshmanan N, Martin M, Horváth B, Maróti G, *et al.*** Evolution of exploitative interactions during diversification in *Bacillus subtilis* biofilms. *FEMS Microbiol Ecol* 2018;94:fix155.

Condition	*hamAT*	*mcpC*	*sigD*	*fliY*	*fliP*	*fliF*	*fliM*	*flhB*	*flhA*	*flil*	*fliR*	*fliG*	*hag*	*yuxH*	*sinR*	*ywcC*	*pstBA*
Bs_pellicle	0.94			0.59													
	0.70			0.62										0.28			
	0.87	0.14		0.40	0.27									0.05			0.12
	0.80	0.18		0.17	0.17												0.13
	1.00	0.16		0.10													0.08
	1.00	0.16		0.32										0.06			
Bs_root									0.15								
														0.23	1.00		
						0.06									0.76		
													0.14				
				0.08		0.26	0.14										
							0.58	0.22									
								0.25	0.13						1.00		
Bs_root_A								0.31		0.90				0.91	0.07	0.15	0.87
								0.23		0.70				0.76	0.70		0.73
								0.20		0.49				0.54	0.14		0.54
								0.28			0.15			0.68	0.17		
	0.13					0.06		0.34			0.07			0.34	0.28		
Bs_root_T	0.08		0.45	0.50									0.49		0.07		
	0.06		0.20	0.44				0.43					0.46	0.43			
			0.28			0.33		0.23					0.36	0.19		1.00	
	0.06		0.16	0.39		0.74		0.21					0.55	0.31		1.00	
			0.10	0.23		0.74	0.19	0.06				0.25	0.56	0.10			
Bs_root_AT						0.14		0.55				0.32	0.48	0.57			
				0.46		0.51		0.39					0.54	0.25			
				0.27		0.23		0.31				0.07	0.29	0.55	0.81		
			0.14			0.15	0.14	0.13					0.22	0.71	0.52		
			0.27			0.17		0.15				0.22	0.26	0.44	0.21	1.00	0.13
Bs_root_TA			0.19			0.05		0.37				0.66	0.69	0.35		0.16	
			0.15					0.12				0.26	0.41	0.15			0.23
			0.43	0.06		0.12		0.42				0.20	0.09	0.56	0.42		
								0.10				0.47	0.19	0.13	0.63		
	0.06		0.13					0.25				0.24	0.36	0.29	0.30	0.10	

Fig. S1 Comparison of several biological functions, i.e., aerotaxis, chemotaxis, motility (regulation) and biofilm regulation between three studies under different evolutional experiment conditions using *B. subtilis*, including a static air-medium floating biofilm transfer mode (Bs_pellicle), an *A. thaliana* root colonization study under shaking hydroponic setup (Bs_root) and plant root colonization study under static hydroponic setup (this study). Each row represents a lineage in corresponding condition, each column represents a gene, and each block shows the highest mutation frequency in corresponding gene and lineage.

6.4 Study 4 (submitted manuscript)

Enhanced niche colonization and competition during bacterial adaptation to a fungus

Anne Richter, Felix Blei, **Guohai Hu**, Jan W. Schwitalla, Carlos N. Lozano-Andrade, Scott A Jarmusch, Mario Wibowo, Bodil Kjeldgaard, Surabhi Surabhi, Theresa Jautzus, Christopher Phippen, Olaf Tyc, Mark Arentshorst, Yue Wang, Paolina Garbeva, Thomas Ostenfeld Larsen, Arthur F.J. Ram, Cees A.M. van den Hondel, Gergely Maróti, Ákos T. Kovács

Note: supplementary figures and tables are attached at the end of the study, the **datasets** are available on bioRxiv:

https://www.biorxiv.org/content/10.1101/2023.03.27.534400v1

Enhanced niche colonisation and competition during bacterial adaptation to a fungus

Anne Richter[1,2], Felix Blei[2], Guohai Hu[1,3,4,5], Jan W. Schwitalla[2], Carlos N. Lozano-Andrade[1], Scott A Jarmusch[6], Mario Wibowo[6], Bodil Kjeldgaard[1], Surabhi Surabhi[2], Theresa Jautzus[2], Christopher B. W. Phippen[6], Olaf Tyc[7], Mark Arentshorst[8], Yue Wang[3,4], Paolina Garbeva[7], Thomas Ostenfeld Larsen[6], Arthur F.J. Ram[8], Cees A.M. van den Hondel[8], Gergely Maróti[9], Ákos T. Kovács[1,2,*]

[1] Bacterial Interactions and Evolution Group, DTU Bioengineering, Technical University of Denmark, 2800 Lyngby, Denmark

[2] Terrestrial Biofilms Group, Institute of Microbiology, Friedrich Schiller University Jena, 07743 Jena, Germany

[3] China National GeneBank, BGI-Shenzhen, 518120 Shenzhen, China

[4] BGI-Shenzhen, 518083 Shenzhen, China

[5] Shenzhen Key Laboratory of Environmental Microbial Genomics and Application, BGI-Shenzhen, 518083 Shenzhen, China

[6] Natural Product Discovery Group, DTU Bioengineering, Technical University of Denmark, 2800 Lyngby, Denmark

[7] Netherlands Institute of Ecology, 6708PB Wageningen, The Netherlands

[8] Microbial Sciences, Institute of Biology, Leiden University, Leiden, The Netherlands

[9] Institute of Plant Biology, Biological Research Centre, Eötvös Loránd Research Network (ELKH), 6726 Szeged, Hungary

*For correspondence. E-mail a.t.kovacs@biology.leidenuniv.nl
Running title: Bacterial evolution in the presence of a fungus
Keywords: *Bacillus subtilis*, *Aspergillus niger*, adaptation, secondary metabolites, bacterial-fungal interaction, volatiles

Word count: 3284 (Introduction to Discussion); Number of Figures: 4

Current affiliations: FB, Department Pharmaceutical Microbiology, Hans-Knöll-Institute, Friedrich-Schiller-Universität, Jena, Germany; OT, Department of Internal Medicine I, Goethe University Hospital, Frankfurt, Germany; MW, Singapore Institute of Food and Biotechnology Innovation (SIFBI), Agency for Science, Technology and Research, Singapore, Republic of Singapore.

Abstract

Bacterial-fungal interactions (BFIs) influence microbial community performance of most ecosystems and elicit specific microbial behaviours, including stimulating specialised metabolite production. Using a simple BFI system encompassing the Gram-positive bacterium *Bacillus subtilis* and the black mould fungus *Aspergillus niger*, we established a co-culture experimental evolution method to investigate bacterial adaptation to the presence of a fungus. In the evolving populations, *B. subtilis* was rapidly selected for enhanced production of the lipopeptide surfactin and accelerated surface spreading ability, leading to inhibition of fungal expansion and acidification of the environment. These phenotypes were explained by specific mutations in the DegS-DegU two-component system. In the presence of surfactin, fungal hyphae exhibited bulging cells with delocalised secretory vesicles and RlmA-dependent cell wall stress induction. Increased surfactin production typically enhances the competitive success of bacteria against fungi, which likely explains the primary adaption path in the presence of *A. niger*.

Significance statement

Experimental evolution and co-cultivation of different microbes are important and useful techniques for discovering new traits and unravelling cryptic regulatory connections. We combined these methods by evolving the Gram-positive bacterium *Bacillus subtilis* in the presence of the black mould fungus *Aspergillus niger* that were previously shown to engage in an intricate and physical interaction. Both are ubiquitous, environmentally and industrially relevant model microbes in the colonisation of rhizo- and endosphere and in the production of enzymes. Our results demonstrate how laboratory adaptation can be exploited to improve biocontrol properties of bacteria.

Introduction

Bacteria and fungi share diverse habitats and consequently, a wide span of interactions is observed between them ranging from mutualism to inhibition. These interactions not only influence the structure and ecology of the respective microbial community but also impact the development and evolution of the interacting species [1,2]. Bacteria and fungi can indirectly affect each other by sensing and responding to diffusible signals such as chemoattractants, quorum-sensing molecules, and volatile substances [3–5]. However, several bacterial-fungal interactions (BFIs) require a close vicinity, and even direct contact between the interacting partners. In certain cases, the bacterium resides inside the cells of its fungal host [1,5]. Often, a combination of indirect influence and physical contact define a BFI. For example, the Gram-negative bacterium *Pseudomonas fluorescens* WCS365 exhibits chemotaxis towards fusaric acid secreted by *Fusarium oxysporum* f. sp. *radicis-lycopersici* hyphae in the rhizosphere of tomato plants [6]. This leads to bacterial colonisation of the fungal mycelium and decreased infection by the fungus in tomato plants [6,7]. In addition to influencing short-term microbial development, BFIs can also impact the evolution of an organism over longer time scales [8]. For example, a mutualistic relationship between fungus-growing ants, their fungal partner *Leucoagaricus gonglyophorus*, and associated actinobacteria was proposed to have existed for at least 45 million years [1,9]. Antimicrobials produced by actinomycetes protect the fungal gardens by selectively targeting parasitic fungi such as *Escovopis* species [10–12].

Investigating BFIs has led to the discovery of numerous secondary metabolites not produced under common laboratory cultivation conditions [12]. The direct co-cultivation of *Streptomyces rapamycinicus* with *Aspergillus nidulans* activates a silent gene cluster in the fungus and triggers the production of orsellinic acid [13,14]. The potential of BFIs has been

exploited to identify new antimicrobial compounds using co-cultivation methods, which are urgently needed due to the emergence of antibiotic-resistant bacteria [12].

Mycelial networks usually cover a large area in soil, and they are used as a highway by bacteria to facilitate their movement along hyphae and thereby disperse and access favourable niches such as the plant endosphere [2,15–17]. In addition to transport, fungal hyphae can also function as attachment sites for bacterial biofilms [18]. The presence of *Aspergillus niger* promotes the growth of *Salmonella enterica*, which forms a biofilm on the fungal mycelium and protects it against antifungal agents [19,20]. During colonisation of maize plants, co-inoculation of both strains leads to a higher reduction of plant growth than inoculation with each strain alone [19].

A direct interaction between the black mould-causing fungus *A. niger* and the plant growth-promoting Gram-positive bacterium *Bacillus subtilis* has previously been described[18,21]. Both organisms are commonly found in soil, thus they potentially coexist in the same habitat and influence each other. Attachment of *B. subtilis* cells to fungal hyphae results in transcriptional changes. Specifically, the production of antimicrobial substances is downregulated in both microorganisms, including the *B. subtilis*-produced lipopeptide, surfactin. Furthermore, genes related to motility and aerobic respiration are also downregulated in the bacterium during attachment [21]. Here, we investigated the effects of long-term cultivation of *B. subtilis* in the presence of *A. niger*, focusing on evolution of the bacterium. During this laboratory adaptation experiment, *B. subtilis* cells with enhanced surfactin production and spreading behaviour were selected, which was mimicked by incorporation of specific mutations in genes encoding a global two-component system. Increased surfactin production and niche colonisation by the bacterium disrupted fungal expansion and acidification of the medium, and caused cell wall stress in *A. niger*.

Results

Adaptation of *B. subtilis* to the presence of *A. niger* leads to enhanced bacterial surface colonisation. Utilising the ability of *B. subtilis* to colonise and grow on mycelia of the fungus *A. niger* [18,21], a simple bacterial-fungal co-culture system was established in which fungal spores and subsequently diluted planktonic bacterial cultures were streaked onto agar medium in a hashtag and square pattern. Areas where bacteria grew over fungal hyphae were dissected (Fig. 1a). This agar block was used to inoculate the bacterium on fresh medium, followed by planktonic growth for 24 h before initiating a new co-culture cycle. Importantly, *A. niger* was not evolved in this setup; a fresh batch of spores was used each time from the same fungal stock. Five parallel co-cultivated evolution BFIs (denoted CoEvo) were used in addition to five control lineages of the bacterium cultivated alone (denoted Bac) following otherwise identical isolation procedures (Supplementary Fig. 1a). After 10 weekly transfers, two endpoint isolates were collected from each lineage of both setups. These evolution endpoint bacterial isolates were tested for growth in the presence of the fungus and their ability to form a colony biofilm.

First, bacterial cultures were spotted between two lines of 1-day-grown *A. niger* mycelia. The ancestor bacterium grew and created a small colony almost surrounded by the fungus after 7 days (Fig. 1b). Most of the evolved isolates behaved similarly to the ancestor, but isolates from two CoEvo lineages, especially CoEvo2 and partially CoEvo4, displayed increased spreading that limited fungal growth and expansion (Fig. 1b, Supplementary Fig. 1b, and Supplementary Video 1 and 2). All Bac isolates behaved like the ancestor. To assess the influence of bacterial spreading on fungal physiology, bacterial cultures were spotted next to a 1-day-grown *A. niger* streak on lysogeny broth (LB) plates containing the pH dye Bromocresol Purple that is purple above pH 6.8 and yellow bellow pH 5.2. When the fungus was cultivated

alone, the entire agar medium displayed a yellow colour corresponding to the ability of *A. niger* to acidify its environment via excretion of citric acid [22–24]. The ancestor bacterium and the CoEvo isolates restricted acidification, and the yellow coloration was apparent on the edge of the fungal streak, while the CoEvo2 isolate caused the strongest reduction in the remaining acidified area (Fig. 1b and Supplementary Fig. 1c). These results suggest increased niche colonisation by the CoEvo2 lineage in the presence of the fungus, whereas such adaptation wasn't observed for replicates of the Bac setup.

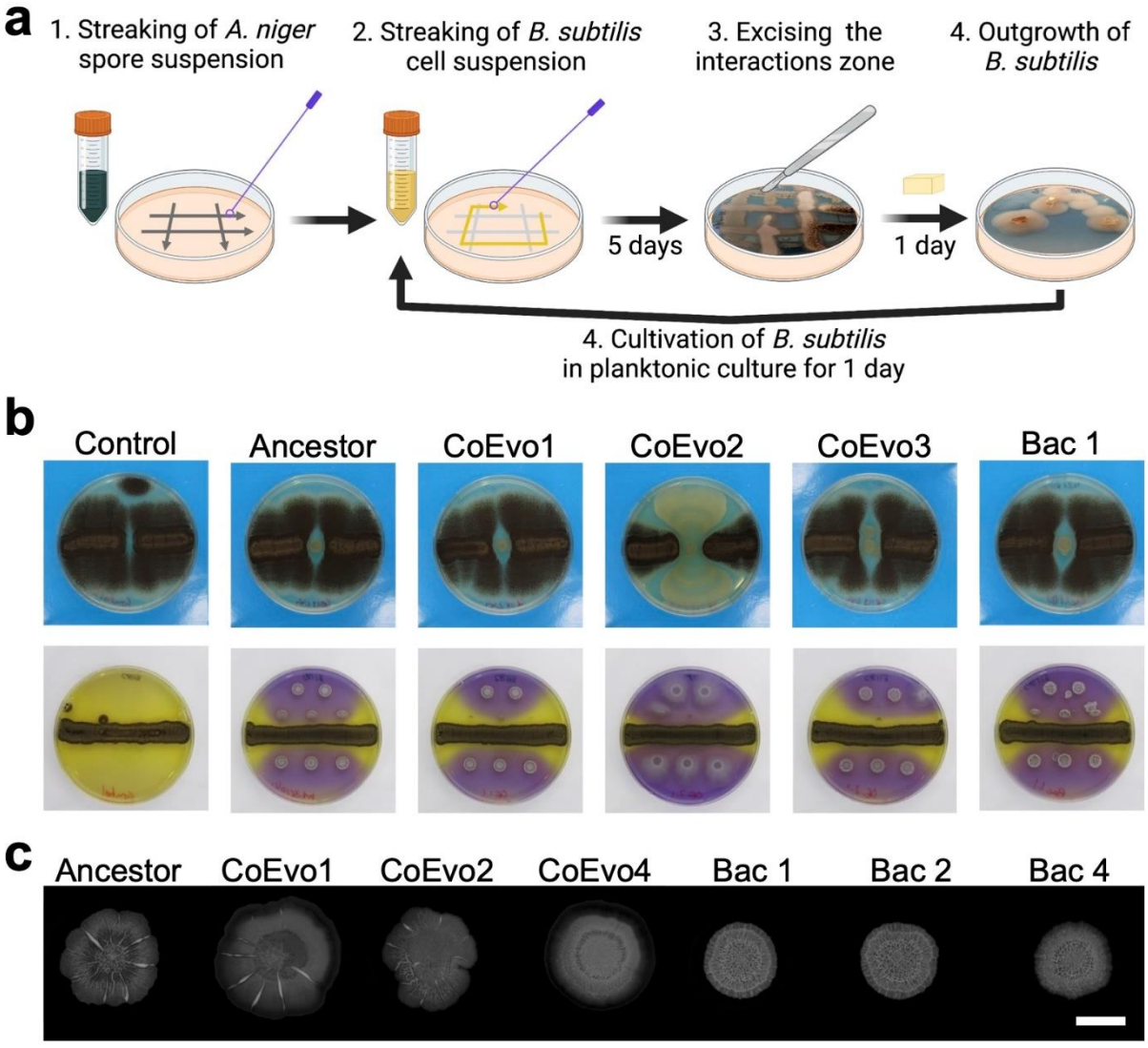

Fig. 1 | *B. subtilis* adaptation to the presence of *A. niger*. a, Schematic representation of the evolution setup. **b,** Top panels showing bacterial growth spotted between two lines of fungal

streaks, and lower panels showing the pH of the medium using Bromocresol Purple, where bacterial cultures were spotted next to a continuous fungal spore streak. Purple and yellow colours indicate pH >6.8 and pH <5.2, respectively. Plate size = 9 cm. CoEvo refers to co-culture evolved isolates, Bac denotes bacteria only evolved isolated. **c,** Biofilm colonies of selected evolved isolates. Scale bar = 10 mm. All isolates for panel b and c are shown in Supplementary Fig. 1.

Evolution of *B. subtilis* on agar medium selects for wrinkled variants. Unlike in the presence of a fungus, evolution of *B. subtilis* on a solid agar surface as pure cultures could potentially be driven by adapting biofilm complexity. Indeed, all but one replicate (Bac 3.2) of Bac isolates displayed increased architecture complexity (Fig. 1c and Supplementary Fig. 1d) reminiscent of biofilm matrix-overproducing wrinkled colonies observed in previous experimental evolution settings[25–28]. In general, isolates from CoEvo lineages exhibited similar colony structure to the ancestor, with a slight increase in complexity of evolved isolate CoEvo 4.1 (Fig. 1c and Supplementary Fig. 1d).

Mutation of the global regulator DegU enhances spreading in the presence of the fungus. To dissect the mutational landscapes of *B. subtilis* adapted in the presence or absence of *A. niger*, sequential populations of each lineage at each transfer were subjected to high-coverage metagenome sequencing (except the first three timepoints of four Bac lineages). Single-nucleotide polymorphisms (SNPs) and short insertions and deletions (indels) were determined using the *breseq* pipeline [29–31] which detected 142 and 157 mutations with >5% frequency in CoEvo and Bac populations, respectively (frequencies of each mutated gene in each lineage are shown in Supplementary Fig. 2a and the mutation types are shown in Supplementary Dataset 1). Subsequently, the genealogical structure of each lineage was determined and visualised as lineage frequencies from shared, nested mutation trajectories over time, using *Lolipop* [32,33]. This approach revealed both unique dominant mutations, including SNPs in *degU*

and *degS* genes in lineages CoEvo2 and CoEvo3, respectively, and parallel genetic changes, such as specific SNPs in *sinR* of Bac lineages (Fig. 2a and Supplementary Dataset 1). In addition, certain genes were commonly mutated under both conditions, including *ywdH* and different *opp* genes. Importantly, while genetic diversity was comparable in both CoEvo and Bac lineages (Fig. 2b), parallelism was higher in control evolved lineages than fungal-adapted lines (Fig. 2c), based on the Jaccard index that reflects the likelihood that the same gene is mutated in two independent lineages [34]. Subsequently, mutations in the genomes of the single endpoint isolates from each lineage were determined to corroborate population sequencing (Supplementary Dataset 1). CoEvo- and Bac-specific mutations were identified in addition to the few commonly mutated genes (Fig. 2d). SNPs in *sinR* were identified in Bac-evolved lineages that were previously associated with increased colony wrinkling [26,28,35,36]. Interestingly, isolate Bac 3.2 lacking increased colony wrinkles harboured no unique SNPs other than those also present in CoEvo isolates. Isolates from lineages CoEvo 2 and 3 possessed SNPs in the genes coding for the two-component regulatory system, DegU and DegS, respectively. The serine to glycine substitution at position 202 of DegU is located at the edge of the helix-turn-helix domain involved in DNA binding (Supplementary Fig. 2b). Mutations in the vicinity (e.g. $DegU^{R184C}$ in [37] and $DegU^{I186M}$ and $DegU^{H200Y}$ in [38]) have been reported to alter the expression of DegU-regulated genes. The alanine to valine substitution at position 193 of DegS (Supplementary Fig. 2c) has been previously characterized and is known to abolish DegS protein kinase activity [39]. Reduced phosphorylation of DegU by DegS results in upregulation of genes related to motility and natural competence for DNA uptake, whereas genes encoding secreted degradative enzymes are upregulated by high levels of phosphorylated DegU [37,39]. When $degU^{S202G}$ and $degS^{A193V}$ mutations were reintroduced into the ancestor, the engineered strains phenocopied the evolved isolates in the presence of *A. niger* (Fig. 2e). By contrast,

deletion of *degU* was comparable to the wild-type ancestor (Fig. 2e), indicating that these mutations modified but did not abolish DegU activity.

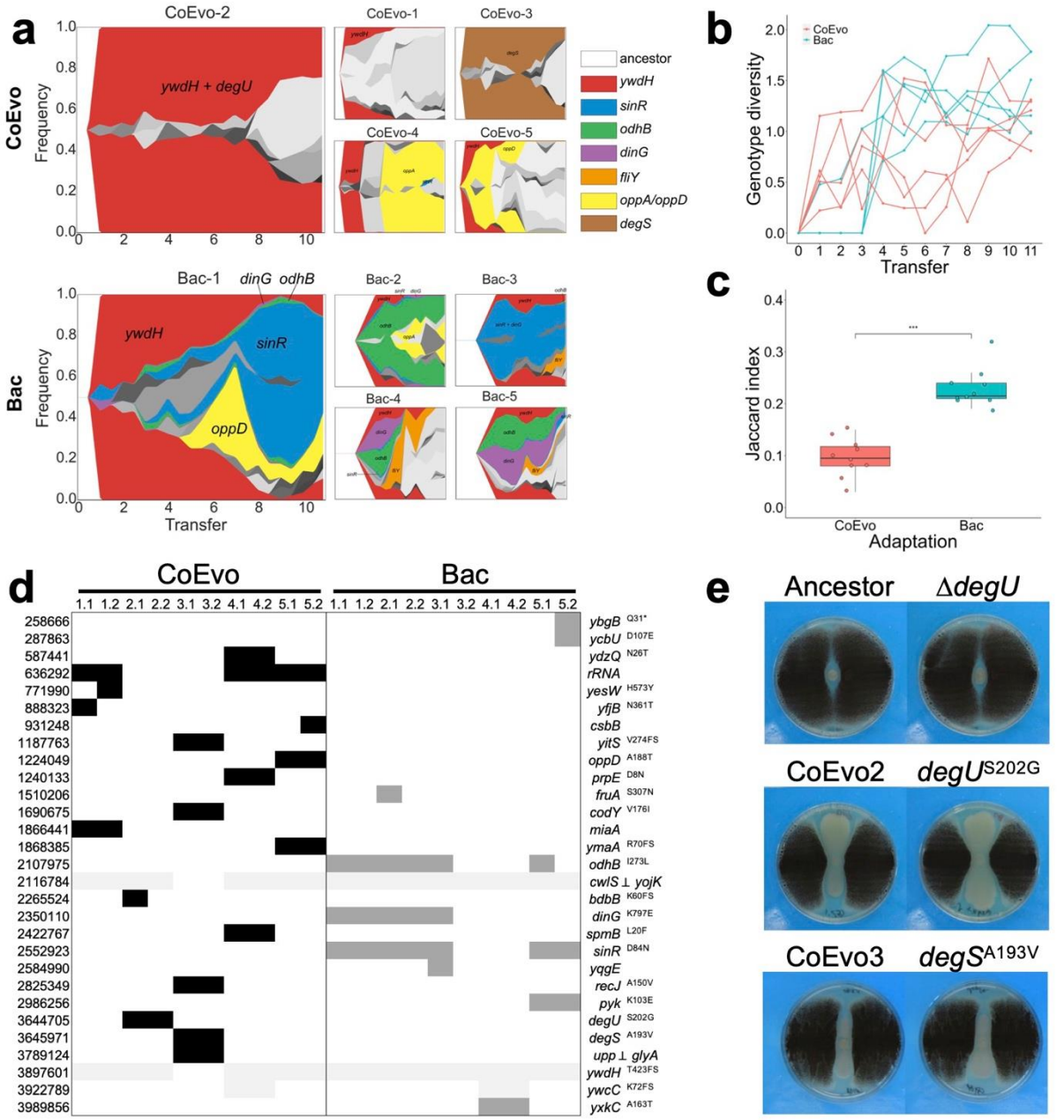

Fig. 2 | Genetic characterisation of *B. subtilis* adaptation to *A. niger*. a, Graphs showing the genealogy and genotype frequencies throughout the transfers. Each colour or shade represents a distinct genotype. The vertical area corresponds to genotype frequency as inferred using Lolipop. Dominant genotypes with a high mutation gene frequency, which are shared in different populations, are highlighted by matching colours within both adaptation models. **b,** Genotype diversity. The dynamic distribution of genotype alpha diversity in each population of the two adaptation models over time was calculated using the Shannon method. **c,** Degree of parallelism within both conditions estimated by Jaccard index. Asterisks denote significant differences (***p <0.001, Student's unpaired two-tailed t-test). Boxes indicate

Q1–Q3, lines indicate the median and dots indicate the J value of each condition. **d,** Detected mutations in endpoint CoEvo and Bac isolates. Black indicates CoEvo-specific mutations, dark grey denotes Bac-specific SNPs and light grey represents common mutations found in both experimental setups. ⊥ indicates intergenic regions between the two genes depicted. * indicates an introduced stop codon. Amino acid changes are indicated unless synonymous mutations were determined. **e,** Bacterial colony growth between two lines of fungal streaks. Plate size = 9 cm.

Selected evolved isolates respond to fungal volatiles, resulting in reduced spreading. While isolating the CoEvo strains, increased spreading over the agar surface was observed compared with the ancestor strain. Intriguingly, while CoEvo2 isolates displayed increased spreading on 1% agar medium regardless of the presence of the fungus, the CoEvo3 clone was only able to expand on the agar surface in the absence of the fungus, even if separated from the fungus by a plastic barrier allowing only volatile-mediated interaction (Supplementary Fig. 3a). The recreated *degS*^{A193V} strain phenocopied the influence of *A. niger* volatiles on colony expansion (Supplementary Fig. 3b). Therefore, for the CoEvo 3 strain, the volatilomes of single and separated co-cultures were determined at day 3 and day 7 after bacterial inoculation (see experimental setup in Supplementary Fig. 3c). Volatilomes contained dimethyl disulphide (DMS), pyrazine and 1-pentyne when *A. niger* was present but not when *B. subtilis* was cultured alone (for a full list see Supplementary Dataset 2). Supplementing either the pure compounds or the mixture of these volatile organic compounds (VOCs) reduced colony spreading of CoEvo 3 (Fig. 3a, one-way ANOVA, $F = 27.04$, $p < 0.001$, Tukey's HSD), demonstrating the volatile-mediated influence of *A. niger* on specific evolved isolates of *B. subtilis*. However, since these experiments were performed using a CoEvo 3 isolate, we cannot exclude the influence of these VOCs on the ancestor strain, which did not display enhanced surface spreading. Further experiments are needed to reveal the direct influence of the identified VOCs on the growth, physiology, or differentiation of *B. subtilis*.

Surfactin production is enhanced in evolved bacterial isolates. The lipopeptide surfactin plays an important role in *B. subtilis* expansion over semi-solid surfaces including swarming or sliding [40–43], and genes encoding the surfactin biosynthesis apparatus were downregulated during the initial attachment of *B. subtilis* to hyphae of *A. niger* in planktonic cultures [21]. Therefore, we hypothesised that surfactin production might be altered in the evolved strains during adaptation to the presence of the fungus. Direct semi-quantification of surfactin produced by the bacterium grown on agar medium confirmed an increase in surfactin production for several CoEvo isolates compared with the ancestor, especially lineages 2 and 3 (Fig. 3b, Student's t-test with Bonferroni-Holm correction), possibly facilitating the improved expansion of the bacterium. By contrast, surfactin production by Bac strains was not increased (Fig. 3b, Student's t-test with Bonferroni-Holm correction). Matrix-assisted laser desorption/ionisation-mass spectrometry imaging (MALDI-MSI) analysis of co-inoculated bacteria-fungi samples further demonstrated increased surfactin production by CoEvo 2 compared with the ancestor strain (Fig. 3c). By contrast, production the lipopeptide plipastatin by CoEvo2 was comparable with the ancestor (Supplementary Fig. 3d).

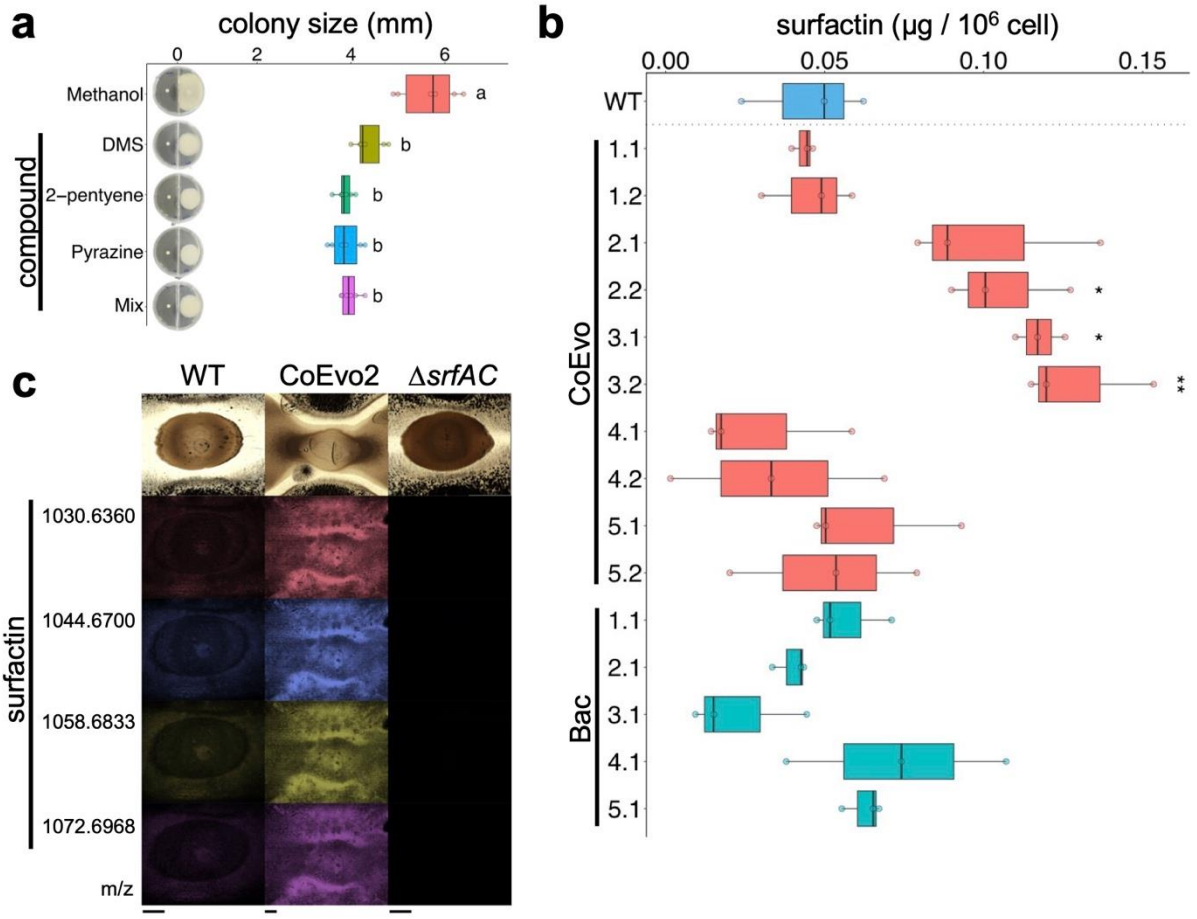

Fig. 3 | The effects of volatile compounds on *B. subtilis* growth, and detection of surfactin in evolved bacterial strains. a, Colony spreading of the CoEvo3 isolate recorded in the presence of methanol, dimethyl disulphide (DMS), 1-pentyne, pyrazine, or their mixture. One-way ANOVA was conducted to compare the effects of pure compounds and the mixture on CoEvo3 colony size. The results indicate a statistically significant difference in colony size between methanol treatment and other treatments ($F = 27.04$, $p < 0.001$). Tukey's HSD test was used to determine significant differences between means, which are denoted by letters. **b,** UHPLC-HRMS quantification of the produced surfactin normalised against the number of cells in colonies on agar medium. Student's t-test with Bonferroni-Holm correction was performed (*p_{adjust} <0.05, **p_{adjust} <0.01). **c,** MALDI-MSI spatial detection of surfactin isoforms in bacterial colonies (wild-type, CoEvo2, and the *srfAC* mutant from left to right) grown between two fungal streak lines. m/z values of surfactin isoforms are indicated on the left. Scale bars = 2 mm.

Surfactin causes hyphal bulging and cell wall stress in *A. niger*. The fungus-adapted bacterial isolate CoEvo2 displayed increased surfactin production and surface colonisation. In addition, acidification of the environment by *A. niger* was slightly reduced in the presence of CoEvo2. Therefore, we hypothesised that increased surfactin production not only stimulated spreading

of bacterial colonies, but also influenced the fungus. Intriguingly, when planktonic cultures of *A. niger* were supplemented with bacterial cell-free supernatant from the *B. subtilis* ancestor, some fungal hyphae displayed bulging (Fig. 4a). However, bulbous fungal cells were absent when surfactin was not produced in the bacterial cultures due to deletion of either *srfAC* (encoding a subunit of the surfactin biosynthesis machinery) or *sfp* (encoding a phosphopantetheinyl transferase involved in activation of the peptidyl carrier protein domains of non-ribosomal synthetases; Fig. 4a). Supplementation the fungal culture with pure surfactin was sufficient to induce bulging (Fig. 4a), and bulbous hyphal cells were still present in mutants lacking the ability to synthesise other non-ribosomal proteins (plipastatin and bacillaene) unless surfactin biosynthesis was simultaneously disrupted (Supplementary Fig. 4a).

To investigate the influence of surfactin on fungal hyphae, we tested a series of fluorescent reporter strains for which specific cell components could be monitored. In the presence of bacterial cell-free supernatant the cell wall, mitochondria, and nuclei were comparable to those of untreated samples, while membranous components including vacuoles, Golgi, and endoplasmic reticulum were aberrant (Supplementary Fig. 4b). In particular, secretory vesicle-specific soluble NSF attachment protein receptor SncA showed a homogenous distribution in bulged cells, and the secretory vesicles were mislocalised (Fig. 4b), unlike in untreated samples where these secretory vesicles are located close to the tips of hyphae to deliver cell wall components and secrete fungal enzymes [44].

The surfactin-induced bulging of *A. niger* hyphae resembles the impact of Calcofluor White (CFW), a chitin and cellulose-binding fluorescent dye, on fungal mycelia [45]. CFW provokes cell wall stress in *A. niger* including upregulation of α-1,3-glucane synthase encoded by the *agsA* gene [45]. Indeed, *agsA* transcription was induced in *A. niger* when treated with

bacterial cell-free supernatant when monitoring using luciferase (Fig. 4c) or a fluorescence reporter (Supplementary Fig. 4c). Furthermore, induction was dependent on production of surfactin by *B. subtilis*, as it could also be promoted by supplementation of pure surfactin (Supplementary Fig. 4c and e). The cell wall stress-sensing pathway in *A. niger* includes the transcription factor RlmA that directly activates *agsA* transcription (Fig. 4d). Accordingly, deletion of the RlmA-binding box within the promoter region of the *agsA* reporter construct tempered induction by bacterial cell-free supernatant (Fig. 4c). Finally, disruption of *rlmA* amplified the number of bulbous hyphal cells in the presence of bacterial cell-free supernatant or purified surfactin (Fig. 4e). As expected, without surfactin in the cell-free culture supernatant, neither wild-type nor *rlmA* mutant *A. niger* hyphae displayed bulging (Fig. 4e).

These results demonstrate that the mode of action of *B. subtilis*-produced surfactin on *A. niger* involves hyphal bulging and inducing cell wall stress. Plipastatin, another lipopeptide synthesised by *B. subtilis*, did not provoke such changes in hyphal cell morphology (Supplementary Fig. 4a). Inhibition of *Fusarium* (another filamentous fungus) by *B. subtilis* is mediated by plipastatin but unaffected by deletion of surfactin [46]. Therefore, potential bulging of *Fusarium* hyphae has been monitored and tested using *B. subtilis* strains lacking either surfactin or plipastatin. In line with the inhibitory activity of plipastatin against *Fusarium*, bulbous cell formation by *Fusarium culmorum* and *Fusarium oxysporum* was dependent on plipastatin in the cell-free supernatant (Supplementary Fig. 5).

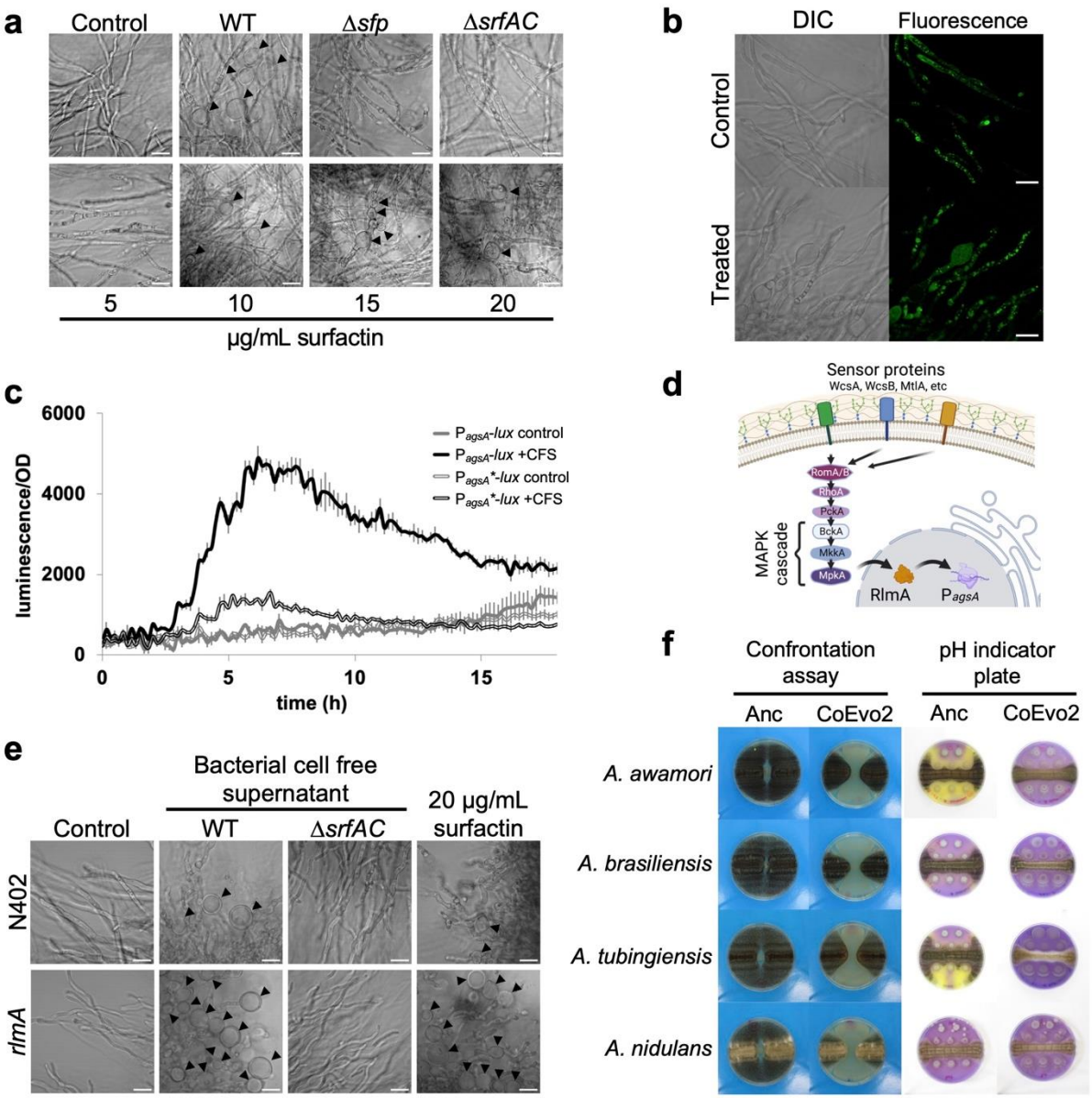

Fig. 4 | Influence of surfactin on fungal hyphae. a, Microscopy visualisation of bulging fungal hyphae with cell-free supernatant (CFS) of wild type (WT), sfp and surfactin mutants (top panels) or increasing amounts of surfactin (bottom panels). **b,** DIC (left) and green fluorescence (right) imaging of the *A. niger* FG7 strain (P_{synA}-GFP::SynA). Scale bar = 20 μm. **c,** Luminescence reporter assay using *A. niger* strains MA297.3 and MA584.2 containing $P_{agsA(3\times RlmA\ box)}$ and $P_{agsA(RlmA\ box\ mutated)}$ before the promoter-less luciferase (grey and black lines, respectively). Cultures were treated with LB medium (double lines) or cell-free supernatant (CFS, filled lines). **d,** Schematic representation of cell wall stress perception in *A. niger* according to a previous report [47]. **e,** Influence of the cell-free supernatant from the WT strain and the surfactin mutant (Δ*srfAC*), and 20 μg/ml surfactin on bulbous hyphae formation in WT and *rlmA* mutant *A. niger* strains (top and bottom panels, respectively). **f,** Impact of the ancestor (Anc) and Coevo2 strains on Aspergillus species *A. awamori*, *A. brasiliensis*, *A. tubingiensis*, and *A. nidulans*. The two columns on the left show bacterial growth spotted between two lines of fungal streaks, while the two columns on the right depict the pH of the

medium measured using Bromocresol Purple, where bacterial cultures were spotted next to a continuous fungal spore streak. Purple and yellow colours indicate pH >6.8 and pH <5.2, respectively. Plate diameter = 9 cm.

Spreading-mediated inhibition of other *Aspergillus* species. To reveal whether the ability of fungus-adapted *B. subtilis* to decrease *A. niger* growth was transferable to other *Aspergillus* species, the CoEvo 2 isolate was tested on them (Fig. 4f). In addition to *A. niger*, spreading enhanced by the CoEvo 2 strain was able to restrict the expansion of *Aspergillus awamori*, *Aspergillus brasiliensis*, *Aspergillus tubingiensis* and *A. nidulans*. Co-inoculation on medium containing a pH indicator revealed that CoEvo isolates could prevent fungal-mediated acidification of the medium during co-cultivation with several *Aspergillus species* (Fig. 4f), demonstrating a general advantage of increased spreading by *B. subtilis* during competition for space and nutrients on a surface.

Discussion

During prolonged co-cultivation with *A. niger*, selected lineages of *B. subtilis* adapted by increasing their surface spreading ability, which allows the bacterium to cover a larger area, reach more nutrients, and thus successfully compete against the fungus. The evolution of such elevated mobility might have been facilitated by the microhabitat generated by the fungal mycelium network. Zhang and colleagues observed rapid movement of single bacterial cells and subsequently groups of cells along a water film around fungal hyphae [48]. The area surrounding a fungal hypha retains water and has a higher humidity than the wider environment, thereby generating conditions that promote bacterial movement even in a dry milieu [48,49]. Spreading along a hypha might be advantageous for *B. subtilis* as the environment dehydrated over the 5-day incubation. Lack of a fungal microhabitat in control experiments may create drier conditions. Indeed, *B. subtilis* generally adapted by increasing matrix production in the absence of fungal mycelia. Investment in biofilm formation and smaller colony size might also be related to the dry environment since biofilms can act as water reservoirs [50,51].

Here, *B. subtilis* adaptation to the presence of *A. niger* increased competition, since in addition to enhanced spreading, several adapted lineages also produced more surfactin. Secondary metabolites such as lipopeptides are often involved in BFIs. These may act as cues to elicit a specific reaction or interfere directly with another microorganism via chemical warfare [12,52]. While the higher surfactin level of certain adapted isolates likely increased the spreading behaviour [41,43], it also directly contributed to fungal inhibition via its antimicrobial properties [53,54]. Importantly, we also revealed that the mode of action of surfactin on *A. niger* involves influencing membranous fungal cell components and provoking cell wall stress. By contrast, rapid adaptation of *B. subtilis* in a 15-day co-culture with the fungus *Setophoma*

terrestris was accompanied by reduced surfactin production, increased biofilm development, reduced swarming, and increased emission of anti-fungal volatile compounds [55]. The distinct adaptation route could be potentially explained by differences in fungal partner sensitivity to antimicrobial compounds.

The fate of a BFI from mutualism and co-existence to competition and elimination of their companion is often not only determined by the specific influence of members on each other, but also influenced by their environment. For example, spatiotemporal organisation is crucial for a stable co-culture and the beneficial influence of *B. subtilis* on the fungus *Serendipita indica* [56]. Interactions can also be influenced by environmental parameters including pH [55]. *A. niger* acidifies its environment by citric acid secretion [22,23]. One potential bacterial strategy to cope with a fungus-constructed niche includes adaptation to growth at low pH, thereby promoting survival in acidic soil, and hence co-occurrence with various fungal species, as reported previously [57,58]. In our experiment, instead of adapting to a lower pH milieu, the evolved *B. subtilis* isolates possibly prevented medium acidification by *A. niger* rather than actively inhibiting the process. The increased spreading of *B. subtilis* could potentially lower nutrient availability for *A. niger*, surfactin could also inhibit the fungus, and a combination of both mechanisms could contribute to reduced growth and acidification by *A. niger*. This observation is further supported by the comparable influence of the evolved isolate on a set of *Aspergillus* species.

Overall, our study demonstrates the potential of combining co-culture and laboratory evolution experiments to deepen our understanding of BFIs. Such co-culture adaptation methodology could offer a general, genetically modified organism-free approach to enhance antifungal activities of biocontrol bacteria against pathogenic fungi.

Methods

Media and cultivation conditions

B. subtilis DK1042 (a naturally competent derivative of the undomesticated biofilm-proficient NCIB3610 strain) and its derivatives were generally grown in lysogeny broth (LB; Lenox, Carl Roth, Germany) from a frozen stock for 18–20 h at 37°C with shaking at 220 rpm. To harvest conidia, *Aspergillus* strains were grown on malt extract agar (MEA) plates (Carl Roth, Germany) at 30°C for 1–2 weeks or on Complete Medium agar plates at 28°C for 3 days. After incubation, 10–20 ml of sterile Saline Tween solution (8 g/l NaCl with 0.005% Tween 80) was added, conidia were scraped off, and conidia-containing liquid was collected. The solution was vortexed, sterile filtered with Miracloth rewetted funnels and stored at 4°C. Interactions of *B. subtilis* and *A. niger* on plates were tested using LB medium supplemented with either 1% or 1.5% agar. To follow pH changes, LB agar medium was supplemented with 0.02 g/l Bromocresol Purple. Interactions of *B. subtilis* with different fungi in liquid cultures were tested in LB medium supplemented with 10 mM $MgSO_4$ and 1 mM $MnCl_2$ as previously reported [21]. Briefly, fungal spores were inoculated in LB medium and cultivated for 24 h. Subsequently, 1 ml cultures of the five fungal microcolonies were supplemented with 10 mM $MgSO_4$ and 1 mM $MnCl_2$ and overnight-grown *B. subtilis* was added at 1000-fold dilution in 24-well plates. Fungal cell morphology was assessed after 24 h of cultivation at 28°C with shaking at 120 rpm.

For luminescence reporter measurement, 7.5×10^4 fungal spores/ml were inoculated in 200 μl LB medium containing 50 μl luciferin (final concentration 0.5 mM) before either 50 μl bacterial cell-free supernatant, CFW (final concentration 50 μg/ml), LB medium or 1% methanol was added.

Strain construction

B. subtilis cells were transformed with genomic DNA (extracted from 168 *degU*) and selected on LB plates supplemented with kanamycin (10 μg/ml) to obtain the *degU* deletion mutant in the DK1042 background. Natural competence was used to transform *B. subtilis* [59]. To obtain the single nucleotide-exchanged strain, DK1042 was first transformed with plasmids pTB693 and pTB694 (for $degU^{S202G}$ and $degS^{A193V}$, respectively) and selected on LB agar plates containing 25 μg/ml lincomycin and 1 μg/ml erythromycin for macrolides (MLS) resistance. The obtained single recombinants were first verified using oligos specific for pMiniMad plasmid (oAR27 or oAR28) and flanking regions of *degU* (oAR25 and oAR26) or *degS* (oAR31 and oAR32) genes. The verified single recombinants were subsequently cultivated in liquid LB medium, cultures were plated on LB medium without antibiotics, single colonies were tested for the loss of integrated plasmid, and clones with specific SNPs ($degU^{S202G}$ and $degS^{A193V}$) were selected. Plasmids pTB693 and pTB694 were obtained by cloning the PCR products obtained using oAR23 and oAR24 ($degU^{S202G}$ from genomic DNA extracted from CoEvo3) and oAR30 and oAR41 ($degS^{A193V}$ from genomic DNA extracted from CoEvo3) into plasmid pMiniMad [60] using restrictions enzymes *Nco*I and *Bam*HI, and *Sal*I and *Bam*HI, respectively. Sequence of oligos are listed in Supplementary Table 1. Incorporation of the ancestor *degU* and *degS* alleles into the evolved variants was verified by sequencing. All other *B. subtilis* strains were constructed previously and the source is indicated in Supplementary Table 1.

The $P_{agsA(3\times RlmA\text{-}box)}$-m*luc*-T*trpC* cassette with *Not*I sites was PCR-amplified using plasmid pBN008 as template and primers PagsAP1f-NotI and TtrpCP2r-NotI. Plasmid pBN008 contains the $P_{agsA(3x\ rlmA\text{-}box)}$ fragment from plasmid P_{agsA}(0.55-kb-rlm2add)-*uidA*-*pyrG** [45] and m*luc*-T*trpC* from plasmid pVG4.1 [61]. The $P_{agsA(3\times RlmA\text{-}box)}$-m*luc*-T*trpC* cassette with *Not*I sites was ligated into pJet1.2 and verified by sequencing. The $P_{agsA(3\times RlmA\text{-}box)}$-m*luc*-T*trpC* cassette was

isolated with *Not*I and ligated into the *Not*I-digested plasmid pMA334 [62], yielding pMA348. The mutation in the RlmA box of the *agsA* promoter to generate the $P_{agsA(\text{RlmA-box mutated})}$-m*luc*-T*trpC* construct was introduced by PCR using primers PagsAP4f-NotI and PagsA-AF-R-mut-RlmA2 (211 bp) and primers PagsA-AF-F-mut-RlmA1 and PagsAP2r (441 bp) with genomic DNA from WT *A. niger* strain N402. Both PCR fragments were fused together by PCR with primers PagsAP4f-NotI and PagsAP2r (622 bp) and the fusion PCR product, containing a mutation in the RlmA box of the *agsA* promoter, was ligated into pJet1.2 and verified by sequencing. The mutated promoter was then isolated using *Not*I and *EcoR*I and ligated into corresponding sites of pBN008, yielding plasmid pMA368 $P_{agsA(\text{RlmA-box mutated})}$-m*luc*-T*trpC*. The $P_{agsA(\text{RlmA-box mutated})}$-m*luc*-T*trpC* cassette with *Not*I sites was PCR-amplified using plasmid pMA368 as template and primers PagsAP1f-NotI and TtrpCP2r-NotI, ligated into pJet1.2, and verified by sequencing. The $P_{agsA(\text{RlmA-box mutated})}$-m*luc*-T*trpC* cassette was isolated using *Not*I and ligated into the *Not*I-digested plasmid pMA334 [62], yielding pMA370. Plasmids pMA348 and pMA370 were digested with *Asc*I to release the complete $P_{agsA(3\times\text{RlmA-box})}$-m*luc*-T*trpC-pyrG*** and $P_{agsA(\text{RlmA-box mutated})}$-m*luc*-T*trpC-pyrG*** targeting cassettes and transformed into *A. niger* strain MA169.4 [63] as described previously [64]. Correct integration of the *pyrG*** targeting construct was confirmed by Southern blot for MA297.3 and MA584.2.

Other *A. niger* strains were constructed previously and the source is indicated in Supplementary Table 1. Species identity of *Aspergillus* strains from the Jena Microbial Resource Collection (JMRC) was validated by sequencing their PCR-amplified calmodulin gene fragment [65] obtained using primers oBK7 and oBK8 (sequencing data included in Supplementary Dataset 3). Fusarium strains from the IBT Culture Collection were used as previously described [46].

Bacterial evolution in the presence of the fungus

For co-cultivation, filtered conidia solution of *A. niger* was streaked on solid 1.5% agar containing LB medium in a hashtag pattern (Fig. 1a) using an inoculation loop. Diluted culture of *B. subtilis* (1:100) was streaked as a square through the inoculation lines of *A. niger* and the plate was incubated for 5 days at 28°C. Small squares of the interaction zone of the bacterium and the fungus were excised and placed on a new LB plate to allow separation of *B. subtilis* by growing out from the old block of the medium over 1 day at 28°C. A sample of the isolated bacteria was collected and incubated overnight in liquid LB medium (shaking at 225 rpm), and the culture was used to incubate a new plate with freshly inoculated *A. niger*, and to create a cryo-stock that was stored at -80°C. Throughout the experiment, dilution of the bacterial culture was increased stepwise to 1:1000 to prevent overgrowth of the fungus by the evolved bacterial strains. As a control, *B. subtilis* was incubated without the fungus and the experiment was performed with five parallel replicates in each group. The experiment was conducted for 10 weeks after which the evolved bacterial populations were clean streaked and two single isolates per replicate were kept for further analysis.

Colony biofilm and surface spreading

To analyse changes in colony biofilm morphology, 2 µl of *B. subtilis* overnight culture was spotted on MSgg medium as previously described [66]. Images of colony biofilms were recorded using an Axio Zoom V16 stereomicroscope (Carl Zeiss, Jena, Germany). A Zeiss CL 9000 LED light source and an AxioCam MRm monochrome camera were employed (Carl Zeiss).

To examine the spreading behaviour of *B. subtilis* in the presence or absence of *A. niger*, two-compartment plates with LB medium and 1% agar were dried for 15 min and 2 µl of *B. subtilis* overnight culture was spotted in the middle of either one or both compartments. In

the case of *A. niger* volatile challenge, fungal spores were inoculated in the other compartment 1 day before inoculation of bacterial cultures. The inoculated plates were dried for 10 min, incubated at 28°C, and expansion of strains was measured after 1 day.

To test the effects of volatile compounds on colony spreading of *B. subtilis*, 5 µl of 500 µM solution of either pyrazine, dimethyl disulphide (DMS), 2-pentyene, or their mixture was spotted on 5 mm filter paper discs placed in one side of the two-compartment plates. Next, 5 µl of an overnight culture of ancestor or CoEvo3 isolate, adjusted to an optical density at 600 nm (OD600) of 1.0, was spotted in the second compartment and plates were dried for 10 min, sealed, and incubated for 96 h at 28°C. Every 24 h, 5 µl of each compound or the mixture was added onto the paper disc. The *B. subtilis* colony size was recorded and plates were photographed at the end of the experiment. The experiment was conducted twice with three biological replicates for each independent assay.

Direct bacterium-fungus interaction on plates

Spreading of *B. subtilis* in the presence of the fungus was analysed by pre-culturing two streaks of the *Aspergillus* strain with a gap of 10 mm in between for 1 day at 28°C. Afterwards, *B. subtilis* was spotted in the gap and the plates were incubated as described above.

To check for pH manipulation by *B. subtilis*, *A. niger* or other *Aspergillus* strains (see strain list and collection numbers in Supplementary Table 1), LB plates containing the pH indicator Bromocresol Purple (0.02 g/l) were prepared. The plates were inoculated with a streak of *Aspergillus* conidia in the middle next to 2 µl spots of *B. subtilis* culture and incubated at 28°C for 2 days.

Population metagenome sequencing and variant calling

For whole-population sequencing, frozen stocks of the evolved bacterial populations and ancestor were cultured for 16 h at 37°C and genomic DNA was extracted using a EURx Bacterial and Yeast Genomic DNA Kit. MGIEasy PCR-free Library Prep Set (MGI Tech) was used for creating acoustic fragmentation PCR-free libraries. Paired-end fragment reads (2 × 150 nucleotides) were generated on a DNBSEQ-Tx sequencer (MGI Tech) according to the manufacturer's procedures. Depth coverage >200× was obtained for all population samples before polymorphism calling.

Low-quality reads were filtered from the raw data using SOAPnuke (version 1.5.6) [67], including reads with >50% of bases with a quality score <12, >10% of unknown bases (N), and adaptor contamination-containing reads. The similar variants calling sensitivity was ensured by normalisation of the clean data to 200× depth for all population samples. Mutations were identified using breseq (version 0.35.7) with default parameters and the -p option for population samples [29,30]. The default parameters called mutations only if they appeared at least twice on each strand and reached a frequency of at least 5% in the population. The reference genome used for population resequencing analysis was the NCIB 3610 genome and the pBS plasmid (GenBank accession no. NZ_CP020102 and NZ_CP020103, respectively). Mutations that were also detected in ancestor strains and in high polymorphism regions were omitted from the list to create the final table of mutations.

Genome resequencing of single evolved bacterial isolates

Genomic DNA of selected isolated strains was obtained as described above for evolved populations. An Illumina NextSeq sequencer was applied for generation of paired-end fragment reads (2 × 150 nucleotides) and bcl2fastq software (v2.17.1.14; Illumina) was applied for primary data analysis (base-calling). SOAPnuke (version 1.5.6)[67] was initially used for

removing low-quality reads as described for the population samples. In addition, the first 10 bases of each read were removed. Mutations were called using breseq (version 0.35.7) with default parameters and the -p option [29,30]. Default parameters called mutations only if they appeared at least twice on each strand and reached a frequency of at least 5% in the sample, and mutations with a frequency <50% were removed. Mutation frequency data for each sequenced strain are included in Supplementary Dataset 1.

Quantification of surfactin production

Bacterial colonies cultivated on LB medium with 1% agar for 2 days were harvested by collecting a plug of agar from the edge of a bacterial colony and subsequently sonicating and diluting for colony-forming counts. PTFE-filtered supernatant was used for semi-quantifying the amount of surfactin. An Agilent Infinity 1290 UHPLC system (Agilent Technologies, Santa Clara, CA, USA) equipped with a diode array detector was used for ultra-high-performance liquid chromatography-high-resolution mass spectrometry (UHPLC-HRMS). An Agilent Poroshell 120 phenyl-hexyl column (2.1 × 250 mm, 2.7 µm) was used for separation using a linear gradient consisting of water (A) and acetonitrile (B) both buffered with 20 mM formic acid, starting at 10% B and increasing to 100% over 15 min, holding for 2 min, returning to 10% B in 0.1 min, and holding for 3 min (0.35 ml/min, 60°C). A 1 µl injection volume was applied. Mass spectra were recorded on an Agilent 6545 QTOF instrument equipped with an Agilent Dual Jet Stream electrospray ion source in positive ion mode as centroid data in the range *m*/*z* 85−1700, with an acquisition rate of 10 spectra/s. A drying gas temperature of 250°C, gas flow of 8 l/min, sheath gas temperature of 300°C and flow of 12 l/min were used. The capillary voltage and nozzle voltage were set to 4000 V and 500 V, respectively. Surfactin A and its isoforms ($C_{53}H_{93}N_7O_{13}$) were semi-quantified using MassHunter quantitative analysis B.07.00

with the $[M + H]^+$ ion (*m/z* 1036.6904) and an isolation window of 10 ppm. A calibration curve was constructed using an authentic standard (Sigma-Aldrich).

Volatile assay and trapping of VOCs

For analysis and trapping of VOCs, two-compartment glass Petri-dishes [68] containing 1% LB agar were employed. *A. niger* was inoculated 24 h before addition of the bacterial strain on the left side of the two-compartment glass Petri dish and incubated overnight at 28°C (Extended Figure 3c). After CoEvo 3 was incubated overnight at 28°C in liquid LB medium, 2 µl of culture was spotted on the opposite compartment of the fungal culture. The glass Petri dishes were kept open for 25 min to allow droplets to dry. Plates were then closed by a lid with an outlet connected to a steel trap containing 150 mg Tenax TA and 150 mg Carbopack B (Markes International Ltd., Llantrisant, UK) and incubated at 28°C. The Tenax steel traps were collected after 3 and 7 days of incubation and stored at 4°C until GC-Q-TOF analysis. Glass Petri dishes containing LB agar medium but without inoculated bacteria or fungi served as controls.

GC-Q-TOF measurement and volatile analysis

The trapped VOCs were analysed as described previously [69]. Briefly, volatiles were desorbed from traps using a Unity TD-100 desorption unit (Markes International Ltd.) at 210°C for 12 min (He flow 50 ml/min) and trapped on a cold trap at -10°C. Volatiles were introduced into the GC-Q-TOF (Agilent 7890B GC and Agilent 7200A QTOF; Agilent Technologies) by heating the cold trap for 12 min to 250°C. The split ratio was 1:10 and the column was a 30 × 0.25 mm ID RXI-5MS with a film thickness of 0.25 µm (Restek 13424-6850, Bellefonte, PA, USA). The temperature program was as follows: 39°C for 2 min, 39°C to 95°C at 3.5°C/min, 95°C to 165°C

at 4°C/min, 165°C to 280°C at 15°C/min, 280°C to 320°C at 30°C/min, holding for 7 min. VOCs were ionised in EI mode at eV and mass spectra were acquired in full scan mode (30–400 U @ 5 scans/s). Mass spectra were extracted with MassHunter Qualitative Analysis Software V B.06.00 Build 6.0.633.0 (Agilent Technologies). The obtained mass spectra were transformed to netCDF files and imported into MZmine V2.20 (Copyright 2005–2012) MZmine Development Team) [70]. Compounds were identified via their mass spectra using the deconvolution function and local minimum search algorithm in combination with two mass spectral libraries, NIST 2014 V2.20 (National Institute of Standards and Technology, USA, http://www.nist.gov) and Wiley 7th edition spectral libraries, and by their linear retention index (LRI) calculated using AMDIS 2.72 (National Institute of Standards and Technology, USA). After deconvolution and mass identification, peak lists containing the mass features of each treatment were exported as csv files for further analysis.

MALDI-MSI

Petri dishes (5 cm diameter) were filled with ~4.5 mL of 1% LB and allowed to dry for 10 min. Subsequently, spores of *A. niger* were inoculated with a plastic loop drawing two separated lines and leaving a non-inoculated area at the centre of the plate. After 24 h of incubation at 28°C, 5 μL of *B. subtilis* ancestor, CoEvo2 or Δ*srfAC* were spotted onto the non-inoculated area. The plates were sealed with parafilm and incubated for 96 h. Samples were excised and mounted on an IntelliSlides conductive tin oxide glass slide (Bruker Daltonik GmbH) precoated with 0.25 ml of 2,5-dihydrobenzoic acid (DHB) by an HTX Imaging TM-Sprayer (HTX Technologies, USA). Slide images were subsequently taken using TissueScout (Bruker Daltonik GmbH) and a Braun FS120 scanner, followed by overnight drying in a desiccator. Subsequently, samples were overlayed by spraying 1.75 ml of DHB (20 mg/ml in ACN/MeOH/H2O (70:25:5,

v/v/v)) in a nitrogen atmosphere and dried overnight in a desiccator prior to MSI measurement. Samples were analysed using a timsTOF flex mass spectrometer (Bruker Daltonik GmbH) for MALDI MSI acquisition in positive MS scan mode with 100 µm raster width and a mass range of 100–2000 Da. Calibration was performed using red phosphorus. The following settings were used in timsControl. Laser imaging 100 µm, Power Boost 3.0%, scan range 26 µm in the XY interval, laser power 90%; Tune Funnel 1 RF 300 Vpp, Funnel 2 RF 300 Vpp, Multipole RF 300 Vpp, isCID 0 eV, Deflection Delta 70 V, MALDI plate offset 100 V, quadrupole ion energy 5 eV, quadrupole loss mass 100 m/z, collision energy 10 eV, focus pre-TOF transfer time 75 µs, pre-pulse storage 8 µs. After data acquisition, SCiLS software was used for data analysis and all data were root mean square normalised.

Statistical analyses

Statistical analysis of volatile metabolite data was performed using MetaboAnalyst V3.0 (www.metaboanalyst.ca) [71]. Prior to statistical analysis, data normalisation was performed via log-transformation and data were mean-centred and divided by the standard deviation of each variable. To identify significant mass features, one-way analysis of variance (ANOVA) with post-hoc TUKEY test (HSD-test) and PLSD analysis were performed between datasets. Mass features were considered statistically significant at $p \leq 0.05$.

One-way ANOVA was conducted to compare the effect of pure compounds and the mixture on the colony size of CoEvo3. Tukey's HSD test was used to determine significant differences between means, which are denoted by letters.

To evaluate differences in surfactin production between strains and to explore the influence of *rlmA* mutation in *A. niger*, Student's t-test with Bonferroni-Holm correction was performed. Student's unpaired two-tailed t-test was used for the Jaccard index.

Data availability

Population sequencing data have been deposited in the CNGB Sequence Archive (CNSA) [72] of the China National GeneBank DataBase (CNGBdb) [73] under accession numbers CNP0002416 and CNP0003923. Data for the DK1042 ancestor strain are available under CNP0002416. Isolate sequencing data have been deposited at the NCBI Sequence Read Archive (SRA) database under BioProject accession numbers PRJNA625867 (ancestor) and PRJNA926387 (evolved clones). VOC data available on Metabolomics Workbench as project PR001621 (http://dx.doi.org/10.21228/M85M6X).

Data points are all included in Supplementary Datasets. All other data generated and analysed during this study are either available in Supplementary Dataset 4 or can be requested from the corresponding author. All supplementary Datasets are available on bioRxiv (https://www.biorxiv.org/content/10.1101/2023.03.27.534400v1)

References

1. Frey-Klett, P. *et al.* Bacterial-fungal interactions: hyphens between agricultural, clinical, environmental, and food microbiologists. *Microbiology and Molecular Biology Reviews* **75**, 583–609 (2011).

2. Deveau, A. *et al.* Bacterial-fungal interactions: Ecology, mechanisms and challenges. *FEMS Microbiol Rev* **42**, 335–352 (2018).

3. Lowery, C. A., Dickerson, T. J. & Janda, K. D. Interspecies and interkingdom communication mediated by bacterial quorum sensing. *Chem Soc Rev* **37**, 1337–1346 (2008).

4. Effmert, U., Kalderás, J., Warnke, R. & Piechulla, B. Volatile mediated interactions between bacteria and fungi in the soil. *J Chem Ecol* **38**, 665–703 (2012).

5. Sadiq, F. A. *et al.* Trans-kingdom interactions in mixed biofilm communities. *FEMS Microbiol Rev* **46**, fuac024 (2022).

6. de Weert, S., Kuiper, I., Lagendijk, E. L., Lamers, G. E. M. & Lugtenberg, B. J. J. Role of chemotaxis toward fusaric acid in colonization of hyphae of *Fusarium oxysporum* f. sp. radicis-lycopersici by *Pseudomonas fluorescens* WCS365. *Molecular Plant-Microbe Interactions* **17**, 1185–1191 (2004).

7. Bolwerk, A. *et al.* Interactions in the tomato rhizosphere of two Pseudomonas biocontrol strains with the phytopathogenic fungus *Fusarium oxysporum* f. sp. radicis-lycopersici. *Molecular Plant-Microbe Interactions* **16**, 983–993 (2003).

8. Zhang, M., Pereira e Silva, M. de C., Chaib De Mares, M. & van Elsas, J. D. The mycosphere constitutes an arena for horizontal gene transfer with strong evolutionary implications for bacterial-fungal interactions. *FEMS Microbiol Ecol* **89**, 516–526 (2014).

9. Mueller, U. G., Schultz, T. R., Currie, C. R., Adams, R. M. M. & Malloch, D. The origin of the attine ant-fungus mutualism. *Quarterly Review of Biology* **76**, 169–197 (2001).

10. Haeder, S., Wirth, R., Herz, H. & Spiteller, D. Candicidin-producing Streptomyces support leaf-cutting ants to protect their fungus garden against the pathogenic fungus Escovopsis. *Proc Natl Acad Sci U S A* **106**, 4742–4746 (2009).

11. Oh, D. C., Poulsen, M., Currie, C. R. & Clardy, J. Dentigerumycin: A bacterial mediator of an ant-fungus symbiosis. *Nat Chem Biol* **5**, 391–393 (2009).

12. Netzker, T. *et al.* Microbial interactions trigger the production of antibiotics. *Curr Opin Microbiol* **45**, 117–123 (2018).

13. Schroeckh, V. *et al.* Intimate bacterial-fungal interaction triggers biosynthesis of archetypal polyketides in *Aspergillus nidulans*. *Proceedings of the National Academy of Sciences* **106**, 14558–14563 (2009).

14. Nutzmann, H.-W. *et al.* Bacteria-induced natural product formation in the fungus *Aspergillus nidulans* requires Saga/Ada-mediated histone acetylation. *Proceedings of the National Academy of Sciences* **108**, 14282–14287 (2011).

15. Kohlmeier, S. *et al.* Taking the fungal highway: Mobilization of pollutant-degrading bacteria by fungi. *Environ Sci Technol* **39**, 4640–4646 (2005).

16. Simon, A., Hervé, V., Al-Dourobi, A., Verrecchia, E. & Junier, P. An *in situ* inventory of fungi and their associated migrating bacteria in forest soils using fungal highway columns. *FEMS Microbiol Ecol* **93**, 1–9 (2017).

17. van Overbeek, L. S. & Saikkonen, K. Impact of bacterial-fungal interactions on the colonization of the endosphere. *Trends Plant Sci* **21**, 230–242 (2016).

18. Kjeldgaard, B. *et al.* Fungal hyphae colonization by *Bacillus subtilis* relies on biofilm matrix components. *Biofilm* **1**, 100007 (2019).

19. Balbontín, R., Vlamakis, H. & Kolter, R. Mutualistic interaction between *Salmonella enterica* and *Aspergillus niger* and its effects on *Zea mays* colonization. *Microb Biotechnol* **7**, 589–600 (2014).

20. Brandl, M. T. *et al. Salmonella* biofilm formation on *Aspergillus niger* involves cellulose - chitin interactions. *PLoS One* **6**, e25553 (2011).

21. Benoit, I. *et al. Bacillus subtilis* attachment to *Aspergillus niger* hyphae results in mutually altered metabolism. *Environ Microbiol* **17**, 2099–2113 (2015).

22. Magnuson, J. K. & Lasure, L. L. Organic acid production by filamentous fungi. in *Advances in Fungal Biotechnology for Industry, Agriculture, and Medicine* 307–340 (2004). doi:10.1007/978-1-4419-8859-1_12.

23. Liaud, N. *et al.* Exploring fungal biodiversity: organic acid production by 66 strains of filamentous fungi. *Fungal Biol Biotechnol* **1**, 1 (2014).

24. Karaffa, L. & Kubicek, C. P. *Aspergillus niger* citric acid accumulation: Do we understand this well working black box? *Applied Microbiology and Biotechnology* vol. 61 189–196 Preprint at https://doi.org/10.1007/s00253-002-1201-7 (2003).

25. Dragoš, A. *et al.* Evolution of exploitative interactions during diversification in *Bacillus subtilis* biofilms. *FEMS Microbiol Ecol* **94**, fix155 (2018).

26. Richter, A. *et al.* Hampered motility promotes the evolution of wrinkly phenotype in *Bacillus subtilis*. *BMC Evol Biol* **18**, 155 (2018).

27. Nordgaard, M. *et al.* Experimental evolution of *Bacillus subtilis* on *Arabidopsis thaliana* roots reveals fast adaptation and improved root colonization. *iScience* **25**, 104406 (2022).

28. Blake, C., Nordgaard, M., Maróti, G. & Kovács, Á. T. Diversification of *Bacillus subtilis* during experimental evolution on *Arabidopsis thaliana* and the complementarity in root colonization of evolved subpopulations. *Environ Microbiol* **23**, 6122–6136 (2021).

29. Barrick, J. E. *et al.* Identifying structural variation in haploid microbial genomes from short-read resequencing data using breseq. *BMC Genomics* **15**, 1039 (2014).

30. Deatherage, D. E. & Barrick, J. E. Identification of mutations in laboratory-evolved microbes from next-generation sequencing data using breseq. *Methods in Molecular Biology* **1151**, 165–188 (2014).

31. Hu, G. *et al.* Species and condition dependent mutational spectrum in experimentally evolved biofilms of *Bacilli*. *bioRxiv* https://doi.org/10.1101/2022.12.07.519423 (2022).

32. Harris, K. B., Flynn, K. M. & Cooper, V. S. Polygenic adaptation and clonal interference enable sustained diversity in experimental *Pseudomonas aeruginosa* populations. *Mol Biol Evol* **38**, 5359–5375 (2021).

33. Scribner, M. R. *et al.* Parallel evolution of tobramycin resistance across species and environments. *mBio* **11**, e00932-20 (2020).

34. Bailey, S. F., Rodrigue, N. & Kassen, R. The effect of selection environment on the probability of parallel evolution. *Mol Biol Evol* **32**, 1436–1448 (2015).

35. Kampf, J. *et al.* Selective pressure for biofilm formation in *Bacillus subtilis*: Differential effect of mutations in the master regulator *sinR* on bistability. *mBio* **9**, e01464-18 (2018).

36. Leiman, S. A., Arboleda, L. C., Spina, J. S. & McLoon, A. L. SinR is a mutational target for fine-tuning biofilm formation in laboratory-evolved strains of *Bacillus subtilis*. *BMC Microbiol* **14**, 301 (2014).

37. Msadek, T. *et al.* Signal transduction pathway controlling synthesis of a class of degradative enzymes in *Bacillus subtilis*: Expression of the regulatory genes and analysis of mutations in *degS* and *degU*. *J Bacteriol* **172**, 824–834 (1990).

38. Barreto, H. C., Cordeiro, T. N., Henriques, A. O. & Gordo, I. Rampant loss of social traits during domestication of a *Bacillus subtilis* natural isolate. *Sci Rep* **10**, 18886 (2020).

39. Dahl, M. K., Msadek, T., Kunst, F. & Rapoport, G. The phosphorylation state of the DegU response regulator acts as a molecular switch allowing either degradative enzyme synthesis or expression of genetic competence in *Bacillus subtilis*. *Journal of Biological Chemistry* **267**, 14509–14514 (1992).

40. Grau, R. R. *et al.* A duo of potassium-responsive histidine kinases govern the multicellular destiny of *Bacillus subtilis*. *mBio* **6**, e00581-15 (2015).

41. Hölscher, T. & Kovács, Á. T. Sliding on the surface: bacterial spreading without an active motor. *Environ Microbiol* **19**, 2537–2545 (2017).

42. Jautzus, T., van Gestel, J. & Kovács, Á. T. Complex extracellular biology drives surface competition during colony expansion in Bacillus subtilis. *ISME J* **16**, 2320–2328 (2022).

43. Kearns, D. A field guide to bacterial swarming motility. *Nat Rev Microbiol* **8**, 634–644 (2010).

44. Kwon, M. J. *et al.* Molecular genetic analysis of vesicular transport in *Aspergillus niger* reveals partial conservation of the molecular mechanism of exocytosis in fungi. *Microbiology (N Y)* **160**, 316–329 (2014).

45. Damveld, R. A. *et al.* The *Aspergillus niger* MADS-box transcription factor RlmA is required for cell wall reinforcement in response to cell wall stress. *Mol Microbiol* **58**, 305–319 (2005).

46. Kiesewalter, H. T. *et al.* Genomic and chemical diversity of *Bacillus subtilis* secondary metabolites against plant pathogenic fungi. *mSystems* **6**, e00770-20 (2021).

47. Yoshimi, A., Miyazawa, K. & Abe, K. Cell wall structure and biogenesis in Aspergillus species. *Bioscience, Biotechnology and Biochemistry* vol. 80 1–12 Preprint at https://doi.org/10.1080/09168451.2016.1177446 (2016).

48. Zhang, Y., Kastman, E. K., Guasto, J. S. & Wolfe, B. E. Fungal networks shape dynamics of bacterial dispersal and community assembly in cheese rind microbiomes. *Nat Commun* **9**, 336 (2018).

49. Furuno, S. *et al.* Fungal mycelia allow chemotactic dispersal of polycyclic aromatic hydrocarbon-degrading bacteria in water-unsaturated systems. *Environ Microbiol* **12**, 1391–1398 (2010).

50. Seminara, A. *et al.* Osmotic spreading of *Bacillus subtilis* biofilms driven by an extracellular matrix. *Proc Natl Acad Sci U S A* **109**, 1116–1121 (2012).

51. Flemming, H. C. & Wuertz, S. Bacteria and archaea on Earth and their abundance in biofilms. *Nat Rev Microbiol* **17**, 247–260 (2019).

52. Kovács, Á. T. A fungal scent from the cheese. *Environ Microbiol* **22**, 4524–4526 (2020).

53. Heerklotz, H. & Seelig, J. Leakage and lysis of lipid membranes induced by the lipopeptide surfactin. *European Biophysics Journal* **36**, 305–314 (2007).

54. Carrillo, C., Teruel, J. A., Aranda, F. J. & Ortiz, A. Molecular mechanism of membrane permeabilization by the peptide antibiotic surfactin. *Biochim Biophys Acta Biomembr* **1611**, 91–97 (2003).

55. Albarracín Orio, A. G. *et al.* Fungal–bacterial interaction selects for quorum sensing mutants with increased production of natural antifungal compounds. *Commun Biol* **3**, 670 (2020).

56. Jiang, X. *et al.* Impact of spatial organization on a novel auxotrophic interaction among soil microbes. *ISME Journal* **12**, 1443–1456 (2018).

57. Stopnisek, N. *et al.* Molecular mechanisms underlying the close association between soil *Burkholderia* and fungi. *ISME Journal* **10**, 253–264 (2016).

58. Stopnisek, N. *et al.* Genus-wide acid tolerance accounts for the biogeographical distribution of soil *Burkholderia* populations. *Environ Microbiol* **16**, 1503–1512 (2014).

59. Anagnostopoulos, C. & Spizizen, J. Requirements for transformation in Bacillus subtilis. *J Bacteriol* **81**, 741–746 (1961).

60. Patrick, J. E. & Kearns, D. B. MinJ (YvjD) is a topological determinant of cell division in *Bacillus subtilis*. *Mol Microbiol* **70**, 1166–1179 (2008).

61. Meyer, V. *et al.* Fungal gene expression on demand: An inducible, tunable, and metabolism-independent expression system for *Aspergillus niger*. *Appl Environ Microbiol* **77**, 2975–2983 (2011).

62. Arentshorst, M., Lagendijk, E. L. & Ram, A. F. A new vector for efficient gene targeting to the *pyrG* locus in *Aspergillus niger*. *Fungal Biol Biotechnol* **2**, 2 (2015).

63. Carvalho, N. D. S. P., Arentshorst, M., Jin Kwon, M., Meyer, V. & Ram, A. F. J. Expanding the ku70 toolbox for filamentous fungi: establishment of complementation vectors and recipient strains for advanced gene analyses. *Appl Microbiol Biotechnol* **87**, 1463–1473 (2010).

64. Arentshorst, M., Ram, A. F. J. & Meyer, V. Using non-homologous end-joining-deficient strains for functional gene analyses in filamentous fungi. *Methods in Molecular Biology* **835**, 133–150 (2012).

65. Samson, R. A. *et al.* Phylogeny, identification and nomenclature of the genus *Aspergillus*. *Stud Mycol* **78**, 141–173 (2014).

66. Gallegos-Monterrosa, R., Mhatre, E. & Kovács, Á. T. Specific *Bacillus subtilis* 168 variants form biofilms on nutrient-rich medium. *Microbiology (N Y)* **162**, 1922–1932 (2016).

67. Chen, Y. *et al.* SOAPnuke: A MapReduce acceleration-supported software for integrated quality control and preprocessing of high-throughput sequencing data. *Gigascience* **7**, gix120 (2018).

68. Garbeva, P., Hordijk, C., Gerards, S. & de Boer, W. Volatiles produced by the mycophagous soil bacterium *Collimonas*. *FEMS Microbiol Ecol* **87**, 639–649 (2014).

69. Tyc, O., Zweers, H., de Boer, W. & Garbeva, P. Volatiles in inter-specific bacterial interactions. *Front Microbiol* **6**, 1412 (2015).

70. Pluskal, T., Castillo, S., Villar-Briones, A. & Orešič, M. MZmine 2: Modular framework for processing, visualizing, and analyzing mass spectrometry-based molecular profile data. *BMC Bioinformatics* **11**, 395 (2010).

71. Xia, J., Sinelnikov, I. v., Han, B. & Wishart, D. S. MetaboAnalyst 3.0-making metabolomics more meaningful. *Nucleic Acids Res* **43**, W251-257 (2015).

72. Guo, X. *et al.* CNSA: A data repository for archiving omics data. *Database* **2020**, baaa055 (2020).

73. Chen, F. Z. *et al.* CNGBdb: China National GeneBank DataBase. *Hereditas* **42**, 799–809 (2020).

Acknowledgements

This work was supported by the Danish National Research Foundation (DNRF137) for the Center for Microbial Secondary Metabolites. Funding was provided by the Novo Nordisk Foundation for infrastructure ‘‘Imaging Microbial Language in Biocontrol (IMLiB)’’ (NNF19OC0055625). GH was supported by the China National GeneBank (CNGB). The authors thank Aaron J.C. Andersen and the DTU Bioengineering Metabolomics Core for support with LC-MS and MALDI-MSI.

Authors contributions

Á.T.K. conceived the project. A.R., F.B., J.W.S., B.K.S., S.B. and Á.T.K. performed the experiments. H.H and Y.W. performed bacterial population metagenomics experiments and corresponding data analysis. G.M. performed genome resequencing of the evolved bacterial clones. S.A.J. and M.W performed MALDI-MSI. O.T. and P.G. performed VOC identification. C.N.L.A. performed microbiology tests on VOCs. C.B.W.P. performed LC-MS on lipopeptides. T.O.L. contributed methods and instrumentation for lipopeptide analysis. M.A., A.F.J.R. and C.A.M.v.d.H. created fungal strains. T.J. and Á.T.K. wrote the manuscript with corrections from all authors.

Competing interests

The authors declare no competing interests.

Correspondence and requests for materials should be addressed to Á.T.K.

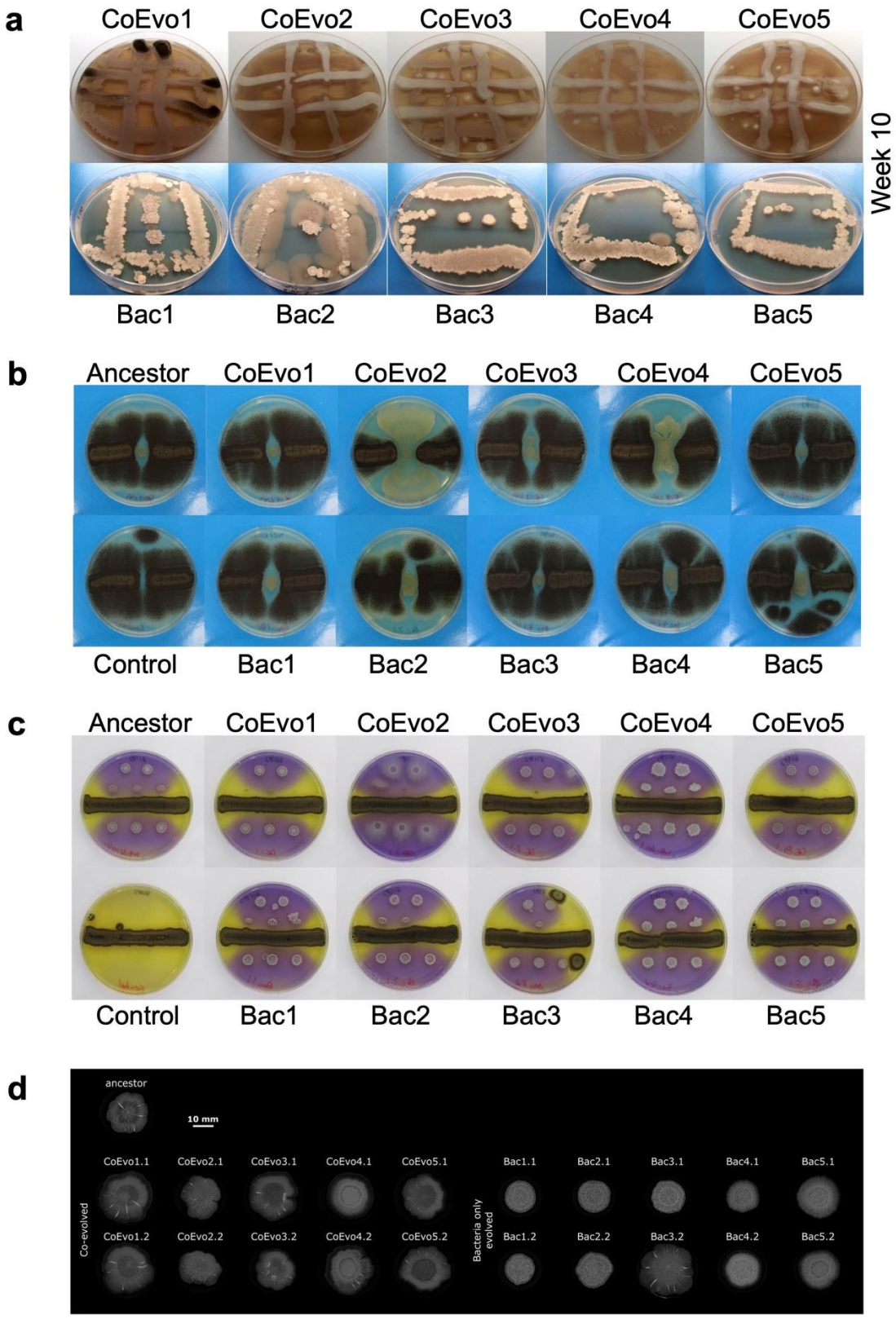

Fig. S1 | *B. subtilis* adaptation to the presence of *A. niger*. a, Experimental evolution plates at the 10th transfer, top panels showing *B. subtilis* evolved in the presence of *A. niger*, and lower panels showing bacteria only cultivations. **b,** Bacterial growth spotted between two lines of fungal streaks. **c,** Lower panels showing the pH of the medium using Bromocresol Purple, where bacterial cultures were spotted next to a continuous fungal spore streak. Purple and yellow colours indicate pH >6.8 and pH <5.2, respectively. In **b** and **c**, the plate size = 9 cm, CoEvo refers to co-culture evolved isolates, Bac denotes bacteria only evolved isolated. **d,** Biofilm colonies of evolved isolates on MSgg agar medium. Scale bar = 10 mm.

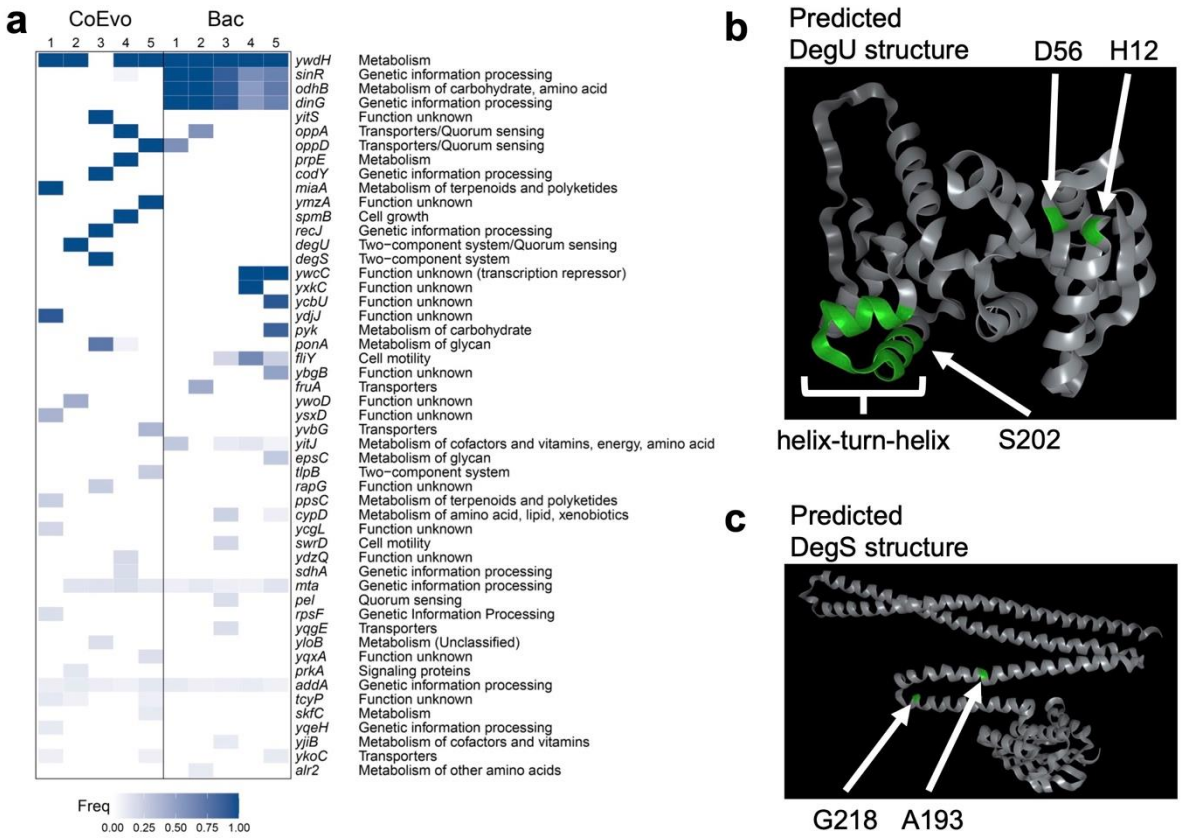

Fig. S2 | Genetic characterisation of *B. subtilis* adaptation to *A. niger*. a, Detected mutations in CoEvo and Bac populations. **b,** Predicted DegU structure based on AlphaFold (https://alphafold.ebi.ac.uk/entry/P13800). H12 and D56 amino acids are highlighted that were previously described to be involved in phosphorylation state of DegU. SNP in CoEvo2, S202 is also highlighted. **c,** Predicted DegS structure based on AlphaFold (https://alphafold.ebi.ac.uk/entry/P13799). G218 amino acid is highlighted that were previously described to be involved in phosphor-activity of DegS. SNP in CoEvo3, A193 is also highlighted.

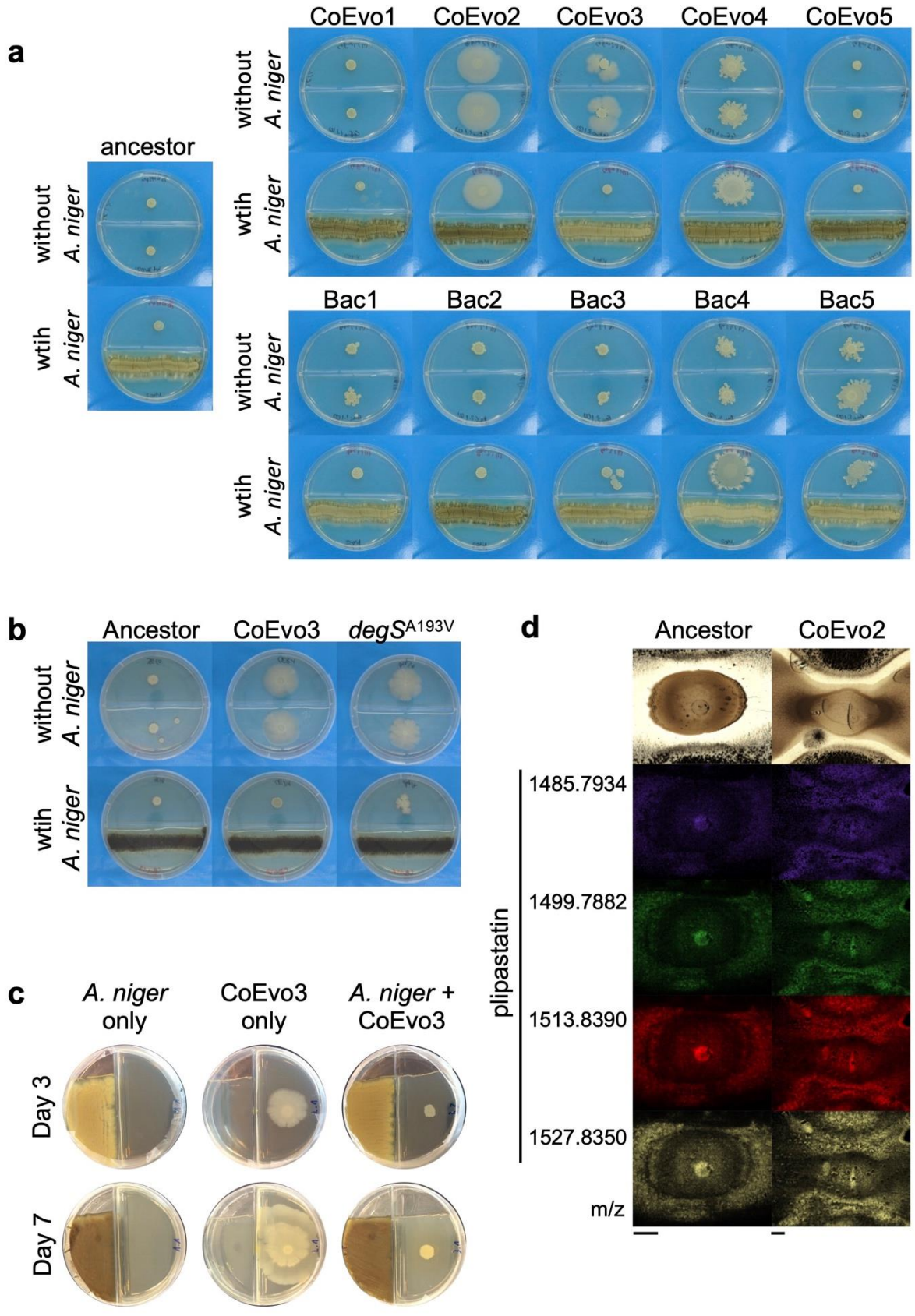

Fig. S3 | The effects of volatile compounds on *B. subtilis* growth, and spatial detection of plipastatin in CoEvo2. a, Colony spreading of the ancestor and evolved isolates in the absence (top panels) and presence of *A. niger* (lower panels). **b,** Colony spreading of the ancestor, CoEvo3 and *degS*^{A193V} mutant in the absence (top panels) and presence of *A. niger* (lower panels). **c,** Experimental setup used to trap VOCs at day 3 and 7. The empty space in the agar medium was used to place the steel traps containing 150 mg Tenax TA and 150 mg Carbopack B. **d,** MALDI-MSI spatial detection of plipastatin isoforms in bacterial colonies (wild-type and CoEvo2) grown between two fungal streak lines.

m/z values of surfactin isoforms are indicated on the left. Scale bars = 2 mm.

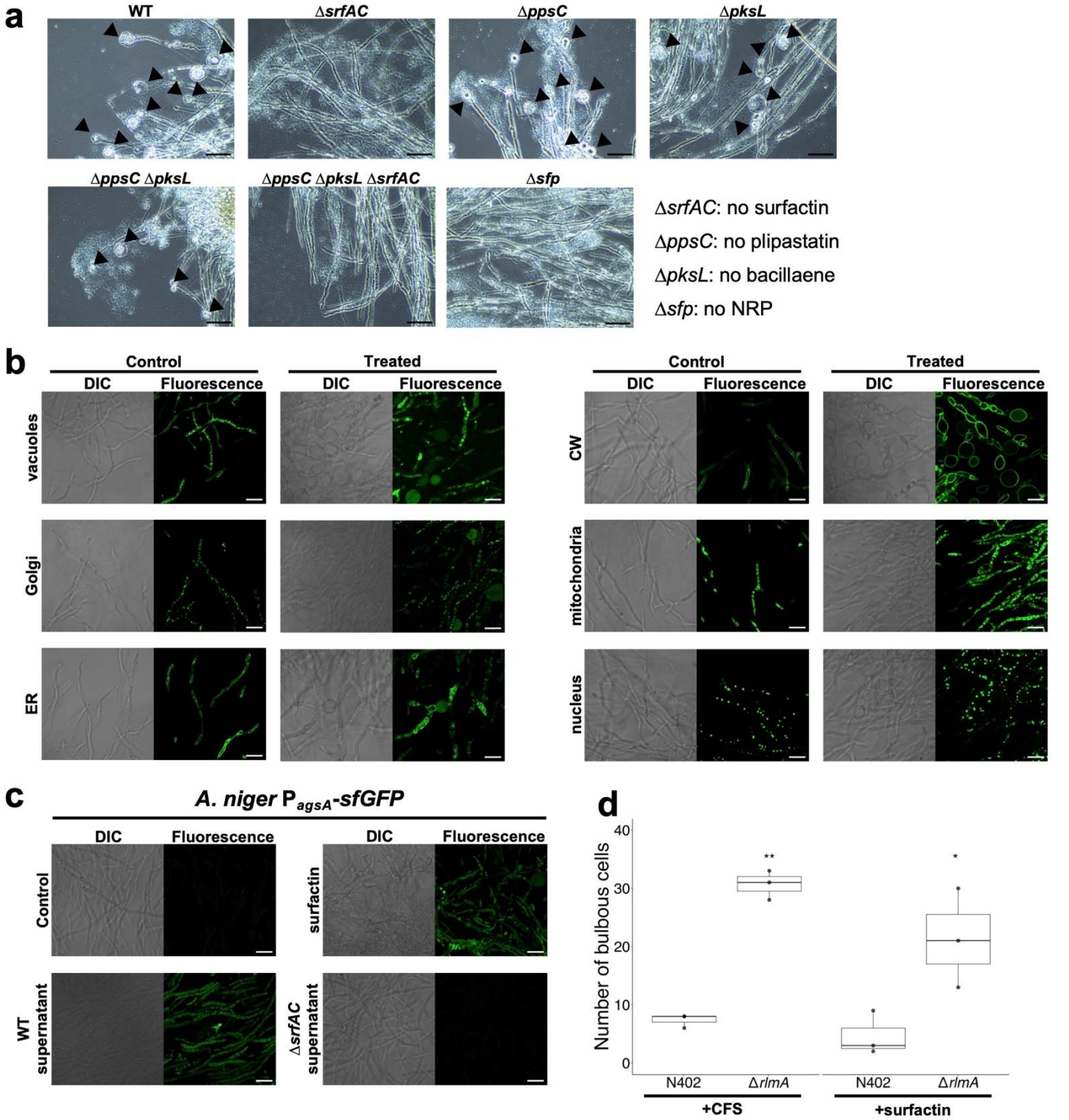
a
WT
ΔsrfAC
ΔppsC
ΔpksL
ΔppsC ΔpksL
ΔppsC ΔpksL ΔsrfAC
Δsfp
ΔsrfAC: no surfactin
ΔppsC: no plipastatin
ΔpksL: no bacillaene
Δsfp: no NRP
b
Control
Treated
DIC
Fluorescence
vacuoles
Golgi
ER
CW
mitochondria
nucleus
c
A. niger PagsA-sfGFP
Control
surfactin
WT supernatant
ΔsrfAC supernatant
d
Number of bulbous cells
N402
ΔrlmA
+CFS
+surfactin
e
luminescence/OD
time [h]
PagsA-lux control
PagsA-lux +WT CFS
PagsA-lux +ΔsrfAC CFS
PagsA-lux +CFW

Fig. S4 | Influence of surfactin on fungal hyphae. a, Microscopy visualisation of bulging fungal hyphae with wild type (WT) and various mutants, including strain lacking surfactin (Δ*srfAC*), plipastatin (Δ*ppsC*), bacillaene (Δ*pksL*), plipastatin and bacillaene (Δ*ppsC* Δ*pksL*), plipastatin, bacillaene, and surfactin (Δ*ppsC* Δ*pksL* Δ*srfAC*), or all non-ribosomal peptides (Δ*sfp*). Scale bar = 20 μm. **b,** DIC (left) and green fluorescence (right) imaging of the *A. niger* MA23.1.1 strain for vacuoles (P_{gpdA}-CpyA::eGFP-T*trpC*); Ren1.10 strain for Golgi (P_{gmtA}-eYFP:: GMTA-T*gmtA*), MA141.1 strain for endoplasmic reticulum, ER (P_{gpdA}-*glaA*:: sGFP-HDEL-T*trpC*); AR0#11 strain for cell wall, CW (P_{gpdA}-*glaA*::sGFP-T*trpC*); BN38.9 strain for mitochondria (P_{gpdA}-CitA::eGFP-T*trpC*); and MA26.1 strain for nucleus (P_{gpdA}-H2B::eGFP-T*trpC*) in the absence (Control) or presence (Treated) of bacterial cell free supernatant. Scale bar = 20 μm. **c,** DIC (left) and green fluorescence (right) imaging of the *A. niger* JvD1.1 strain carrying P_{agsA}-eGFP-T*trpC* for detection of *agsA* gene expression in the absence (control) and presence of cell-free WT supernatant, 20 μg/ml surfactin, and cell-free Δ*srfAC* supernatant. Scale bar = 20 μm. **d,** Number of bulbous cells by the wild-type N402 and Δ*rlmA* mutant *A. niger* in the presence of cell-free WT supernatant (CFS) or 20 μg/ml surfactin. Student's t-test with Bonferroni-Holm correction was performed (*p_{adjust} <0.05, **p_{adjust} <0.01). **e,** Luminescence reporter assay using *A. niger* strains MA297.3 containing $P_{agsA(3\times RlmA\ box)}$ before the promoter-less luciferase. Cultures were treated with LB medium (black dashed line), cell-free WT supernatant (CFS, solid line), cell-free Δ*srfAC* supernatant (Δ*srfAC* CSF, dotted line), or Calcofluor White (CFW, grey dashed line).

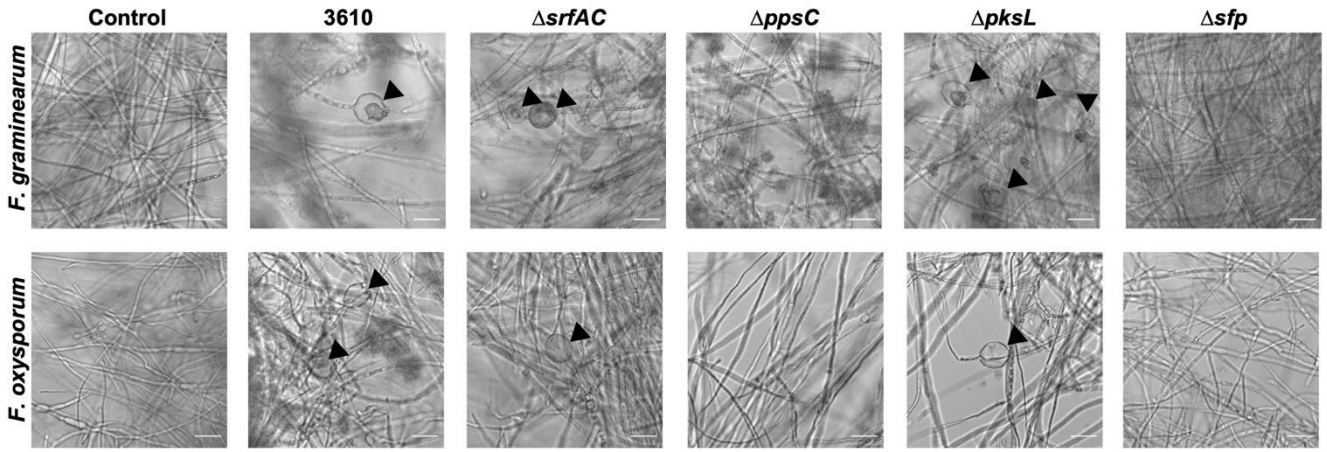

Fig. S5 | Influence of plipastatin on hyphae of Fusarium species. Microscopy visualisation of bulging Fusarium hyphae with wild type (WT) and various mutants, including strain lacking surfactin (Δ*srfAC*), plipastatin (Δ*ppsC*), bacillaene (Δ*pksL*), or all non-ribosomal peptides (Δ*sfp*). Scale bar = 25 μm.

Supplementary Table 1 for strains, plasmids and oligos

B. subtilis strains	Genotype, description	Reference
NCIB 3610	undomesticated wild type strain	[1,2]
DK1042	NCIB 3610, but *comI*^{Q12L} (naturally competent)	[3]
168 *degU*	*trpC* Δ*degU*::Km^{R}	[4]
TB742	DK1042 Δ*degU*::Km^{R}	This work
TB938	DK1042 *degU*^{S202G}	This work
TB939	DK1042 *degS*^{A193V}	This work
DS4085	NCIB 3610 Δ*pksL*::Cm^{R}	[5]
DS4114	NCIB 3610 Δ*ppsC*::Tet^{R}	[5]
DS1122	NCIB 3610 *srfAC*::Tn10 Spec^{R}	[6]
DS3337	NCIB 3610 Δ*sfp*::Mls^{R}	[7]
DS4113	NCIB 3610 Δ*ppsC*::Tet^{R} Δ*pksL*::Cm^{R}	[5]
DS4124	NCIB 3610 Δ*ppsC*::Tet^{R} Δ*pksL*::Cm^{R} *srfAC*::Tn10 Spec^{R}	[5]

A. niger strains	Genotype	Reference
N402	wild-type fungal strain	[8]
MA297.3	N402 $P_{agsA(3\times RlmA\ box)}$-m*luc*-T*trpC-pyrG***	This work
MA584.2	N402 $P_{agsA(RlmA\ box\ mutated)}$-m*luc*-T*trpC-pyrG***	This work
Δ*rlmA*	N402 Δ*rlmA*::hyg^{R}	[9]
AR0#11	N402 P_{gpdA}-*glaA*::sGFP-T*trpC*	[10]
MA141.1	N402 P_{gpdA}-*glaA*:: sGFP-HDEL-T*trpC*	[11]
Ren1.10	N402 P_{gmtA}-eYFP:: GMTA-T*gmtA*	[11]
MA23.1.1	N402 P_{gpdA}-CpyA::eGFP-T*trpC*	[12]
FG7	N402 P_{synA}-eGFP::SynA-T*synA*	[13]
BN38.9	N402 P_{gpdA}-CitA::eGFP-T*trpC*	[14]
MA26.1	N402 P_{gpdA}-H2B::eGFP-T*trpC*	[12]
JvD1.1	N402 P_{agsA}-eGFP-T*trpC*	[15]

Fungal strains		
A. awamori	FSU 11418	JMRC
A. brasiliensis	FSU 35902 (DSM 1988)	JMRC
A. tubingiensis	FSU 11408	JMRC
A. nidulans	HKI G034	JMRC
F. graminearum	IBT 41925	IBT
F. oxysporum	IBT 40872	IBT

JMRC: Jena Microbial Resource Collection at Leibniz Institute for Natural Product Research and Infection Biology Hans Knöll Institute, Jena, Germany (https://www.leibniz-hki.de/en/jena-microbial-resource-collection.html)
IBT: IBT Culture Collection at DTU Bioengineering, Kongens Lyngby, Denmark (https://www.bioengineering.dtu.dk/research/strain-collections/ibt-culture-collection-of-fungi)

Plasmids	description	Source
pMiniMad	*ori*^{BsTs} *Amp*^{R} *Mls*^{R}	[16]
pTB693	pMiniMad with *degU*^{S202G}	This work
pTB694	pMiniMad with *degS*^{A193V}	This work
pMA334	vector with *pyrG* flanking regions	[17]
pBN008	vector with P_{agsA}(0.55-kb-rlm2add)-*uidA-pyrG*	[9]
pVG4.1	vector with m*luc*-T*trpC*	[18]
pMA348	pMA334 with $P_{agsA(3\times RlmA\text{-}box)}$-m*luc*-T*trpC-pyrG***	This work
pMA370	pMA334 with $P_{agsA(RlmA\text{-}box\ mutated)}$-m*luc*-T*trpC-pyrG***	This work

Oligos		sequence	gene targeted
oAR23	*Nco*I	ATCCATGGTGGCGGCTGAGAAGTCGTCG	*degU* in CoEvo2
oAR24	*Bam*HI	GCGGATCCAAGAGGTTATCTGCTGAAAG	*degU* in CoEvo2
oAR30	*Sal*I	CCGTCGACTTGGCGATAAACTTGAAGTG	*degS* in CoEvo3
oAR41	*Bam*HI	ATGGATCCTGAAGAGCGCAACCTCAAAC	*degS* in CoEvo3
oAR25		AGACTTGCCAAGCTCTTC	*degU*
oAR26		GCTTGTAGAGCTGTATCC	*degU*
oAR31		TCAGGTCGAACCCTTTAC	*degS*
oAR32		AACAGCTGGTCGAAGAAC	*degS*
oAR27		TCCTCTGGCCATTGCTCTG	pMiniMad MCS
oAR28		CGAAGTTAGGCTGGTAAG	pMiniMad MCS
PagsAP1f-NotI		GCGGCCGCTCTAGAACTAGT	
TtrpCP2r-NotI		AAGGAAAAAAGCGGCCGCTCTAGAAAGAAGGATTACCTC	
PagsAP4f-NotI		AAGGAAAAAAGCGGCCGCCTGCAGTAGTGGCGGCTGCTTC	
PagsA-AF-R-mut-RlmA2		CTCGGTGGTCGCCGCCGAGAAACGTCATATCAGGATAGC	
PagsA-AF-F-mut-RlmA1		ATATGACGTTTCTCGGCGGCGACCACCGAGAGTAGAGAATGA	
PagsAP2r		CTCGATCTTTCTGCGACCCATGATGGCAAGCGGCGTGTGGTA	
oBK7		CCGAGTACAAGGARGCCTTC	CaM
oBK8		CCGATRGAGGTCATRACGTGG	CaM

References

1. Branda, S. S., González-Pastor, J. E., Ben-Yehuda, S., Losick, R. & Kolter, R. Fruiting body formation by *Bacillus subtilis*. *Proc Natl Acad Sci U S A* **98**, 11621–11626 (2001).
2. Zeigler, D. R. *et al.* The origins of 168, W23, and other *Bacillus subtilis* legacy strains. *J Bacteriol* **190**, 6983–6995 (2008).

3. Konkol, M. A., Blair, K. M. & Kearns, D. B. Plasmid-encoded comI inhibits competence in the ancestral 3610 strain of *Bacillus subtilis*. *J Bacteriol* **195**, 4085–4093 (2013).
4. Kovács, Á. T. & Kuipers, O. P. Rok regulates *yuaB* expression during architecturally complex colony development of *Bacillus subtilis* 168. *J Bacteriol* **193**, 998–1002 (2011).
5. Müller, S. *et al.* Bacillaene and sporulation protect *Bacillus subtilis* from predation by *Myxococcus xanthus*. *Appl Environ Microbiol* **80**, 5603–5610 (2014).
6. Chen, R., Guttenplan, S. B., Blair, K. M. & Kearns, D. B. Role of the σD-dependent autolysins in *Bacillus subtilis* population heterogeneity. *J Bacteriol* **191**, 5775–5784 (2009).
7. Patrick, J. E. & Kearns, D. B. Laboratory strains of *Bacillus subtilis* do not exhibit swarming motility. *J Bacteriol* **191**, 7129–7133 (2009).
8. Bos, C. J. *et al.* Genetic analysis and the construction of master strains for assignment of genes to six linkage groups in *Aspergillus niger*. *Curr Genet* **14**, 437–443 (1988).
9. Damveld, R. A. *et al.* The *Aspergillus niger* MADS-box transcription factor RlmA is required for cell wall reinforcement in response to cell wall stress. *Mol Microbiol* **58**, 305–319 (2005).
10. Gordon, C. L. *et al.* Glucoamylase::green fluorescent protein fusions to monitor protein secretion in *Aspergillus niger*. *Microbiology (N Y)* **146**, 415–426 (2000).
11. Carvalho, N. D. S. P. *et al.* Functional YFP-tagging of the essential GDP-mannose transporter reveals an important role for the secretion related small GTPase SrgC protein in maintenance of Golgi bodies in *Aspergillus niger*. *Fungal Biol* **115**, 253–264 (2011).
12. Weenink, X. O. Protein secretion in the filamentous fungus *Aspergillus niger*. (Leiden University, 2008).
13. Kwon, M. J. *et al.* Molecular genetic analysis of vesicular transport in *Aspergillus niger* reveals partial conservation of the molecular mechanism of exocytosis in fungi. *Microbiology (N Y)* **160**, 316–329 (2014).
14. Nitsche, B. M., Burggraaf-Van Welzen, A. M., Lamers, G., Meyer, V. & Ram, A. F. J. Autophagy promotes survival in aging submerged cultures of the filamentous fungus *Aspergillus niger*. *Appl Microbiol Biotechnol* **97**, 8205–8218 (2013).
15. Meyer, V. *et al.* Survival in the presence of antifungals: Genome-wide expression profiling of *Aspergillus niger* in response to sublethal concentrations of caspofungin and fenpropimorph. *Journal of Biological Chemistry* **282**, 32935–32948 (2007).
16. Patrick, J. E. & Kearns, D. B. MinJ (YvjD) is a topological determinant of cell division in *Bacillus subtilis*. *Mol Microbiol* **70**, 1166–1179 (2008).
17. Arentshorst, M., Lagendijk, E. L. & Ram, A. F. A new vector for efficient gene targeting to the *pyrG* locus in *Aspergillus niger*. *Fungal Biol Biotechnol* **2**, 2 (2015).

18. Meyer, V. *et al.* Fungal gene expression on demand: An inducible, tunable, and metabolism-independent expression system for *Aspergillus niger*. *Appl Environ Microbiol* **77**, 2975–2983 (2011).